Investigating cellular senescence during gliomagenesis

Rana Salam

SORBONNE UNIVERSITÉ
CRÉATEURS DE FUTURS DEPUIS 1257

Thèse de la faculté des sciences de
Sorbonne Université

Ecole doctorale Cerveau, Comportement, Cognition (ED3C)

Investigating cellular senescence during gliomagenesis

Présentée par

Rana SALAM

POUR OBTENIR LE GRADE DE DOCTEUR

Spécialité Neurosciences

Soutenue publiquement le 7 Juillet 2021

Devant un jury composé de :

Pr. Marie-Claude POTIER	Présidente
Dr. Julie GAVARD	Rapportrice
Dr. Jean-Yves THURET	Rapporteur
Dr. Franck BOURDEAUT	Examinateur
Dr. Marco DEMARIA	Examinateur
Dr. Isabelle LE ROUX	Directrice de thèse

ICM Institut du Cerveau

Thèse de la faculté des sciences de
Sorbonne Université

Ecole doctorale Cerveau, Comportement, Cognition (ED3C)

Investigating cellular senescence during gliomagenesis

Présentée par

Rana SALAM

POUR OBTENIR LE GRADE DE DOCTEUR

Spécialité Neurosciences

Soutenue publiquement le 7 Juillet 2021

Devant un jury composé de :

Pr. Marie-Claude POTIER	Présidente
Dr. Julie GAVARD	Rapportrice
Dr. Jean-Yves THURET	Rapporteur
Dr. Franck BOURDEAUT	Examinateur
Dr. Marco DEMARIA	Examinateur
Dr. Isabelle LE ROUX	Directrice de thèse

Illustration by Sergio López Manzaneda

March on. Do not tarry. To go forward is to move toward perfection. March on, and fear not the thorns, or the sharp stones on life's path.

Gibran Khalil Gibran

Seek the company of the wise, who know. Agree with what they say, for one understands only that with which one agrees. Be sincere in what you say - a single tongue should not speak two different words. No deceit or fraud should enter into your thoughts. Do not belittle anyone or anything, for everyone and everything in its inner being wishes for the same thing.

Ibn Arabi

Wear gratitude like a cloak and it will feed every corner of your life

Jalāl al-Dīn Rūmī

Acknowledgements

I want to express my deepest gratitude to all the jury members, Dr. **Marco Demaria**, Dr. **Franck Bourdeaut**, Pr. **Marie-Claude Potier** and especially Dr. **Jean-Yves Thuret** and Dr. **Julie Gavard** for taking the time and accepting to review my work.

I am extremely thankful to all the persons without whom my project would not be achieved. Thank you.

Je remercie Dr. **Emmanuelle Huillard** et Pr. **Marc Sanson** pour m'avoir accueillie dans leur équipe.

Je remercie le Dr. **Isabelle Le Roux** de m'avoir donné l'opportunité de poursuivre ma thèse. Tout au long de ma thèse, tu m'as énormément guidée, appris en rigueur, en méthodologie sur les plans technique et théorique. Merci pour ton soutien et ta disponibilité, malgré les moments douloureux que nous avons vécus, chacune, à titre personnel.

Merci également au SiRIC CURAMUS d'avoir financé ce projet. Merci aux membres de mes comités de suivi de thèse notamment pour m'avoir donné l'opportunité de participer au AEK de Heidelberg dès ma deuxième année.

A toutes les **plateformes** de l'Institut, de cyto-ICAN ainsi qu'à l'animalerie du 105 je vous suis plus que reconnaissante, sans vous, nous n'aurions pu mener à bien ce projet. Merci pour votre patience et vos précieux conseils, en particulier à **Yannick**, **Emeline** et **Delphine**, **Philippe**, **Clémentine** et **Blandine**, **David**, **Aymeric**, **Annick**, **Célia**, **Nicolas** et **Dominique**, **Florence** et **Aurélie**, **Olivier**, **Dave**, **Julianne** et **Maria**. Un très grand merci également aux deux équipes de bio-informatique, **Justine** et **Mathilde** chez Iconics, **Christophe** et **Léa** chez ArtBio, pour votre travail de grande qualité, vos efforts sans relâche, et nos maintes réunions au cours de ces deux dernières années.

Merci à **Tomek**, pour l'aide apportée sur la technique de l'iDISCO, ta gentillesse et ta disponibilité.

Alexa, ce fut un plaisir de te transmettre les techniques que j'ai pu moi-même apprendre au cours de ma thèse. Merci pour toute l'aide que tu as pu apporter à la fin de ce projet ! Je te souhaite un bon courage pour ta thèse, et je ne me fais aucun souci !

Force à tous les futurs doctorants de l'équipe ! **Alice**, merci pour ces discussions qui m'ont ouvert les yeux sur d'autres aspects de la thèse, **Charlotte**, merci pour ta patience et la relecture de l'article, **Cristina** pour tes propositions de conférences et ta bonne humeur et merci à vous tous pour nos échanges et votre belle énergie !

Sophie et **Julie La.** merci pour votre soutien et le partage des blagues pas drôles qui nous font quand même bien rire. Merci à Sophie, qui a su trouver les mots quand il le fallait. **Caroline**, **Julie Le**., **Yseult**, **Marine** pour nos échanges et votre aide, ainsi que **Marion**, pour avoir partagé ton expertise et toujours répondu à mes questions.

Merci à **Nolwenn** de m'avoir encouragée et soutenue ainsi que **Bertille** surtout pendant l'écriture. **Sandra** et **Nathalie** merci pour tous nos échanges scientifiques et non-scientifiques, vos guides et conseils ! Nat, ça va me manquer ma tête sur ton épaule !

Mus' et **Boussif** merci pour votre bonne humeur (et toutes ces boîtes !), il n'y a pas eu un jour sans que vous n'affichiez votre sourire communicatif. Merci beaucoup **Antoine** pour votre aide chaleureuse, je ne l'oublierai pas.

Lucas, le nombre de fois où on devait prendre un verre/café ensemble ! Merci à toi **Lamia** pour m'avoir toujours encouragée à poursuivre mes futurs projets. **Emeric**, il faut vraiment qu'on crée notre antisocial social club avec **Sofia** et **Rémi** avant la fin de notre thèse ! Merci **Pierre**, ta bonne humeur a été motivante.

Nicolas, merci pour toute ton aide, ton soutien, ton respect, tu m'as toujours poussée à réfléchir hors des sentiers battus.

Sofia, having you by my side is one of my biggest luck and soothed my thesis adventure. I cannot thank you enough for all your support and patience, thank you for our biggest laughs ("to not cry"), for accompanying me in the craziest moments and for "searching for the light" together. Thank you for all our discussions on simple and complex issues and for validating our view on what should be normal or not! You kept opening my eyes on many levels, and you are a true inspiration for pursuing goals no matter what. I will miss helping you searching for stuff with you haha! Keep wearing all your evil eyes. God preserves you, your family and your mom, she is the sweetest I could encounter in my life, I also thank her for her support and all the kind messages.

Maha, thank you for consistently pushing me to achieve my best, for your understanding and our long conversations that taught me a lot. Thank you for seeking with me the bright side out of every situation, and always dancing! Your consistent fight and your perspectives on always reaching our dreams was a second wind for me. And you know, as long as "we're good, health is good, family is ok", everything is ok haha! May God help us on our path, in our families and countries and as Mawlana said "as long as, there is not someone, pointing a knife at your heart, everything is fine!" J'en profite pour remercier **Laurène** et **Charlotte** pour leur gentillesse et bienveillance !

SuperSergio, eres uno de los encuentros más "random" y bonitos de esta experiencia. Eres unas de las personas más profundamente buenas que he conocido, y siempre dispuesto a ayudar. Nuestras largas discusiones sobre tantos temas científicos, sociales, culturales y religiosos fueron una bocanada de oxígeno para mí. Por tu experiencia en la vida, tu cultura y tu "open-minded" opiniones, no te hemos llamado Mawlana para nada. Miles gracias.

Merci à vous **Isabelle** pour votre patience infinie, et nos échanges presque thérapeutiques.

Hazal, **Evelyne**, **Angélique**, **Marina** merci d'avoir été un soutien important pour moi, depuis maintenant... en tous cas, bieeen avant de commencer ma thèse! Vous êtes chacune formidable, et nos moments passés ensemble m'ont permis de m'échapper du quotidien, merci pour tout.

Coralie, je suis tellement contente que nos chemins se soient croisés, merci de ton soutien et de nos discussions libératrices, je serai toujours admirative devant la femme forte et libre que tu es devenue.

Seynabou, ma Seynabou, combien de fois tu m'as sauvée de situations irréelles ? Merci pour ta présence protectrice mashallah, merci d'avoir toujours veillé sur moi et de m'avoir toujours guidée.

Cornel e **Ana**, non lo so come posso ingraziarvi per il vostro amore. Ho crescuto e imparato tantissimo con voi. Grazie per tutti questi belli momenti. Ci vediamo prossimo si Dio vuole. Pisicuta.

Je souhaite également remercier tous les **patients** ainsi que leur **famille** pour leur précieuse aide.

Une pensée à toutes les **souris** sacrifiées pour ce projet.

Amine, **Manal**, **Ayman** et **Bouchra** merci pour votre amour et votre soutien inconditionnels si précieux, foyer dans lequel je savais que je pouvais toujours me réfugier.

To my whole family in Lebanon, thank you for your unconditional love, the nurturing environment and all your endless support you gave me until now. During this thesis, we assisted to multiple catastrophes. Although I believe we did not reach the end of our healing process path, we should persevere in our hope for a better place.

To **Teta**, **Atti**, **Khalo Walid** and **Amal**, to **Amine**, to **Mama** and **Baba**, this thesis symbolizes the accomplishment of all the sacrifices you did for me. I am the proudest to have you as my family.

بحبكن، الله يحمكن، أشتقتلكن، بشوفكن عن قريب

I am grateful to all the persons in my life who made who I am today, and help me build who I will be tomorrow.

بشكرك يا الله على كل الخير والبركة يلي اعطيتني يها كل حياتي

Abstract

Glioblastoma (GBM) is the most common primary brain tumor in adults yet with limited treatment efficacy. In cancer, recent studies describe senescent cells removal as a new emerging therapeutic strategy. Senescent cells are characterized by a stable cell cycle arrest and by the secretion of a plethora of factors referred as the senescence-associated secretory phenotype (SASP). The aim of my PhD was to decipher the role of cellular senescence in GBM progression. We first identified senescent cells in patient and in a mouse model of GBM. We then showed that the removal of senescent cells expressing high levels of *p16*^{Ink4a}, using the p16-3MR transgene, significantly increased the survival of GBM-bearing mice. Single-cell RNA sequencing (scRNAseq) analysis revealed that senescent p16$^{Ink4a\ Hi}$ cells are malignant, they represent less than 10% of the tumor cells and their removal modify the tumoral ecosystem. By combining scRNAseq and bulk RNAseq with immunohistochemistry, we identified NRF2 transcription factor as a regulator of the SASP. Moreover, we defined a specific senescence signature in the mouse model of GBM. Remarkably, the senescence signature is conserved in patient GBMs and its high score is correlated with a lower survival. These results pave the way for the use of senotherapy as a companion therapy for patients with GBM.

Key words: Glioblastoma, Cellular Senescence, NRF2, scRNAseq, Senotherapy.

Résumé

Le glioblastome (GBM) est une tumeur cérébrale maligne primitive la plus fréquente chez l'adulte. L'efficacité des traitements reste très limitée et le taux de survie est faible. Dans le domaine du cancer, l'élimination des cellules sénescentes a récemment émergé comme une potentielle stratégie thérapeutique. Les cellules sénescentes sont caractérisées par un arrêt permanent du cycle cellulaire ainsi que par la sécrétion d'une multitude de facteurs regroupés sous le terme phénotype sécrétoire associé à la sénescence (SASP). Le but de mon projet de thèse a été d'étudier le rôle de ces cellules au cours de la progression tumorale des GBM. Nous les avons tout d'abord identifiées dans les GBMs de patients et dans un modèle murin de GBM. En utilisant le transgène p16-3MR, nous avons montré que l'élimination des cellules sénescentes exprimant des niveaux élevés de *p16*^{Ink4a} améliore significativement la survie des souris porteuses d'un GBM. Des analyses de séquençage d'ARN en cellule unique (scRNAseq) ont révélé que les cellules sénescentes p16$^{Ink4a\ Hi}$ ont une identité maligne, qu'elles représentent moins de 10% de la tumeur totale, et que leur élimination modifie l'écosystème tumoral. En combinant les techniques de séquençage de l'ARNm sur tissu (bulk RNAseq) et sur cellule unique (scRNAseq) avec l'immunohistochimie, nous avons identifié le facteur de transcription NRF2 comme régulateur du SASP. Enfin, nous avons défini une signature de la sénescence dans le modèle murin de GBM qui est conservée dans les GBMs de patients. De manière remarquable, un score élevé de la signature de la sénescence est corrélé à un mauvais pronostic chez les patients. Ces résultats ouvrent la voie à l'utilisation de la sénothérapie en thérapie d'accompagnement pour les patients atteints de GBM.

Mots-clés : Glioblastome, Sénescence Cellulaire, NRF2, scRNAseq, Sénothérapie.

TABLE OF CONTENTS

List of abbreviations

AC: astrocyte
AKT: kinase
ARE: antioxidant response element
Areg: amphiregulin
ARF: alternate reading frame protein
ATM: ataxia telangiectasia mutated
ATR: ataxia telangiectasia and rad3-related
BBB: blood-brain barrier
BMDM: bone marrow-derived macrophages
BMI1: BMI1 proto-oncogene, polycomb ring finger
BRD4: bromodomain 4
CAR: chimeric antigen receptor
CBX7: chromobox 7
CCF: cytoplasmic chromatin fragment
CDK: cyclin dependent kinase
CDKN: cyclin dependent kinase inhibitor
cGAS/STING: cytosolic GMP-AMP synthase/stimulator of interferon genes
CL: classical
CNS: central nervous system
CNV: copy number variation
COP: committed OPC-like
CSC: cancer stem cell
CXCL: C-X-C motif ligand
CX43: connexin 43
GATA4: GATA binding protein 4
GBM: glioblastoma
DDR: DNA-damage response
DNA: deoxyribonucleic acid
DNA-SCARS: DNA-segments with chromatin alterations reinforcing senescence
DPI: days post injection
DTA: diphtheria toxin subunit A
DSB: double strand breaks
ECM: extracellular matrix
EdU: 5-ethynyl-2'-deoxyuridine
EGFR: epidermal growth factor receptor
EMT: epithelial-to-mesenchymal transition
Ereg: epiregulin
EZH2: enhancer of zeste homolog 2
FACS: fluorescence activated cell sorting
FFPE: formalin-fixed paraffin embedded
FGFR: fibroblast growth factor receptor
G-CIMP: glioma-CpG island methylator phenotype
GCV: ganciclovir
GEMM: genetically engineered mouse model
GFP: green fluorescent protein
GFAP: glial fibrillary acidic protein
GLAST: glutamate aspartate transporter
GSEA: gene set enrichment analysis
HGF: hepatocyte growth factor
HIF-1: hypoxia-inducible factor 1
HLA: human leukocyte antigen
HR: homologous recombination
HSV-TK: herpes simplex virus 1-thymidine kinase
IBA1: ionized calcium binding adaptor molecule 1
IDH: isocitrate dehydrogenase
iDISCO: immunolabeling-enabled three-dimensional imaging of solvent-cleared organs
IGFBP: insulin-like growth factor–binding protein
IHC: immunohistochemistry
IL: interleukin
INK4A: inhibitors of CDK4A
INK-ATTAC: INK4a-apoptosis through targeted activation of caspase
IR: ionizing radiations
JAK/STAT: janus kinase/signal transducer and activator of transcription
KEAP1: kelch-like ECH-associated protein 1
LAD: lamina-associated domain
LSEC: liver sinusoid endothelial cell
Luc: luciferase
Lv: lentivirus
MDM2: murine double minute 2
MDSC: myeloid-derived stromal cell
MES: mesenchymal
MGMT: O^6-methylguanine-DNA methyltransferase
MHC: major histocompatibility complex
miRNA or **miR**: micro RNA
MMP: matrix metalloprotease
mOL: myelinating oligodendrocyte
mTOR: mammalian target of rapamycin
mRFP: monomeric red fluorescent protein
NF1: neurofibromatosis factor 1
NF-κB: nuclear factor kappa light chain enhance of activated B cells
NFE2L2, **NRF2**: nuclear factor-erythroid 2-related factor 2
NHEJ: nonhomologous end joining
NK: natural killer
NP: neural progenitor
NPC: neural-precursor-cell
NSC: neural stem cell
OLIG2: oligodendrocyte transcription factor 2

OPC: oligodendrocyte precursor cell
OIS: oncogene-induced senescence
PAI-1: plasminogen activator inhibitor-1
PCR: poly chain reaction
PD1: programmed cell death protein 1
PDL1: programmed death-ligand 1
pOPC: pri-OPC
Rb: retinoblastoma protein
ROS: reactive oxygen species
RT-qPCR: retro-transcription quantitative poly chain reaction
p16-3MR:
p38MAPK: p38 mitogen-activated protein kinase
PDGF-AA: platelet-derived growth factor-AA
PDGFR: platelet-derived growth factor receptor
PICS: PTEN-induced cellular senescence
PI3K: phosphatidylinositol 3-kinase
PN: proneural
PRC: polycomb repressive complex
PTEN: phosphatase and TENsin homolog
Ras: rat sarcoma
RB: retinoblastoma protein
RTK: receptor tyrosine kinase
SAHF: senescence-associated heterochromatin foci
SASP: senescence-associated secretory phenotype
SA-β-Gal: senescence-associated beta galactosidase
SERPIN: serine protease inhibitor
sEV: small extracellular vesicles
sMAF: small musculoaponeurotic fibrosarcoma
T reg: regulatory T
TAM: tumor associated macrophage
TCGA The Cancer Genome Atlas
TERT: telomerase reverse transcriptase
TIMP: tissue inhibitor of metalloprotease
TIS: therapy-induced senescence
TK: thymidine kinase
TME: tumor microenvironment
TMZ: temozolomide
TNC: tenascin-C
UMAP: uniform manifold approximation and projection
VEGF: vascular endothelial growth factor
VEGFR: vascular endothelial growth factor receptor
VIM: vimentin
WT: wild-type
γH2AX: gamma H2A histone family
3'LTR: 3' long terminal repeat
53BP1: p53-binding protein 1

Introduction

I. Glioblastoma: a poor patient prognosis

1. Gliomas: the most common malignant brain tumors

Primary tumors of the central nervous system (CNS) represent 2% of overall cancer types. They are classified according to the World Health Organization recommendations which are regularly updated by the cIMPACT-NOW (Consortium to Inform Molecular and Practical Approaches to CNS Tumor Taxonomy). Gliomas are the most frequent malignant primary brain tumors in adult and their global incidence is 3.22 newly diagnosed cases per 100,000 population each year, according to the Central Brain Tumor Registry of the United States (Ostrom et al., 2020).

Gliomas display features of glial cells which are one of the two main cell types of the CNS, along with neurons. Glial cells in the brain include astrocytes, the most abundant CNS cells that regulate neuronal activity and homeostasis, oligodendrocytes that produce myelin wrapping axons, ependymal cells, a cell component of the blood-brain barrier (BBB), and microglial cells, the resident immune cells of the CNS. Noteworthy, neural stem cells (NSCs) give rise to neurons, oligodendrocytes and astrocytes. Deep sequencing of triple-matched resected patient tissues of (i) normal subventricular zone (SVZ) tissue away from the tumor mass, (ii) tumor tissue, and (iii) normal cortical tissue (or blood), identified NSCs as the cell of origin of the human high grade gliomas (Lee et al., 2018). In addition, gliomas are infiltrated by tumor-associated macrophages. They are of two kinds: the microglial cells which arise from embryonic yolk sac precursors and the macrophages derived from the bone marrow (named bone marrow-derived macrophages, BMDM) which infiltrate the brain when the BBB has lost its integrity.

Gliomas are classified into four grades (grade I-III for low grade gliomas and grade IV for high grade glioma, or glioblastomas (GBM)) based on their histological features, on the most represented physiological cell type (oligodendrocyte or astrocyte), on their malignity and on their genetic alterations (Louis et al., 2016; Ostrom et al., 2020). As pediatric gliomas display different clinical and molecular characteristics, I will focus my introduction on adult gliomas and more particularly, on GBM, a grade IV astrocytoma. They represent more than half of all malignant primary brain tumors (***Figure 1***) and are the focus of my PhD work.

2. Glioblastoma: the most frequent and aggressive glioma

2.1. Epidemiology and symptoms

GBM is the most aggressive grade of glioma. Patients have a median age of 62 years at diagnosis. The median survival is of only 8 months with a dramatic 5-year overall survival of 6.8% (Ostrom et al., 2020). A study conducted in England demonstrated that GBM incidence has significantly risen across all ages over the last two decades (***Figure 1***) (Philips et al., 2018). Its etiology is not yet well understood, and patients do not present clear inheritable predispositions. Only exposition to ionizing radiations were demonstrated to increase the risk of incidence (Ostrom et al., 2020; Todorova et al., 2019).

Patients with GBMs are diagnosed after presenting various symptoms, which depend on the tumor localization and the infiltration degree of malignant cells in the parenchyma. These symptoms include headaches, epileptic seizures, focal neurologic signs and increased intracranial pressure (Hanif et al., 2017; Weller et al., 2017). Although GBM is a highly invasive tumor, they rarely metastasize (Louis et al., 2016). In GBM, malignant cells are defined by two main characteristics: they display molecular alterations identified by the copy number variations (CNV), and they are negative for the pan-leucocyte marker CD45 (Neftel et al., 2019). They are composed of about 20% of cycling cells and 80% of non-cycling cells (Couturier et al., 2020; Wang et al., 2019b). In contrast, non-malignant cells gather CD45+ immune cells, and brain cells including endothelial, neuronal and glial cells (Neftel et al., 2019).

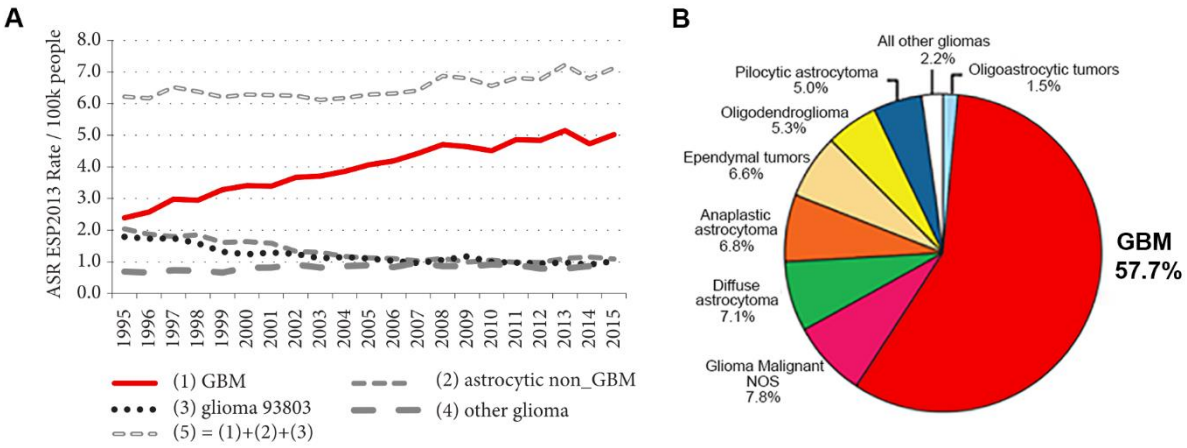

Figure 1. **GBM incidence increased over the last two decades and represent half of all gliomas**
A. Age-standardized incidence rates (ASR) per 100 000 people for gliomas diagnosed between 1995 and 2015 by type and year (adapted from Philips et al., 2018).
B. Distribution of gliomas according to their histology (adapted from Ostrom et al., 2020).
ESP2013: European Standard Population of 2013; NOS: not otherwise specified.

2.2. Patient diagnosis

After the apparition of the first symptoms and the observation by magnetic-resonance imaging (MRI) of an invasive tumor, the patient undergoes a maximal safe resection of the tumor, which helps decreasing the intracranial pressure. The surgery depends on the patient condition, the tumor localization and the surrounding functional brain regions. Otherwise, a biopsy is necessary to obtain a representative tissue sample and confirm the patient diagnosis.

The diagnosis of a GBM is validated based on neuropathologist observations of hematoxylin and eosin (HE) and immunohistochemistry (IHC) stainings of tumor resection or biopsy samples. The main cellular identity composing the tumor are therefore identified, as well as its mitotic index and the main altered molecular markers. GBMs are poorly differentiated yet with a predominant (glial fibrillary acidic protein, GFAP+) astrocytic differentiation. They display a diffuse growth pattern with a wide heterogeneity in cell morphologies (e.g., malignant cells with nuclear atypia and cellular pleomorphism, important immune infiltrates) and histological structures (e.g., microvascular proliferation, high cellular density and extent necrosis or pseudo-palissadic necrosis) (Louis et al., 2016) (***Figure 2***).

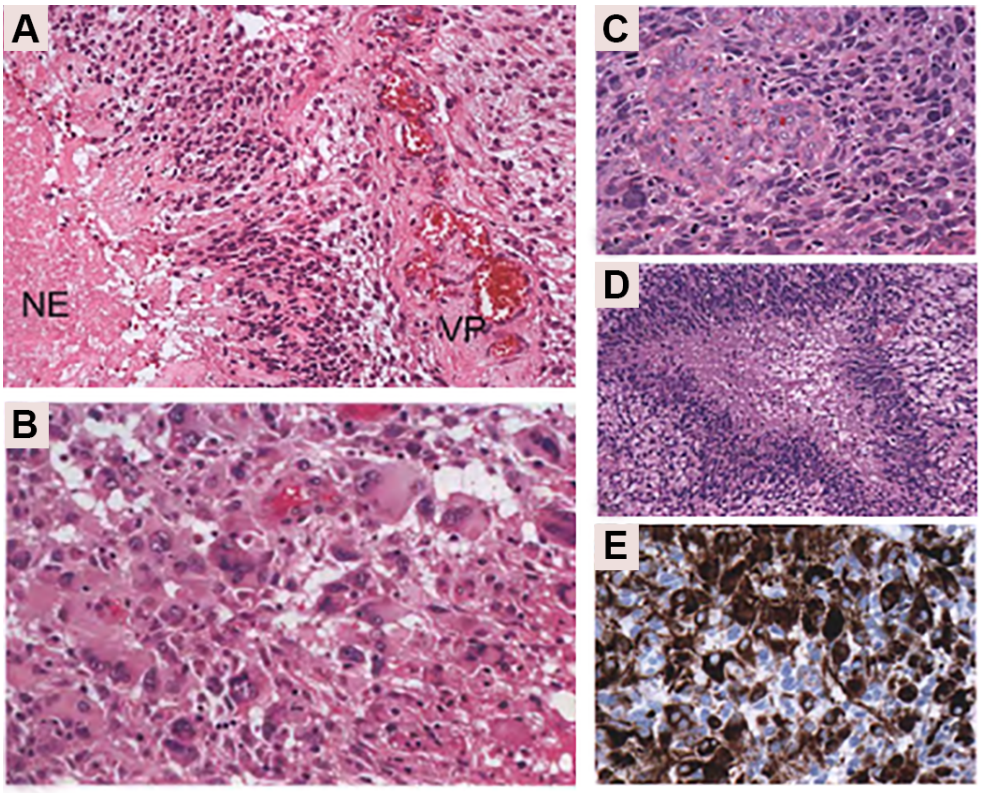

Figure 2. **Hematoxylin/Eosin (HE) and immunohistochemistry (IHC) stainings representative of GBM main histological features**
HE staining representative of (**A**) necrosis (NE) and vascular proliferation (VP); (**B**) giant cells with pleiomorphic nuclei; (**C**) microvascular proliferation and (**D**) palissadic necrosis.
(**E**) IHC staining representative of GFAP+ malignant cells (adapted from Louis et al., 2016).

2.3. Standard of care

Once the GBM diagnosis is confirmed, the neurooncologist starts the standard procedure which corresponds to a multimodal treatment combining radio- and chemotherapy. As GBM are invasive, the complete tumor resection is impossible. In order to remove the remaining malignant cells, surgery is followed by a heavy protocol developed by Stupp and colleagues, consisting of a radiotherapy (60 Gray of ionizing radiations (IR) in 30 fractions on a period of 6 weeks) combined with concomitant treatment of Temozolomide (TMZ) an alkylating agent (75 mg/m² of body surface per day), and followed by an adjuvant chemotherapy of 6 cycles of 28 days, 5 days per cycle (50-200 mg/m² of body surface per day) (Stupp et al., 2005).
Both IR and TMZ aim at inducing DNA damage. On the one hand, IR causes irreversible DNA damage including crosslinks, single and double strand breaks DNA. On the other hand, TMZ exerts a cytotoxic effect by exploiting a weakness of the mismatch repair (MMR) mechanism. It methylates guanine bases on the O^6 position (O^6-meG) to create a mismatch with the complementary base. To remove the alkylated base, the MMR machinery creates a single strand break. The DNA polymerase inserts a thymine which in turn creates another MMR cycle response. These cycles of MMR and single strand DNA breaks trigger a DNA damage response (DDR). IR- and TMZ-induced damages lead to a mitotic catastrophe or mitotic bypass which results in apoptosis or therapy-induced senescence (TIS) respectively (Aasland et al., 2019; Günther et al., 2003; Li, 2008; McFaline-Figueroa et al., 2015) (***Figure 3***).

Mutations in the O^6-methylguanine-DNA methyltransferase (MGMT) gene occur in only 0.5% of GBMs (cbioportal.org; TCGA Cell 2013 and Nature Med. 2019 cohorts). However, approximately half of GBMs display a hypermethylated MGMT promoter; they lack the expression of this enzyme and are more sensitive to TMZ. Indeed, MGMT removes the O^6-meG marks and prevents the action of TMZ (Hegi et al., 2005). A recent multicentric study which included our team, shows that MMR deficiency in GBMs increases the mutational burden upon TMZ treatment. These hypermutated tumors become resistant to TMZ but not to other alkylating agents such as the nitrosourea compound Lomustine (also abbreviated as CCNU) (Touat et al., 2020).

Despite the combined protocol of radiotherapy with TMZ, patients present an overall survival of 14.6 months (compared with 12.1 months with radiotherapy only) (Stupp et al., 2005) (***Figure 3***). Many novel therapies have been tested on patients with GBM including targeted molecular therapies, growth factor inhibitors, angiogenesis inhibitors, immuno- and viral therapies, yet with no significant amelioration of the overall survival of patients (Wen et al., 2020). GBMs are incurable and ultimately relapse. Several hypotheses could explain the

treatment inefficacy including the presence of the BBB which limits the drug delivery to the brain, the high growth rate of the tumor, the invasiveness of the malignant cells, the inter- and intratumoral heterogeneities, the presence of cancer stem cells (CSCs) and the immunosuppressive environment (Castellan et al., 2020; Garofano et al., 2021; Louis et al., 2016; Richards et al., 2021; Wang et al., 2017b). Therefore, a better understanding of these cellular processes becomes critical for developing novel GBM therapeutic strategies (Bhat et al., 2013; Lu et al., 2016; Wang et al., 2017b).

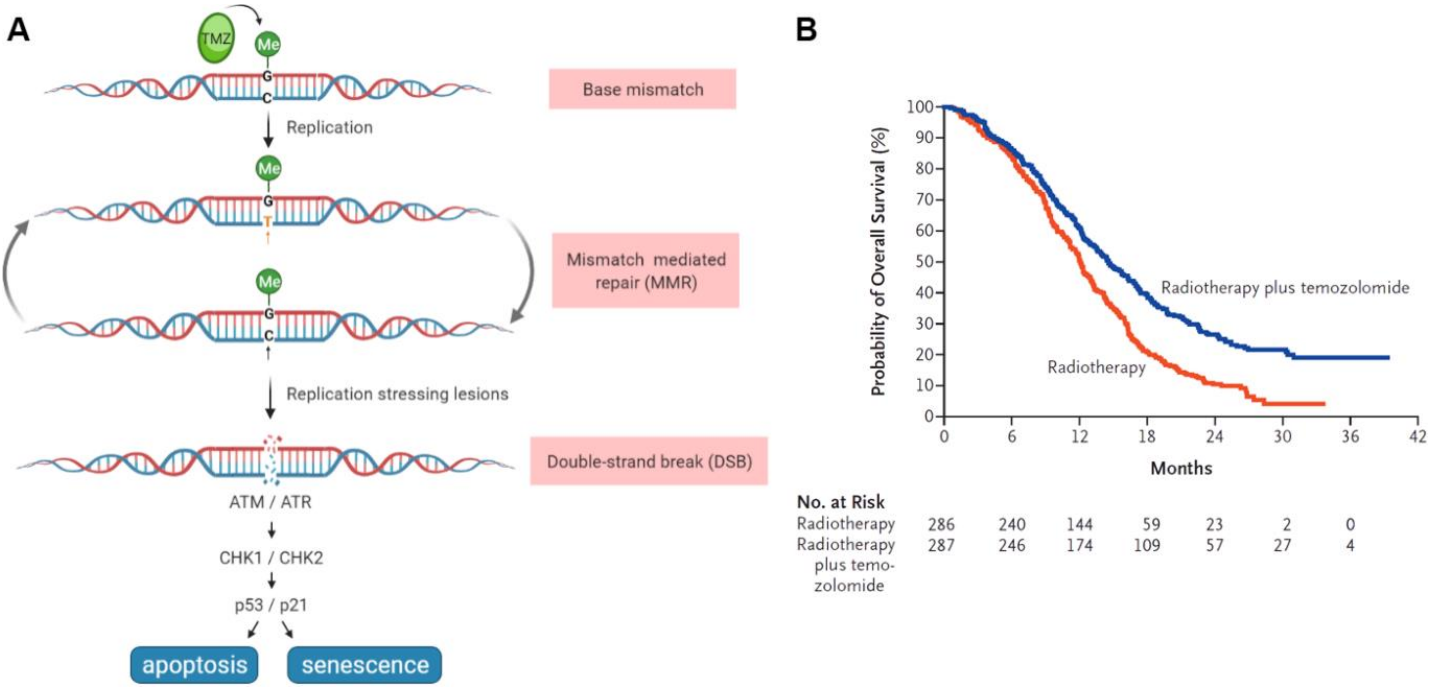

Figure 3. Combined treatment of Temozolomide with radiation increases modestly patient survival
A. Temozolomide (TMZ) mechanism of action triggering either apoptosis or therapy-induced senescence.
B. Kaplan-Meier estimates of overall survival according to treatment group (Stupp protocol in blue vs radiotherapy only in red) (adapted from Stupp et al., 2005).

3. Intertumoral heterogeneity of GBMs

3.1. Main altered genetic pathways

Along with histological analysis, the genetic analysis upgraded the GBM classification which now includes genetic alterations (mainly gene mutations, amplifications, deletions and translocations). GBMs can further be classified into two main groups: primary (*de novo*) and secondary tumors.

Secondary GBMs generally derive from a previous lower grade glioma. Although primary and secondary GBMs are histologically very similar, they can be distinguished based on their isocitrate dehydrogenase (IDH) mutational status. IDH1 and IDH2 enzymes play metabolic functions by converting the α-ketoglutarate to isocitrate. However, the mutation R132H in IDH enzymes results in the formation of the D-2-hydroxyglutarate which functions as an oncometabolite by notably contributing to the genome hypermethylation. Secondary IDH-mutant GBMs represent 10% of all GBMs, they occur more frequently in younger patients and are associated with a better prognosis (Sanson et al., 2009) (***Figure 4***). Conversely, IDH-wild type (IDH-WT) GBMs correspond mostly to primary GBMs and represent 90% of all GBMs. My PhD project focused on IDH-WT GBMs, which I will detail here after.

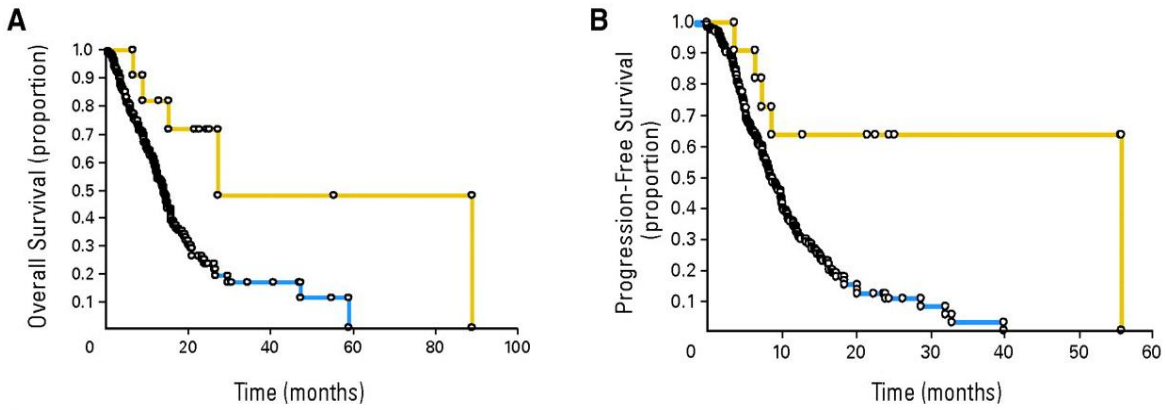

Figure 4. Patients with an IDH-WT GBM present a worst survival
(**A**) Overall survival curves and (**B**) progression-free survival curves in GBM according to IDH1 codon 132 status (yellow line, mutated; blue line, non-mutated).
(adapted from Sanson et al., 2009).

The most frequently altered pathways in GBMs include RTK/RAS/PI3K (receptor tyrosine kinases/rat sarcoma/phosphatidylinositol 3-kinases), $p16^{INK4A}$/RB ($p16^{INK4A}$/retinoblastoma protein) and p53/$p21^{CIP1}$ signaling pathways (***Figure 5***). The p53/$p21^{CIP1}$, as well as the $p16^{INK4A}$/RB pathway, induce a cell cycle arrest which results either in apoptosis or cellular senescence. Furthermore, most common genetic alterations in GBM include loss of heterozygosity of the chromosome 10 where *PTEN* (phosphatase and tensin homologue) is located, loss of chromosome 9 containing *INK4A/ARF* locus, and amplification of chromosome 7 containing *EGFR* (epidermal growth factor receptor) and *FGFR* (fibroblast growth factor receptor). These altered pathways are almost always associated with mutations in the telomerase reverse transcriptase (TERT) promoter and other deletions/amplifications of oncogenes or tumor suppressor genes (McLendon et al., 2008; Verhaak et al., 2010) (***Figure 5***).

RTK/RAS/PI3K pathway

Receptor tyrosine kinases (RTKs) are composed of cell surface receptors of various molecules including growth factors, hormones, and cytokines. When ligand binds to the RTK, Ras/MAPK (rat sarcoma/mitogen-activated protein kinases) and Ras/PI3K/AKT (rat sarcoma/phosphatidylinositol 3-kinases/Akt) downstream pathways are activated and further regulate multiple cellular processes such as proliferation, differentiation, survival or angiogenesis. RTK/RAS/PI3K pathway is altered either by the RTKs or by the downstream signaling components. The main altered RTKs in GBMs include EGFR, FGFR, and PDGFR (platelet-derived growth factor receptor) (Louis et al., 2016; McLendon et al., 2008).
For instance, EGFR is amplified in more than 50% of GBMs. EGFR can also be mutated into an EGFRvIII variant that constitutively stimulates tumor growth (Knobbe and Reifenberger, 2003; Reni et al., 2017; Wikstrand et al., 1997). In addition, PDGFRα is the second most frequently amplified RTK in GBM after EGFR, and is involved in similar cellular processes.

The PI3K/AKT/mTOR (phosphatidylinositol 3-kinases/Akt/mammalian target of rapamycin) pathway regulates cell cycle through a cascade of phosphorylation involving AKT and mTOR activation. For instance, the tumor suppressor PTEN antagonizes PI3K and prevents AKT activation. Loss of *PTEN* function, either upon mutation or deletion, is associated with tumor progression and a shorter survival (Srividya et al., 2011; Wang et al., 1997; Yang et al., 2010). Although Ras mutations are rare in GBMs, *NF1* (neurofibromatosis factor 1), a tumor suppressor inhibiting the Ras pathway, can be mutated or deleted which in turn activates the Ras pathway and promotes tumor growth (Jeong and Yee, 2014; McLendon et al., 2008; Verhaak et al., 2010). Overall 86% of GBMs harbor at least one genetic alteration in the RTK/RAS/PI3K pathway (McLendon et al., 2008) (***Figure 5***).

p53/p21^{CIP1} pathway

The tumor suppressor p53 inhibits the cell cycle but also regulates various non-canonical functions, including cellular metabolism, autophagy, angiogenesis and ferroptosis (Kruiswijk et al., 2015). Importantly, high levels of p53 and downstream signaling trigger apoptosis while low levels trigger cellular senescence (Campisi and D'Adda Di Fagagna, 2007; Chen et al., 2000; Childs et al., 2014). Oncogenic stress and DNA damage response (DDR) can directly induce p53 and p19^{ARF} expression and repress MDM2 (murine double minute 2). p19^{ARF} activates p53 expression while MDM2, an E3 ubiquitin ligase, targets p19^{ARF} and p53 degradation. Once p53 protein is expressed and stabilized, it promotes the transcription of the cyclin-dependent kinase inhibitor p21^{CIP1}. In turn, p21^{CIP1} can trigger two downstream processes. On the one hand, it activates the transcription of pro-apoptotic genes leading to

apoptosis. On the other hand, it inhibits the binding of CDK2/CDK4 (cyclin dependent kinase 2/ cyclin dependent kinase 4) to cyclins which phosphorylates RB (retinoblastoma) protein. Therefore, RB remains in a hypo-phosphorylated state and prevents the release of E2F transcription factors necessary for cell-cycle-progress gene activation. This in turn leads to a growth arrest in the G1/S phase (Rowland et al., 2002). The p53 pathway is the most frequently altered in GBM via mutations in TP53 and RB coding sequences, as well as ARF deletions and amplifications of MDM2 (McLendon et al., 2008) (***Figure 5***).

p16^{INK4A}/RB pathway

p16^{INK4A} is encoded by the *INK4A/ARF* locus which encompasses three cyclin-dependent kinase inhibitors, namely: *CDKN2A* gene coding for p16^{INK4A}, *CDKN2B* gene coding for p15^{INK4B} and *ARF* coding for p14^{ARF} (p19^{Arf} in mice), all being senescent mediators. Importantly, p16^{INK4A} and p15^{INK4B} are inhibitors of the CDK4/6-cyclins complex binding which in turn prevent RB phosphorylation and cell cycle progression (Narita et al., 2003) (***Figure 5***). In physiological conditions, the *INK4A/ARF* locus is epigenetically silenced by the Polycomb repressive complexes 1 and 2 (PRC1, 2). PRC1 and PRC2 deposit repressive marks on chromatin histones to inhibit downstream transcription. However, these histones marks may be lost upon disruption of PRC1 and 2 subcomponents (e.g., CBX7, BMI1, EZH2) which activates the expression of *CDKN2A* and induces senescence entry (Bracken et al., 2007; Gil et al., 2004; Jacobs et al., 1999). In GBM, the most common genetic events are deletion of the *CDKN2A/CDKN2B* locus on chromosome 9, followed by amplification of the *CDK4* locus in 14% of GBMs (McLendon et al., 2008) (***Figure 5***). Of note, *TP53/MDM2* mutations and *INK4A/ARF* locus alterations generally occur in a mutually exclusive way (Fulci et al., 2000).

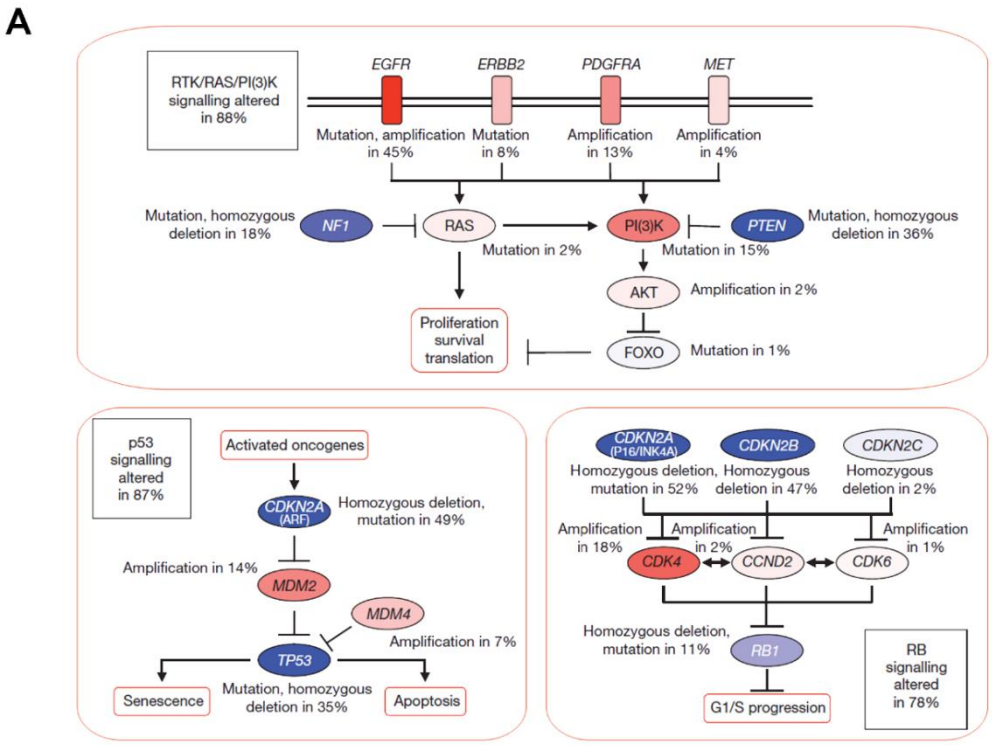

(legend on next page)

Figure 5. **Frequent genetic alterations in the three critical signaling pathways in GBM**
A. Red and blue indicates activating and inactivating genetic alterations respectively in RTK/RAS/PI3K, p53/p21^{CIP1} and p16^{INK4A}/RB pathways (adapted from McLendon et al., 2008).
B. cBioportal analysis showing distinct main genetic alterations in 585 GBMs from two cohorts (TCGA Cell 2013 and Nature Med. 2019) (generated from https://www.cbioportal.org/).

3.2. Transcriptional classification

Classification based on the genetic alterations

To better understand the molecular mechanisms of primary GBMs and better predict patient outcome, Verhaak and colleagues further classified GBMs based on genetic alterations. In 2010, initial analysis of bulk RNAseq of GBMs from The Cancer Genome Atlas (TCGA) revealed four molecular subtypes: classical, proneural, mesenchymal (GBM-CL, GBM-PN, GBM-MES) and neural. The neural subtype was later identified as a contamination from non-malignant tissue (Verhaak et al., 2010; Wang et al., 2017b) (***Table 1***). The GBM-CL and GBM-PN subtypes are associated with neurodevelopmental programs while the GBM-MES is

associated with injury response programs (Richards et al., 2021; Verhaak et al., 2010; Wang et al., 2017b). Interestingly, distinct subtypes can coexist in different locations of the same tumor (Patel et al., 2014; Wang et al., 2017b).

GBM-CL displays an amplification of chromosome 7, a loss of chromosome 10, and a focal loss of 9p21.3 locus targeting *CDKN2A*, but lacks *TP53* mutations. In addition, GBM-CL overexpresses neural precursor and stem cell marker NES, as well as Notch and Sonic hedgehog signaling pathways.

GBM-PN presents *PDGFRA* alteration, point mutations in *IDH1* gene (in secondary GBMs), a reduced *CDKN1A* expression (encoding $p21^{CIP1}$), and frequent *TP53* mutations. GBM-PN expresses oligodendrocytic and proneural developmental genes such as *PDGFRA*, *OLIG2, NKX2-2*, *DCX*, *ASCL1, TCF4* and *SOX* genes. Interestingly, loss of OLIG2 in a mouse model of GBM leads to a shift from the GBM-PN to the GBM-CL subtype and was sufficient to promote radiosensitivity of patient GBM cell lines (Lu et al., 2016; Mehta et al., 2011). Of note, GBM-PN is overall associated with a better prognosis.

GBM-MES is characterized by mutations/deletions in the *NF1* region, which is frequently co-mutated with *PTEN*. GBM-MES expresses *CHI3L1* and *MET* mesenchymal markers. In addition, GBM-MES presents increased expression of genes in the NF-κB and TNF (tumor necrosis factor) signaling pathways (Verhaak et al., 2010; Wang et al., 2017b). Importantly, this subtype correlates with a worst survival and GBMs frequently shift from the GBM-PN to the GBM-MES subtype upon recurrence (Patel et al., 2014; Wang et al., 2017b).

Classification based on the methylation status

Sturm and colleagues analyzed adult, pediatric and young adult cohorts and further classified GBMs into six epigenetic subgroups: “IDH”, “G34”, “K27”, “mesenchymal”, RTK I “PDGFRA” and RTK II “Classic”.

The IDH (with IDH1/2 mutations) subgroup is enriched in young adult GBMs and associates with GBM-PN displaying a glioma-CpG island methylator phenotype (G-CIMP). G-CIMP+ tumors present overall hypermethylated regions which confers a less aggressive phenotype and correlates with a more favorable prognosis to patients (Noushmehr et al., 2010; de Souza et al., 2018). In contrast, the RTK I “PDGFRA” subgroup (with PDGFRA amplifications) is enriched in G-CIMP- GBM-PN and present a lower prognosis.

The mesenchymal and RTK II "Classic" correlate with the GBM-MES and GBM-CL subtypes. Noteworthy, the last two subgroups, K27 and G34 (with K27M and G34R/V mutations in *H3F3A* histone H3.3 coding sequence) are enriched in pediatric and adolescent GBM respectively. Although K27 GBMs were associated with G-CIMP+ proneural subtype, G34 GBMs was not associated with a particular GBM transcriptional subtype (Sturm et al., 2012) (***Table 1***).

Verhaak subtypes / Subgroup classification	**GBM-PN**			**GBM-MES**	**GBM-CL**	**N/A**
Noushmehr *et al.*	G-CIMP -	G-CIMP +		G-CIMP -	G-CIMP -	G-CIMP +
Sturm *et al.*	RTK I "PDGFRA"	IDH	K27	Mesenchymal	RTK II "Classic"	G34
Neftel *et al.*	OPC-like and NPC-like states			MES-like state	AC-like state	N/A
Main alterations	PDGFRA amplif. p53 mut. CDKN1A downreg.	IDH mut. p53 mut.	H3F3A K27 mut. p53 mut.	PTEN loss NF1 loss p53 mut.	Ampli of chrom 7 Loss of chrom 10 CDKN2A del. EGFR ampli	H3F3A G34 mut. p53 mut. Hypomethylated

Table 1. Table recapitulating the different classifications of GBMs based on the transcriptional subtype classification of Wang et al., 2017
Amplif: amplification, mut: mutation, downreg: downregulation.

4. Intratumoral heterogeneity of GBMs

The advances of single cell transcriptomics largely contributed to demonstrate the different degrees of transcriptional and cellular heterogeneities among the malignant cells, within a single GBM. In addition, these studies revealed the plasticity of malignant cells which can be defined by their cellular states and the diversity of glioma stem cells (GSCs) (Bhaduri et al., 2020; Couturier et al., 2020; Richards et al., 2021; Wang et al., 2019b).

4.1. Cellular states

In 2019, Neftel and colleagues classified the intratumoral heterogeneity of malignant cells and subdivided them into four main cellular plastic states: oligodendrocyte-precursor-cell-like (OPC-like), neural-precursor-cell-like (NPC-like), astrocyte-like (AC-like) and mesenchymal-like (MES-like) states. One given cellular state is defined by the relative score of a meta-module

(a network of genes enriched in a recurrent expression program) and bears different proliferative potentials, the OPC-like and NPC-like states being the most proliferative ones. Malignant cells can display intermediate hybrid states and the proportion of these cellular states within the tumor defines the tumor transcriptional subtype. Indeed, GBM-PN are enriched in OPC-like and NPC-like states whereas GBM-CL and GBM-MES are enriched in AC-like and MES-like states respectively (Neftel et al., 2019) (***Figure 6***).

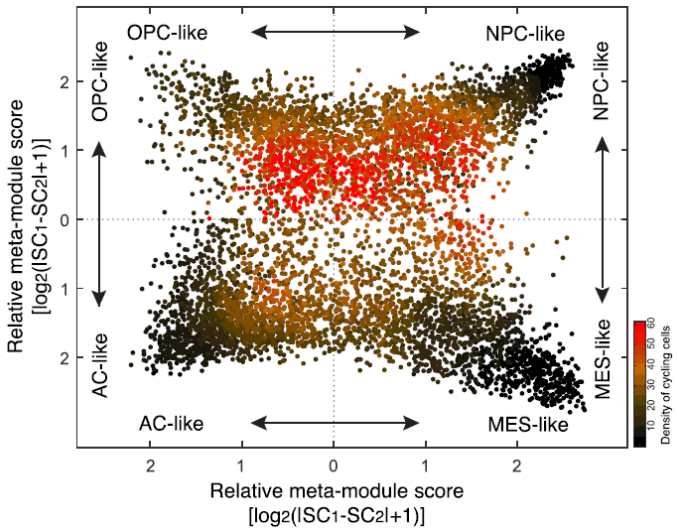

Figure 6. **Two-dimensional representation of cellular states of malignant cells as defined by Neftel et al., 2019**
Each quadrant corresponds to one cellular state, the exact position of malignant cells (dots) reflects their relative scores for the meta-modules (AC-like, OPC-like, NPC-like, MES-like), and their colors reflect the density of cycling cells (from Neftel et al., 2019).
AC: astrocyte; OPC: oligodendrocyte precursor cell; NPC: neural progenitor cell; MES: mesenchymal.

4.2. Glioma stem cells

Glioma stem cells (GSCs) correspond to a subpopulation of malignant cells. They present features of stem cells from healthy tissue such as the ability to self-renew and to give rise to some or all the cells of the tissue they reside in (Lathia et al., 2015). Stemness programs of GSCs are diverse and are characterized by heterogenous marker gene combinations. Multiple GSC subtypes, identified by scRNAseq, can reside within a single tumor and promote tumor invasion via their secreted factors (e.g., periostin (POSTN)) (Bhaduri et al., 2020). The heterogeneity of GSCs between patients participates in the intertumoral heterogeneity (Richards et al., 2021). To date, no universal marker has been discovered to identify them, rather a combination of markers is required (e.g., CD133, CD44, A2B5, SSEA1) (Suvà and Tirosh, 2020). Castellan and colleagues identified a glioma stem cell (G-STEM) signature

reflecting the stemness property, and is differentially expressed in GSCs compared with differentiated GBM cells. Moreover, they found YAP/TAZ as master transcriptional regulators of the GSC state, which was further validated in an inducible YAP/TAZ knock out mouse model (Castellan et al., 2020). Noteworthy, GSCs are resistant to radio- and chemotherapy and contributes to the GBM adaptive response to treatments (Bao et al., 2006; Chen et al., 2012). Several characteristics can explain therapy resistance, including GSC metabolism, the influence of the microenvironment on GSC and GSC heterogeneity. I will focus here on the last two features.

GSC heterogeneity

Recent single cell transcriptomics studies combined with TCGA bulk analysis, further described the diversity and plasticity of GSCs (Castellan et al., 2020; Garofano et al., 2021; Richards et al., 2021). Richards and colleagues identified a metabolism gradient, from "developmental" to "injury response" states, along which GSCs can range from one state to the other. GSCs from the developmental state were grouped into a core GSC proliferation module, in agreement with what was previously described by Neftel and colleagues where OPC-like, NPC-like and AC-like states are associated with a reminiscent neurodevelopmental program. Similarly, injury response state GSCs express genes within the MES-like signature (including NF-κB, STAT signaling, reactive astrocytes and inflammatory wound response genes) (Neftel et al., 2019; Richards et al., 2021). However, the GSC state of the engrafted cell lines does not correlate with the survival of the orthotopic xenograft mice suggesting that GBM aggressiveness may be independent of the GSC state (Richards et al., 2021).
Another study performed by Garofano and colleagues identified four cellular states scores of activated pathways which are involved either in the metabolism (mitochondrial vs glycolytic/plurimetabolic) or the developmental program (neuronal vs proliferative/progenitor) and emphasizes the importance of GBM cells states on therapy response (Garofano et al., 2021). Overall, GSCs are now considered as a gradient of different states which include stemness, metabolism and cellular specialization (Castellan et al., 2020; Garofano et al., 2021; Richards et al., 2021) (***Figure 7***).

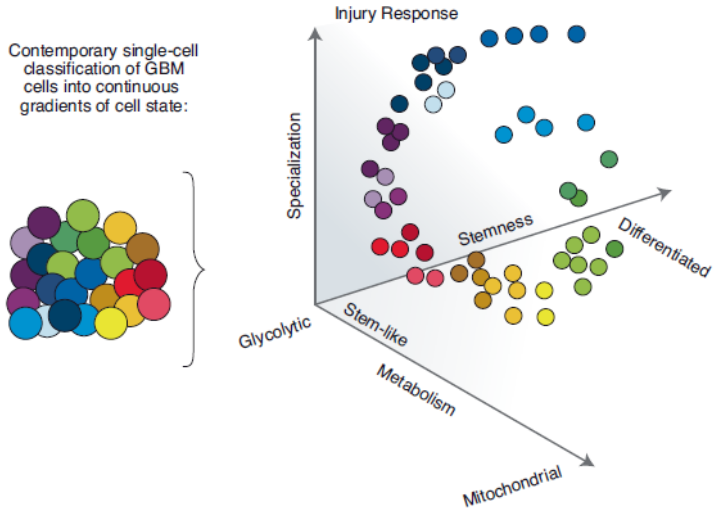

Figure 7. **Continuous gradients of cell state define GBM cellular heterogeneity**
Transcriptional profiles of single GBM cells can be distributed along continuous axes based on a cellular property such as stemness (Richards et al., 2021; Castellan et al., 2020), metabolism (Garofano et al., 2021) or cellular specialization (Richards et al., 2021). (from Lathia et al., 2021)

Influence of the microenvironment on GSC

The microenvironment of GSCs plays a major role in therapy resistance. Indeed, GSCs are enriched in vascular niches where they are in close contact with malignant cells and necrotic areas (***Figure 8***). Necrosis generates a hypoxic environment which increases the expression of molecules such as the hypoxia-inducible factor 1 (HIF-1). HIF-1 is a key regulator of cell responses to hypoxia and angiogenesis. It activates the expression of pro-angiogenic factors including VEGF, VEGFR, PDGFR and TGF-β and in turn promotes tumor vascularization (Lathia et al., 2015). Angiogenesis corresponds to the formation of *de novo* blood vessels by endothelial cells. Blood vessels provide oxygen and nutrients to the tumor, and contributes to the overall progression and invasion of GBM (Guarnaccia et al., 2018). Notably, GSCs and their perivascular niches establish a cross-talk whereby endothelial cells support GSCs survival and stemness while GSCs secrete vesicles with pro-angiogenic factors (e.g., VEGF-A) in an mTOR-dependent manner to target endothelial cells (***Figure 8***) (Calabrese et al., 2007; Galan-Moya et al., 2011; Treps et al., 2017). Using *in vitro* functional study and lineage tracing in a mouse model of GBM, a study showed that GSCs can transdifferentiate into CD31+ vascular endothelial cells to ensure their own vascularization which can contribute to GBM invasion and therapy resistance (Soda et al., 2011).

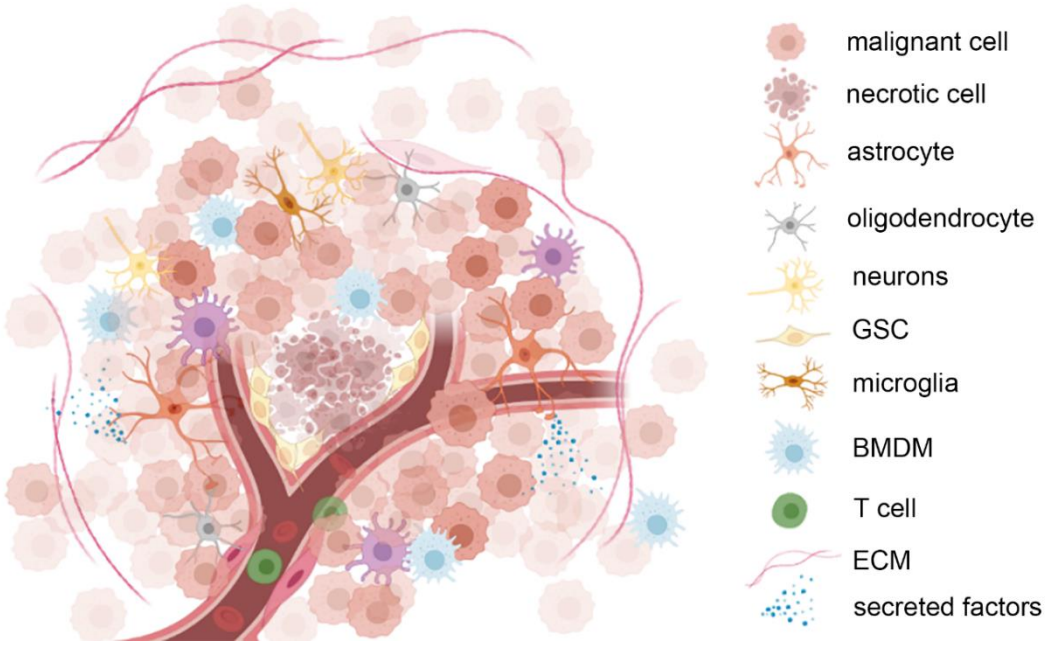

Figure 8. **GBM perivascular niche and tumor microenvironment**
The tumor microenvironment is heterogenous and comprises various non-malignant cells. Necrotic area results in hypoxia which participates in the formation of the GSC perivascular niche. GBMs are hypervascularized tumors. Although neoangiogenic vessels are poorly formed, endothelial cells establish a crosstalk with GSCs and support their stemness. Infiltrative immune cells comprise tumor-associated macrophages (microglia and BMDM) and lymphoid cells (T cells among others). Malignant and non-malignant cells secrete factors and ECM which modulate the tumor survival, growth, angiogenesis, immunosuppression and malignant cell invasion.
GSC: glioma stem cell; BMDM: bone marrow-derived macrophages; ECM: extracellular matrix

5. The tumor microenvironment

The tumor microenvironment (TME) is composed of various non-malignant cells and non-cellular components including immune cells, astrocytes, neurons, endothelial cells and the extracellular matrix. Importantly, the GBM-MES subtype is characterized by a highly necrotic and hypoxic environment which can induce angiogenesis and immune cell recruitment (Bhat et al., 2013; Lu et al., 2016; Wang et al., 2017b). The TME plays a pivotal role in tumor growth, dissemination and therapy resistance. A better understanding of GBM microenvironment becomes critical to develop novel treatments (Neftel et al., 2019; Richards et al., 2021; Wang et al., 2017b). Here, I will focus on two of aspects of the TME: the immune compartment and the extracellular matrix.

5.1. Immune compartment

From bulk RNAseq analysis to single-cell transcriptomics analysis, the mesenchymal subtype is shown to be associated with increased epithelial-to-mesenchymal transition, migration, hypoxia and immune infiltration (Castellan et al., 2020; Garofano et al., 2021; Neftel et al., 2019; Richards et al., 2021; Verhaak et al., 2010; Wang et al., 2017b). Along with a hypoxic environment, loss of *NF1* (one of the main GBM-MES alterations) also correlates with the recruitment of immune cells to the tumor site (Gangoso et al., 2021; Verhaak et al., 2010; Wang et al., 2017b). Accordingly, the GBM-MES subtype displays the highest percentage of tumor-associated macrophages (TAM) and lymphocyte infiltration compared with the other subtypes (Wang et al., 2017b). Several studies suggest that the infiltration of TAMs promote the establishment of a GBM-MES subtype via anti-inflammatory, pro-angiogenic and extracellular matrix remodeling factors and is involved in tumor growth, survival and invasion (Doucette et al., 2013; Wang et al., 2017b; Zanotto-Filho et al., 2017).

Moreover, the immune populations of the GBM-MES subtype are heterogeneous. IHC staining and deconvoluted analysis from bulk RNAseq data (CIBERSORT) reveals enrichment in neutrophils, TAM and distinct T cell populations such as cytotoxic CD8 T cells, natural killer (NK) cells, CD4 T cells, and regulatory T (T reg) cells (Kaffes et al., 2019; Wang et al., 2017b). These cells are of two types, resident and infiltrating cells. Microglia cells are the brain-resident macrophages while the peripheral immune cells are composed of dendritic cells, T cells and bone marrow-derived macrophages (BMDM) (Bowman et al., 2016; Quail and Joyce, 2017). The TAMs (microglia and BMDM) contribute to tumor growth, survival, and invasion (Zhang et al., 2020). They have been traditionally categorized into two polarization states according to their secreted factors, namely the M1 and the M2 states. The M1-like TAMs are characterized by the expression of a pro-inflammatory and anti-tumoral program with the secretion of cytokines such as TNF-α, IL1-β and CXCL10. In contrast, the M2-like TAMs are considered as anti-inflammatory/pro-angiogenic as they display a program composed of anti-inflammatory molecules (e.g., TGFβ1, CXCL2, IL10, MIF), pro-angiogenic factors (e.g., HIF1α, VEGFA/B) and secrete tissue remodeling factors (e.g., ADAM8, TIMP1/2, MMP2) (Darmanis et al., 2017; Hambardzumyan et al., 2015). Of note, the pro-inflammatory TAM state is enriched in microglia and is mostly present in the periphery of the tumor, in contrast to the anti-inflammatory state enriched in BMDM and preferentially located in the tumor core (Darmanis et al., 2017). Interestingly, the M2 anti-inflammatory gene signature is associated with the GBM-MES subtype and blocking macrophage polarization into the M2 state, by CSF-1R inhibition, improves GBM-bearing mouse survival (Pyonteck et al., 2013; Wang et al., 2017b).

Several studies demonstrated that macrophage polarization is complex and is better represented by a spectrum of overlapping M1 and M2 in gene expressions (Quail and Joyce, 2017). Importantly, one pan-cancer study clustered intratumoral immune states into six groups (C1-C6) based on immune signature gene sets. Gliomas exhibit “lymphocyte depleted” (C4) and “immunologically quiet” (C5) immune subtypes associated with high macrophages and low lymphocytes scores (Thorsson et al., 2018). In addition, TAMs in GBM lack expression of co-stimulating T cell molecules (including CD40, CD80, and CD86). Thus, the induction of T cell responses by TAMs is impaired which partly contributes to T cell exhaustion, and the immunosuppressive microenvironment (Hussain et al., 2006; Otvos et al., 2016). Myeloid-derived suppressor cells (MDSC) also suppress T cell activity and are associated with a bad prognosis (Alban et al., 2018; Dubinski et al., 2016; Gielen et al., 2016; Kamran et al., 2017). In summary, GBMs are termed “cold” tumors due to the immunosuppressed microenvironment and the rare infiltrating effector T cells (Duan et al., 2020; Quail and Joyce, 2017). These GBMs properties could explain the absence of increased overall survival after immune checkpoint blockade treatments in patients with recurrent GBMs (Litak et al., 2019).

5.2. Extracellular matrix

The extracellular matrix (ECM) is a network of macromolecules that supports cells in a tissue and regulates intercellular communications (Brösicke and Faissner, 2015). In GBM, the ECM is stiffer than in physiological brain tissue and is mainly composed of proteoglycans, glycosaminoglycans and glycoproteins. Interestingly, increased ECM concentration and stiffness is associated with the presence of vascular and tumor stem cell niches. For instance, the expression of Tenascin-C (TNC), a glycoprotein, is correlated with cell motility and tumor invasion (Yoshida et al., 2015). TNC is found in higher concentration around blood vessels, along with other factors (e.g., IGFBP7 and SPARC). It plays a key role in angiogenesis notably by modulating the activity of pro-angiogenic factors (e.g., VEGF) (Brösicke et al., 2013; Rupp et al., 2016). ECM stiffness also regulates cell motility, proliferation and immunosuppression. Indeed, T cell can be “trapped” in ECM to block their migration to the tumor site and inhibit their activity (Huang et al., 2010). Importantly, TNC regulates cell plasticity in a mouse GBM-MES model by promoting the expression of the mesenchymal marker NF-κB (Angel et al., 2020).

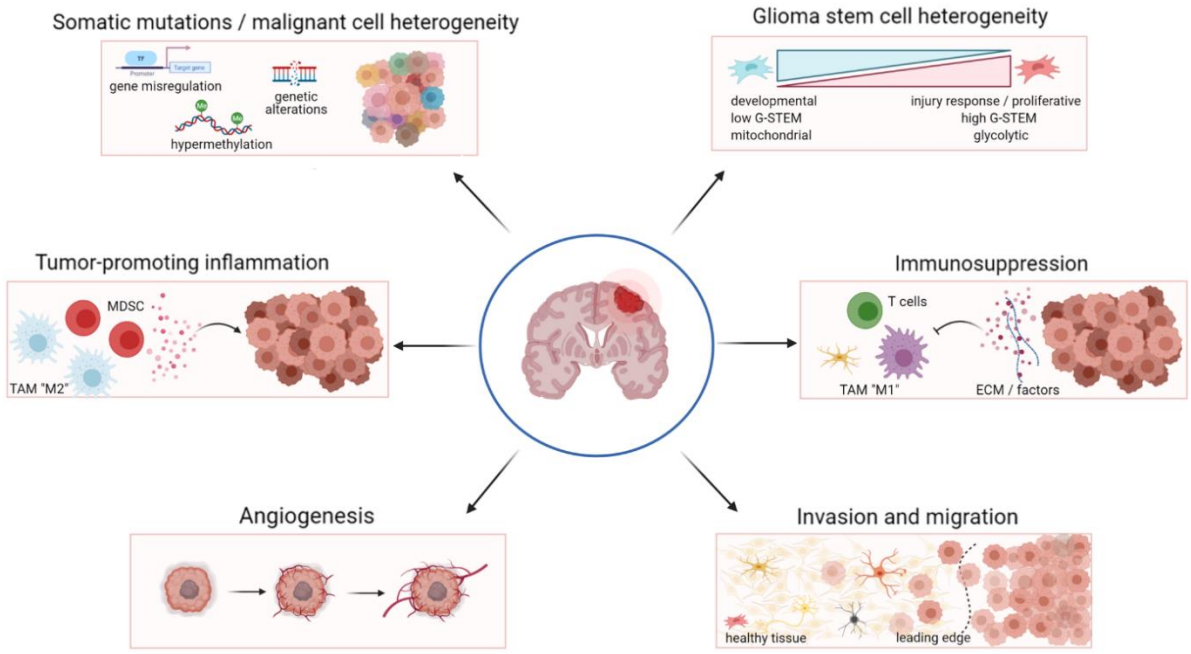

Figure 9. The main GBM characteristics challenging the efficacy of current therapies
(adapted from Roberts and Munson, 2020)

As a conclusion to this introductory part on GBM, one can state that despite the growing molecular and cellular knowledge on GBM (***Figure 9***), the clinical transposition to find novel therapeutic breakthroughs remains difficult. Various studies unveiled the possibility of exploiting cellular senescence to limit tumorigenesis. This hypothesis was the focus of my PhD work and the state of art of senescence in cancer will be the subject of the next chapter.

II. Cellular senescence: a novel actionable target for GBM?

1. Senescent cells: a crossroad for multiple processes

Cellular senescence is a mechanism characterized by a permanent cell cycle arrest and the secretion of a plethora of molecules called the senescence-associated secretory phenotype (SASP) (Childs et al., 2015). Leonard Hayflick and Paul Moorhead first described senescence in 1961 when they observed *in vitro* human fibroblasts with a finite number of population doublings. This phenomenon is now known as replicative senescence, and the authors had hypothesized at the time that it could play a role during organismal aging (Hayflick, 1965). Since then, numerous studies showed that senescence is induced in multiple physiological processes and age-related pathologies including cancer.

Senescence is a multistep process triggered by various stresses such as telomere shortening, oxidative stress, oncogenes, mitochondrial dysfunction or conventional anticancer therapies, including radio- and chemotherapy (Childs et al., 2015; Gorgoulis et al., 2019). In contrast to quiescent cells, senescent cells display a generally irreversible cycle arrest, macromolecule damages, and a deregulated metabolism (Gorgoulis et al., 2019). Nevertheless in certain conditions, cells can escape from senescence (Milanovic et al., 2018). Cellular senescence is mediated by the DNA damage response (DDR), the p53/p21^{CIP1} or p16^{INK4A}/RB signaling pathways. Importantly, senescent cells develop a SASP program which can either promote their own immune clearance or contribute to a persistent inflammation (Childs et al., 2015).
The roles of senescence are context-dependent. They can be considered as an example of an evolutionary antagonistic balance between the beneficial developmental/anti-tumoral mechanisms, and the detrimental roles in inflammation during aging (or “inflammaging”) /cancer progression (Franceschi and Campisi, 2014).

Programmed senescence regulates embryonic development and tissue patterning (Gal et al., 2020; Muñoz-Espín et al., 2013; Storer et al., 2013). Furthermore, cellular senescence is essential for tissue homeostasis and tissue remodeling processes including wound healing, regeneration and tissue plasticity (Chiche et al., 2017; Demaria et al., 2014; Hiebert et al., 2018; Mosteiro et al., 2016; Ritschka et al., 2017; Le Roux et al., 2015). However, when senescence becomes chronic during aging and in immunodeficient contexts, it can contribute to several age-related diseases including neurodegenerative diseases such as Alzheimer’s and Parkinson’s diseases (Bhat et al., 2012; Bussian et al., 2018; Chinta et al., 2018; Zhang et al., 2019), obesity (Ogrodnik et al., 2019; Yoshimoto et al., 2013), type 2 diabetes (Sone and Kagawa, 2005; Thompson et al., 2019), atherosclerosis (Childs et al., 2016), osteoarthritis (Jeon et al., 2017; Lee et al., 2021), and osteoporosis (Farr et al., 2017) among others.

In cancer, oncogene-induced senescence (OIS) was first described as a protective barrier against neoplastic progression, in addition to apoptosis (Collado et al., 2007; Michaloglou et al., 2005). Of note, senescent cells generally express an anti-apoptotic program (Childs et al., 2014; Yosef et al., 2016). Furthermore, senescent cells are heterogenous. They can be malignant or non-malignant cells and they can act as tumor suppressor or tumor activator depending on the tumor type and its immune status. Great efforts have been made to develop therapies using senescence as an actionable target to treat cancer. In this section, I will describe the senescence hallmarks, the mechanisms of action of senescent cells in cancer and the current state of the art in the growing domain of senotherapies.

2. Senescence hallmarks

One of the main challenges in the field of senescence is to discriminate cells temporarily entering a cell cycle arrest (such as quiescent G0-phase) from senescent cells. *In vitro* senescent cells display enlarged morphology and irregular shape (Robbins et al., 1970). However, these changes are readily difficult to detect *in vivo*. Senescent cells are heterogenous and to date there is no unique universal senescent marker. Rather, these cells are characterized by a combination of presence or absence of markers based on the senescence hallmarks (Gorgoulis et al., 2019; Kohli et al., 2021).

2.1. Activation of tumor suppressor signaling pathways

The activation of three main pathways, namely the DDR, the p53/p21^{CIP1} and p16^{INK4A}/RB pathways can induce the cell cycle arrest at G1/S stage, the first step of senescence entry (***Figure 10***). These pathways can be activated upon several inducers, including the shortening of telomeres, oxidative stress upon increased reactive oxygen species (ROS) levels, genomic damage (such as oncogenic Ras, loss of *Pten*, *Nf1* and *Rb1*) or conventional therapies. They can trigger double strand breaks (DSBs) which are repaired either by homologous recombination (HR) or less accurately by non-homologous end joining (NHEJ) (Essers et al., 2000; Di Micco et al., 2021). When HR or NHEJ are no longer efficient to repair DSB, prolonged DDR is activated. ATM/ATR protein kinases are recruited to the DSBs, phosphorylate H2AX (γH2AX) histones and facilitate the assembly of nuclear foci composed of γH2AX and p53-binding protein 1 (53BP1). The signal is then transduced to downstream kinases (CHK1 and CHK2) which in turn activate the p53/p19^{ARF} pathway and lead to cellular senescence entry (***Figure 10***). Antibodies against γH2AX, 53BP1, p53, p19^{ARF} and p21^{CIP1} are commonly used to label senescent cells (Burma et al., 2001; Fumagalli et al., 2014).

Other proteins mediating growth arrest can be used to identify senescent cells, such as the cell cycle inhibitors $p27^{KIP1}$ and the ones encoded by the *INK4A* locus ($p16^{INK4A}$, $p15^{INK4B}$, $p19^{ARF}$). However, the use of these markers can encounter some challenges. Indeed, the antibodies against the murine $p16^{INK4A}$ lack specificity and these proteins are not exclusively expressed in senescent cells. For instance, $p16^{INK4A}$ can be expressed in non-senescent macrophages and RB-deficient cancer cells (Hall et al., 2017; Shapiro et al., 1995). Furthermore, $p21^{CIP1}$ is required for the differentiation program of oligodendrocytes (Zezula et al., 2001). To solve this issue, these markers are combined with the absence of proliferation markers such as Ki67 expression or EdU incorporation (Collado et al., 2005; Fumagalli et al., 2014; Kohli et al., 2021). In addition, the expression of reporter genes under the regulatory sequences of *p16*^{Ink4a} are used in mouse transgenic models to track *in vivo* $p16^{Ink4a}$ senescent cells (Demaria et al., 2014; Grosse et al., 2020; Ohtani et al., 2010).

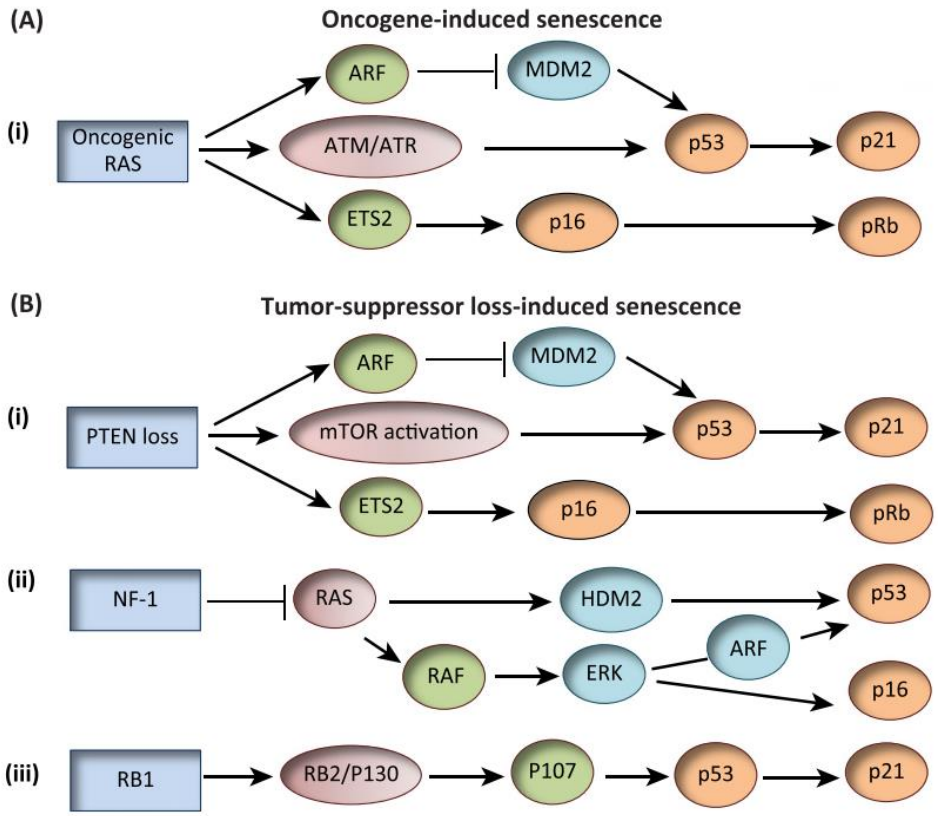

Figure 10. Main cellular senescence signaling pathways in cancer
Cellular senescence can be induced by multiple genetic alteration including (**A**) the overexpression of oncogenes (e.g., *Ras*) or (**B**) the inactivation of tumor suppressor genes (e.g., *Pten*, *Nf1* and *Rb1*) (adapted from Di Mitri et al., 2016).

2.2. Alteration of senescent cell compartments

Besides the cell cycle arrest, senescent cells undergo changes in different cellular compartments which induce mitochondrial dysfunction, altered lipid metabolism, increase in lysosomal content, disruption of the nuclear envelop and change in the chromatin structure (***Figure 11***) (Cho and Hwang, 2012; Freund et al., 2012; Wiley and Campisi, 2016; Yamada et al., 2012).

In 1995, Dimri and collaborators made use of the increased lysosomal compartment to develop a staining for senescent cells. The activity of the β-galactosidase enzyme, a lysosomal enzyme, is readily detectable in suboptimal acidic condition (pH 5.5-6.0) with the X-gal substrate, which becomes blue once cleaved by the enzyme (Dimri et al., 1995) (***Figure 11***). This senescence-associated β-galactosidase (SA-β-gal) histochemical staining is now used as a "gold-standard" hallmark of senescent cells. Noteworthy, this staining can also be detected in non-senescent cells including macrophages or hippocampal pyramidal cells (Geng et al., 2010; Hall et al., 2017).

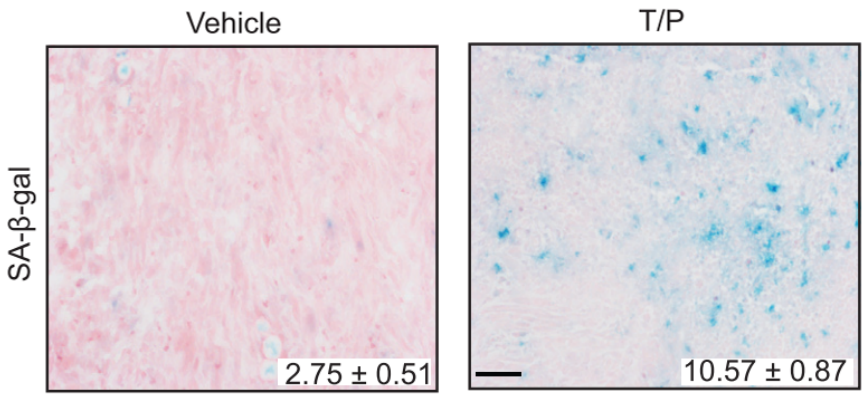

Figure 11. Example of SA-β-gal staining of TIS cells in pancreatic tumor mouse tissue
Numerical values correspond to the SA-β-gal positive area quantification.
T/P: trametinib/palbociclib (adapted from Ruscetti et al., 2020).

Loss of LAMIN B1, a structural protein of the nuclear envelop, occurs upon senescence entry in a $p16^{INK4A}$- and p53-dependent manner, both *in vitro* and *in vivo* (Freund et al., 2012; Hernandez-Segura et al., 2017) (***Figure 12***). Of note, several cancers, including GBM, present a disruption of the nuclear envelop accompanied by altered levels of LAMIN B1 (Gupta et al., 2019). Therefore, the loss of this protein cannot be solely used a senescence marker in the context of cancer.

The disruption of the nuclear envelop leads to the dispersal of cytoplasmic chromatin fragments (CCFs) from the nucleus to the cytoplasm, which are recognized by the cytosolic GMP-AMP synthase/stimulator of interferon genes (cGAS/STING) immune machinery and in turn activates the expression of genes reinforcing senescence and the SASP (***Figure 12***) (Glück et al., 2017; Yang et al., 2017).

Another hallmark of senescent cells is the formation of specific chromatin structures termed senescence-associated heterochromatin foci (SAHF) which are enriched in repressive histone marks (H3K9me3, H3K27me3) and in heterochromatin proteins (such as HP1, HMGA proteins, and macroH2A histone variant 1) (Narita et al., 2003; Zhang et al., 2005). These foci together with the γH2AX and 53BP1 foci form the DNA segments with chromatin alterations, reinforcing senescence (DNA-SCARS) (***Figure 12***) (Rodier et al., 2011). Chromatin remodeling represses proliferative gene transcription which contributes to cell cycle arrest reinforcement as well as the SASP maintenance (Narita et al., 2003; Rodier et al., 2009; Sharpless and Sherr, 2015).

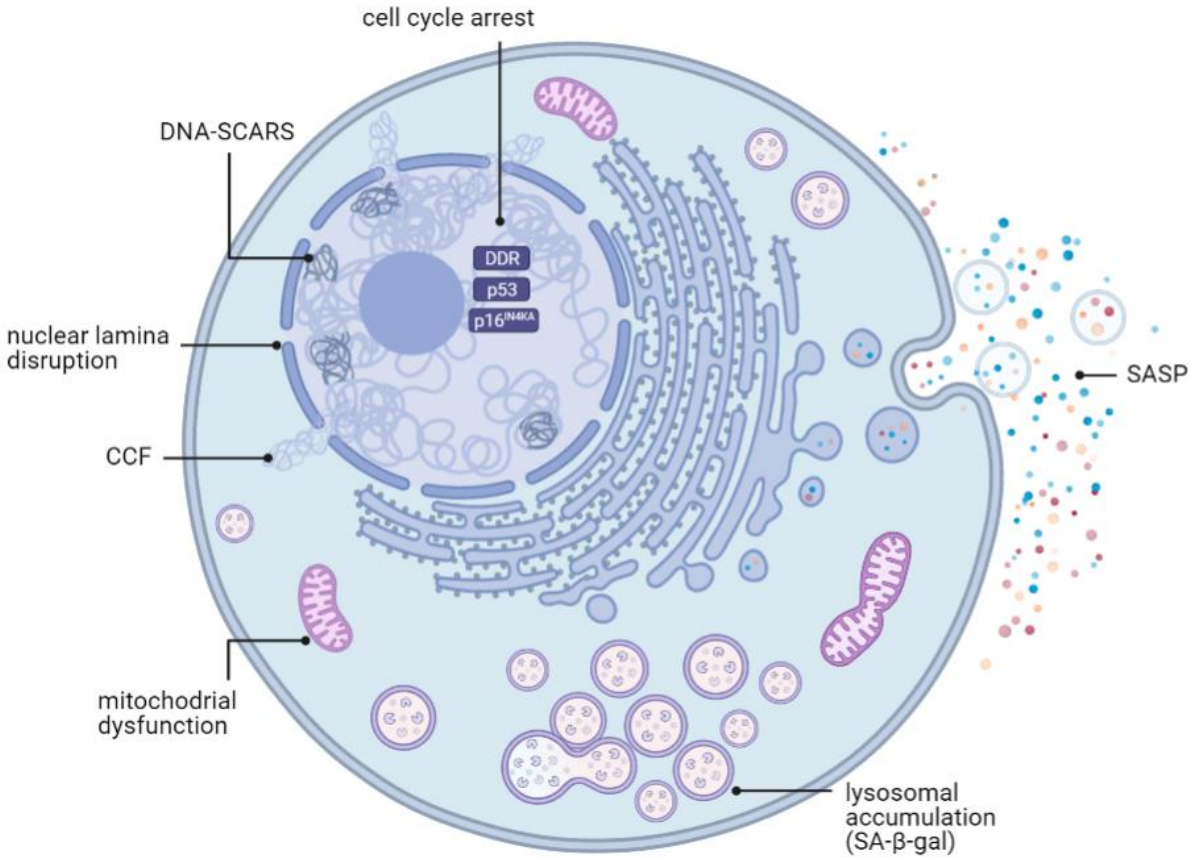

Figure 12. Senescence hallmarks are recapitulated in different cellular compartments

DNA-SCARS: DNA segments with chromatin alterations reinforcing senescence; CCF: cytoplasmic chromatin fragment; sEV: small extracellular vesicle; SASP: senescence-associated secretory phenotype; SA-β-gal: senescence-associated β-galactosidase

2.3. SASP regulation program

Senescent cells represent a low percentage of cells within physiological or pathological tissues, nevertheless they exert long range paracrine pleiotropic functions via their SASP (Baker et al., 2008; Demaria et al., 2014; Wang et al., 2009a). The SASP program modulates malignant cells and the tumor microenvironment including, the immune cells (macrophages, T cells, MDSCs), the stromal cells and the ECM (Louis et al., 2016; Ruhland et al., 2016a). The components of the SASP are context-dependent and vary according to the senescence inducer and the cell type. They are mainly composed of cytokines (e.g., pro-inflammatory interleukins (IL)1α, IL1β, IL6, IL8 and immunosuppressive factors IL10, IL13), chemokines (e.g., CXCL1/2, CCL2, CCL20), ECM remodeling enzymes (e.g., metalloproteases (MMPs), tissue inhibitor of metalloproteases (TIMPs), serine protease inhibitors (SERPINs)) and growth factors (e.g., PDGF-A, VEGF, TGF, insulin growth factor binding proteins (IGFBPs), hepatocyte growth factor (HGF), amphiregulin (AREG)) (Basisty et al., 2020; Coppé et al., 2010, 2008).

The SASP program is activated in a hierarchical manner where senescence inducers such as the DDR, the ROS-induced p38MAPK and cGAS/STING pathways converge to the activation of two main transcription factors: NF-κB and CCAAT/enhancer binding protein β (C/EBPβ). These factors synergistically activate the expression of the SASP master regulators IL1α, IL6 and IL8 which reinforce, in an autocrine manner, the senescent growth arrest and the SASP program via a positive feedback of the NF-κB and C/EBPβ activities (Acosta et al., 2008; Chien et al., 2011; Kuilman et al., 2008; Rodier et al., 2009) (***Figure 13***). In addition, *in vitro* study showed that OIS human fibroblasts secrete IL1α (with other factors such as VEGF, CCL2, CCL20) and promote a paracrine senescence (or bystander senescence) by upregulating the expression of p53/p21^{CIP1} and p15^{INK4B} in recipient cells (Acosta et al., 2013; Hubackova et al., 2012).

Several studies demonstrated the variety of SASP activation programs (***Figure 13***). For instance, NF-κB, C/EBPβ and IL1α regulate the SASP production and amplify the inflammatory cytokine signaling, including CCL2 and IL8 (Acosta et al., 2008; Kuilman et al., 2008; Laberge et al., 2015). Furthermore, prolonged DDR inhibits the autophagy regulator p62 leading to the stabilization the transcription factor GATA4, which in turn induces the SASP program via the IL1α-activated NF-κB pathway (Kang et al., 2015). Along this line, the mTOR pathway regulates the NF-κB/IL1α pathway by inhibiting the translation repressor

protein 4EBP1. The latter triggers the degradation of IL1α mRNA and the MAPKAPK2-mediated degradation of other SASP factors mRNA. Hence, inhibiting mTOR signaling pathway with rapamycin prevents the secretion of cytokines (Herranz et al., 2015; Laberge et al., 2015). Noteworthy, mTOR function can also be inhibited in hypoxic conditions (Brugarolas et al., 2004). Accordingly, van Vliet and colleagues demonstrated that the mTOR signaling pathway inhibition in senescent cells, under hypoxic conditions, hampered NF-κB and SASP inductions (van Vliet et al., 2021).

NOTCH1 can also modulate the SASP composition, on the one hand by activating an enriched TGFβ secretion, and on the other hand by inhibiting C/EBPβ-mediated pro-inflammatory factors secretion (Hoare et al., 2016). The SASP can also be induced by BRD4 (an acetylated histone-binding protein which binds to super-enhancers) or by HMGB proteins and ultimately activate the expression of SASP genes (Basisty et al., 2020; Davalos et al., 2013; Tasdemir et al., 2016).

Importantly, some SASP factors are expressed by non-senescent cells, such as immune and endothelial cells, and it is the combination of core (e.g., NF-κB, C/EBPb, IL1α) and regulating (e.g., mTOR, NOTCH1, BRD4) SASP factors that can be used to identify senescent cells.

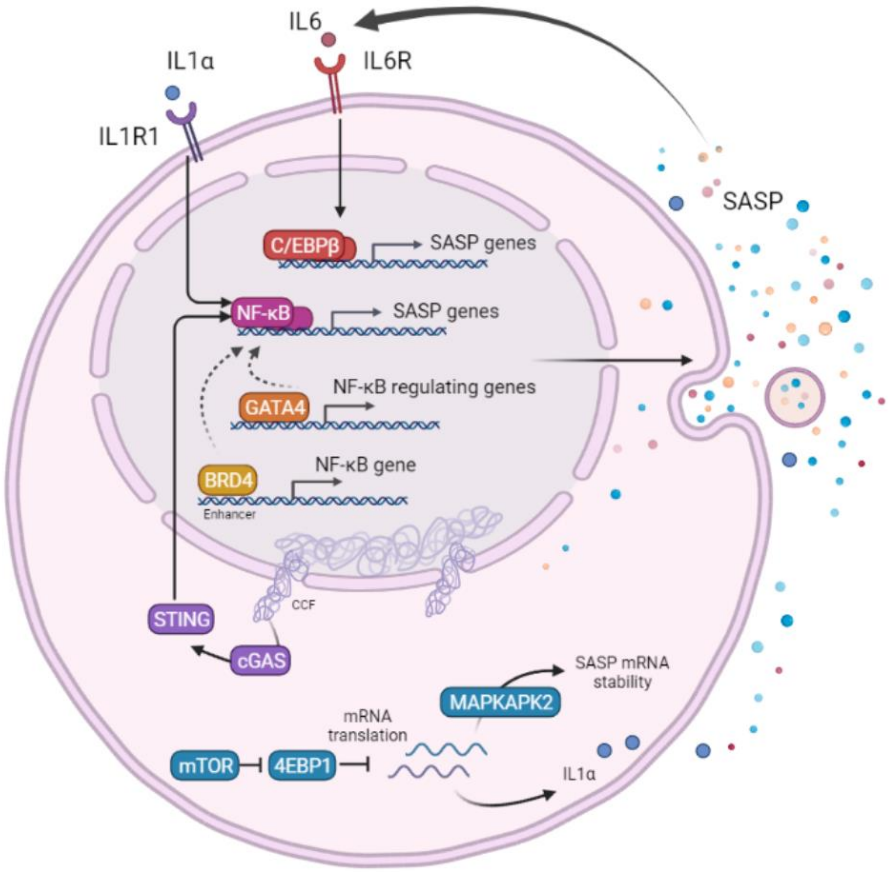

Figure 13. The diverse activation programs of the SASP
CCF: cytoplasmic chromatin fragment; SASP: senescence-associated secretory phenotype

3. The senescence mechanisms of action in cancer

In cancer, cellular senescence can be triggered upon oncogenic cues (e.g., *Ras, Akt, Braf, E2f1, Cyclin E*), loss of tumor suppressor genes (e.g., *Pten*, *Nf1*) high levels of ROS, soluble factors in the tumor microenvironment (e.g., IGFBP7, IL6/IL8 via C/EBPβ) or radio- and chemotherapy which in turn induce cells to enter a cell cycle arrest, via the DDR, the p53/p21^{CIP1} and p16^{INK4A}/Rb pathways (Collado et al., 2005; Kuilman et al., 2008; Michaloglou et al., 2005; Serrano et al., 1997). Depending on the context, senescence is a "double-edged sword" where the various SASP factors can either prevent or promote tumor progression (Sieben et al., 2018).

3.1. Beneficial roles

Senescence is a key cell-intrinsic mechanism of tumor suppression. OIS was first described in human fibroblasts expressing oncogenic Ras (HRasV12), which induces a stable cell cycle arrest either in a DDR-dependent manner or upon activation of the ROS-mediated p38MAPK pathway (Collado et al., 2005; Debacq-Chainiaux et al., 2010; Serrano et al., 1997). Consequently, p53-dependent senescence mediates anti-tumoral functions. For instance, in hepatocarcinoma and lymphoma/sarcoma genetically engineered mouse models, tumor progression is promoted in absence of p53 but regresses upon its re-activated expression, and therefore restricts the *in vivo* tumor progression (Ventura et al., 2007; Xue et al., 2007). In mouse models of prostate cancer, loss of *Pten* induces cellular senescence in a p53-dependent manner. In turn, tumor progression was prevented via cell growth arrest and reduction of the NF-κB-mediated anti-inflammatory SASP program (Chen et al., 2005; Parisotto et al., 2018; Toso et al., 2014). Of note, loss of *Pten* also induces cellular senescence in primary GBM neurospheres and decreases tumor formation in a xenograft model (Banasavadi-Siddegowda et al., 2017). Moreover, the p53 heterozygous deletion in a mouse model of GBM diminishes the percentage of SA-β-gal+ cells, favors the escape of OIS and worsens the GBM-bearing mice survival (Marumoto et al., 2009).

Depending on the context, SASP components can recruit and/or activate immune cells to target the clearance of senescent cells. This process is called senescence surveillance. The immune cell types responsible for the immune surveillance vary depending on the pathological conditions. Several studies on hepatocarcinoma mouse models have shed light on this process. Indeed, cytokines within the SASP (e.g., IL15, CXCL1 and MCP1) can direct the innate (NK cells) or the adaptive immune system (tumor-infiltrating CD4 T cells, macrophages) to mediate the senescent tumor cells clearance and terminate inflammation (Kang et al., 2011; Xue et al., 2007). Senescent cells can further secrete CCL2 chemokine or NKG2D ligand which

recruit CCR2 expressing myeloid cells or NK cells respectively and trigger senescence clearance (***Figure 14***) (Eggert et al., 2016; Iannello et al., 2013). Furthermore, IL1β-mediated SASP production can either modulate the macrophages polarization to an M1 anti-tumorigenic state or recruit M1 macrophages via CXCL1 and promote a microenvironment less favorable to tumor growth (Lesina et al., 2016; Lujambio et al., 2013). Inhibition of mTOR (using rapamycin) and BRD4 (using a BET inhibitor) hampers the SASP production and reduces the immune cell infiltration, thus impairing senescence surveillance and tumor suppression (Herranz et al., 2015; Tasdemir et al., 2016) (***Figure 14***).

Interestingly, senescent cells can also be induced by anticancer therapies and play beneficial roles by acting as an adjuvant for therapies. Chemotherapeutic agents such as TMZ, doxorubicin and cisplatin can trigger TIS (Demaria et al., 2017). In addition, in a lung cancer mouse model, the combo of a chemotherapeutic agent (palbociclib, a CDK4/6 inhibitor), with an inhibitor of MEK (downstream effector of Ras) potentiates the induction of senescence in malignant cells. These cells are further eliminated by NK cells that mediate the immune surveillance (Ruscetti et al., 2018). The SASP of TIS cells can also promote vascular remodeling in a pancreatic ductal adenocarcinoma mouse model and facilitates the chemo- and immune therapies delivery (Ruscetti et al., 2020) (***Figure 14***).

3.2. Detrimental roles

Senescent cells can contribute to tumor growth in an autocrine and a paracrine manner. In the hematopoietic context, few senescent cancer cells can escape the senescent state and acquire *de novo* self-renewing properties which further increases tumor aggressiveness (Milanovic et al., 2018). While cells undergoing OIS and TIS can be efficiently cleared by immune cells, they can also evade immune clearance and persist (Michaloglou et al., 2005). In this case, chronic senescence takes place and promotes tumorigenesis via the production of a pro-tumorigenic SASP.

Tumor growth

Several SASP factors, such as IL6, contribute to tumor growth in various cancer, including GBM (Faget et al., 2019). Indeed, although the link with senescence was not established, IL6 promotes patient GSCs growth and contributes to glioma malignancy of mouse patient-derived xenograft (PDX) model (Wang et al., 2009b). In addition, a multitude of secreted factors present in the GBM tumor environment are known SASP cytokines, chemokines and MMPs contributing to tumor progression (Louis et al., 2016). For instance, osteopontin (*Spp1*, a CD44 ligand) promotes stemness properties in the perivascular niche of GBM-PN, and contributes to tumor aggressiveness via C/EBPβ-mediated HIF2α expression (Pietras et al., 2014).

Moreover, in the diffuse intrinsic pontine glioma tumor, a pediatric low-grade glioma, TIS is triggered upon inhibition of the BMI1 (a PRC2 component) and the SASP promotes tumor recurrence (Balakrishnan et al., 2020).

Noteworthy, exosomes (small extracellular vesicles (sEV) with lipid bilayer membrane) containing mainly proteins, nucleotidic fragments and lipids, are secreted 30 to 50-fold more in senescent cells than in non-senescent cells and participate in the senescent secretory machinery (Basisty et al., 2020; Takasugi et al., 2017). Senescent human fibroblasts and cancer cell lines induce, via the secreted sEV containing SASP factors (e.g., IFTIM3), bystander senescence and promote tumor growth and inflammation (Borghesan et al., 2019; Takasugi et al., 2017).

Although TIS can act as an adjuvant for anticancer therapies, in an immunosuppressive environment, TIS cells that are not cleared contribute to the therapy side effects and toxicity. Elimination of doxorubicin induced senescent cells reduces metastasis of a mammary mouse model and alleviates the burden of several chemotherapy side effects including fatigue and cardiac dysfunction (Demaria et al., 2017).

Immunosuppression

Degradation of the innate and adaptive immune system associated with aging favors the accumulation of senescent cells. During aging, the SASP favors a low level of chronic inflammation, also known as “inflammaging” in a non-cell autonomous way, which is causal to some age-related diseases including cancer (Franceschi and Campisi, 2014).

During tumor progression, senescent cells contribute to the establishment of an immunosuppressive environment by triggering TAM re-education (Eggert et al., 2016; Di Mitri and Alimonti, 2016; Di Mitri et al., 2019). Senescent cells of advanced hepatocarcinoma secrete CCL2 which recruits anti-inflammatory M2 macrophages and inhibits NK cells-mediated elimination of tumor cells. In turn, it promotes a poor survival and early tumor recurrence of hepatocarcinoma-bearing mice (Eggert et al., 2016). Noteworthy, CCL2 is also produced in patient and murine GBMs where it recruits MDSCs and T reg cells to mediates immunosuppression. CCL2 expression correlates with a reduced overall survival of patients with GBM (Chang et al., 2016a). In the same line, the IL6/Jak2/Stat3 and NF-κB signaling pathways activate an immunosuppressive SASP which induces MDSC-mediated T cell inhibition and contribute to the progression of skin and prostate tumor *in vivo* (***Figure 14***) (Ruhland et al., 2016b; Toso et al., 2014). Interestingly, NF-κB, C/EBPβ and STAT3 are also master transcriptional regulators of the GBM-MES; they induce the expression of mesenchymal genes such as CD44, N-CADHERIN, VIMENTIN (VIM), and promote an

inflammatory microenvironment via the action of TNFα, CCL2 and IL6 (Bhat et al., 2013; Carro et al., 2010; Doucette et al., 2013).

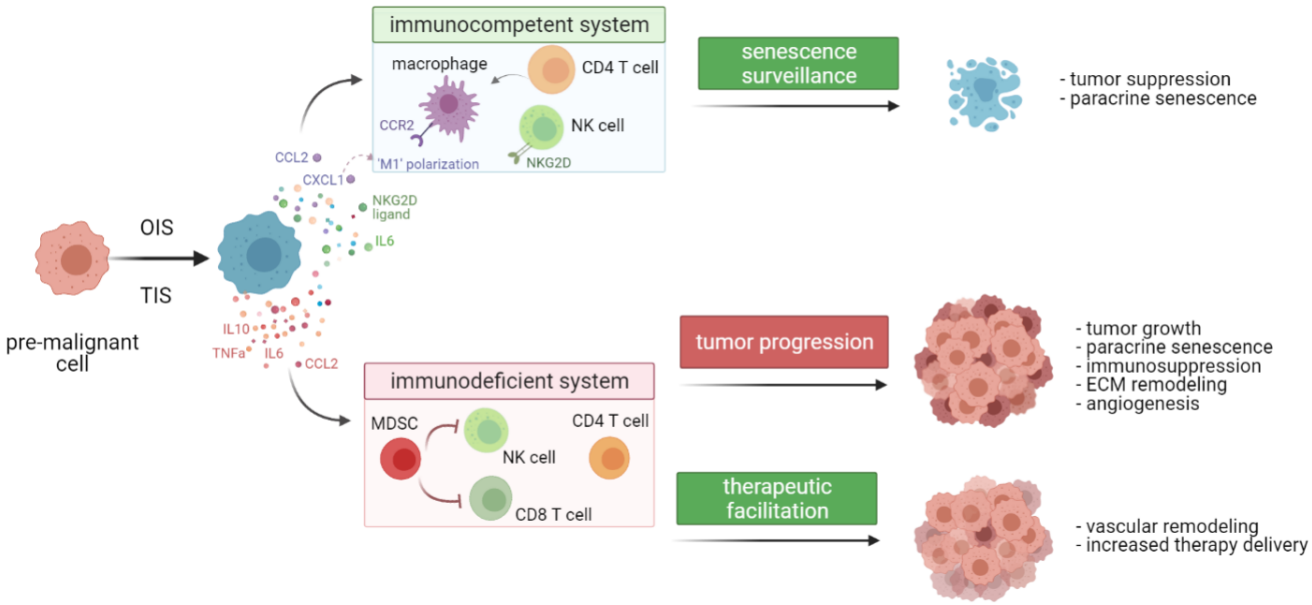

Figure 14. Senescent cell roles depend on the activation state of the immune system
OIS: oncogene-induced senescence; TIS: therapy-induced senescence; NK cell: natural killer cell; MDSC: myeloid-derived suppressor cell; ECM: extracellular matrix.

ECM remodeling and angiogenesis

The SASP contains ECM remodeling enzymes (e.g., MMPs, TIMPs, SERPINs) and ECM components (e.g., laminins, integrins) which support tumor invasion and metastasis by facilitating cell motility and epithelial-to-mesenchymal transition (EMT) (Coppé et al., 2008; Demaria et al., 2017; Malaquin et al., 2013). IL6/IL8/STAT3 signaling and mTOR pathway via 4EBP1 inhibition activate an EMT gene program characterized by increased *VIM* and reduced *β-CATENIN* and *E-CADHERIN* (Canino et al., 2012; Herranz et al., 2015). Of note, the GBM-MES meta-module, associated with poor radiotherapy response and worse patient survival, includes ECM remodelers such as YKL40, SERPINE1, TIMP1, and TGFB, which are known SASP factors (Bhat et al., 2013; Wang et al., 2017b).

Interestingly, the transcription factor NRF2 (nuclear factor-erythroid 2-related factor 2) activates ECM gene expression which alters ECM secretion and promotes *in vivo* senescence in fibroblast. Senescent fibroblasts further adopt a cancer-associated fibroblast phenotype and promote tumor expansion (Hiebert et al., 2018).

Another important feature associated with tumor propagation is angiogenesis. VEGF secreted by OIS fibroblasts promotes blood vessel formation and angiogenesis. Indeed, co-injected

senescent fibroblasts with malignant epithelial cells increased tumor vasculature which in turn promote tumor growth (Coppé et al., 2010, 2006; Krtolica et al., 2001).

4. The senotherapies: using senescence as a therapeutic target

In light of current data on cellular senescence on the one hand, and on GBM biology on the other hand, studying the functions of senescence in the context of GBM appears relevant. GBMs are good candidates to display OIS and TIS which could account for detrimental senescence in the context of the GBM immunosuppressive environment (Aasland et al., 2019; Marumoto et al., 2009). Multiple studies demonstrated the benefit of eliminating senescent cells in various age-related diseases and the development of drugs targeting senescent cells has been expanding throughout the last decade (Childs et al., 2017). Senotherapy consists in either eliminating senescent cells, by senolytics or to inhibiting their functions. An optimal senotherapy should then target senescent cells, without affecting beneficial senescent cells. To date, there are two main types of senotherapeutic agents known: senolytics (from the words senescence and lysis) which specifically kill senescent cells and senomorphics which modulates their activation without inducing their death (***Figure 15***).

Senolytics

One feature of senescent cells is the development of an anti-apoptotic program induced by the expression of anti-apoptotic genes such as BCL-2, BCL-XL and BCL-W (Childs et al., 2014; Yosef et al., 2016) and the downregulation of pro-apoptotic genes such as Bax (Sanders et al., 2013). Various senolytic drugs have been developed to inhibit their resistance to apoptosis. Among them the BCL2 inhibitor family (also known as BH3-mimetics) represents an important category including ABT263 (inhibiting BCL-2, BCL-XL and BCL-W) (Chang et al., 2016b; Yosef et al., 2016) and ABT737 (inhibiting BCL-2 and BCL-XL) (Kohlhapp et al., 2021; Ovadya et al., 2018; Ritschka et al., 2020). Importantly, Chang and colleagues demonstrated the efficacy of the ABT263 to eliminate senescent bone marrow hematopoietic and muscle stem cells in irradiated mice (Chang et al., 2016b). ABT263 also increased the survival of IDH-mutant GBM xenograft models via mTOR pathway inhibition (Karpel-Massler et al., 2017). Although senescence was not addressed in this study, it shows that ABT263 crosses the BBB. This property of ABT263 was confirmed in a mouse model of tauopathy (Bussian et al., 2018). Of note, initial clinical trials of ABT263 as an anti-cancer agent were limited by its toxicity, in particular due to thrombocytopenia which reduces the ABT263 dose in patients (Wyld et al., 2020). One way to efficiently reduce the drug side effects is to increase the specificity of the drug delivery by exploiting senescent cells features, such as the accumulation of β-galactosidase in lysosomes. Recently, pro-drugs composed of a combination ABT263

(or Duocarmycin, a cytostatic antibiotic) with a galactose molecule were successfully developed to selectively target and induce apoptosis of TIS cells in irradiated mice (González-Gualda et al., 2020; Guerrero et al., 2020).

Furthermore, great efforts are invested into the identification of novel senolytic molecules including Fisetin (Li et al 2018), cardiac glycosides (such as Ouabain and Digoxin) (Guerrero et al., 2019; Triana-Martínez et al., 2019), Foxo4-p53 interfering peptides (Baar et al., 2017), p53-mdm2 interaction inhibitors (Jeon et al., 2017), and Dasatinib and Quercetin combination (Musi et al., 2018; Schafer et al., 2017; Xu et al., 2018; Zhang et al., 2019) (***Figure 15***). Dasatinib and Quercetin reduce lung fibrosis and alleviate senescent phenotypes induced in neurodegenerative mouse models, strongly suggesting that the combo crosses the BBB (Musi et al., 2018; Schafer et al., 2017; Zhang et al., 2019). This combo therefore could be relevant for GBM therapy. Upcoming drug screening will significantly expand the list of senolytics which will further need to be tested on *in vivo* tumor models.
Noteworthy, Amor and colleagues exploited the cytotoxic activity of chimeric antigen receptor (CAR) T cells in a mouse model, to mirror the physiological senescence clearance. They engineered CAR T cells to recognize and kill target cells expressing a specific antigen. In this study, uPAR is expressed at the surface of senescent cells and this approach alleviates senescence burden in liver fibrosis and lung adenocarcinoma (Amor et al., 2020).

Senomorphics

Senomorphic (also called senostatic) drugs bypass the action of senescent cells without removing them. For instance in an oncogenic context, clobetasol, a glucocorticoid, delays BRAF-V600E induced senescence entry in human fibroblasts (Carvalho et al., 2019). Another class of senomorphic inhibits the SASP program. On the one hand, inhibitors of SASP components include neutralizing antibodies against known cytokines (IL6, IL8, TNFα), or growth factors (PDGF-A) (Acosta et al., 2008; Chiche et al., 2017; Demaria et al., 2014; Mosteiro et al., 2016). On the other hand, targeting the transcriptional regulatory program of SASP can be achieved in OIS and TIS contexts using inhibitors of IL1α (Acosta et al., 2013), NF-κB (Chien et al., 2011), mTOR pathway (Herranz et al., 2015; Laberge et al., 2015), JAK1/2 (Farr et al., 2017; Toso et al., 2014), BRD4 (BET inhibitors) (Tasdemir et al., 2016; Wakita et al., 2020) and hypoxia mimetics (van Vliet et al., 2021) (***Figure 15***). Notably, hypoxia-mimetics inhibit SASP production in aged mice and in mice treated with doxorubicin chemotherapy agent. This approach can therefore be used as a companion therapy to eliminate TIS side effects (van Vliet et al., 2021).

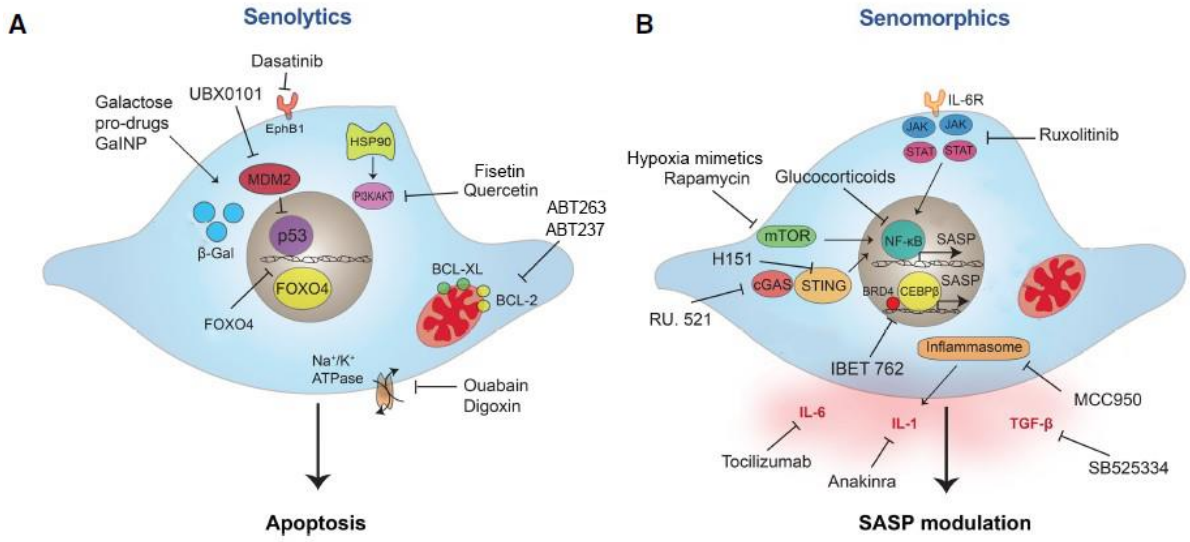

Figure 15. Senotherapies target senescent cells and the SASP
A. Senolytics induce senescent cell death.
B. Senomorphics modulates the activity of senescent cells notably by interfering with SASP regulatory pathways.
(adapted from Birch and Gil, 2020)

The one-two punch strategy

The “one-two punch” approach consists in using drugs promoting senescence entry of cancer cells and in a second step, inducing their elimination with senolytics (Wang et al., 2017a). Notably, it has been demonstrated in a mouse model of hepatocarcinoma where senescent cells are first induced by antidepressant Sertraline (DNA-replication kinase CDC7 inhibitor). Consequently, senescent tumor cell are sensitizes to two mTOR inhibitors (AZD8055 and AZD2014) and induce cell death (Wang et al., 2019a).

III. An optimal model to study senescence in GBM

To study the function of cellular senescence during gliomagenesis and screen potential therapeutics, the use of both *in vitro* models and *in vivo* mouse models is complementary. On the one hand, 2D, 3D *in vitro* GBM cultures allow large chemical, genetic screens and "-omics" approaches to study the potential response to novel drugs. On the other hand, *in vivo* mouse models are essential for several reasons, including the recapitulation of the complex GBM biology, the potential interactions of senescent cells with their microenvironment (e.g., the immune compartment, blood vessels), and the presence of a BBB for testing the permeability to senotherapeutic agents (Robertson et al., 2019).

Few *in vivo* studies point to the function of senescence in the context of gliomas, yet with contradictory outcomes. While IL6 promotes growth of patient GSCs and contributes to tumor progression in a PDX model, loss of PTEN-PRMT5 pathway inducing GSCs senescence slows down tumorigenesis in an immunodeficient mouse model (Banasavadi-Siddegowda et al., 2017; Wang et al., 2009b). Furthermore, a mouse model of GBM bypasses HRasV12-mediated OIS upon the loss of p53 leading to a decrease in SA-β-gal staining and a better survival of the mice (Marumoto et al., 2009). In addition, a study demonstrated the dual role of BMI1 inhibitor mediated-TIS in diffuse intrinsic pontine glioma tumor which attenuates cell self-renewal and growth in a short-term but promotes SASP-mediated tumor recurrence in a long-term (Balakrishnan et al., 2020).

To date, functional models to understand the role of senescence in GBM are greatly lacking. Nevertheless, a myriad of experimental models has been developed to study either senescence or GBMs.

1. Models for GBM study

1.1. *In vitro* models

2D GBM cultures

GBM cell lines (e.g., U87, U251MG) in adherent or non-adherent (spheres) conditions were first established in 1968. Although they are commonly used in GBM research, their use is controversial as they can diverge at a genetic level from the tumor of origin (Allen et al., 2016). To recapitulate more faithfully patient tumors, patient-derived primary GBM cell line (PDCL) were generated as preclinical models and conserve 85% of copy number variations after 8 passages (Rosenberg et al., 2017). Of note, when injected in immunocompromised mice, PDCLs conserve important histopathological features of the parental tumor compared with GBM cell lines (Lee et al., 2006). Nonetheless, the cell-cell interactions and the microenvironment of the tumor of origin are not conserved in 2D cell culture. This can be

compensated by the culture of organoids which widespread over the last decade in GBM studies.

GBM organoid culture

Organoids have been defined by De Souza as 3 dimensional multicellular *in vitro* tissue constructs that mimic its corresponding *in vivo* organ, such that it can be used to study aspects of that organ in the tissue culture dish (De Souza, 2018). They can be kept in culture for several months. In cancer research, organoids aim at modeling human cancer more faithfully to reveal new biological insights and to further be used as predictive models for personalized cancer treatments (Tuveson et al., 2021). They are currently four main types of organoids to model GBM: embedded tumor cells or minced tissues in ECM (Hubert et al., 2016), minced tissues without dissociation and without embedding (Jacob et al., 2020), cerebral organoids grafted with tumor cells or genetically modified to generate *de novo* GBMs (Ogawa et al., 2018; Pine et al., 2020; da Silva et al., 2018), and 3D bioprinted GBM organoids (Tang et al., 2020). Each of these methods are complementary and dedicated to specific questions (***Tableau 2***).

Hubert and colleagues first developed GBM in organoids which consist of dissociated patient GBMs cells embedded in droplets of ECM (Matrigel or Geltrex) (Hubert et al., 2016). Organoids recapitulate tumor heterogeneity with regionalized structures including a hypoxic core and a proliferative outer rim. In addition, the histological and invasiveness features of organoids were representative of the patient tissue, although they lack cells from the TME. Of note, this technique was used in our work to generate mouse GBM-derived organoids, which grow faster than patient GBM-derived organoids and display cells from the microenvironment (***Tableau 2***).

Jacob and colleagues developed in 2020 patient-derived GBM organoids from minced but non-dissociated patient GBM tissue directly cultivated in an appropriate culture medium (Jacob et al., 2020). Remarkably, the authors reduced the time needed to establish GBM organoids which recapitulate histological and morphological features of the parental tumor. GBM organoids display intratumoral heterogeneity with the presence of immune cells (TAM and T cells) for about two weeks, recapitulate treatment responses to conventional treatments (TMZ/IR) and were efficiently used as a tool to test CAR-T cell immunotherapy.

Human cerebral organoids generated from embryonic or induced pluripotent stem cell lines, provide a platform to generate and study novel mutations and oncogenes by gene-editing CRISPR/Cas9 tool, during gliomagenesis (Ogawa et al., 2018) and to investigate GBM heterogeneity and cell invasion (Pine et al., 2020; da Silva et al., 2018). Interestingly, 3D bioprinted organoids give insights in cell-cell interactions between bioprinted cells (e.g., immune cells) and malignant cells within the GBM organoids (Tang et al., 2020).

	Embedded tumor cells or minced tissues in ECM		**Minced tissues without dissociation/ without embedding**	**Cerebral organoids (1) grafted with tumor cells (2) de novo genetically modified**	**3D bioprinted GBM organoids**
References	Hubert et al., 2016		Jacob et al., 2020	Da Silva et al., 2018 Ogawa et al., 2018 Pine et al., 2020	Tang et al., 2020
Materials	Patient GBM-derived	Mouse GBM-derived	Patient GBM-derived	- Organoid: Patient hiPSCs or ESCs - Graft: Patient GBM-derived	GSC, macrophages, astrocytes, NSCs bioprinted in ECM
Properties	- Low vs high success rate - Slow vs short growing - Slow vs presence TME - Histological features and heterogeneity of parental tumor in both patient and mouse GBM-derived		- High success rate - Short growing - Histological features and heterogeneity of parental tumor	- High success rate - Short growing - No TME	- High success rate - Short growing - TME
Applications	- Treatments - Multi-omics - Xenograft		- Treatments - Drug screening - Xenograft - CAR-T cell immunotherapy	- Invasion - Specific mutation study	- Invasion - Malignant-immune cell interactions - Specific mutation study - Drug screening

Tableau 2. Table recapitulating the different types of organoid cultures available to study GBM
hiPSC: human induced pluripotent stem cells; ESC: embryonic stem cells; TME: tumor microenvironment, CAR: chimeric antigen receptor; ECM: extracellular matrix.

Despite the increasing efforts to recapitulate patient GBM features and cell interactions in organoid cultures, important structures (e.g., BBB, brain vasculature, full competent immune system) are lacking to study GBM biology. Whole-animal models can overcome these limitations as they display shared organ systems and physiology (Robertson et al., 2019).

1.2. *In vivo* models

Experimental mouse models are utilized in order to better understand GBM molecular and cellular mechanisms, identify new potential targets and for preclinical tests of new therapeutic strategies. Nonetheless, results obtained from *in vivo* mouse models should further be validated with complementary approaches such as *in vitro* models or *in silico* patient data. No single model can encompass all GBM features, yet a reliable GBM model should mimic the histological and molecular characteristics of patient GBM, the inter- and intratumoral heterogeneity, be immunocompetent and indicative of patient treatment response (Robertson et al., 2019).

The anatomical location of the generated tumor is crucial in order to recapitulate the local tissue microenvironment. In the case of the GBM, malignant cells diffuse into the healthy brain

tissue while immune cells infiltrate the tumor, and the BBB is required to test the crossing of pre-clinical drugs. Thus, orthotopic models using intracranial stereotactic surgery should be preferred over subcutaneous grafting (Robertson et al., 2019).

Given the major roles of the immune system in GBM progression and the increasing studies on immunotherapies in cancer, mouse models of GBM should ideally be immunocompetent. Although patient-derived xenograft models allow functional studies of patient GBM subpopulations, patient-derived cells are transplanted into immunodeficient mice which limits the study on the TME. Syngeneic models can overcome this issue where grafted cells and the host animal are of the same genetic background. In addition, specific mutations can be introduced in the genome of the grafted cells via gene-editing CRISPR/Cas9 tool prior to be injected (Gangoso et al., 2021). However, this model does not faithfully recapitulate the initial steps of tumorigenesis (Robertson et al., 2019) (**Figure *16***).

Conversely, genetically engineered mouse models (GEMMs) allow *de novo* tumor formation. The choice of the cell of origin (e.g., astrocyte, neuron, neural stem cell) and the use of inducible approach (e.g., Cre-lox system) give a spatial and temporal control on tumor initiation, respectively. GEMMs are generated via the combination of oncogene (e.g., *EGFRvIII*, *Pdgfra*) and tumor suppressors (e.g. *Pten*, *Nf1*, *Tp53*, *Cdkn2a*, *Rb1*) genetic alterations known in patient GBMs. These genetic alterations are expressed via either stable inducible transgenes or by lentiviral induction (Alcantara Llaguno et al., 2019; Marumoto et al., 2009) (***Figure 16***). Noteworthy, Alcantara Llaguno and colleagues demonstrated the importance of the cell of origin in a series of studies. They induced a loss of *Pten*, *Nf1*, *Tp53*, mediated by the Cre recombination in the neural lineage and showed that the more the cells are differentiated the less potent the tumor induction is (Alcantara Llaguno et al., 2009, 2019, 2015). These studies were further confirmed in patient GBMs, where neural stem cells from the subventricular zone (SVZ) were identified as the cell of origin of patient GBMs (Lee et al., 2018).

Depending on the induced genetic alterations, the GBM can recapitulate the known transcriptional subtypes (Wang et al., 2017b). For instance, a GBM-PN model can be generated by using the RCAS-tva strategy which allows the somatic gene transfer of oncogene (e.g., PDGFB) and/or loss of tumor suppressor (e.g., *Ink4a/Arf* locus) into targeted brain cells (here Nestin+ neural progenitors) engineered to express the tva receptor. Another team developed a GBM-MES mouse model with a lentivirus expressing HRasV12 or AKT, which is injected in the SVZ to target GFAP+ neural stem cells expressing the Cre recombinase. Although Ras mutations are rare in patient GBMs, HRasV12 here mimics the loss of NF1 found in patient GBMs (Marumoto et al., 2009). An shRNA against p53 was further integrated into the lentiviral construction to recapitulate the loss of p53 expression in GBM-MES (Friedmann-

Morvinski et al., 2012). The choice of the adequate GBM model is dependent on the raised research question.

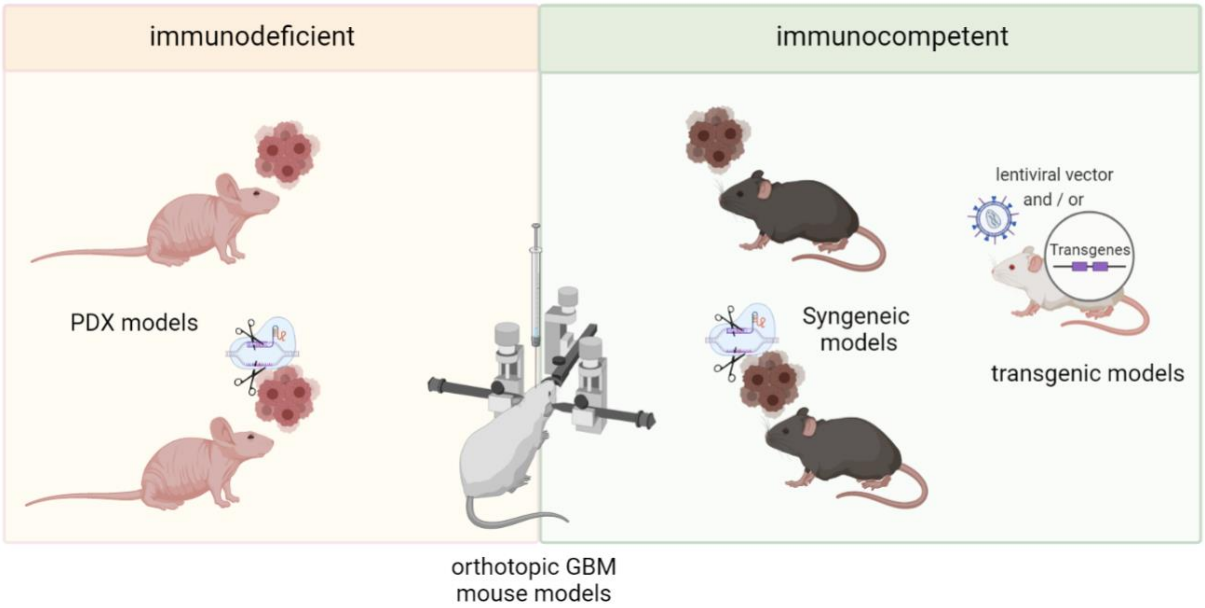

Figure 16. Orthotopic GBM mouse models
PDX mice are transplanted with patient-derived GBM cells, and syngeneic mice are transplanted with mouse glioma cells. Transplanted cells can be genetically modified. Transgenic models are genetically modified and can be injected with lentiviral vector to induce *de novo* tumorigenesis.
PDX: patient-derived xenograft;

2. Mouse models for senescence study

Mouse models have been generated to functionally study *in vivo* senescence during organismal aging, physiological and pathological processes by removing senescent cells. Importantly, this strategy initiated the development of senotherapies and these models are often used to validate the benefits of senotherapeutic drugs (Bussian et al., 2018; Chang et al., 2016b; Farr et al., 2017). Here, I will focus on three main transgenic mouse models that use distinct regions of the *p16*^{Ink4a} regulatory sequences to drive the expression of inducible reporters in cells expressing *p16*^{Ink4a}, further leading to apoptosis.

Baker and colleagues generated the INK-ATTAC transgenic mouse model which selectively eliminates p16^{Ink4a} senescent cells (***Figure 17***). The transgene encodes for a FK506-binding-protein-caspase 8 (FKBP-Casp8) fusion protein under the p16^{Ink4a} promoter (2.6 kb). This protein is localized on the cell membrane. In the presence of the AP20187 drug, the FKBP-Casp8 dimerization is induced, the caspases adopt an active conformation and trigger apoptosis of p16^{Ink4a} cells.

Demaria and colleagues generated the p16-3MR transgenic mouse model allowing the identification, isolation, and the selective elimination of senescent cells expressing high levels of $p16^{Ink4a}$ (Demaria et al., 2014) (***Figure 17***). The transgene encodes for a 3MR trimeric fusion protein under the regulatory sequences of $p16^{Ink4a}$ (50 kb). The 3MR trimeric protein is composed of the functional domains of the Renilla luciferase (LUC) to monitor senescent cells by bioluminescence, the monomeric red fluorescent protein (mRFP) for *in situ* labeling, and the truncated herpes simplex virus 1-thymidine kinase (HSV-TK) to specifically kill senescent cells expressing $p16^{Ink4a}$ upon ganciclovir (GCV) treatment. GCV is a nucleoside analog of the 2′-deoxy-guanosine and it is phosphorylated by thymidine kinase (TK). Noteworthy, HSV-TK has a higher affinity for GCV than the endogenous cellular TK. Once the GCV is phosphorylated, it is converted into a toxic DNA chain terminator which ends the DNA replication process. As senescent cells are in a cell cycle arrested, the phosphorylated GCV inhibits the mitochondrial DNA replication, resulting in the cell death of $p16^{Ink4a}$ senescent cells (Laberge et al., 2013).

As previously evoked, organismal aging is often associated with age-related diseases. The direct causality between cellular senescence and aging was demonstrated by crossing an accelerated aging BubR1 progeroid mouse model with the INK-ATTC model. In both accelerated and naturally aging mice, *in vivo* clearance of $p16^{Ink4a}$ positive senescent cells extended mice lifespan and healthspan, reduced age-associated disorders (in kidneys, heart, lungs and skeletal muscles) and delayed tumorigenesis (Baker et al., 2008, 2011). In addition, INK-ATTAC and p16-3MR models were used to demonstrate the role of senescence in a plethora of pathologies. For instance, INK-ATTAC was used mouse model of obesity (Yoshimoto et al., 2013), bone loss (Farr et al., 2017) and tauopathy (Bussian et al., 2018). p16-3MR was initially developed to study wound healing (Demaria et al., 2014), and later in atherosclerosis (Childs et al., 2016), *in vivo* reprograming (Chiche et al., 2017) and in osteoarthritis (Jeon et al., 2017). Although these mouse models target the elimination of $p16^{Ink4a}$-expressing senescent cells in various organs, some organs are yet not targeted.

In an attempt to target all the cells expressing $p16^{Inka}$, Grosse and colleagues generated a third mouse model. They inserted a Cre (or CreERT2) recombinase by homologous recombination in the end of the last exon of the Ink4b-ARF-Ink4a locus (Grosse et al., 2020). In this model, the recombinase induces the expression of the diphtheria toxin subunit A (DTA) and or the mTmG (Tomato/GFP) inserted in the Rosa26 locus. Consequently, cells expressing high levels of $p16^{Ink4a}$ ($p16^{High}$) are removed (by the DTA) or permanently labeled (by the GFP). The authors confirmed the presence of $p16^{High}$ senescent cells in multiple organs including the lung, heart, kidney, white adipocyte tissue and the liver. The senescent liver sinusoid

endothelial cells (LSECs) display enhanced toxin elimination capacities compared to non-senescent LSECs and their elimination promotes buildup of macromolecular waste. In contrast, Dasatinib and Quercetin combo treatment only removed $p16^{High}$ macrophages but not $p16^{High}$ LSECs and adipocytes. These results highlight the need for specific and local delivery of senolytics to prevent the elimination of beneficial senescent cell types. To sum up, each mouse model has its advantage and limitation. Of note, the model of Grosse and colleagues would need to be modified to study senescence in the central nervous system as the Rosa26 locus is not active in all brain cells of adult mice (Madisen et al., 2010).

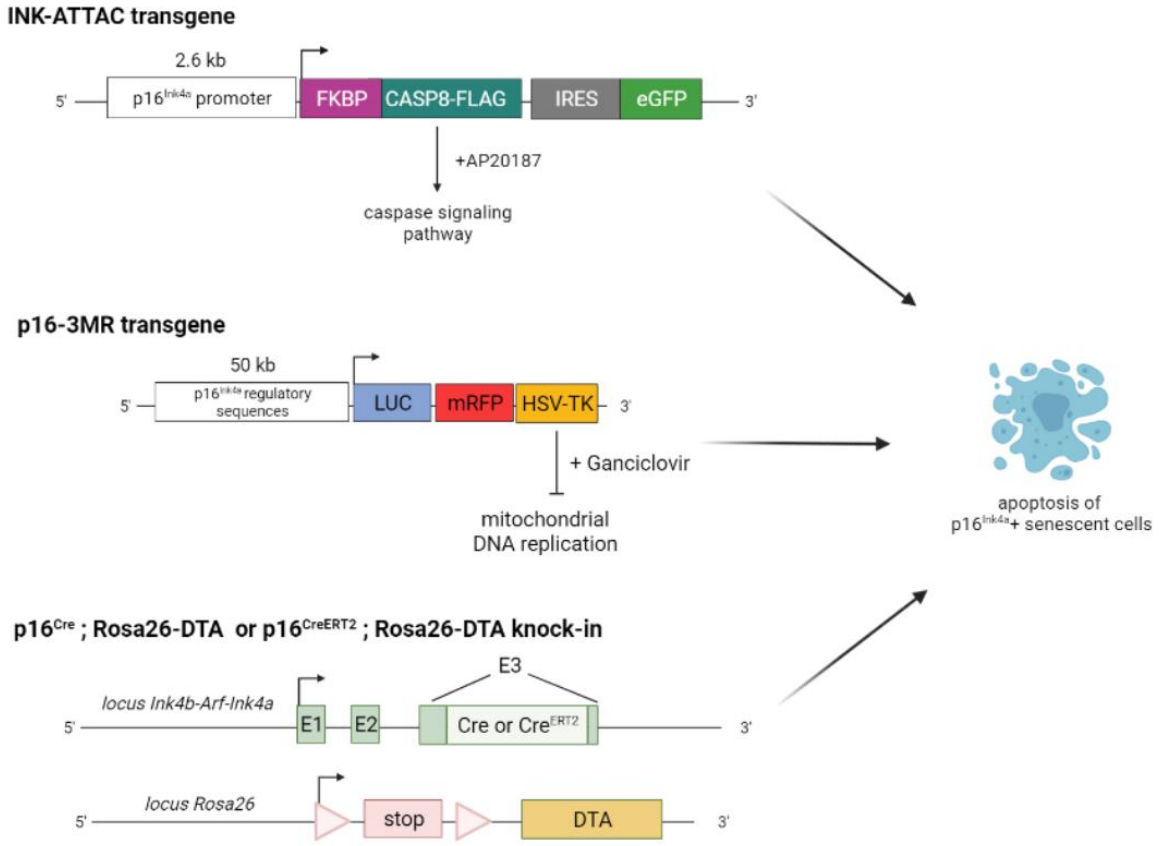

Figure 17. Mouse models to eliminate $p16^{Ink4a}$ senescent cells
The INK-ATTAC (Baker et al., 2008, 2011) and p16-3MR (Demaria et al., 2014) models express a transgene under the regulatory sequences of the $p16^{Ink4a}$ promoter and the $p16^{Cre}$;Rosa26-DTA and $p16^{CreERT2}$;Rosa-26-DTA are knock-in mouse models (Grosse et al., 2020). They induce the apoptosis of senescent cells expressing high levels of $p16^{Ink4a}$.
FKBP-Casp8: FK506-binding-protein-caspase 8; IRES: internal ribosome entry site; eGFP: enhanced green fluorescent protein; Luc: renilla luciferase; mRFP: mouse red fluorescent protein; HSV-TK: herpes simplex virus-thymidine kinase; E: exon; DTA: diphtheria toxin subunit A.

Project rational and objectives

Despite the aggressive conventional therapies, GBM always recur and patient survival remains less than 15 months after diagnosis (Stupp et al., 2005). Novel approaches are therefore required to find effective therapeutic strategies for diagnosed GBM patients.

Considering the present knowledge, investigating the functions of senescence in GBM appears relevant for multiple reasons:

- Senescence inducers are present in GBMs. Indeed, GBMs are characterized by the presence of hypoxic regions, the activation of oncogenic and tumor suppressor pathways and the induction of the DDR upon conventional therapies (TMZ/IR). In addition, the immunosuppressive environment in GBM could favor the establishment of chronic senescence (Chang et al., 2016a; Eggert et al., 2016; Kamran et al., 2017; Ruhland et al., 2016b).
- The high amount of secreted cytokines, chemokines, and metalloproteases in the GBM tumor microenvironment is consistent with the expression of a SASP program by senescent cells (Basisty et al., 2020; Louis et al., 2016; Pietras et al., 2014). Notably, the main SASP program inducers (namely NF-κB and C/EBPβ) are key regulators of the GBM-MES subtype, and loss of *Pten*, one of the main GBM-MES genetic alteration, induces senescence (Banasavadi-Siddegowda et al., 2017; Chen et al., 2005; Parisotto et al., 2018; Toso et al., 2014; Wang et al., 2017b).
- The mesenchymal GBM model generated by Marumoto and colleagues displayed a high percentage of SA-β-gal+ cells. Although one marker is not sufficient to label senescent cells, it may reflect the presence of OIS cells (Marumoto et al., 2009).

We therefore hypothesized that **senescent cells present in GBM may represent an actionable target to slow down the process of tumorigenesis**.

To address this question, the main objective of my PhD project was to determine the functions of cellular senescence in patient and mouse GBMs. To this end, we adapted an immunocompetent GBM mouse model and introduced the p16-3MR transgene into the mouse genome to functionally eliminate senescent cells expressing high levels of *p16^{Ink4a}* (Demaria et al., 2014; Friedmann-Morvinski et al., 2012). We investigated the impact of senescence removal on GBM-bearing mouse survival, and its mechanisms of action by combining bulk and single-cell transcriptomics. We validated our results with published patient GBM datasets (TCGA data and Neftel et al., 2019).

Results

Cellular Senescence in Malignant Cells Promotes Tumorigenesis in Mouse and Patient Glioblastoma

Before starting my thesis, preliminary results generated in the team established the presence of senescent cells in primary and recurrent patient GBMs. They display an SA-β-gal activity (SA-β-gal+), do not proliferate (Ki67-) and express the $p16^{INK4A}$ cell cycle arrest marker ($p16^{INK4A}$+). In order to functionally study the role of cellular senescence in GBM, I developed and generated an immunocompetent GBM mouse model harboring the p16-3MR transgene. During the course of the project, I implemented the model with a Firefly luciferase cassette to monitor tumor growth *in vivo*. I generated all the mouse data of the manuscript. The transcriptomic analysis of the bulk and single RNA sequencing were done in collaboration with the iCONICS platform at the Brain Institute (Justine Guégan and Mathilde Bertrand) and the ARTbio Bioinformatics Analysis Facility at the Institut Français de Bioinformatique (IFB) (Christophe Antoniewski and Léa Bellanger).

The results of my PhD work are presented below in a manuscript format; this version is currently under review in Cell Reports.

Graphical abstract

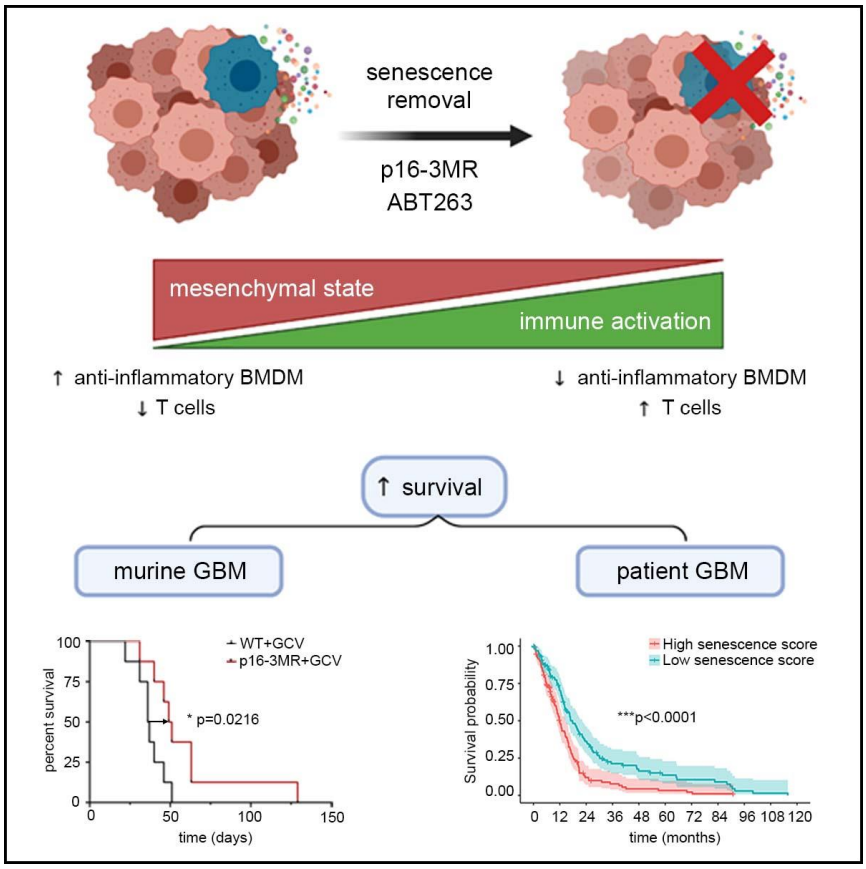

Highlights

- Patient and mouse primary GBMs display senescent cells
- Removal of p16$^{Ink4a\ Hi}$ senescent cells increases the survival of the mice bearing GBM
- scRNAseq identifies p16$^{Ink4a\ Hi}$ senescent cells as malignant
- p16$^{Ink4a\ Hi}$ senescent cells promote mesenchymal cell identity and immunosuppression
- The transcription factor NRF2 regulates the SASP
- High score of senescence signature correlates with a poor prognosis for patients with GBM

Title:

Cellular Senescence in Malignant Cells Promotes Tumorigenesis in Mouse and Patient Glioblastoma

Authors:

Rana Salam[1], Alexa Saliou[1], Franck Bielle[1,2,3], Mathilde Bertrand[4], Christophe Antoniewski[5], Agusti Alentorn[1,6], Laurent Capelle[7], Marc Sanson[1,3,6], Emmanuelle Huillard[1], Léa Bellenger[5], Justine Guégan[4] and Isabelle Le Roux[1]

Affiliations:

[1]Paris Brain Institute (ICM), Hôpital Pitié-Salpêtrière, Inserm U 1127, CNRS UMR 7225, Sorbonne Université, Genetics and Development of Brain Tumors Team, Paris, France. [2]AP-HP, Hôpital de la Pitié-Salpêtrière – Charles Foix, Département de Neuropathologie, Paris, France. [3]Paris Brain Institute (ICM), Hôpital Pitié-Salpêtrière, Inserm U 1127, CNRS UMR 7225, Sorbonne Université, Onconeurotek Tumor Bank, Paris, France. [4]Paris Brain Institute (ICM), Hôpital Pitié-Salpêtrière, Inserm U 1127, CNRS UMR 7225, Sorbonne Université, Iconics, Paris, France. [5]Sorbonne Université, CNRS FR3631, Inserm US037, Institut de Biologie Paris Seine (IBPS), ARTbio Bioinformatics Analysis Facility, Paris, Institut Français de Bioinformatique (IFB), France. [6]AP-HP, Hôpital de la Pitié-Salpêtrière - Charles Foix, Service de Neurologie 2-Mazarin, Paris, France. [7]AP-HP, Hôpital de la Pitié-Salpêtrière - Charles Foix, Service de Neurochirurgie, Paris, France.

Corresponding Author: Isabelle Le Roux, Paris Brain Institute, Hôpital de la Pitié-Salpêtrière CNRS UMR 7225 - Inserm U 1127 – Sorbonne Université 47, boulevard de l'Hôpital CS 21414 75646 Paris Cedex 13 France. Phone: 33 1 57 27 44 84. Email: isabelle.leroux@icm-institute.org

SUMMARY

Glioblastoma (GBM) is the most common primary malignant brain tumor in adults yet with limited treatment efficacy. Elimination of senescent cells has emerged as a new strategy against cancer. In this study, we investigate the contribution of senescent cells to GBM progression. We identify senescent cells in patient and mouse GBMs. The removal of $p16^{Ink4a}$ malignant senescent cells that represent less than 10% of the tumor, improves the survival of GBM-bearing mice and modifies the tumor ecosystem. By combining single cell and bulk RNA sequencing with immunohistochemistry, we identify the NRF2 transcription factor as an upstream regulator of the senescence-associated secretory phenotype, composed of extracellular matrix components or remodelers. Remarkably, the mouse senescent signature and the underlying mechanisms of senescence are conserved in patient GBMs whose high score of senescence is correlated with a lower survival. These findings provide insights into the benefit of senotherapy for patients with GBM.

KEYWORDS

Glioblastoma, Cellular Senescence, NRF2, scRNAseq, Senotherapy.

INTRODUCTION

Gliomas are the most common primary malignant brain tumors in adults (Ostrom et al., 2013). Glioblastoma (GBM, grade IV astrocytoma) is the most aggressive glioma and its incidence has significantly risen in the last two decades across all ages (Philips et al., 2018). Despite intensive conventional therapy which includes surgery, radiation with both concurrent and adjuvant temozolomide (TMZ) chemotherapy, GBM remains resistant and disease progression is fatal with a median survival below 15 months (Stupp et al., 2005). Distinct factors may account for current treatments' failure including the invasiveness, the immunosuppressive microenvironment and the intra-tumoral heterogeneity of these tumors. Novel approaches are therefore required to find effective therapeutic strategies (Geraldo et al., 2019).

Cellular senescence is a permanent cell cycle arrest mediated by p53/p21^{CIP1} or/and p16^{INK4A}/Rb pathways and is defined by a combination of features including senescence-associated secretory phenotype (SASP), anti-apoptotic program or increased lysosomal content (allowing histochemical detection of senescence associated-β-galactosidase activity, SA-β-gal) (Gorgoulis et al., 2019). In cancer, cellular senescence is triggered by multiple stresses among which are DNA damage, oncogene activation, therapeutic agents or elevated reactive oxygen species (ROS). The SASP of senescent cells is composed of a plethora of factors such as cytokines, chemokines, growth factors, extracellular matrix (ECM) components and proteases, which stimulate angiogenesis, modulate the ECM and promote epithelial-to-mesenchymal transition (Coppé et al., 2010; Faget et al., 2019). Depending on the context, senescence exerts two opposite effects during tumorigenesis (Sieben et al., 2018). On the one hand, senescent cells prevent the proliferation of pre-malignant cancer cells, and SASP factors stimulate the immune clearance of oncogene or therapy-induced senescent tumor cells (Xue et al., 2007; Kang et al., 2011; Ruscetti et al., 2018). On the other hand, SASP of persistent senescent cells can either directly induce tumor growth (Yoshimoto et al., 2013) or contribute to the immune suppression thus allowing tumor progression (Toso et al., 2014; Ruhland et al., 2016). Many studies assessed the function of senescence in developing tissues and age-related disease using the *in vivo* removal of senescent cells either by chemical or genetic senolytics (Baker et al., 2011; Demaria et al., 2014; Zhu et al., 2015; Chang et al., 2016; Kohlhapp et al., 2021). In the genetic approach, the regulatory sequences of *p16^{Ink4a}* drive the expression of inducible reporters INK-ATTAC or p16-3MR in cells expressing high levels of *p16^{Ink4a}* in mouse models, leading to apoptosis (Baker et al., 2011; Demaria et al., 2014). This senolytic strategy efficiently reduces the adverse effects of therapy-induced senescent cells in a mouse breast cancer model (Demaria et al., 2017).

Few *in vivo* studies point to the function of cellular senescence in the context of gliomas. Mouse patient-derived xenograft (PDX) models showed that IL6, a universal SASP component as well

as a cytokine express by immune cells, promotes growth of patient glioma stem cells (GSCs) and contributes to glioma malignancy, whereas loss of PTEN-PRMT5 pathway-induced senescent GSCs slow down tumorigenesis (Wang et al., 2009; Banasavadi-Siddegowda et al., 2017). Furthermore, an orthotopically-lentiviral GBM mouse model bypassed H-RasV12 oncogene-induced senescence upon p53 loss and displayed decreased SA-β-gal staining and increased mouse survival (Marumoto et al., 2009). Recently, a study demonstrated the dual role of therapy-induced senescence (TIS) upon BMI1 inhibitor treatment. TIS attenuated cell self-renewal and growth of diffuse intrinsic pontine glioma tumor (a pediatric high-grade glioma), but promoted SASP-mediated tumor recurrence in a long-term (Balakrishnan et al., 2020). These studies suggest that senescent cells could represent an actionable target to mitigate the process of gliomagenesis.

Recent single-cell RNA expression profiling studies classified the intra-tumoral heterogeneity (Neftel et al., 2019; Wang et al., 2019; Bhaduri et al., 2020; Couturier et al., 2020; Richards et al., 2021) of malignant GBM cells which can be subdivided in four main cellular plastic states: oligodendrocyte-precursor-cell-like (OPC-like), neural-precursor-cell-like (NPC-like), astrocyte-like (AC-like) and mesenchymal-like (MES-like) states (Neftel et al., 2019). The relative abundance of these cellular states within the tumor defines three GBM transcriptomic subtypes namely proneural and classical (PN-GBM, CL-GBM) associated with neurodevelopmental programs and mesenchymal (MES-GBM) associated with injury response programs (Verhaak et al., 2010; Wang et al., 2019; Wang et al., 2017; Bhaduri et al., 2020; Couturier et al., 2020; Richards et al., 2021). OPC-like and NPC-like states are enriched in PN-GBM whereas AC-like and MES-like states are enriched in CL-GBM and MES-GBM, respectively (Neftel et al., 2019). In addition, stemness programs are heterogeneous even within a single tumor and PN and MES GSCs could contribute to the genetic heterogeneity observed in patient GBM (Wang et al., 2019; Bhaduri et al., 2020; Castellan et al., 2020). Each transcriptional GBM subtype is associated with distinct molecular alterations and patient outcomes. MES-GBM is correlated to a poorer prognosis and with enhanced expression of anti-inflammatory (or tumor-promoting) macrophages (Bhat et al., 2013; Darmanis et al., 2017; Wang et al., 2017; Schmitt et al., 2020).

Mutations in *NF1*, *TP53*, *PTEN* genes are prevalent in this GBM subtype, as well as an increased NF-κB signaling pathway (Verhaak et al., 2010). Interestingly, *Pten* loss induces cellular senescence and NF-κB signaling pathway, initiates and maintains the SASP (Chen et al., 2005; Acosta et al., 2008; Chien et al., 2011). These findings indicate that cellular senescence could contribute to the intra-tumoral heterogeneity of GBM.

In this study, we investigated whether cellular senescence participates to GBM tumor progression using patients' resected GBM tissues, mouse GBM and mouse GBM-derived organoids as models (Friedmann-Morvinski et al., 2012; Hubert et al., 2016). We identify senescent cells in patient and mouse GBMs. The inducible removal of cells expressing high levels of $p16^{Ink4a}$ by the use of the p16-3MR transgene (Demaria et al., 2014) upon ganciclovir injection improves the survival of GBM-bearing mice. We combined single cell and bulk RNA sequencing (RNAseq) analysis at early and late timepoints after the senolytic treatment. This approach enabled us to identify the cells expressing high levels of $p16^{Ink4a}$, to characterize the paracrine action of these cells on the tumor ecosystem and revealed the NRF2 pathway and its selected targets as a candidate to trigger the pro-tumoral function of $p16^{Ink4a}$ senescent cells. Finally, we propose an unbiased senescence signature that we successfully applied to interrogate GBM patient data sets.

RESULTS

Identification of senescent cells in patient and mouse GBMs

We first searched for senescent cells on freshly resected gliomas from patients. To accomplish this, we performed SA-β-gal staining coupled with immunohistochemistry (IHC) on cryosections. We analyzed 14 tumors from patient resected tissues (4 GBMs, 7 low-grade gliomas; 3 recurrent low-grade gliomas; Figure S1A) and identified 13/14 gliomas with senescent cells that are positive for SA-β-gal (SA-β-gal+) and negative for the cell cycle marker Ki67 (Ki67-). Depending on the molecular alterations found in gliomas, these cells express the cell cycle inhibitor $p16^{INK4A}$ (Figures 1A and S1A). Many of the SA-β-gal+ cells co-express the glial marker GFAP; these cells could either be parenchymal astrocytes or tumor cells (Figure 1A). In gliomas harboring a mutation of p53, senescent malignant cells are identified by the strong expression of this mutant protein (Figure 1A). Some of the SA-β-gal+ cells co-express the oligodendrocyte progenitor cell (OPC) marker OLIG2, or the microglia/macrophage marker IBA1.

We then studied senescence in an immuno-competent GBM mouse model that is a modified version of one developed by Friedmann-Morvinski *et al.* (2012). This model recapitulates the molecular alterations identified in the MES-GBM: the loss of *Pten* and *p53* and the inactivation of *Nf1* via the ectopic expression of HRasV12 (Figure 1B). Six-to-eight week $Glast^{creERT2/+}$; $Pten^{fl/fl}$ mice were intracranially injected with the lentivirus encoding HRasV12-IRES-eGFP and shp53, into the subventricular zone (SVZ) and mice were sacrificed when they reached end points (Figure 1B). These tumors display the heterogenous histopathology described for patient GBM (Figure S1B) (Louis et al., 2016). In addition, the *Ink4/ARF* (encoding $p16^{Ink4a}$, $p15^{Ink4b}$, $p19^{Arf}$) and *p21* loci, which encode senescence-mediating proteins, are active in the

tumor (GFP+) compared with the surrounding parenchyma (GFP-) (Figure 1C). In contrast, *p53* mRNA levels are similarly low within the tumor and the adjacent tissue, confirming the efficacy of the shp53 (Figure 1C). We further identify SA-β-gal+ Ki67- LAMINB1- $p19^{ARF}$+ senescent cells in mouse GBM (Figure 1D). Of note, the expression of $p16^{Ink4a}$ in mouse tissues is not reported due to the lack of antibody specificity. Moreover, senescent cells are of distinct cell types, either malignant (GFP+), glial (GFAP+, OLIG2+) or microglia/macrophage (IBA1+) cells (Figure 1D). We do not detect any senescent endothelial cells (CD31+; Figure 1D). Senescent cells are sparse in the tumor, mostly located in proliferative areas and adjacent to necrotic regions (Figure S1C).

All together these data show that cellular senescence is a mechanism associated with primary and recurrent gliomagenesis. The GBM mouse model recapitulates the histopathology, the senescence features and cell identities of patient GBMs, allowing us to further use this model to address the function of senescence during primary gliomagenesis.

Senescent cells removal increases the survival of GBM-bearing mice

We introduced the p16-3MR transgene in the mouse model to selectively remove senescent cells expressing high levels of $p16^{Ink4a}$ upon ganciclovir (GCV) injections (Demaria et al., 2014). Remarkably, the median survival of GBM-bearing mice harboring p16-3MR and treated with GCV (p16-3MR+GCV) increases significantly compared with WT mice treated with GCV (WT+GCV) or p16-3MR mice treated with vehicle (p16-3MR+vhc) (Figures 2A, 2B, 2C and 2D). Similarly, the survival of GBM-bearing mice treated with the senolytic drug ABT263 (Navitoclax, an inhibitor of the anti-apoptotic proteins BCL2 and BCL-xL; Chang et al., 2016) increases significantly compared with control mice (WT+vhc) (Figures 2C and 2E). Together these results strongly suggest that senescent cells act as a pro-tumoral mechanism during primary gliomagenesis.

In order to confirm the pro-tumorigenic function of senescent cells, we next focused our analysis on the p16-3MR paradigm. We analyzed whether the senescence hallmarks decrease in p16-3MR+GCV GBMs compared with controls. The SA-β-gal area in the tumor (GFP+ area) decreases significantly in p16-3MR+GCV compared with WT+GCV GBMs (Figures 2F and 2G). Of note this area represents less than 5% of the total tumor area, strongly suggesting a paracrine action of these cells on the whole tumor. We then performed bulk RNA sequencing (RNAseq). In agreement with the inter-tumoral heterogeneity of patient GBMs, heatmaps of the bulk RNAseq reveals inter-tumoral heterogeneity of the mouse GBMs independently of the treatment (Figures S2A and S2D). Gene Set Enrichment Analysis (GSEA, Figures S2B and S2E and data not shown) of p16-3MR+GCV GBMs compared with controls highlights an upregulation of the cell cycle pathway (E2F targets), a downregulation of pathways involved in cancer (epithelial-mesenchymal transition, mTORC1 signaling, angiogenesis), and

a modulation of the metabolism (oxidative phosphorylation, glycolysis, hypoxia) and the immune system (interferon responses, TNFA signaling via NFKB).

In addition, bulk RNAseq analysis shows in p16-3MR+GCV GBMs compared with control GBMs a slight decrease of p16^{Ink4a} transcripts (Figure 2H) and GSEA demonstrates significant downregulation of senescence pathways (Figures 2I and S2G; Table S1). This analysis led to the identification of SASP genes (*Fn1*, *Plau*, *Timp1*, *Mmp10*, *Plaur*, *Ereg*, *Bmp2*) whose expression is significantly decreased in p16-3MR+GCV compared with WT+GCV GBMs (Figures 2J, S2C and S2F). These SASP genes encode for growth factors and extracellular matrix components or remodelers. Collectively our data show at the endpoint of the mice, the efficacy of the p16^{Ink4a} senescent cells removal, therefore pointing to their pro-tumorigenic action during gliomagenesis.

Identification of p16$^{Ink4a\ Hi}$ cells in a subset of malignant cells

To unveil the identity of the p16^{Ink4a} senescent cells, we performed droplet-based single cell RNAseq (scRNAseq) on FACs sorted cells from WT and p16-3MR GBMs collected 7 days after the last GCV injection (Figures 3A and 3B). At this early timepoint, WT+GCV GBMs (n=2) exhibit increased tumor growth compared to p16-3MR+GCV GBMs (n=2) (Figures S3A, S3B and S3C). Uniform Manifold Approximation and Projection (UMAP) clustering at the 0.5 resolution reveals 22 clusters with distinct gene expression signatures in each sample in the two conditions (Figures 3C and S3D). Malignant and non-malignant cells are identified based on the expressions of the 3' long terminal repeat (3'*LTR*) of the injected lentivirus and of the pan-leucocyte marker *Cd45* (*Ptprc*), and on the copy number variations (CNV) (Figures 3D, 3E and S3E). Cells in each cluster express variable levels of *p16^{Ink4a}* (*Cdkn2a*) transcripts however, only malignant cells express high levels of *p16^{Ink4a}*. Hereafter, we refer to as p16$^{Ink4a\ Hi}$ cells, those cells expressing *p16^{Ink4a}* to a level ≥ 4 (Figures 3E and 3H).

This result prompted us to focus our analysis on the malignant cell compartment. The p16$^{Ink4a\ Hi}$ senescent cells are mostly present in cluster 0 which comprises the highest cell number in WT+GCV GBMs (2910 out of 13 563 cells; Figure 3E). Further UMAP clustering of malignant cells at the 0.6 resolution reveals 17 clusters in the two conditions (Figure 3F). GSEA using the gene lists published by Weng et al., 2019 allows the labelling of these clusters into subpopulations including predominantly cycling cells, pri-oligodendrocyte precursor cell-like (pri-OPC-like), committed OPC-like (COP-like), myelinating oligodendrocyte (mOL), astrocyte (AC), neural precursor-like (NP-like), and hypoxic cells (HC) (Figures 3F, 3G and S3F; Table S1). Some clusters exhibit mixed cell identities. The astrocyte cluster shares gene signatures of astrocytes, endothelial cells and ependymal cells whereas the pri-OPC-like 1 (pOPC1) and pri-OPC-like 2 (pOPC2) clusters share gene signatures of pri-OPC-like cells, astrocytes and COP cells (Figure 3G). Of note, the enrichment score of each subpopulation

differs very little between p16-3MR+GCV and WT+GCV GBMs, except for the pOPC1-3 clusters (Figure 3G; see below).

The p16$^{Ink4a\ Hi}$ cells are mainly grouped in the astrocyte cluster and to a lesser extent in the NP-like cluster (Figure 3H). Remarkably, the cell numbers of these two clusters decrease in p16-3MR+GCV GBMs compared with WT+GCV GBMs (astrocyte cluster from 7.75% to 3.21%; NP cluster from 20.88% to 17.76%; Figure 3I), in agreement with the removal of p16$^{Ink4a\ Hi}$ cells by the p16-3MR transgene in the presence of GCV.

The removal of p16$^{Ink4a\ Hi}$ malignant cells impacts the remaining malignant cells

We then tested whether the removal of p16$^{Ink4a\ Hi}$ cells influences the remaining malignant cells. Strikingly, three clusters of the oligodendroglial lineage pOPC2, COP and mOL increase in cell numbers upon the removal of p16$^{Ink4a\ Hi}$ cells (pOPC2 from 6.81% to 13.10%; COP from 1.24% to 4.60%; mOL from 1.31% to 4.30%; Figure 3I) suggesting a shift of the malignant cellular states upon the removal of p16$^{Ink4a\ Hi}$ cells. We thus explored the abundance of cellular states as defined by Neftel et al., 2019. The two-dimensional (2D)-representation in quadrants shows that malignant cells in control GBMs are distributed between the four cellular states with a small bias towards the MES-like and NPC-like states (MES-like state 31.28%, NPC-like state 28.10%, OPC-like state 23.23%, AC-like state 17.37%; Figure 3J). Upon p16$^{Ink4a\ Hi}$ cells removal, the number of AC-like cells increases to reach 26.27% whereas the overall proportion of the other cellular states is maintained (MES-like state 29.69%, NPC-like state 25.17%, OPC-like state 18.85% Figure 3J). The position of the majority of the cells in the center of the 2D-representation in the two conditions reflects a homogenous cell population (for comparison see Figure 7G). Noteworthy, the cells from the astrocyte, COP and mOL clusters spread away from the center showing the mixed AC-like and MES-like states of the astrocyte cluster and validating the OPC-like state of the COP and mOL clusters. The 2D-representation also shows the increased numbers of COP and mOL cells and the decreased numbers of astrocytes in p16-3MR GBMs compared to controls (Figure 3J).

Unexpectedly, although the size of the tumors at this early timepoint differs between the two conditions (Figures S3A-S3C), the percentage of cycling cells (G2/M1, G2/M2, G1/S1, G2/S2 clusters) remains stable (WT+GCV: 24.46%; p16-3MR+GCV: 23.08%; Figure 3I). The 2D-representation suggests a shift of these cycling cells from an OPC-like state to a MES-like state in p16-3MR GBMs compared to controls (Figure S3G) nonetheless, this trend is not confirmed by GSEA (data not shown). We thus conclude that the number and the cellular states of the cycling cells do not significantly vary upon removal of p16$^{Ink4a\ Hi}$ cells.

We then investigated the cellular state of the pri-OPC-like cells whose gene signatures and numbers vary between the two experimental conditions (Figures 3G and 3I). The 2D-representation reveals a shift from an OPC-like state to an AC-like state upon removal

of p16$^{Ink4a\ Hi}$ cells (Figure 3K). GSEA confirms this result and reveals an upregulation of the AC-like state in the pOPC1 cluster (Figure 3L; Table S1). Further GSEA shows a downregulation of the mesenchymal transcriptional subtype in the pOPC1 and the pOPC2 clusters of p16-3MR GBMs compared with controls (Verhaak_GBM_MES; Figure 3L). We next tested whether the change in the cellular state and the GBM transcriptional subtype between p16-3MR GBMs and WT+GBMs persists at the late timepoint. GSEA on the bulk RNAseq reveals a decrease in the MES-like state and the MES-transcriptional subtype upon p16$^{Ink4a\ Hi}$ cell removal. Additional GSEA shows an increase in the OPC-like and NPC-like states and its associated proneural transcriptional subtype (Verhaak_GBM_PN; Figure S3I, S3J and Table S1). The increase of the AC-like state observed in one pri-OPC-like cluster at the early timepoint is not detected at the late timepoint in the whole tumor.

All together the scRNAseq analysis identifies the p16$^{Ink4a\ Hi}$ senescent cells in a small subset of malignant cells. Their removal impacts the remaining malignant cells: it transiently increases the AC-like cellular state, permanently increases the oligodendroglial lineage and favors the loss of a mesenchymal cell identity.

Modulation of the immune compartment following p16$^{Ink4a\ Hi}$ cells removal

The MES transcriptional GBM subtype is associated with enhanced expression of anti-inflammatory and tumor-promoting macrophages (Bhat et al., 2013; Wang et al., 2017; Neftel et al., 2019). We therefore examined the immune fraction at the early timepoint following the removal of p16$^{Ink4a\ Hi}$ cells. UMAP clustering of *Cd45*+ cells reveals seven clusters in the two experimental conditions (Figures 3C, S3D and 4A). Differentially expressed (DE) genes and GSEA allow the labelling of these clusters into infiltrating bone marrow-derived macrophages (BMDM), resident microglia and T cells (Figures 4B, 4C, S4A and S4B; Table S1) (Bowman et al., 2016). All the BMDM and microglia clusters harbor an anti-inflammatory gene signature. Furthermore, the BMDM-like1 and microglia clusters share an antagonist pro-inflammatory gene signature (Figure 4C) (Darmanis et al., 2017). Here again, the enrichment score of each subpopulation differs very little between the two conditions (Figure 4C). In addition, the proportion of the immune fraction within the tumor hardly varies between WT+GCV and p16-3MR+GCV GBMs. However, the number of T cells increases (from 9% to 27%) at the expense of TAMs (BMDM and microglia) upon p16$^{Ink4a\ Hi}$ cells removal (Figure 4D).

We next examined whether the activity of these cell types differs from one condition to another. Although few genes are DE per cluster between the two conditions (Table S2), GSEA reveals an upregulation of the TNFA signaling via NFKB pathway in the microglia cluster and a downregulation of the inflammatory and hypoxia pathways in the BMDM clusters in p16-3MR GBMs compared with WT+GCV GBMs (Figure 4E). Close examination of the DE genes in these pathways highlights an increase in the expression of genes associated with the

pro-inflammatory signature (*Ccl4*, *Tnf*, *Il1a*, *Il1b*, *Csf1*) in the microglia cluster and a decrease in the expression of genes related to the anti-inflammatory signature (*Cxcl2*, *Vegfa*, *Tgfbi*, *Spp1*, *Thbs1*, *Hmox1*, *Hif1a*) in the BMDM clusters (Figure 4F). In addition, the T cell cluster analysis reveals a decrease in the expression of genes regulating the activity of T cells including the immune checkpoints *Ctla4, Lag3* and *Pdcd1* (*PD1*) (Figure 4F).

We then assessed whether this phenotype is maintained at the late timepoint. We estimated the abundances of the main immune cell types in the bulk RNAseq using CIBERSORT. The macrophage fraction significantly decreases in p16-3MR+GCV compared with WT+GCV GBMs (Figures S4C and S4D). Consistently GSEA reveals a decrease in core BMDM and anti-inflammatory pathways following the removal of $p16^{Ink4a\ Hi}$ cells (Figures S4E and S4F) (Bowman et al., 2016; Darmanis et al., 2017). This result shows that the downregulation of BMDM cells and the decrease of the anti-inflammatory signatures observed at the early timepoint are maintained at the end points of the mice.

Collectively, the transcriptomic analysis shows that the removal of $p16^{Ink4a\ Hi}$ malignant cells mitigates the anti-inflammatory and the immuno-suppressive phenotype of the GBM microenvironment and points to the paracrine action of senescent cells.

NRF2 activity in $p16^{Ink4aHi}$ cells can mediate pro-tumoral senescent functions

To explore the upstream regulators of senescence in malignant cells, we performed pathway enrichment analysis with the ENCODE and ChEA consensus TFs from ChIP-X database using Enrichr (Kuleshov et al., 2016) on three gene sets enriched in $p16^{Ink4a\ Hi}$ senescent cells: (i) differentially downregulated genes in the p16-3MR+GCV vs the WT+GCV astrocyte cluster from the scRNAseq at the early timepoint (Early; Figures 5A and 5B; Table S3); (ii) differentially upregulated genes in $p16^{Ink4a}$ positive vs $p16^{Ink4a}$ negative malignant cells from a scRNAseq at end points (Late (1); Figures 5C, 5D and S5A-S5E; Table S3); (iii) differentially downregulated genes in the p16-3MR+GCV vs the WT+GCV GBMs from the bulk RNAseq at end points (Late (2); Figures 5E and 5F; Table S3). Remarkably, the *Nuclear Factor Erythroid 2 Like 2* (*Nfe2l2*) signaling pathway is enriched in the three gene sets. NRF2 encoded by *Nfe2l2* is an antioxidant defense system that appears to be a plausible candidate to trigger the pro-tumoral action of $p16^{Ink4a\ Hi}$ senescent cells as it induces cellular senescence in fibroblasts (Hiebert et al., 2018) and confers a selective advantage in cancer cells (Rojo de la Vega et al., 2018). Among the identified NRF2 putative targets, three genes are common to all data sets (*Tgif1*, *Plaur*, *Gja1*) whereas four more genes are shared between only two gene lists (*Tnc*, *Igfbp3*, *Areg*, *Esd*) (Figure 5G; Table S3). As illustrated on the heatmap, the combined expression of *Nfe2l2* and its seven putative targets is unique to the $p16^{Ink4a\ Hi}$ cells in WT+GCV GBMs (Figure 5H).

Immunohistochemistry on GBM cryosections collected at end points shows NRF2 in a few scattered cells (Figures 5I and S5F). Quantification of the NRF2 expression area in the tumor shows a modest decrease in p16-3MR compared with WT+GCV GBMs. Of note, the expression of NRF2 in cells expressing low levels of $p16^{Ink4a}$, most probably CD45+ cells, may conceal a decrease of NRF2 in senescent cells (Figure 5H). We further examined the expression of three NRF2 putative targets whose encoded proteins are associated with senescence, glioma progression or glioma resistance namely urokinase plasminogen activator receptor (uPAR encoded by *Plaur*; (Gilder et al., 2018), Tenascin-C (TNC) (Brösicke and Faissner, 2015) or Connexin43 (CX43 encoded by *Gja1*) (Osswald et al., 2015), respectively. These proteins are expressed in a few scattered cells throughout the tumor. TNC is expressed in more numerous cells than uPAR and CX43 in agreement with their transcript expression at the single cell level (Figures 5H, 5I and S5F). Quantifications of CX43 by IHC and TNC by western blot reveal a significant downregulation of these proteins in p16-3MR GBMs compared with WT+GCV GBMs, strengthening *Gja1* and *Tnc* as NRF2 target genes in GBM (Figures 5K, 5L and S5G). We then assessed whether interactions between NRF2 selected targets and the immune fractions can occur in GBM. We interrogated for ligand-receptor interactions between the cluster 0 enriched in $p16^{Ink4a\ Hi}$ cells and the immune clusters in the scRNAseq data at the early timepoint using CellPhoneDB (Figure 3E). *In silico* analysis highlights possible interactions between TNC and PLAUR expressed in malignant cells and integrins receptors expressed in the immune clusters. Remarkably, putative TNC-aVb3 and PLAUR-aVb3 complexes between malignant cells and T cells are abolished upon $p16^{Ink4a\ Hi}$ cell removal (Figure S5H).

All together these data strongly suggest that NRF2 activity in $p16^{Ink4a\ Hi}$ senescent cells can in part trigger the pro-tumoral action of these cells, notably through the identified targets that can act on adjacent cells.

Senolytic treatment in mouse GBM-derived organoids decreases NRF2 signaling

We next moved to a mouse GBM-derived organoid model to confirm the function of NRF2 in malignant senescent cells (Figure 6A). Whole mount immunofluorescence reveals after 7 days in culture that organoids are composed of malignant (GFP+) and non-malignant cells (GFP-) (Figure 6B). SA-β-gal+ cells are identified after 14 days in culture; they are negative for Ki67 and some of them express $p19^{ARF}$, similar to patient and mouse GBMs (Figures 6C and 6D). We applied the senolytic ABT263 to the organoids after 14 days in culture and analyzed them a week later by immunofluorescence and bulk RNAseq (Figures 6A and S6A-S6C). The significant downregulation of the expression of $p16^{Ink4a}$, $p15^{Ink4b}$ and $p21^{Cip1}$ validates ABT263 efficacy (Figure 6E). We further identified upon senolytic treatment downregulated genes encoding for SASP factors (*Timp1*, *Mmp3*, *Cxcl1*, *Vegfa*, *Ereg*, *Cxcl2*) (Figures 6E and S6C).

Importantly, GSEA reveals a significant downregulation of NRF2 pathway upon senolytic treatment (Figure 6F). Whole mount immunofluorescence shows NRF2 in control and ABT263 treated organoids. NRF2 is expressed in GFP+ and GFP- cells and localized mainly in the nucleus. Furthermore, some cells co-express NRF2 with $p19^{ARF}$ (Figure 6G). Of note, the high cell density prevented protein quantification in malignant cells. In contrast to NRF2 and in agreement with *Tnc* transcripts in the tumor, TNC is only expressed in GFP+ cells. CIBERSORT analysis reveals that organoids display different immune cell abundance compared with tumor samples. For instance, the macrophage fraction is expended *in vitro* (Figure S7D). We next tested whether the above identified NRF2 targets are differentially expressed upon senolytic treatment in GFP+ organoid sorted-cells. The expression of *Nfe2l2*, *Igfbp3*, *Tnc*, *Gja1* but not *Plaur* decrease after ABT263 treatment as well as canonical NRF2 targets such as *Srxn1, Txrd1, Hk2* (Figures S6E and S6F).
Overall *in vivo* and *in vitro* experiments using either genetic or chemical senolytic agents reveal NRF2 pathway as a candidate to trigger the pro-tumoral function of $p16^{Ink4a\ Hi}$ senescent cells.

Mouse senescent signature is conserved in patient GBM and its high score is predictive of a worse survival

We next explored whether $p16^{Ink4a\ Hi}$ senescent cells are conserved in patient GBMs. We first established a senescent signature from the scRNAseq data at the early timepoint (Figure 3). We compared the transcriptome of the $p16^{Ink4a\ Hi}$ cells in the astrocyte and NP clusters ($p16^{Ink4a\ Hi}$ group) with those of the remaining malignant cells in the WT+GCV GBMs (Figures 3H, 7A and 7B). In agreement with the features of senescence, GSEA reveals in the $p16^{Ink4a\ Hi}$ group, a downregulation of cell cycle pathways (E2F targets, G2/M checkpoint) and an upregulation of pathways involved in inflammation (IL2 Stat5 signaling, inflammatory response, TNFA signaling via NFKB, inflammatory response, IL6 Jak Stat3 signaling) (Figure S7A). We further selected a list of 31 genes to define a GBM senescence signature. To accomplish this, among the 278 differentially upregulated genes in the $p16^{Ink4a\ Hi}$ group compared with the remaining malignant cells, we selected the genes that are expressed in more than 90% of $p16^{Ink4a\ Hi}$ cells and presented a fold change superior to 0.8 between the two groups. As expected, these genes are enriched in the astrocyte cluster and to a lesser extent in the NP cluster (Figure 7C). The encoded proteins are associated with diverse cellular processes compatible with cellular senescence such as cell cycle arrest (*Cdkn1a*, *Cdkn2a*, *Cdkn2b*), lysosomal function (*Ctsb*, *Ctsd*, *Ctsl*, *Ctsz*, *Lamp1*, *Lamp2*), cellular growth (*Igfbp2*, *Igfbp3*), extracellular matrix interaction (*Sparc*, *Tnc*, *Sdc4*, *Lgals1*, *Timp1*, *Mt1*), cytoskeleton interaction (*Pdlim4*, *S100a11*, *Tmsb4x*, *Sep11*) or cancer (*Tm4sf1*, *Ociad2*, *Emp3*) (Figure 7C). We then computed the senescence scores which correspond to the geometric mean of the expression of these genes in the WT+GCV and p16-3MR GBM transcriptomes. In WT+GCV

GBMs, 6.85% of the malignant cells harbor a senescence score ≥ 2 and belong mostly to the astrocyte cluster (493 cells out of 725 cells, 68%) recapitulating the proportions of SA-β-gal+ and $p16^{Ink4a\ Hi}$ cells in the GBM mouse model. In p16-3MR+GCV GBMs, the number of these cells drops to 1.82% and their majority still belongs to the astrocyte cluster (123 cells out of 188 cells; 65.43%), in agreement with the removal of $p16^{Ink4a\ Hi}$ senescent cells in p16-3MR mice upon GCV injections (Figure 7D). The cells with a senescence score ≥ 2 cells display mostly MES-like and AC-like cellular states (Figure 7E). Consistently, 9 out of the 31 genes of the signature belong to the MES-like meta-module.

We then applied the senescence score to the Smart Seq2 scRNAseq data set of patient GBMs from Neftel et al., 2019. Beforehand, we excluded pediatric GBMs and *CD45*+ cells from the analysis. We first analyzed patient GBMs without *CDKN2A*/*CDK4* genomic alterations, as our senescence scoring is based on $p16^{Ink4a}$ malignant senescence. For unbiased analysis, we considered that cells with a high senescent score are those with a score in the highest decile of senescent scores in all patient GBM cells (Figure 7F). Two groups of tumors emerge: GBMs with a percentage of high senescent score cells superior to 5% (n=8; MGH100, MGH101, MGH104, MGH105, MGH106, MGH121, MGH129, MGH66) and GBMs with a percentage of high senescent score cells inferior to 5% (n=7, MGH102, MGH110, MGH113, MGH115, MGH122, MGH124, MGH125) (Figure 7F). The cellular state of the senescent cells from patient GBMs follows the same trend as those in the mouse GBMs: cells with a high senescent score are mostly MES-like and AC-like independently of the predominant cellular state of the GBM (Figure 7G). Furthermore, two out of five GBMs (MGH128, MGH143) with *CDKN2A* and/or *CDK4* alterations possess more than 5% of cells with a high senescent score (Figure S7B), suggesting that the senescence score is not solely dependent on CDKN2A activity. These high senescent score cells are also enriched in AC-like and MES-like cellular states (Figure S7C).

We next investigated whether the senescence score could be used as a prognostic factor for patients with GBM. We interrogated the senescence score in The Cancer Genome Atlas (TCGA) GBM data sets, by stratifying patients into high and low senescence scores when they belong to the highest and lowest score quartiles, respectively. Consistent with the mouse study, a high senescent score predicts a worse survival in patients with GBM (Figure 7H). We then tested if the same molecular mechanisms could account for the pro-tumoral function of senescence in mice and patients with GBMs. First, SA-β-gal staining coupled with IHC on cryosections reveals the expression of NRF2, TNC and CX43 in SA-β-gal+ cells in patient GBMs (Figures 7I and S7E). Then, similarly to the senescence score, we interrogated the NRF2 targets score corresponding to the geometric mean of the expression of *NRF2* and its seven identified targets (*TGIF1*, *PLAUR*, *GJA1*, *TNC*, *IGFBP3*, *AREG*, *ESD*) in the TCGA GBM data sets. Remarkably, a high NRF2 targets score predicts a worse survival in patients with

GBM (Figure 7J). Importantly, the high expression of solely *NRF2* has no impact on the survival of patients with GBM, emphasizing the detrimental function of the identified NRF2 targets in malignant senescent cells (Figure S7D).

In summary, our data show that the mouse senescent signature and the underlying mechanisms of senescence are conserved in patient GBMs and that the high scores of senescence and of NRF2 targets are correlated with a lower survival in patients with GBM.

DISCUSSION

Depending on the context, cellular senescence plays both beneficial and detrimental roles during tumorigenesis. Here, we reveal the pro-tumorigenic action of malignant senescent cells in mouse and patient GBMs. The GBM mouse model used in the present study recapitulates the histopathology and the senescent features of patient GBMs. We show that $p16^{Ink4a\ Hi}$ malignant senescent cells account for less than 10% of the total tumor cells. Their partial removal increases significantly the survival of GBM-bearing mice and modifies the tumor ecosystem, therefore pointing to the paracrine action of the malignant senescent cells. By combining single cell and bulk RNA sequencing with immunohistochemistry, we identify the NRF2 transcription factor as an upstream regulator of SASP factors. Although GBM malignant cells largely express inflammatory cytokines and chemokines (Louis et al., 2016), these molecules are not enriched in $p16^{Ink4a\ Hi}$ malignant cells. In contrast, identified SASP factors are growth factors and components or modifying enzymes of the ECM (Figures 2J, 5G, 6E and 7B). These findings provide insights into previously reported functions of ECM in malignant and non-malignant cell mobility and of ECM as a potential target to improve response to therapy (Winkler et al., 2020). For instance, TNC appears from our study as one of the SASP components (Basisty et al., 2020) whose functions can partly be responsible for the pro-tumoral phenotype of the $p16^{Ink4a\ Hi}$ malignant senescent cells including the delay of tumor growth, the loss of MES-like cellular state and the decrease of the anti-inflammatory and immunosuppressive phenotypes. TNC is a component of the ECM of glioma that binds to integrin receptors, EGF receptor (EGFR), SYNDECAN 4 (SDC4) and regulates angiogenesis, proliferation and cell migration (Brösicke and Faissner, 2015). Previous studies, independently of the senescence context, described the pro-tumoral functions of TNC (Mirzaei et al., 2018; Faget et al., 2019; Haage et al., 2019; Angel et al., 2020). Our data show that targeting senescent cells in GBM decreases TNC and its adverse functions during gliomagenesis.

In addition, we identify *Tnc* as a putative target of NRF2. We show that in patients with GBM a high score of *TNC* expression correlates with a significantly lower survival although to a lesser extent than the high combined NRF2 targets score. This result suggests that TNC together with other NRF2 targets convey the pro-tumoral function of $p16^{Ink4a\ Hi}$ malignant

senescent cells (Figures 7J and S7D). All together our findings point to NRF2 acting as a hub for pro-tumoral senescence in GBM. Along this line, many studies demonstrated that chronic activation of this transcription factor contributes to tumor growth, metastasis, treatment resistance and poorer prognosis in patients with cancer (Rojo de la Vega et al., 2018). NRF2 binds to antioxidant responsive elements (AREs) and controls the expression of a battery of genes regulating metabolism, intracellular redox-balance, apoptosis, and autophagy (Rojo de la Vega et al., 2018). Depending on the context, NRF2 promotes or delays fibroblasts senescence (Hiebert et al., 2018; Rojo de la Vega et al., 2018). Nrf2 transcription can be induced by oncogenes (e.g. KRAS) and its activity is modulated by environmental cues (e.g. hypoxia, ROS) (Mitsuishi et al., 2012; Rojo de la Vega et al., 2018). Under homeostatic state, cytoplasmic NRF2 binds to KEAP1, which mediates its proteasomal degradation. However, impairment of NRF2-KEAP1 binding, either by p62 or by elevated ROS permits NRF2 nuclear translocation and activation of target genes (Inoue et al., 2012; Menegon et al., 2016; Harris and DeNicola, 2020). The p62-mediated degradation of NRF2 promotes *in vitro* glioma stem cell survival and NRF2 is hyperactivated in the MES-GBM subtype (Pölönen et al., 2019). The NRF2 putative targets identified in the present study are not canonical NRF2 targets and belong to SASP components which function as growth factors (AREG, IGFBP3, TGIF1), ECM remodelers (uPAR, ESD) or cell-cell interactors (CX43) (Gorgoulis et al., 2019). CONNEXIN 43 is of particular interest as it participates in the formation of microtubes that interconnect malignant cells, creating a cellular network resistant to treatment (Osswald et al., 2015). Our study together with previous work, lead us to propose that NRF2 triggers SASP expression in malignant senescent cells, further promoting gliomagenesis. Nonetheless, NRF2 is also expressed in the immune fraction where it exerts an antagonist function. In a mouse lung cancer model, NRF2 activity in the immune cells contributes to the suppression of the tumor progression (Hayashi et al., 2020). Hence, this result raises the question of the cell specificity when using NRF2 inhibiting or activating based therapies (Gao et al., 2014). In addition, it highlights the benefit of a senotherapeuthic strategy that would target NRF2 in malignant senescent cells in the context of GBM.

Single cell RNAseq analysis of mouse GBMs allowed the comprehensive characterization of the pro-tumorigenic malignant senescent cells. Although this approach focused primarily on $p16^{Ink4a\ Hi}$ senescent cells in a mouse MES-GBM model, our findings suggest that the senescence signature that we established is applicable to all transcriptional GBM subtypes independently of their molecular alterations. Hence, we identified high score senescent cells in all patient GBM subtypes and in patient GBMs with genomic alterations in *CDKN2A* gene (Figures 7F, 7G, S7B and S7C). This latest result is crucial, as 54% of patient GBMs carry a deep deletion in *CDKN2A* gene (cbioportal.org). Cyclin dependent kinase inhibitors warrant

cell cycle exit and entry into senescence. Our data suggest that the presence of three genes (*Cdkn2a*, *Cdkn2b*, *Cdkn1a*) encoding for these proteins, in the senescence signature, makes the senescence score independent of the CDKN2A molecular status. Of note, *CDKN1A* (*$p21^{CIP1}$*) is rarely mutated in patient GBMs (0.4%) and mediates senescence in many tissues (Gorgoulis et al., 2019). Furthermore, we presume that the senescent signature defined in the study is specific to detrimental senescence. Indeed, it contains genes encoding for SASP components of which activities are associated with tumor aggressiveness and/or worse patient prognosis (Yuan et al., 2017; Gilder et al., 2018; Morita and Hayashi, 2018; Yue et al., 2018; Chen et al., 2019; Angel et al., 2020). Furthermore, the high score of senescence correlates with a MES-like meta-module, also associated with a poor prognosis. Future studies are needed to determine if the senescence scoring in the diagnosis of patients with GBM at the time of the surgery improves the design of personalized treatment and effective combinatorial strategies.

In this study we show that senolytic treatments applied to GBM-bearing mice delay significantly tumor growth (Figures 2B, 2D and 2E). These findings raise the question of the benefit of combining senotherapy to improve response to other therapies. The field of senotherapies, which includes drugs eliminating senescent cells (senolytic drugs: anti- BCL2 and BCL-xL, Dasatinib and Quercitin, cardiac glycosides) or drugs inhibiting their function (senostatic drugs such as Metformin) is under active investigation (Moiseeva et al., 2013; Guerrero et al., 2019; Triana-Martínez et al., 2019; Wyld et al., 2020). A recent study reported in a MC38 mouse syngeneic tumor model, that Venetoclax (anti-BCL2) augments the antitumor efficacy of an anti-PD1 treatment by increasing the T effector memory cells although Venetoclax reduces the overall T cell number, a known function of the anti-apoptotic protein inhibitors (Kohlhapp et al., 2021). The authors reported the absence of cancer cell-intrinsic effects of the Venetoclax. In sharp contrast, our data provide evidence that the senolytic p16-3MR transgene in a GBM mouse model removes malignant senescent cells and mitigates the immunosuppressive phenotype, notably by increasing the T cell pool. This result suggests that senolytic treatment could prime GBM to respond to immunotherapy. This hypothesis is attractive as the immunotherapies with the anti-PD1 and PD-L1 antibodies did not show an extension of the overall survival in treating patients with recurrent GBM (Litak et al., 2019). One possible explanation for this failure could be that GBMs contain very few immune effector cells (Quail and Joyce, 2017). Further work on immunocompetent GBM models is now needed to evaluate the effect of novel senolytic/senostatic treatments on gliomagenesis and assess their efficacy as companion therapy.

ACKNOWLEDGEMENTS

The authors acknowledge the service of the ICM platforms: iGenSeq, iVector, icm-QUAN-Imaging, Pheno-ICMice, Histomics-Histology, Celis-Cell culture in particular David Akbar (Nikon confocal acquisition and 3D reconstruction), the service of the animal facility UMS28 (Sorbonne University) and the service of the flow cytometry platform CYTO-ICAN especially Florence Deknuydt (Hôpital Pitié-Salpétrière). The authors are grateful to Judith Campisi, Inder Verma, Magdalena Götz, Anton Berns and the Centro Nacional de Investigaciones Oncológicas (CNIO) for providing reagents and to Christopher Hubert for teaching the organoid technique. We also thank members of the Huillard-Sanson laboratory for discussions and help with the experiments, in particular Sophie Paris for teaching the intracranial injection. This work was supported by institutional fundings from Paris Brain Institute (ICM), the Institut National de la Santé Et de la Recherche Médicale and the Centre National de la Recherche Scientifique and grants from the ATIP-AVENIR (EH), the Cancéropole Ile de France (Emergence Program, ILR), the Ligue contre le cancer, comité Ile de France (ILR); the Fondation ARC pour la Recherche sur le Cancer (EH, ILR); the SIRIC-CURAMUS (joint Emergence program ILR and CA). R. Salam was supported by fellowships from the French Ministry of Education and Research and the Ligue Nationale Contre le Cancer; A. Saliou was supported by a fellowship from the Ligue Nationale Contre le Cancer.

AUTHOR CONTRIBUTIONS

Conceptualization, RS and ILR; Methodology, RS, AS, FB, CA, LB, JG and ILR; In vivo and in vitro experiments, RS, AS and ILR; Formal analysis, RS, AS, FB, MB, CA, LB, JG and ILR; Bioinformatics, MB, CA, AA, LB and JG; Resources, EH, FB and LC; Funding acquisition, EH, MS, CA and ILR. Writing - Original Draft, RS, AS, CA, LB, JG and ILR; Supervision, ILR.

DECLARATION OF INTERESTS

F. Bielle reports employment of next-of-kin from Bristol-Myers Squibb; research grants from Sanofi and Abbvie outside the submitted work; travel, accommodations expenses from Bristol-Myers Squibb for travel expenses, outside the submitted work.

Figure 1

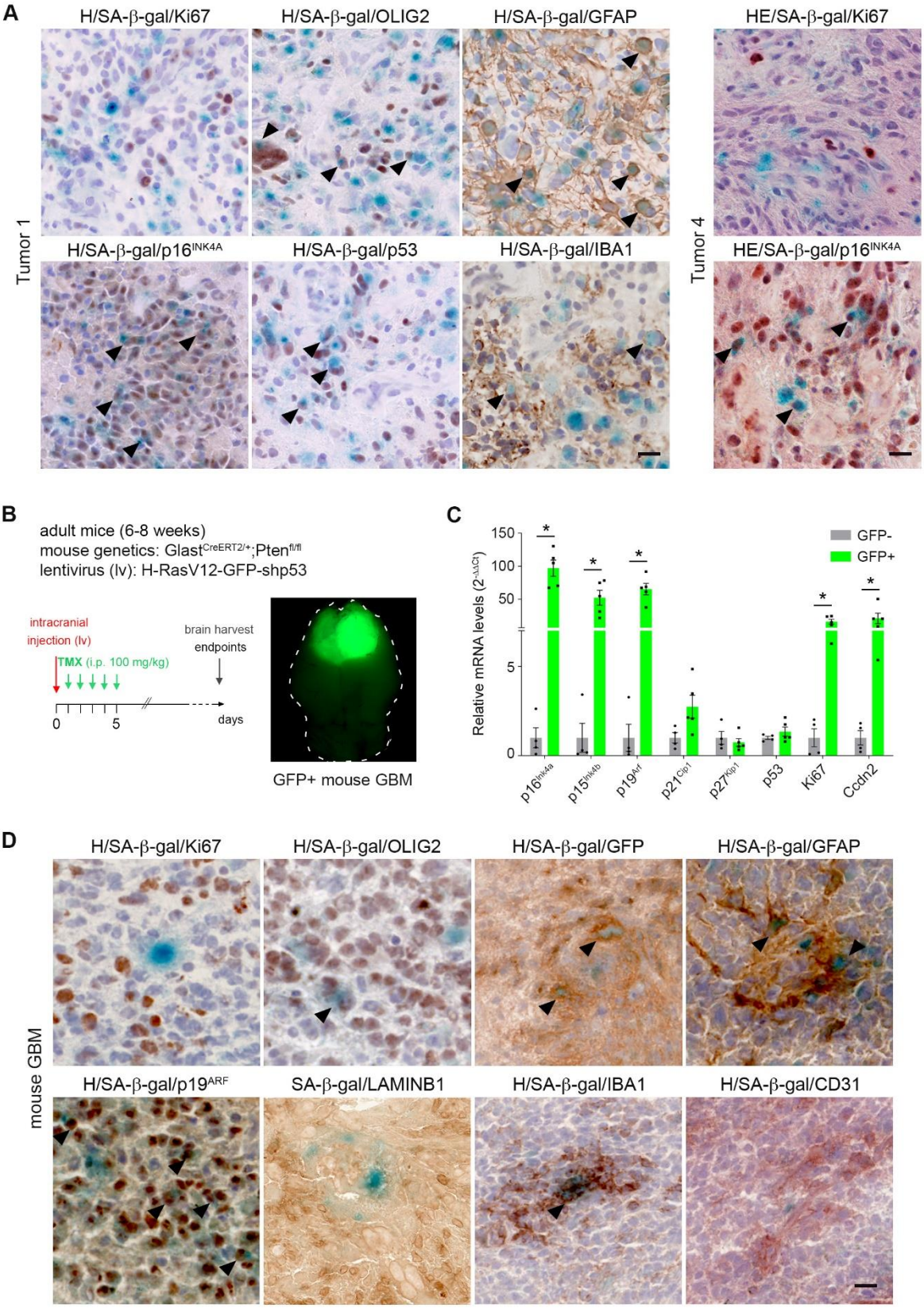
A
H/SA-β-gal/Ki67
H/SA-β-gal/OLIG2
H/SA-β-gal/GFAP
HE/SA-β-gal/Ki67
Tumor 1
Tumor 4
H/SA-β-gal/p16INK4A
H/SA-β-gal/p53
H/SA-β-gal/IBA1
HE/SA-β-gal/p16INK4A
B
adult mice (6-8 weeks)
mouse genetics: GlastCreERT2/+;Ptenfl/fl
lentivirus (lv): H-RasV12-GFP-shp53
intracranial injection (lv)
TMX (i.p. 100 mg/kg)
brain harvest endpoints
0
5
days
GFP+ mouse GBM
C
Relative mRNA levels (2-ΔΔCt)
GFP-
GFP+
p16Ink4a
p15Ink4b
p19Arf
p21Cip1
p27Kip1
p53
Ki67
Ccdn2
D
mouse GBM
H/SA-β-gal/Ki67
H/SA-β-gal/OLIG2
H/SA-β-gal/GFP
H/SA-β-gal/GFAP
H/SA-β-gal/p19ARF
SA-β-gal/LAMINB1
H/SA-β-gal/IBA1
H/SA-β-gal/CD31

Figure 1. Identification of senescent cells in patient and mouse GBMs.

(A) Representative SA-β-gal staining (blue) coupled with immunohistochemistry (IHC, brown) on two non-fixed patient GBM cryosections samples.

(B) Left: genetics of the mouse mesenchymal GBM model (mouse and injected lentivirus (lv)). The time line represents the induction of the tumorigenesis upon tamoxifen intraperitoneal (i.p.) injections (TMX, 1mg/kg/day for 5 days). Brains are harvested when mice reach end points. Right: representative stereomicroscopic image of a mouse brain with a GFP+ GBM.

(C) Relative transcript levels shown as ratios of normalized values of mouse GBM (GFP+, n=4) over surrounding parenchyma (GFP-, n=4). Statistical significance was determined by Wilcoxon-Mann-Whitney test (*, $p<0.05$).

(D) Representative SA-β-gal staining coupled with IHC on mouse GBM cryosections. A minimum of 4 GBMs were examined per antibody.

H: hematoxylin; HE: hematoxylin and eosin. Arrow heads in A, D point to double positive cells. Scale bars, A and D: 20 µm.

Figure S1

A

Name	Type	IHC	Molecular alterations	P/R/T	SA-β-gal
Tumor 1	GBM IDH mut	p53 overex	IDH1 mut	P	+
Tumor 2	GBM IDH wt			P	+
Tumor 3	GBM IDH wt	p53 overex		P	+
Tumor 4	GBM IDH wt	p53 overex		P	+
Tumor 5	AA III IDH mut	p53 overex	IDH1 mut	P	+
Tumor 6	O III		IDH1 mut; 1p19q codel; hTERT C250T; CICmut	P	+
Tumor 7	AA III IDH mut	p53 overex	IDH1 mut, p53 mut	P	+
Tumor 8	O III		IDH1 mut;1p19q codel; hTERT C250T; CICmut	P	+
Tumor 9	O III		IDH1 mut; 1p19q codel; hTERT C228T; CICmut	P	+
Tumor 10	O II		IDH1 mut; 1p19q codel; CICmut	P	+
Tumor 11	O II		IDH2 mut; 1p19q codel; hTERT C228T	P	-
Tumor 12	AA III IDH mut	p53 overex	IDH1 mut	R/T	+
Tumor 13	O III		IDH1 mut; 1p19q codel; hTERT C228T; PTENmut	R	+
Tumor 14	O III		IDH1 mut; 1p19q codel; hTERT C228T	R/T	+

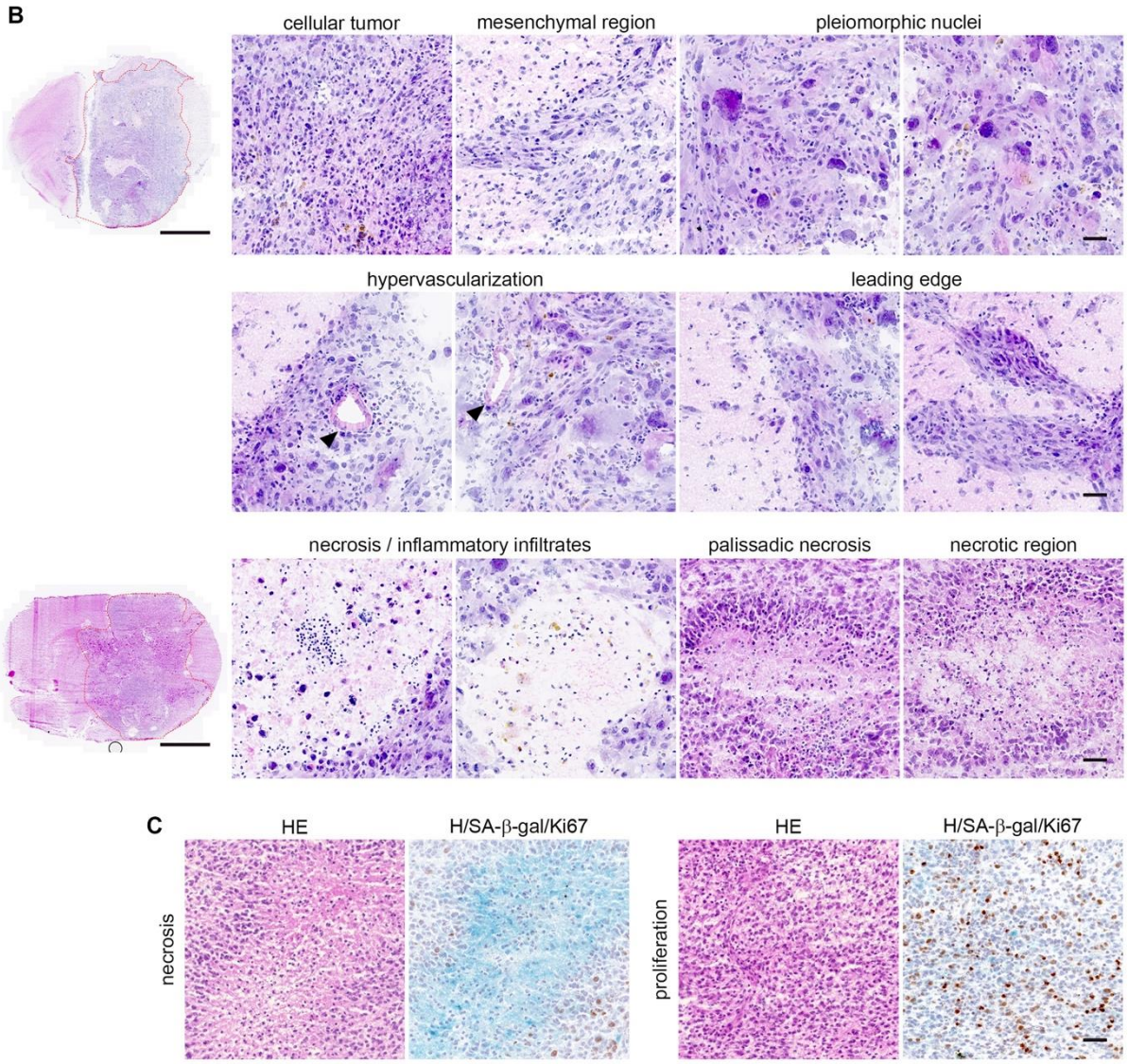

Figure S1. Identification of senescent cells in patient and mouse GBMs.

(A) Table recapitulating the patient resected gliomas stained for SA-β-gal. The presence of the SA-β-gal cells for each tumor is indicated by +. P: primary; R: recurrent; T: treated.

(B) Hematoxylin and eosin (HE) staining on mouse GBM cryosections. The two left panels correspond to low magnifications of the right panels. The GBM mouse model recapitulates the patient GBM histological features.

(C) HE and SA-β-gal/Ki67 staining on adjacent mouse GBM cryosections highlighting the presence SA-β-gal+ cells in proliferative and necrotic areas.

Scale bars, B left panels: 2 mm, right panels: 20 µm; C: 100 µm.

Figure 2

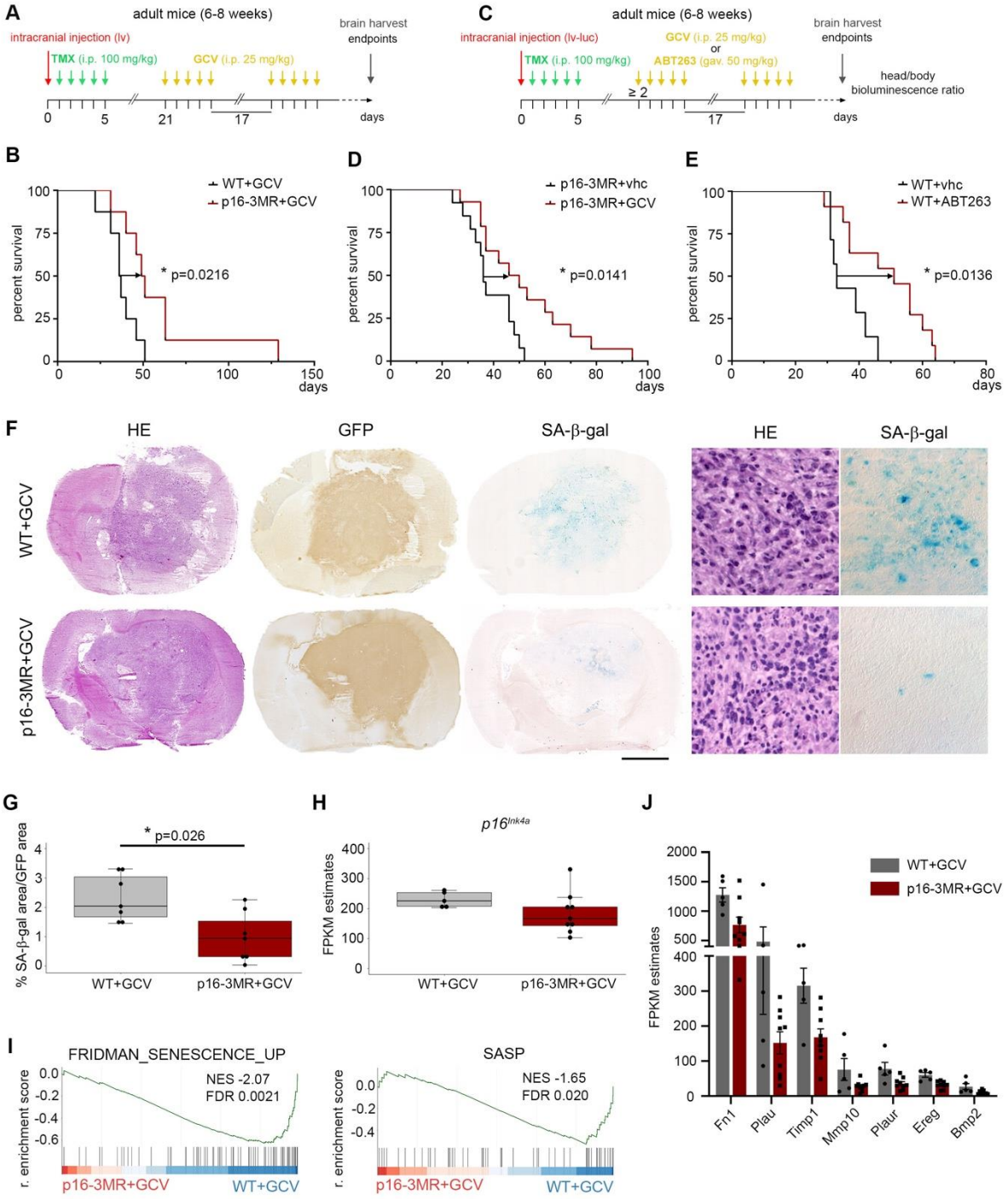
A
adult mice (6-8 weeks)
intracranial injection (iv)
TMX (i.p. 100 mg/kg)
GCV (i.p. 25 mg/kg)
brain harvest endpoints
0
5
21
17
days
C
adult mice (6-8 weeks)
intracranial injection (iv-luc)
TMX (i.p. 100 mg/kg)
GCV (i.p. 25 mg/kg)
or
ABT263 (gav. 50 mg/kg)
≥ 2
brain harvest endpoints
head/body bioluminescence ratio
0
5
17
days
B
WT+GCV
p16-3MR+GCV
percent survival
* p=0.0216
days
D
p16-3MR+vhc
p16-3MR+GCV
percent survival
* p=0.0141
days
E
WT+vhc
WT+ABT263
percent survival
* p=0.0136
days
F
HE
GFP
SA-β-gal
HE
SA-β-gal
WT+GCV
p16-3MR+GCV
G
* p=0.026
% SA-β-gal area/GFP area
WT+GCV
p16-3MR+GCV
H
p16Ink4a
FPKM estimates
WT+GCV
p16-3MR+GCV
J
WT+GCV
p16-3MR+GCV
FPKM estimates
Fn1
Plau
Timp1
Mmp10
Plaur
Ereg
Bmp2
I
FRIDMAN_SENESCENCE_UP
NES -2.07
FDR 0.0021
r. enrichment score
p16-3MR+GCV
WT+GCV
SASP
NES -1.65
FDR 0.020
r. enrichment score
p16-3MR+GCV
WT+GCV

Figure 2. Senescent cells removal increases the survival of GBM-bearing mice

(A) Timeline of tumorigenesis induction (lv: H-RasV12-GFP-shp53) and removal of $p16^{Ink4a}$ senescent cells by the p16-3MR transgene upon ganciclovir (GCV) i.p. injections, 21 days post lv injection.

(B) Kaplan-Meier survival curves of WT (n=8) and p16-3MR (n=8) mice treated with GCV. Statistical significance was determined by Mantel-Cox log-rank test (*, $p<0.05$).

(C) Timeline of tumorigenesis induction (lv-luc: H-RasV12-GFP-P2A-Luc2-shp53) and removal of senescent cells by the p16-3MR transgene upon GCV i.p. injections or ABT263 gavage when head to body bioluminescence ratio reached 2.

(D, E) Kaplan-Meier survival curves of p16-3MR mice treated with vehicle (vhc, n=13) or GCV (n=14) (D), and WT mice treated with vhc (n=7) or ABT263 (n=11) (E).

(F) Representative HE, GFP IHC and SA-β-Gal stainings on adjacent mouse GBM cryosections. GFP IHC was used to delineate the tumor area. Right panels represent higher magnifications of the left panels. Scale bars, F left panels: 2.5 mm, right panels: 20 µm.

(G) Quantification of the SA-β-Gal area over the tumor (GFP+) area. Statistical significance was determined by Wilcoxon-Mann-Whitney test (*, $p<0.05$).

(H) Relative transcript levels of $p16^{Ink4a}$, shown as FPKM estimates extracted from the bulk RNAseq analysis (WT+GCV, n=5; p16-3MR+GCV, n=9).

(I) GSEA graphs representing the enrichment score of two senescence pathways in p16-3MR+GCV GBMs compared to WT+GCV GBMs. The barcode plot indicates the position of the genes in each gene set; red represents positive Pearson's correlation with p16-3MR+GCV expression, blue with WT+GCV expression. The SASP gene list is a custom list established from Gorgoulis et al., 2019.

(J). Relative transcript levels of genes in WT+GCV and p16-3MR+GCV GBMs; FPKM estimates were extracted from bulk RNAseq data. These genes are differentially expressed between the two conditions (FDR<0.05; logFC>0.5).

lv: lentivirus; lv-luc: lentivirus-luciferase; i.p.: intraperitoneal; gav.: gavage; HE: hematoxylin eosin; r. enrichment score: running enrichment score. G, H: Data are represented as the mean ± SD.

Figure S2

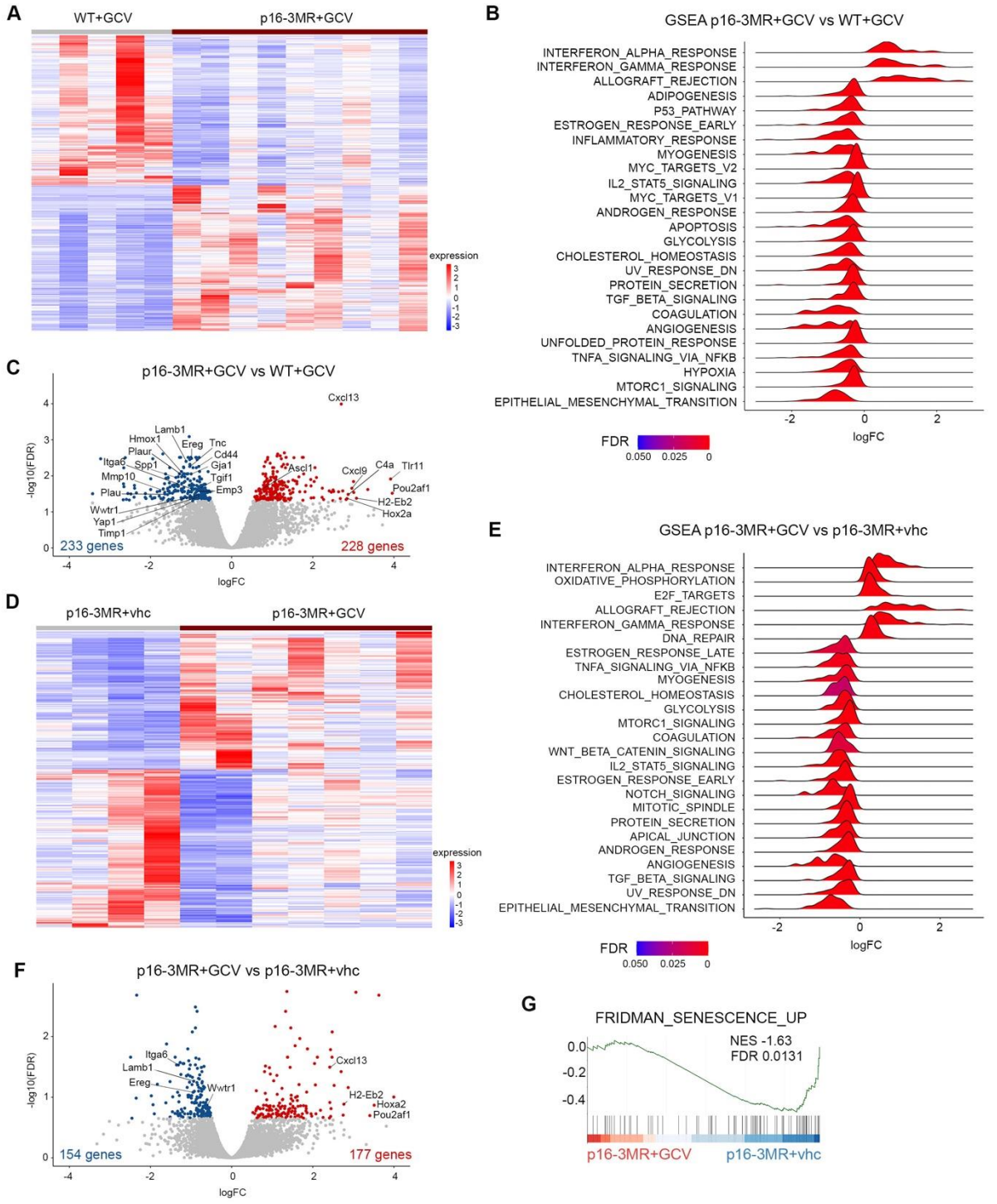
A
WT+GCV
p16-3MR+GCV
expression
B
GSEA p16-3MR+GCV vs WT+GCV
INTERFERON_ALPHA_RESPONSE
INTERFERON_GAMMA_RESPONSE
ALLOGRAFT_REJECTION
ADIPOGENESIS
P53_PATHWAY
ESTROGEN_RESPONSE_EARLY
INFLAMMATORY_RESPONSE
MYOGENESIS
MYC_TARGETS_V2
IL2_STAT5_SIGNALING
MYC_TARGETS_V1
ANDROGEN_RESPONSE
APOPTOSIS
GLYCOLYSIS
CHOLESTEROL_HOMEOSTASIS
UV_RESPONSE_DN
PROTEIN_SECRETION
TGF_BETA_SIGNALING
COAGULATION
ANGIOGENESIS
UNFOLDED_PROTEIN_RESPONSE
TNFA_SIGNALING_VIA_NFKB
HYPOXIA
MTORC1_SIGNALING
EPITHELIAL_MESENCHYMAL_TRANSITION
logFC
FDR
C
p16-3MR+GCV vs WT+GCV
-log10(FDR)
logFC
233 genes
228 genes
D
p16-3MR+vhc
p16-3MR+GCV
expression
E
GSEA p16-3MR+GCV vs p16-3MR+vhc
INTERFERON_ALPHA_RESPONSE
OXIDATIVE_PHOSPHORYLATION
E2F_TARGETS
ALLOGRAFT_REJECTION
INTERFERON_GAMMA_RESPONSE
DNA_REPAIR
ESTROGEN_RESPONSE_LATE
TNFA_SIGNALING_VIA_NFKB
MYOGENESIS
CHOLESTEROL_HOMEOSTASIS
GLYCOLYSIS
MTORC1_SIGNALING
COAGULATION
WNT_BETA_CATENIN_SIGNALING
IL2_STAT5_SIGNALING
ESTROGEN_RESPONSE_EARLY
NOTCH_SIGNALING
MITOTIC_SPINDLE
PROTEIN_SECRETION
APICAL_JUNCTION
ANDROGEN_RESPONSE
ANGIOGENESIS
TGF_BETA_SIGNALING
UV_RESPONSE_DN
EPITHELIAL_MESENCHYMAL_TRANSITION
logFC
FDR
F
p16-3MR+GCV vs p16-3MR+vhc
-log10(FDR)
logFC
154 genes
177 genes
G
FRIDMAN_SENESCENCE_UP
NES -1.63
FDR 0.0131
p16-3MR+GCV
p16-3MR+vhc

Figure S2. Senescent cells removal increases the survival of GBM-bearing mice

(A-C). Bulk RNAseq analysis of p16-3MR+GCV (n=9) compared with WT+GCV (n=5) GBMs collected at the end points of the mice.

(A) Heatmaps of the differentially expressed (DE) genes (FDR<0.05; logFC>0.5).

(B). GSEA ridge plots of the most significant representative Hallmark gene lists.

(C) Volcano plots of the DE genes. D-F. Bulk RNAseq analysis of p16-3MR+GCV (n=7) compared with p16-3MR+vhc GBMs (n=4) collected at the end points of the mice.

(D) Heatmaps of the DE genes (FDR<0.05; logFC>0.5).

(E) GSEA ridge plots of the most significant representative Hallmark gene lists.

(F) Volcano plots of the DE genes. Annotated genes are common to those in C.

(G) GSEA graph representing the enrichment score of the Fridman senescence pathway in p16-3MR+GCV compared with p16-3MR+vhc GBMs.

Figure 3

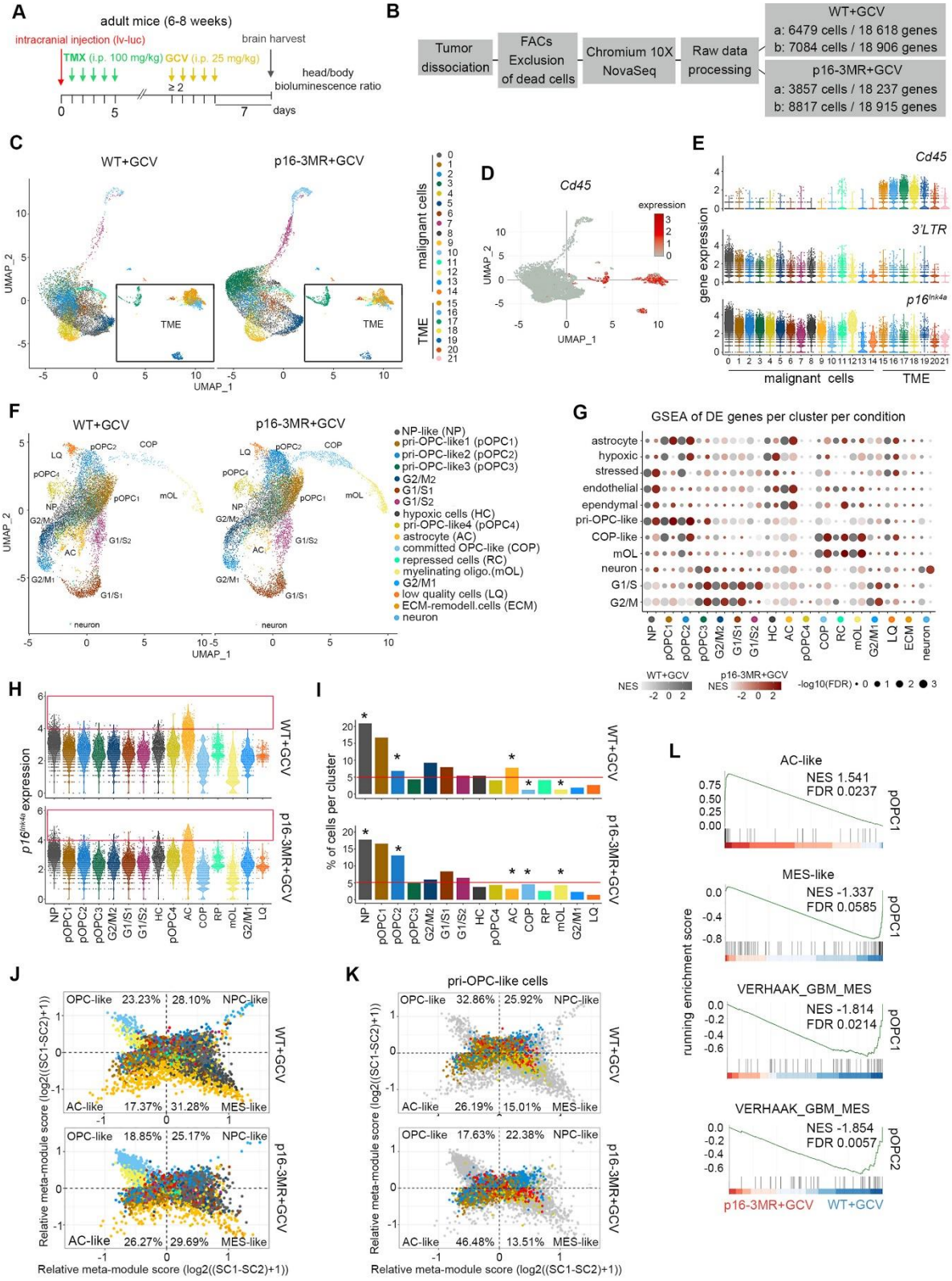
A
adult mice (6-8 weeks)
intracranial injection (lv-luc)
brain harvest
TMX (i.p. 100 mg/kg) GCV (i.p. 25 mg/kg)
head/body bioluminescence ratio
≥ 2
0
5
7
days
B
Tumor dissociation
FACs Exclusion of dead cells
Chromium 10X NovaSeq
Raw data processing
WT+GCV
a: 6479 cells / 18 618 genes
b: 7084 cells / 18 906 genes
p16-3MR+GCV
a: 3857 cells / 18 237 genes
b: 8817 cells / 18 915 genes
C
WT+GCV
p16-3MR+GCV
TME
UMAP_1
UMAP_2
malignant cells
TME
D
Cd45
expression
E
Cd45
3'LTR
p16Ink4a
gene expression
malignant cells
TME
F
WT+GCV
p16-3MR+GCV
NP-like (NP)
pri-OPC-like1 (pOPC1)
pri-OPC-like2 (pOPC2)
pri-OPC-like3 (pOPC3)
G2/M2
G1/S1
G1/S2
hypoxic cells (HC)
pri-OPC-like4 (pOPC4)
astrocyte (AC)
committed OPC-like (COP)
repressed cells (RC)
myelinating oligo.(mOL)
G2/M1
low quality cells (LQ)
ECM-remodell.cells (ECM)
neuron
G
GSEA of DE genes per cluster per condition
astrocyte
hypoxic
stressed
endothelial
ependymal
pri-OPC-like
COP-like
mOL
neuron
G1/S
G2/M
NES
-log10(FDR)
H
p16Ink4a expression
WT+GCV
p16-3MR+GCV
I
% of cells per cluster
J
OPC-like 23.23% 28.10% NPC-like
AC-like 17.37% 31.28% MES-like
OPC-like 18.85% 25.17% NPC-like
AC-like 26.27% 29.69% MES-like
Relative meta-module score (log2((SC1-SC2)+1))
K
pri-OPC-like cells
OPC-like 32.86% 25.92% NPC-like
AC-like 26.19% 15.01% MES-like
OPC-like 17.63% 22.38% NPC-like
AC-like 46.48% 13.51% MES-like
L
AC-like
NES 1.541
FDR 0.0237
MES-like
NES -1.337
FDR 0.0585
VERHAAK_GBM_MES
NES -1.814
FDR 0.0214
VERHAAK_GBM_MES
NES -1.854
FDR 0.0057
running enrichment score
pOPC1
pOPC2
p16-3MR+GCV
WT+GCV

Figure 3. Identification of p16$^{Ink4a\ Hi}$ cells in a subset of malignant cells

(A) Timeline of the mouse GBM generation for scRNAseq at the early timepoint.

(B) Scheme of the scRNAseq experiment.

(C) UMAP plots of WT+GCV (n=2) and p16-3MR+GCV (n=2) GBM cells at a 0.5 resolution and annotated malignant cells and tumor microenvironment (TME) cells.

(D) UMAP plots of the expression of the pan-leucocyte marker *Cd45* in WT+GCV GBM cells.

(E) Violin plots of the expression of *Cd45*, 3'*LTR* and *p16^{Ink4a}* WT+GCV GBM cells per cluster.

(F) UMAP plots of WT+GCV (n=2) and p16-3MR+GCV (n=2) GBM malignant cells and annotated cell type at a 0.6 resolution.

(G) GSEA dot plots of DE genes (FDR<0.05; avlogFC>0.25) in WT+GCV (grey dots) and p16-3MR+GCV (red dots) GBMs of gene lists from Weng *et al.* 2019.

(H) Violin plots of the expression of *p16^{Ink4a}* in malignant cells per cluster. The red box indicates the cells with an expression of *p16^{Ink4a}* ε 4 (p16$^{Ink4a\ Hi}$ cells).

(I) Barplots representing the percentage of malignant cells per cluster in WT+GCV and p16-3MR+GCV GBMs. The asterisk points to clusters which cell number varies between the two conditions.

(J) Two-dimensional (2-D) representations of cellular states of malignant cells. Each quadrant corresponds to one cellular state, the exact position of malignant cells reflects their relative scores for the meta-modules as previously described (Neftel et al., 2019), and their colors correspond to clusters.

(K) 2-D representations of cellular states of the pri-OPC-like cells.

(L) GSEA graphs representing the enrichment score of cellular states and transcriptional GBM subtypes in pri-OPC-like clusters in p16-3MR+GCV compared to WT+GCV GBMs.

Figure S3

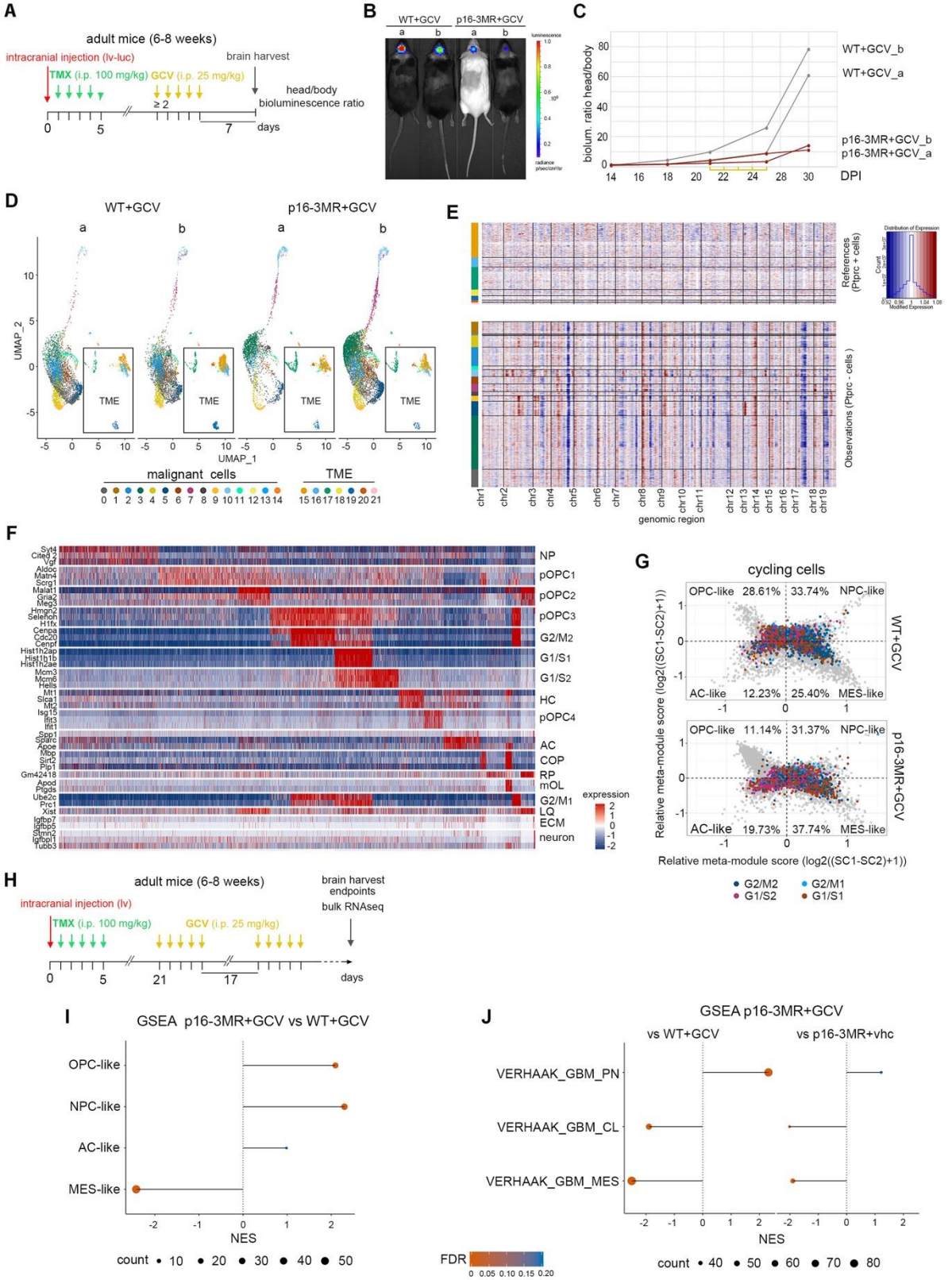
A
adult mice (6-8 weeks)
intracranial injection (lv-luc)
brain harvest
TMX (i.p. 100 mg/kg) GCV (i.p. 25 mg/kg)
≥ 2
head/body bioluminescence ratio
0
5
7
days
B
WT+GCV
p16-3MR+GCV
a
b
a
b
C
biolum. ratio head/body
WT+GCV_b
WT+GCV_a
p16-3MR+GCV_b
p16-3MR+GCV_a
DPI
D
WT+GCV
p16-3MR+GCV
UMAP_2
UMAP_1
TME
malignant cells
E
References (Ptprc + cells)
Observations (Ptprc - cells)
genomic region
F
NP
pOPC1
pOPC2
pOPC3
G2/M2
G1/S1
G1/S2
HC
pOPC4
AC
COP
RP
mOL
G2/M1
LQ
ECM
neuron
expression
G
cycling cells
OPC-like 28.61% 33.74% NPC-like
AC-like 12.23% 25.40% MES-like
OPC-like 11.14% 31.37% NPC-like
AC-like 19.73% 37.74% MES-like
WT+GCV
p16-3MR+GCV
Relative meta-module score (log2((SC1-SC2)+1))
G2/M2
G1/S2
G2/M1
G1/S1
H
adult mice (6-8 weeks)
intracranial injection (lv)
TMX (i.p. 100 mg/kg)
GCV (i.p. 25 mg/kg)
brain harvest endpoints
bulk RNAseq
0
5
21
17
days
I
GSEA p16-3MR+GCV vs WT+GCV
OPC-like
NPC-like
AC-like
MES-like
NES
count
J
GSEA p16-3MR+GCV
vs WT+GCV
vs p16-3MR+vhc
VERHAAK_GBM_PN
VERHAAK_GBM_CL
VERHAAK_GBM_MES
NES
FDR
count

Figure S3. Identification of p16$^{Ink4a\ Hi}$ cells in a subset of malignant cells

(A) Timeline of the mouse GBMs generation for scRNAseq at the early timepoint.

(B) *In vivo* bioluminescence imaging of WT+GCV and p16-3MR+GCV GBM-bearing mice.

(C) Graph representing the head to body ratio bioluminescence of GBM-bearing mice over time. Yellow lines correspond to GCV injections.

(D) UMAP plots of WT+GCV and p16-3MR+GCV GBM cells per biological sample at a 0.5 resolution and annotated malignant cells and cells from the tumor microenvironment (TME).

(E) Heatmap representing inference of chromosomal copy number variations (CNVs) in WT+GCV GBMs with cells as rows, grouped in clusters, and genes as columns, ordered according to chromosome.

(F) Heatmap of the top 3 DE genes (FDR<0.05; avlogFC>0.25) in malignant clusters (0.6 resolution) in WT+GCV GBMs. When the same gene is DE in more than one cluster, it appears only once.

(G) 2-D representation of the cellular states of the cycling cells (G2/M and G1/S clusters).

(H) Timeline of the mouse GBMs generation for bulk RNAseq at the late timepoint.

(I) GSEA dot plots representing the enrichment score of cellular states in p16-3MR+GCV compared with WT+GCV GBMs.

(J) GSEA dot plots representing the enrichment score of GBM transcriptional subtype in p16-3MR+GCV compared with WT+GCV GBMs. NES: normalized enrichment score.

Figure 4

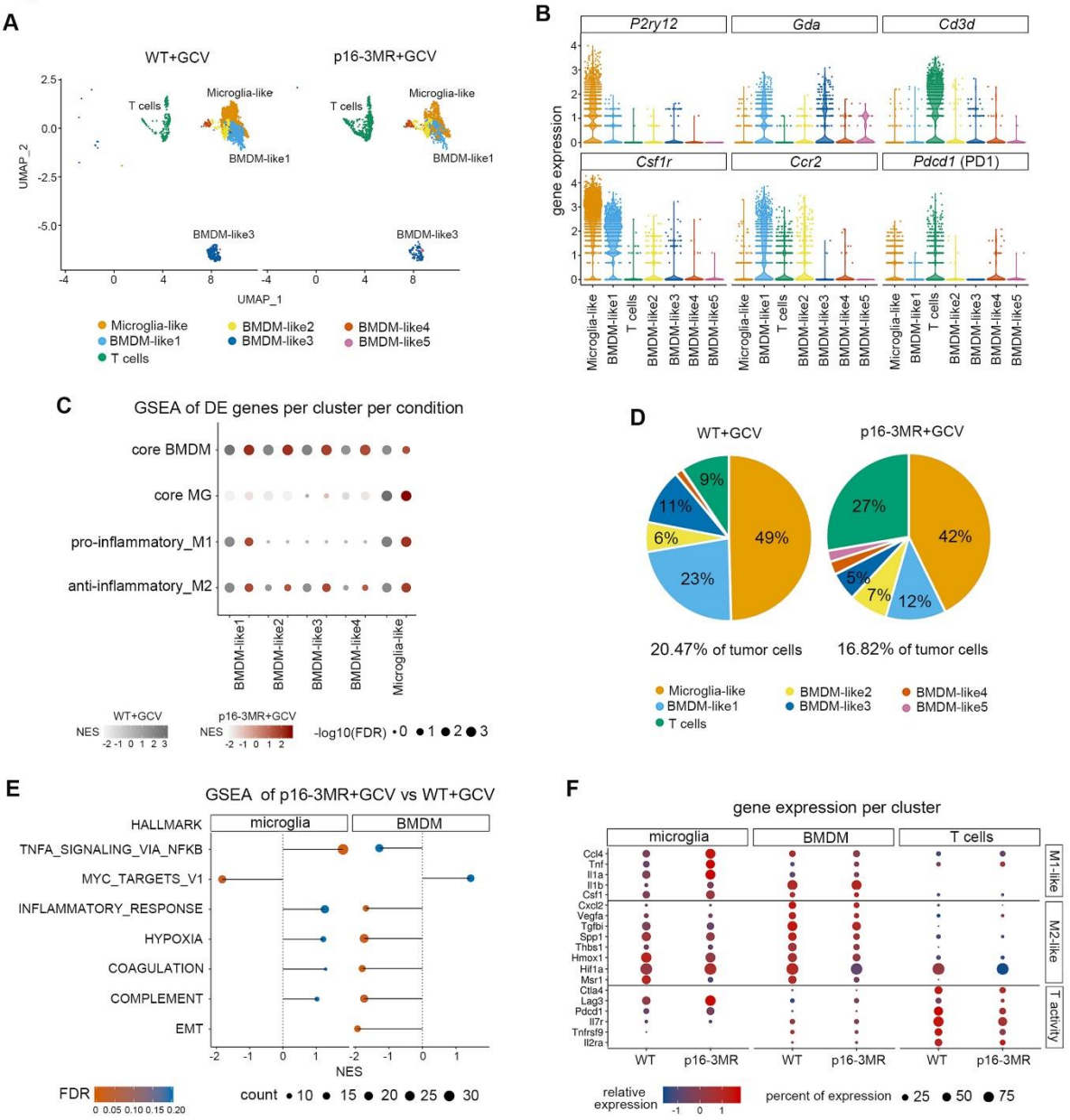
A
WT+GCV
p16-3MR+GCV
T cells
Microglia-like
BMDM-like1
BMDM-like3
UMAP_2
UMAP_1
Microglia-like
BMDM-like1
T cells
BMDM-like2
BMDM-like3
BMDM-like4
BMDM-like5
B
P2ry12
Gda
Cd3d
Csf1r
Ccr2
Pdcd1 (PD1)
gene expression
C
GSEA of DE genes per cluster per condition
core BMDM
core MG
pro-inflammatory_M1
anti-inflammatory_M2
BMDM-like1
BMDM-like2
BMDM-like3
BMDM-like4
Microglia-like
WT+GCV
p16-3MR+GCV
NES
-log10(FDR)
D
WT+GCV
p16-3MR+GCV
9%
11%
6%
49%
23%
27%
42%
5%
7%
12%
20.47% of tumor cells
16.82% of tumor cells
E
GSEA of p16-3MR+GCV vs WT+GCV
HALLMARK
TNFA_SIGNALING_VIA_NFKB
MYC_TARGETS_V1
INFLAMMATORY_RESPONSE
HYPOXIA
COAGULATION
COMPLEMENT
EMT
microglia
BMDM
NES
FDR
count
F
gene expression per cluster
microglia
BMDM
T cells
Ccl4
Tnf
Il1a
Il1b
Csf1
Cxcl2
Vegfa
Tgfbi
Spp1
Thbs1
Hmox1
Hif1a
Msr1
Ctla4
Lag3
Pdcd1
Il7r
Tnfrsf9
Il2ra
M1-like
M2-like
T activity
WT
p16-3MR
relative expression
percent of expression

Figure 4. Modulation of the immune compartment following p16$^{Ink4a\ Hi}$ cells removal

(A) UMAP plots of *Cd45*+ cells in WT+GCV and p16-3MR+GCV GBMs at a 0.5 resolution and annotated cell type.

(B) Violin plots representing the expression of selected DE genes (FDR<0.05; avlogFC>0.25) per cluster in WT+GCV GBMs.

(C) GSEA dot plot of DE genes (FDR<0.05; avlogFC>0.25) in WT+GCV (grey dots) and p16-3MR+GCV (red dots) *Cd45*+ clusters of core-BMDM, core-microglia (MG), pro-inflammatory and anti-inflammatory pathways as defined in Bowman et al., 2016 and Darmanis et al., 2017.

(D) Chart pies representing the percentage of *Cd45*+ cells per cluster in WT+GCV and p16-3MR+GCV GBMs.

(E) GSEA dot plots representing the enrichment score of Hallmark gene lists in p16-3MR compared to WT+GCV GBM clusters.

(F) Dot plots of the relative expression of selected genes in WT+GCV and p16-3MR+GCV GBM clusters.

Figure S4

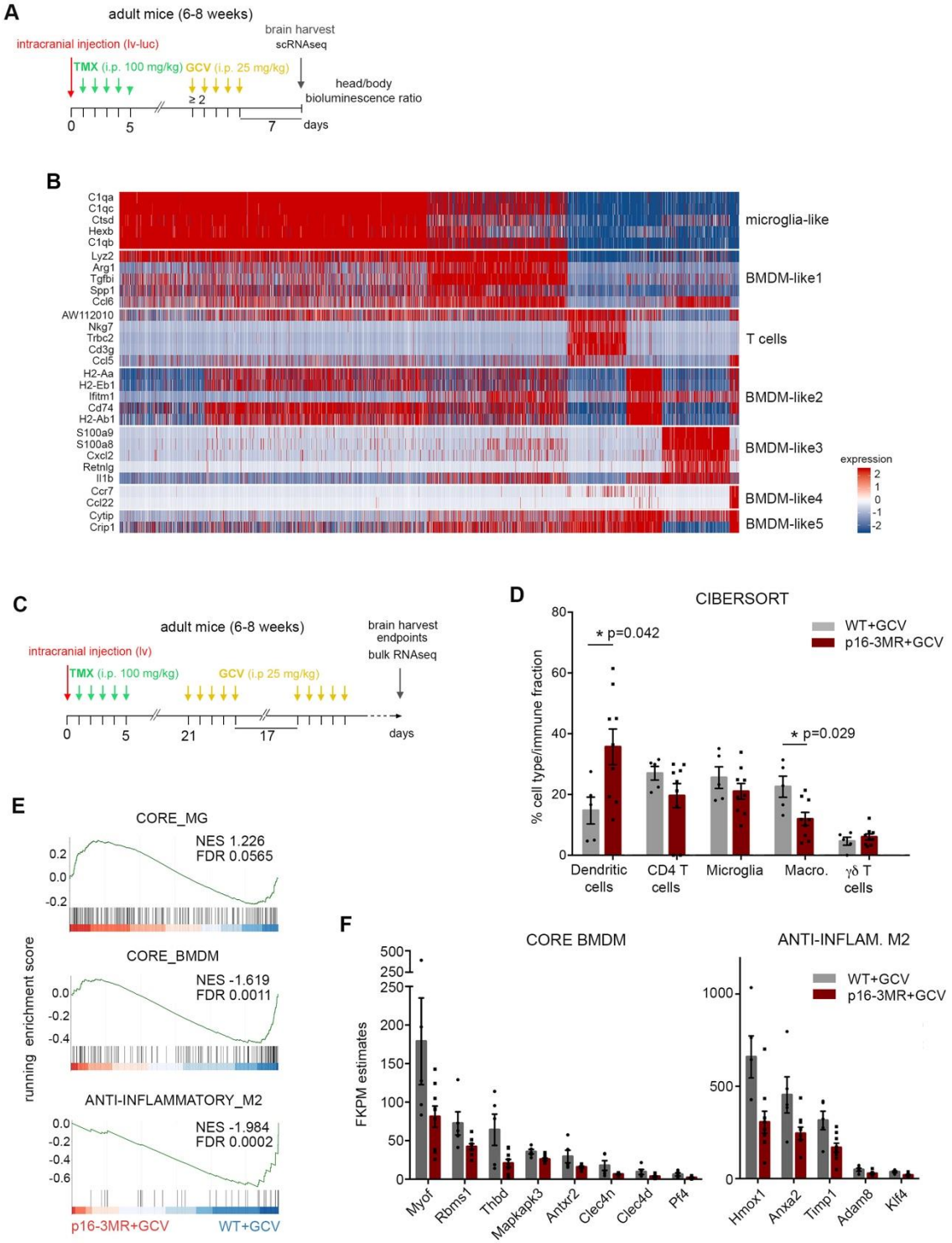
A
adult mice (6-8 weeks)
brain harvest
scRNAseq
intracranial injection (lv-luc)
TMX (i.p. 100 mg/kg) GCV (i.p. 25 mg/kg)
≥ 2
head/body
bioluminescence ratio
0
5
7
days
B
C1qa
C1qc
Ctsd
Hexb
C1qb
microglia-like
Lyz2
Arg1
Tgfbi
Spp1
Ccl6
BMDM-like1
AW112010
Nkg7
Trbc2
Cd3g
Ccl5
T cells
H2-Aa
H2-Eb1
Ifitm1
Cd74
H2-Ab1
BMDM-like2
S100a9
S100a8
Cxcl2
Retnlg
Il1b
BMDM-like3
Ccr7
Ccl22
BMDM-like4
Cytip
Crip1
BMDM-like5
expression
2
1
0
-1
-2
C
adult mice (6-8 weeks)
brain harvest
endpoints
bulk RNAseq
intracranial injection (lv)
TMX (i.p. 100 mg/kg)
GCV (i.p 25 mg/kg)
0
5
21
17
days
D
CIBERSORT
WT+GCV
p16-3MR+GCV
* p=0.042
* p=0.029
% cell type/immune fraction
Dendritic cells
CD4 T cells
Microglia
Macro.
γδ T cells
E
CORE_MG
NES 1.226
FDR 0.0565
CORE_BMDM
NES -1.619
FDR 0.0011
ANTI-INFLAMMATORY_M2
NES -1.984
FDR 0.0002
running enrichment score
p16-3MR+GCV
WT+GCV
F
CORE BMDM
ANTI-INFLAM. M2
WT+GCV
p16-3MR+GCV
FKPM estimates
Myof
Rbms1
Thbd
Mapkapk3
Antxr2
Clec4n
Clec4d
Pf4
Hmox1
Anxa2
Timp1
Adam8
Klf4

Figure S4. Modulation of the immune compartment following p16$^{Ink4a\ Hi}$ cells removal

(A) Timeline of the mouse GBM generation for scRNAseq.

(B) Heatmap of the top 5 DE genes (FDR<0.05; avlogFC>0.25) in *Cd45*+ clusters (0.5 resolution) in WT+GCV GBMs. When the same gene is DE in more than one cluster, it appears only once.

(C) Timeline of the mouse GBM generation for bulk RNAseq.

(D) Bar plot representing the estimation of the abundance of immune cell types in WT+GCV and p16-3MR+GCV GBMs using CIBERSORT (reference data set GSE124829). Statistical significance was determined by Wilcoxon-Mann-Whitney test (*, p<0.05).

(E) GSEA graphs representing the enrichment score of CORE_MG (microglia), CORE_BMDM and ANTI_INFLAMMATORY_M2 pathways (Bowman et al., 2016; Darmanis et al., 2017) in p16-3MR+GCV compared with WT+GCV GBMs at endpoints.

(F) Relative transcript levels of genes in WT+GCV and p16-3MR+GCV GBMs; FPKM estimates were extracted from bulk RNAseq data. These genes from the CORE_BMDM and ANTI_INFLAMMATORY_M2 gene lists are DE between the two conditions (FDR<0.05; logFC>0.5).

Figure 5

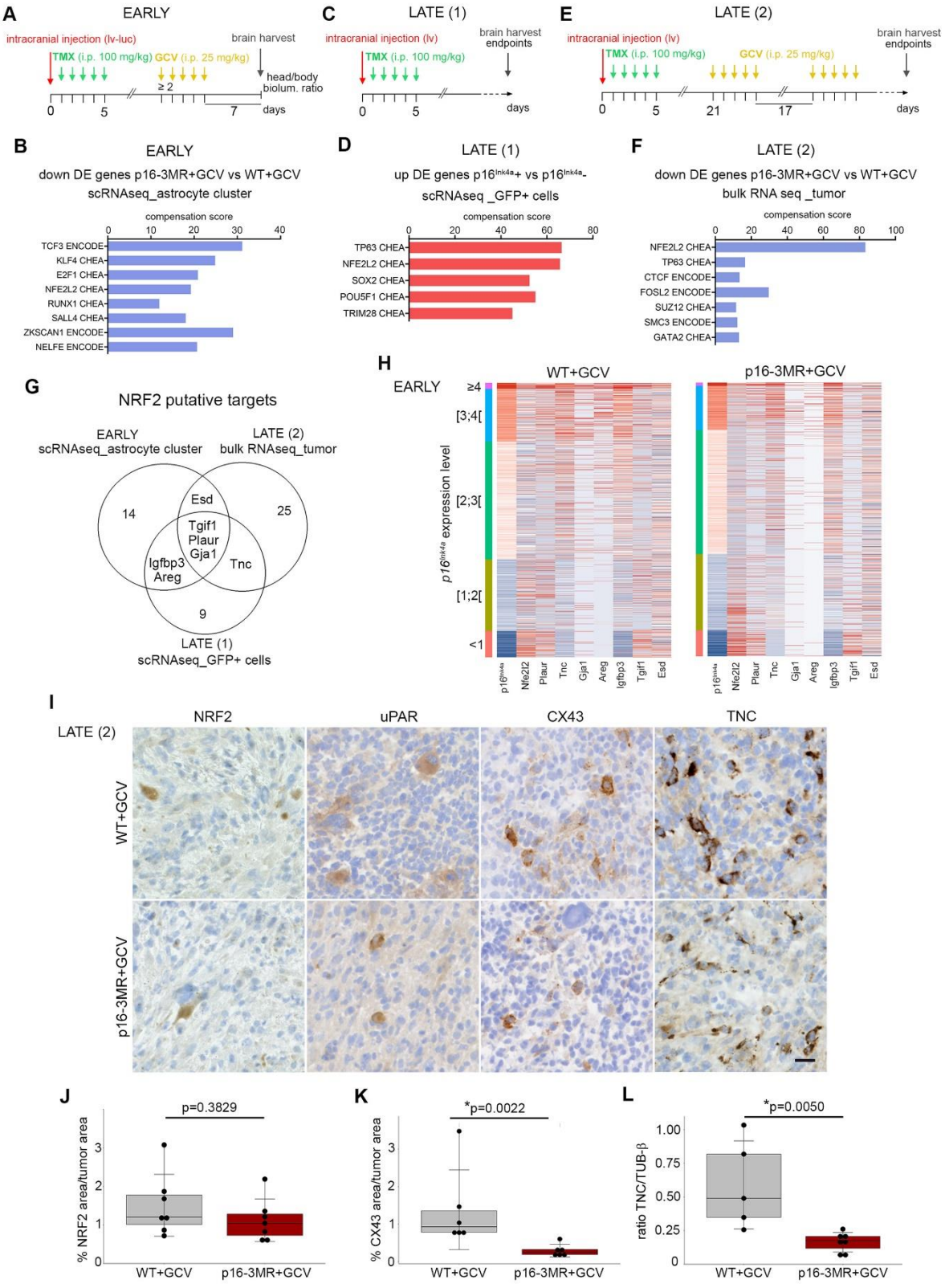
A
EARLY
intracranial injection (lv-luc)
brain harvest
TMX (i.p. 100 mg/kg) GCV (i.p. 25 mg/kg)
≥ 2
head/body biolum. ratio
0
5
7
days
C
LATE (1)
intracranial injection (lv)
brain harvest endpoints
TMX (i.p. 100 mg/kg)
0
5
days
E
LATE (2)
intracranial injection (lv)
brain harvest endpoints
TMX (i.p. 100 mg/kg)
GCV (i.p. 25 mg/kg)
0
5
21
17
days
B
EARLY
down DE genes p16-3MR+GCV vs WT+GCV
scRNAseq_astrocyte cluster
compensation score
TCF3 ENCODE
KLF4 CHEA
E2F1 CHEA
NFE2L2 CHEA
RUNX1 CHEA
SALL4 CHEA
ZKSCAN1 ENCODE
NELFE ENCODE
D
LATE (1)
up DE genes p16Ink4a+ vs p16Ink4a-
scRNAseq _GFP+ cells
compensation score
TP63 CHEA
NFE2L2 CHEA
SOX2 CHEA
POU5F1 CHEA
TRIM28 CHEA
F
LATE (2)
down DE genes p16-3MR+GCV vs WT+GCV
bulk RNA seq _tumor
compensation score
NFE2L2 CHEA
TP63 CHEA
CTCF ENCODE
FOSL2 ENCODE
SUZ12 CHEA
SMC3 ENCODE
GATA2 CHEA
G
NRF2 putative targets
EARLY
scRNAseq_astrocyte cluster
LATE (2)
bulk RNAseq_tumor
LATE (1)
scRNAseq_GFP+ cells
14
25
9
Esd
Tgif1
Plaur
Gja1
Igfbp3
Areg
Tnc
H
WT+GCV
p16-3MR+GCV
EARLY
≥4
[3;4[
[2;3[
[1;2[
<1
p16Ink4a expression level
p16Ink4a
Nfe2l2
Plaur
Tnc
Gja1
Areg
Igfbp3
Tgif1
Esd
I
LATE (2)
NRF2
uPAR
CX43
TNC
WT+GCV
p16-3MR+GCV
J
p=0.3829
% NRF2 area/tumor area
WT+GCV
p16-3MR+GCV
K
*p=0.0022
% CX43 area/tumor area
WT+GCV
p16-3MR+GCV
L
*p=0.0050
ratio TNC/TUB-β
WT+GCV
p16-3MR+GCV

Figure 5. NRF2 activity in p16^{Ink4aHi} cells can mediate pro-tumoral senescent functions

(A) Timeline of the mouse GBM generation for scRNAseq at the early timepoint.

(B) Barplot corresponding to significantly enriched pathways (ENCODE and ChEA consensus TFs from ChIP-X, Enrichr) in differentially downregulated genes (FDR<0.05; avlogFC>0.25) in the p16-3MR+GCV compared with the WT+GCV astrocyte clusters from the scRNAseq data (as shown in A).

(C) Timeline of the mouse GBM generation for scRNAseq at the late timepoint.

(D) Barplot corresponding to significantly enriched pathways in differentially up-regulated genes (FDR<0.05; logFC>0.5) in p16^{Ink4a} positive vs p16^{Ink4a} negative malignant cells from the scRNAseq data (as shown in C).

(E) Timeline of the mouse GBM generation for bulk RNAseq at the late timepoint.

(F) Barplot corresponding to significantly enriched pathways in differentially down-regulated genes (FDR<0.05; logFC>0.5) in p16-3MR+GCV compared with WT+GCV GBMs from the bulk RNAseq data (as shown in E).

(G) Venn diagram of NRF2 putative targets between the 3 gene sets.

(H) Heatmaps of *Nrf2* and its 7 identified putative targets in WT+GCV and p16-3MR GBMs. Cells are classified in 5 categories according to *p16^{Ink4a}* expression levels.

(I) Representative IHC staining on mouse GBM cryosections at the late timepoint. H: hematoxylin. A minimum of 3 GBMs was analyzed per antibody in the two conditions. Scale bar, I: 20 µm.

(J) Quantification of the NRF2 area (IHC) over the tumor area (WT+GCV, n=7; p16-3MR+GCV, n=7).

(K) Quantification of the CX43 area (IHC) over the tumor area (WT+GCV, n=5; p16-3MR+GCV, n=6).

(L) Quantification of the ratio of TNC over β-TUBULIN expression (western blot) (WT+GCV, n=5; p16-3MR+GCV, n=7).

Data in I, J and K are represented as the mean ± SD. Statistical significance was determined by Wilcoxon-Mann-Whitney test (*, p<0.05).

Figure S5

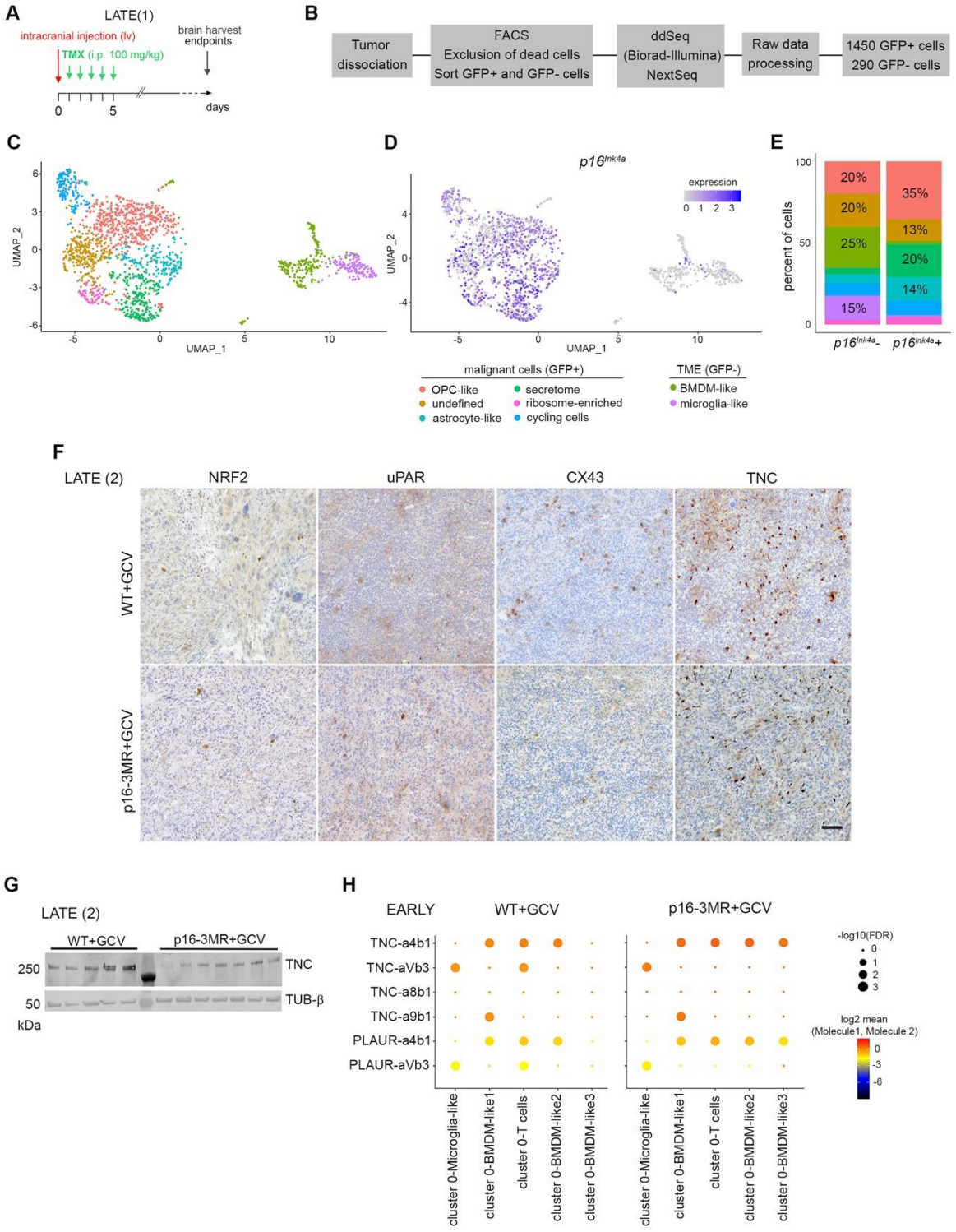
A
LATE(1)
intracranial injection (Iv)
TMX (i.p. 100 mg/kg)
brain harvest endpoints
0
5
days
B
Tumor dissociation
FACS
Exclusion of dead cells
Sort GFP+ and GFP- cells
ddSeq
(Biorad-Illumina)
NextSeq
Raw data processing
1450 GFP+ cells
290 GFP- cells
C
UMAP_2
UMAP_1
D
p16Ink4a
expression
0 1 2 3
malignant cells (GFP+)
OPC-like
undefined
astrocyte-like
secretome
ribosome-enriched
cycling cells
TME (GFP-)
BMDM-like
microglia-like
E
percent of cells
20%
20%
25%
15%
35%
13%
20%
14%
p16Ink4a- p16Ink4a+
F
LATE (2)
NRF2
uPAR
CX43
TNC
WT+GCV
p16-3MR+GCV
G
LATE (2)
WT+GCV
p16-3MR+GCV
250
50
kDa
TNC
TUB-β
H
EARLY
WT+GCV
p16-3MR+GCV
TNC-a4b1
TNC-aVb3
TNC-a8b1
TNC-a9b1
PLAUR-a4b1
PLAUR-aVb3
-log10(FDR)
0
1
2
3
log2 mean
(Molecule1, Molecule 2)
0
-3
-6
cluster 0-Microglia-like
cluster 0-BMDM-like1
cluster 0-T cells
cluster 0-BMDM-like2
cluster 0-BMDM-like3

Figure S5. NRF2 activity in p16^{Ink4aHi} cells can mediate pro-tumoral senescent functions

(A) Timeline of the mouse GBM generation for scRNAseq at the late timepoint.

(B) Scheme of the scRNAseq experiment.

(C) UMAP plots of GBM cells and annotated cell type at a 0.6 resolution.

(D) UMAP plots of the expression of *p16^{Ink4a}* in GBM cells.

(E) Barplot representing the percentage of cells per cluster positive and negative for *p16^{Ink4a}* expression.

(F) Representative IHC staining on mouse GBM cryosections at the late timepoint. H: hematoxylin counterstaining. Scale bar: 40 µm.

(G) Western blot for TNC from GBMs collected at the late timepoint.

(H) Dot plot representing ligand-receptor interactions between the cluster 0 and the immune clusters in the scRNAseq data at the early timepoint using CellPhoneDB. The colors indicate the mean expression of the ligand-receptor complexes.

Figure 6

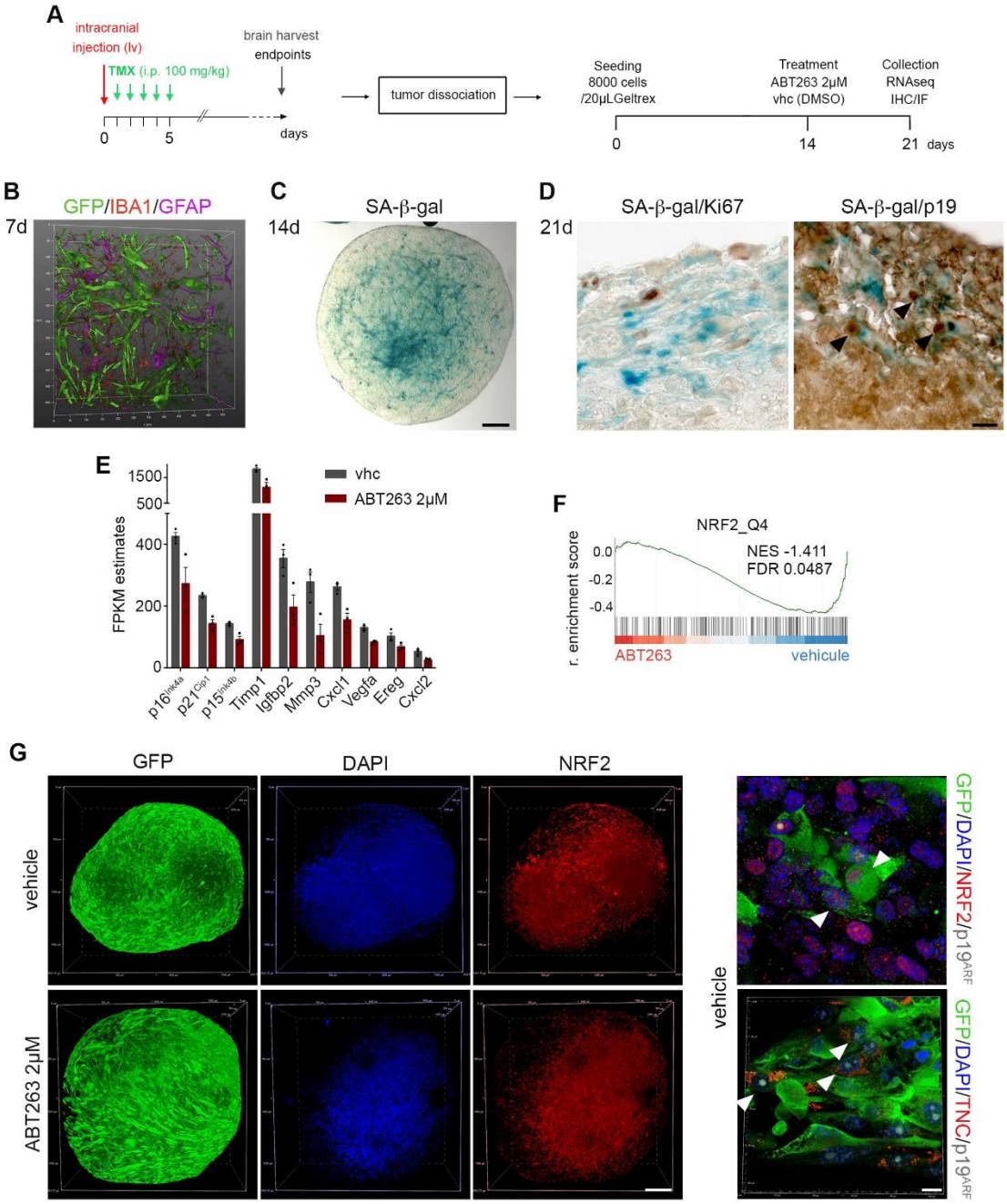
A
intracranial injection (Iv)
TMX (i.p. 100 mg/kg)
brain harvest endpoints
0
5
days
tumor dissociation
Seeding 8000 cells /20µLGeltrex
Treatment ABT263 2µM vhc (DMSO)
Collection RNAseq IHC/IF
0
14
21 days
B
7d
GFP/IBA1/GFAP
C
14d
SA-β-gal
D
21d
SA-β-gal/Ki67
SA-β-gal/p19
E
FPKM estimates
vhc
ABT263 2µM
p16Ink4a
p21Cip1
p15Ink4b
Timp1
Igfbp2
Mmp3
Cxcl1
Vegfa
Ereg
Cxcl2
F
NRF2_Q4
NES -1.411
FDR 0.0487
r. enrichment score
ABT263
vehicule
G
GFP
DAPI
NRF2
vehicle
ABT263 2µM
GFP/DAPI/NRF2/p19ARF
GFP/DAPI/TNC/p19ARF

Figure 6. Senolytic treatment in mouse GBM-derived organoids decreases NRF2 signaling

(A) Scheme of the mouse GBM-derived organoid generation.

(B) Whole mount immunofluorescence of organoids after 7 days in culture.

(C) Representative whole mount SA-β-gal staining of an organoid after 14 days in culture.

(D) Representative SA-β-gal staining coupled with IHC on cryosections of organoids collected after 21 days. Black arrowheads point to double positive cells.

(E) Relative transcript levels of genes in vehicle (vhc) and ABT263 treated organoids; FPKM estimates were extracted from bulk RNAseq data. These genes are differentially expressed between the two conditions (FDR<0.05; logFC >0.5).

(F) GSEA graph representing the enrichment score of NRF2_Q4 enriched pathway in ABT263 compared with vhc treated organoids.

(G) Representative whole mount immunofluorescence in vhc and ABT263 treated organoids after 21 days in culture (controls n=5; ABT263 2 µM n=4). White arrowheads point to GFP+/NRF2+ or GFP+/TNC+ cells.

Scale bars, C: 50 µm; D: 20 µm; G (left): 50 µm; (right): 5 µm.

Figure S6

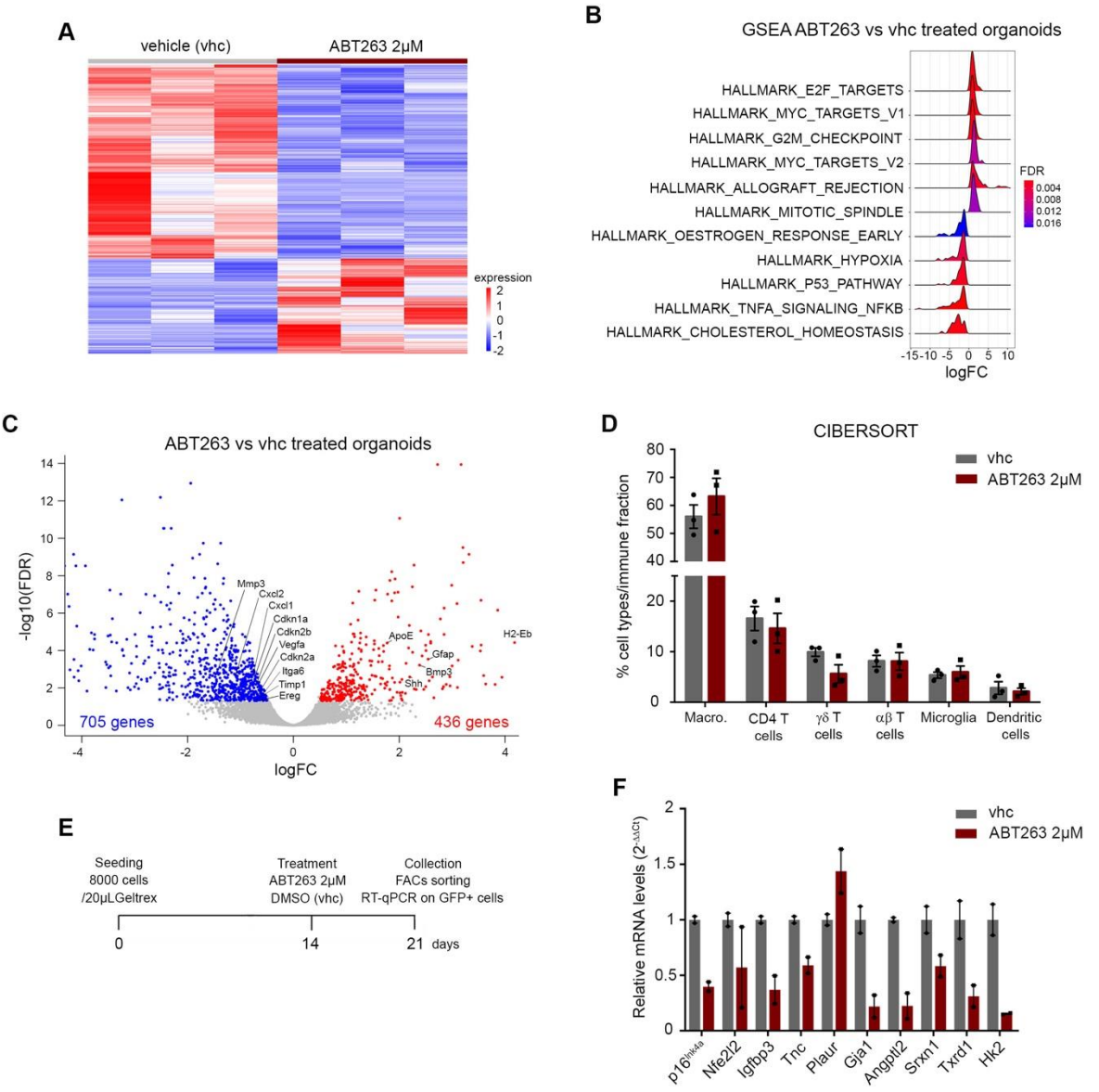
A
vehicle (vhc)
ABT263 2µM
expression
2
1
0
-1
-2
B
GSEA ABT263 vs vhc treated organoids
HALLMARK_E2F_TARGETS
HALLMARK_MYC_TARGETS_V1
HALLMARK_G2M_CHECKPOINT
HALLMARK_MYC_TARGETS_V2
HALLMARK_ALLOGRAFT_REJECTION
HALLMARK_MITOTIC_SPINDLE
HALLMARK_OESTROGEN_RESPONSE_EARLY
HALLMARK_HYPOXIA
HALLMARK_P53_PATHWAY
HALLMARK_TNFA_SIGNALING_NFKB
HALLMARK_CHOLESTEROL_HOMEOSTASIS
FDR
0.004
0.008
0.012
0.016
-15 -10 -5 0 5 10
logFC
C
ABT263 vs vhc treated organoids
-log10(FDR)
Mmp3
Cxcl2
Cxcl1
Cdkn1a
Cdkn2b
Vegfa
Cdkn2a
Itga6
Timp1
Ereg
ApoE
Gfap
Bmp3
Shh
H2-Eb
705 genes
436 genes
logFC
D
CIBERSORT
vhc
ABT263 2µM
% cell types/immune fraction
Macro.
CD4 T cells
γδ T cells
αβ T cells
Microglia
Dendritic cells
E
Seeding
8000 cells
/20µLGeltrex
Treatment
ABT263 2µM
DMSO (vhc)
Collection
FACs sorting
RT-qPCR on GFP+ cells
0
14
21 days
F
vhc
ABT263 2µM
Relative mRNA levels (2-ΔΔCt)
p16Ink4a
Nfe2l2
Igfbp3
Tnc
Plaur
Gja1
Angptl2
Srxn1
Txrd1
Hk2

Figure S6. Senolytic treatment in mouse GBM-derived organoids decreases NRF2 signaling

(A) Heatmap of bulk RNAseq analysis of ABT263 2 µM (n=3) compared with vehicle (vhc, n=3) treated organoids, each triplicate represents 3 pooled organoids.

(B) GSEA ridge plots of the most significant representative Hallmark gene lists in ABT263 treated organoids compared with vhc.

(C) Volcano plots of the DE genes (FDR<0.05; logFC>0.5) between ABT263 treated compared with vhc organoids.

(D) Bar plot representing the estimation of the abundance of immune cell types using CIBERSORT (reference data set GSE124829) in vhc and ABT263 treated organoids.

(E) Timeline of the organoid culture protocol.

(F) Relative transcript levels shown as ratios of normalized values of ABT263 over vhc treated organoids. Data represent technical duplicates of three pooled organoids in each condition.

Figure 7

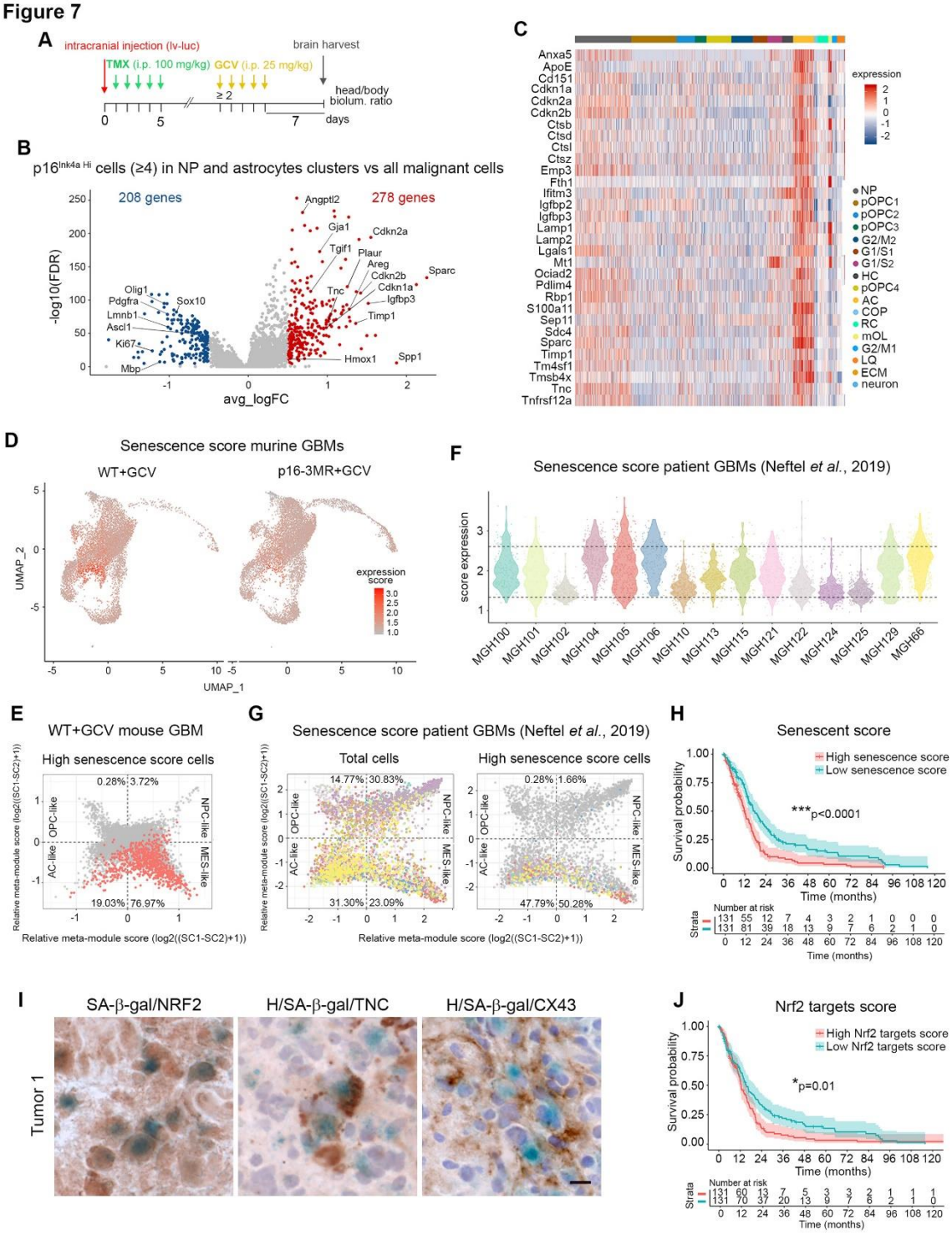
A
intracranial injection (lv-luc)
brain harvest
TMX (i.p. 100 mg/kg) GCV (i.p. 25 mg/kg)
≥ 2
head/body biolum. ratio
0
5
7
days
B
p16Ink4a Hi cells (≥4) in NP and astrocytes clusters vs all malignant cells
208 genes
278 genes
-log10(FDR)
avg_logFC
Olig1
Pdgfra
Sox10
Lmnb1
Ascl1
Ki67
Mbp
Angptl2
Gja1
Cdkn2a
Tgif1
Plaur
Areg
Cdkn2b
Cdkn1a
Igfbp3
Timp1
Tnc
Sparc
Hmox1
Spp1
C
expression
Anxa5
ApoE
Cd151
Cdkn1a
Cdkn2a
Cdkn2b
Ctsb
Ctsd
Ctsl
Ctsz
Emp3
Fth1
Ifitm3
Igfbp2
Igfbp3
Lamp1
Lamp2
Lgals1
Mt1
Ociad2
Pdlim4
Rbp1
S100a11
Sep11
Sdc4
Sparc
Timp1
Tm4sf1
Tmsb4x
Tnc
Tnfrsf12a
NP
pOPC1
pOPC2
pOPC3
G2/M2
G1/S1
G1/S2
HC
pOPC4
AC
COP
RC
mOL
G2/M1
LQ
ECM
neuron
D
Senescence score murine GBMs
WT+GCV
p16-3MR+GCV
UMAP_2
UMAP_1
expression score
F
Senescence score patient GBMs (Neftel et al., 2019)
score expression
MGH100
MGH101
MGH102
MGH104
MGH105
MGH106
MGH110
MGH113
MGH115
MGH121
MGH122
MGH124
MGH125
MGH129
MGH66
E
WT+GCV mouse GBM
High senescence score cells
0.28%
3.72%
19.03%
76.97%
OPC-like
NPC-like
AC-like
MES-like
Relative meta-module score (log2((SC1-SC2)+1))
G
Senescence score patient GBMs (Neftel et al., 2019)
Total cells
High senescence score cells
14.77%
30.83%
31.30%
23.09%
0.28%
1.66%
47.79%
50.28%
H
Senescent score
High senescence score
Low senescence score
***p<0.0001
Survival probability
Time (months)
Number at risk
Strata
131 55 12 7 4 3 2 1 0 0 0
131 81 39 18 13 9 7 6 2 1 0
0 12 24 36 48 60 72 84 96 108 120
I
SA-β-gal/NRF2
H/SA-β-gal/TNC
H/SA-β-gal/CX43
Tumor 1
J
Nrf2 targets score
High Nrf2 targets score
Low Nrf2 targets score
*p=0.01
Survival probability
Time (months)
Number at risk
Strata
131 60 13 7 5 3 3 2 1 1 1
131 70 37 20 13 9 7 6 2 1 0
0 12 24 36 48 60 72 84 96 108 120

Figure 7. Mouse senescent signature is conserved in patient GBM and its high score is predictive of a worse survival

(A) Timeline of the mouse GBM generation for scRNAseq at the early timepoint.

(B) Volcano plot of DE genes (-0.5<log2FC>0.5; FDR<0.05) between $p16^{Ink4a\ Hi}$ cells (gene expression ≥ 4) of NP and astrocyte clusters compared with the remaining malignant cells in WT+GBMs.

(C) Heatmap of the 31 senescence signature genes in WT+GCV GBMs.

(D) UMAP plots of senescent score signature expression in WT+GCV and p16-3MR+GCV GBMs.

(E) 2-D representation of cellular states in WT+GCV GBM cells with a high senescent score (score ≥ 2).

(F) Violin plots of the senescent score expression in wild-type CDKN2A/CDK4 patient GBMs. The top and bottom dot lines correspond to the highest and lowest deciles respectively. Patient GBMs data were extracted from Neftel et al., 2019.

(G) 2-D representation of cellular states in all malignant cells (left panel) and in malignant cells with a high senescent score (first decile, right panel) in wild-type CDKN2A/CDK4 patient GBMs (Neftel et al., 2019).

(H) Kaplan-Meier survival curve of TGCA GBMs with high and low senescent score. The high and low cohorts are based on the highest and lowest quartiles.

(I) Representative SA-β-gal staining coupled with IHC staining on patient GBM cryosections. 3 patient GBMs were analyzed per antibody. H: hematoxylin. Scale bar :10 µm.

(J) Kaplan-Meier survival curves of TGCA GBMs with high and low Nrf2 targets score. The high and low cohorts are based on the highest and lowest quartiles.

Statistical significance for the Kaplan-Meier survival curves was determined by Mantel-Cox log-rank test (*, p<0.05; ***, p<0.001).

Figure S7

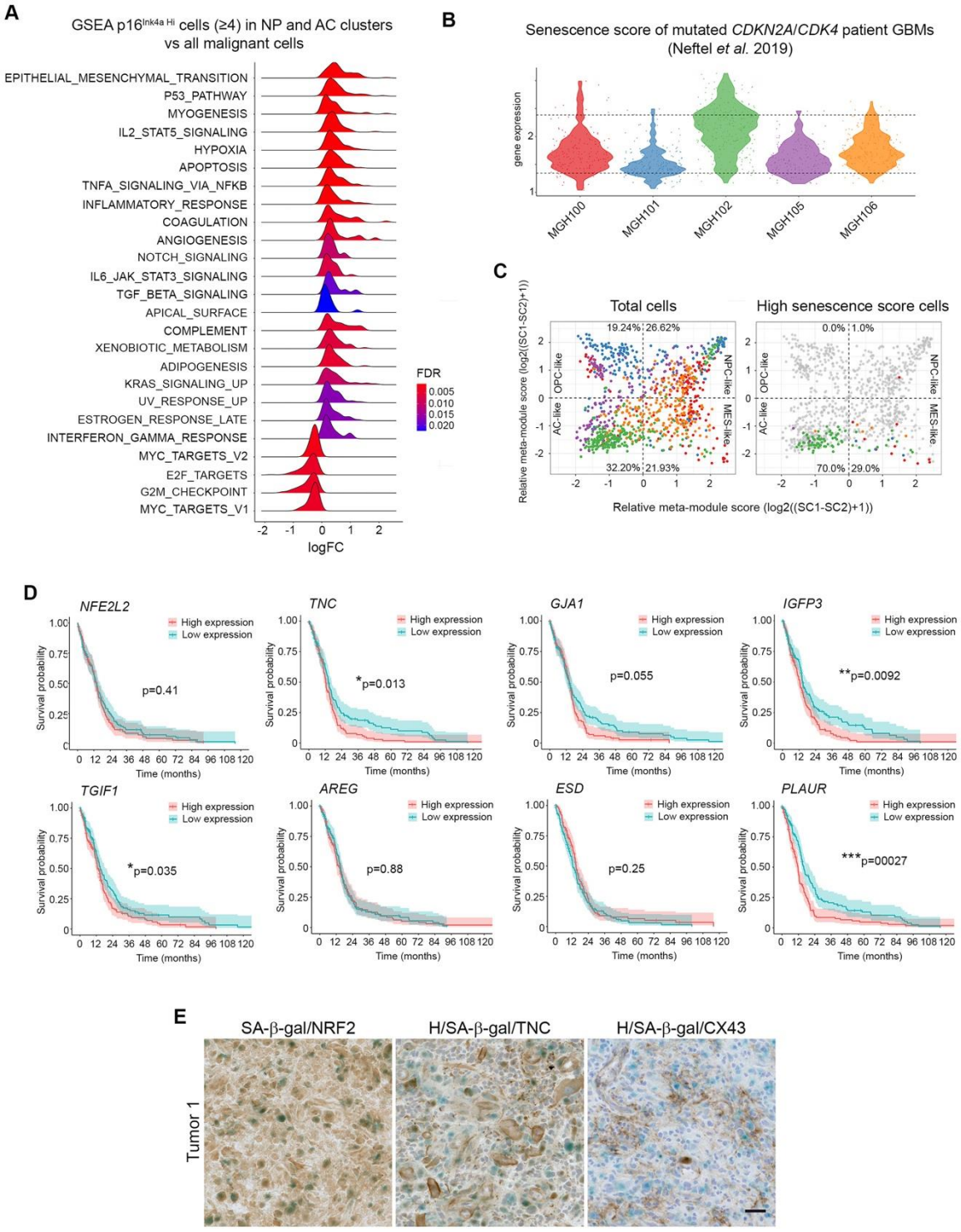
A
GSEA p16Ink4a Hi cells (≥4) in NP and AC clusters vs all malignant cells
EPITHELIAL_MESENCHYMAL_TRANSITION
P53_PATHWAY
MYOGENESIS
IL2_STAT5_SIGNALING
HYPOXIA
APOPTOSIS
TNFA_SIGNALING_VIA_NFKB
INFLAMMATORY_RESPONSE
COAGULATION
ANGIOGENESIS
NOTCH_SIGNALING
IL6_JAK_STAT3_SIGNALING
TGF_BETA_SIGNALING
APICAL_SURFACE
COMPLEMENT
XENOBIOTIC_METABOLISM
ADIPOGENESIS
KRAS_SIGNALING_UP
UV_RESPONSE_UP
ESTROGEN_RESPONSE_LATE
INTERFERON_GAMMA_RESPONSE
MYC_TARGETS_V2
E2F_TARGETS
G2M_CHECKPOINT
MYC_TARGETS_V1
FDR
0.005
0.010
0.015
0.020
logFC
B
Senescence score of mutated CDKN2A/CDK4 patient GBMs (Neftel et al. 2019)
gene expression
MGH100
MGH101
MGH102
MGH105
MGH106
C
Total cells
High senescence score cells
19.24%
26.62%
32.20%
21.93%
0.0%
1.0%
70.0%
29.0%
AC-like
OPC-like
NPC-like
MES-like
Relative meta-module score (log2((SC1-SC2)+1))
D
NFE2L2
p=0.41
TNC
*p=0.013
GJA1
p=0.055
IGFP3
**p=0.0092
TGIF1
*p=0.035
AREG
p=0.88
ESD
p=0.25
PLAUR
***p=00027
High expression
Low expression
Survival probability
Time (months)
E
SA-β-gal/NRF2
H/SA-β-gal/TNC
H/SA-β-gal/CX43
Tumor 1

Figure S7. Mouse senescent signature is conserved in patient GBM and its high score is predictive of a worse survival

(A) GSEA ridge plot of the most significant representative Hallmark gene lists between $p16^{Ink4a\ Hi}$ cells (gene expression ≥4) of NP and astrocytes clusters compared with the remaining malignant cells in WT+GCV GBMs.

(B) Violin plots of the senescent score expression in *CDKN2A*/*CDK4* mutated patient GBMs. The top and bottom dot lines correspond to the highest and lowest deciles respectively. Adult patient GBMs data were extracted from (Neftel et al., 2019).

(C) 2-D representation of cellular states in total cells (left panel) and in cells with a high senescent score (first decile, right panel).

(D). Kaplan-Meier survival curves of TGCA GBMs with high and low score of NRF2 and its identified targets. The high and low cohorts are based on highest and lowest quartiles. Statistical significance was determined by Mantel-Cox log-rank test (*, $p<0.05$; **, $p<0.01$; ***, $p<0.001$).

(E) Representative SA-β-gal staining coupled with IHC staining on patient GBM cryosections. H: hematoxylin. Scale bar, 40 µm.

STAR★METHODS

KEY RESOURCES TABLE

REAGENT or RESOURCE	SOURCE	IDENTIFIER
Antibodies		
Rabbit monoclonal anti-Ki67	Vector Laboratories	Cat# VP-RM04; RRID: AB_2336545
Rabbit monoclonal anti-p16INK4A (clone EPR1473)	Abcam	Cat# ab108349; RRID: AB_10858268
Mouse monoclonal anti-Lamin B1(clone B-10)	Santa Cruz Biotechnology	Cat# sc-374015; RRID: AB_10947408
Mouse monoclonal anti-GFAP (Clone G-A-5)	Sigma-Aldrich	Cat# G3893; RRID: AB_477010
Rabbit monoclonal anti-OLIG2	Millipore	Cat# AB9610; RRID: AB_570666
Rabbit monoclonal anti-IBA1	Wako	Cat# 019-19741; RRID: AB_839504
Chicken monoclonal anti-GFP	Aves Labs	Cat# GFP-1020; RRID: AB_10000240
Rat polyclonal anti-p19 (clone 340C/B3)	CNIO	N/A
Rabbit monoclonal anti-NRF2	Thermo Fisher Scientific	Cat# PA5-27882; RRID: AB_2545358
Mouse monoclonal anti-TNC (clone 4C8MS)	Novus	Cat# NB110-68136; RRID: AB_1110904
Rabbit polyclonal anti-CX43	Cell Signaling Technology	Cat# 3512; RRID: AB_2294590
Goat polyclonal anti-uPAR	R and D Systems	Cat# AF534; RRID: AB_2165351
Biotinylated Goat Anti-Mouse IgG Antibody	Vector Laboratories	Cat# BP-9200; RRID: AB_2827937
Goat anti-Mouse IgG1 Cross-Adsorbed Secondary Antibody, Biotin-XX	Thermo Fisher Scientific	Cat# A10519; RRID: AB_2534028
Biotinylated Goat Anti-Rat IgG Antibody	Vector Laboratories	Cat# BA-4001; RRID: AB_10015300
Biotinylated Goat Anti-Rabbit IgG Antibody	Vector Laboratories	Cat# PI-1000; RRID:AB_2336198
Biotinylated Goat Anti-Chicken IgG Antibody	Vector Laboratories	Cat# BA-9010; RRID:AB_2336114
Biological samples		
Patient resected glioma tissues	OncoNeuroTek	N/A
Chemicals, peptides, and recombinant proteins		
Tamoxifen	Sigma-Aldrich	Cat# T5648-1Gi
Corn oil	Sigma-Aldrich	Cat# C8267
Ganciclovir	Selleck Chemicals	Cat# S1878
Navitoclax (ABT-263)	Selleck Chemicals	Cat# S1001
DMSO	Sigma-Aldrich	Cat# D8418-50ML
Poly(ethylene glycol) BioUltra400 (PEG400)	Sigma-Aldrich	Cat# 91893-250ML-F
Phosal 50 PG	Lipoid	Cat# 368315
Xenolight D-Luciferin	Perkin Elmer	Cat# 122799
X-Gal	Sigma-Aldrich	Cat# 15520-018
Buprenorphin (Buprenovet)	Bayer Health Care	Cat# 794-996
Lidocain (Laocain)	Centravet	Cat# QN01BB02
Mini-PROTEAN TGX Protein Gels	Bio Rad	Cat# 4568096

Nitrocellulose membrane	Thermo Fisher Scientific	Cat# 88018
Super Block Blocking buffer	Thermo Fisher Scientific	Cat# 37535
Neurobasal medium	Life Technologies	Cat# 12348-017
DNAse	Worthington	Cat# LS002139
Ovomucoid	Worthington	Cat# LS003085
L-Cystein	Sigma	Cat# C78805
Glutamax	Life Technologies	Cat# 35050-061
Human EGF	Peprotech	Cat# 100-18B
Human FGF-basic	Peprotech	Cat# AF-100-15
B27	Life Technologies	Cat# 17504-044
GelTrex	Thermo Fisher Scientific	Cat# A14132-02
Rapidclear@1.49	SunJinLab	Cat# RC149001
LightCycler 480 SYBR Green I Master Mix	Roche	Cat# 4707516001
Critical commercial assays		
VECTASTAIN Elite ABC HRP Kit	Vector Laboratories	Cat# PK-6100-NB
Pierce BCA protein assay kit	Thermo Fisher Scientific	Cat# 23225
Debris removal	Miltenyi	Cat# 130-109-398
Red blood lysis buffer	Roche	Cat# 11 814 389 001
TRI-reagent	Molecular Center Research	Cat# TR 118
Macherey-Nagel Mini kit Nucleospin	Macherey-Nagel	Cat# 740955.50
Maxima 1str cDNA Synth Kit	LifeTechnologies	Cat# K1642
NextSeq 500/550 High Output Kit v2 (150 cycles)	Illumina	Cat# 20024907
High Sensitivity RNA ScreenTape	Agilent Technologies	Cat# 5067-5579
High Sensitivity D5000 ScreenTape	Agilent Technologies	Cat# 5067-5592
High Sensitivity D1000 ScreenTape	Agilent Technologies	Cat# 5067-5584
KAPA mRNA HyperPrep Kit	Roche	Cat# 8098123702
SureCell™ WTA 3′ Library Prep Kit for the ddSEQ System	Illumina	Cat# 20014280
Chromium Next GEM Single Cell 3' Reagent Kits v3.1	10X Genomics	Cat# 20012850
Chromium Next GEM Chip G Single Cell Kit, 48 rxns	10X Genomics	Cat# PN-1000120
Deposited data		
Bulk and single cell RNA sequencing data of murine GBM and its derived organoids	This paper	GEO: GSE168014
Smartseq2 dataset of patient GBMs	Neftel et al., 2019	GEO: GSE131928
ImmGen immune cell genes signature	Newman et al., 2015	GEO: GSE124829
Experimental models: organisms/strains		
Mouse: $Pten^{fl/fl}$/FVB	Marino et al., 2002	N/A
Mouse: $Glast^{creERT2/+}$/129/SVJ x C57BL/6	Mori et al., 2006	N/A
Mouse: p16-3MR/C57BL/6	Demaria et al., 2014	N/A
Oligonucleotides		
Primers for RT-qPCR	This paper	Table S4
Recombinant DNA		
pTomo HRasV12-shp53-(IRES)-GFP	Friedmann-Morvinski et al. 2012	N/A
pTomo HRasV12-shp53-(IRES)-GFP-(2a)-Firefly-luciferase	This paper	N/A
Software and algorithms		

Fiji	Schindelin et al., 2012	RRID:SCR_002285
CIBERSORT	Newman et al., 2015	RRID:SCR_016955
Enrichr	Chen et al., 2013 Kuleshov et al., 2016	RRID:SCR_001575
GSEA 2.2.3	Subramanian et al., 2005	RRID:SCR_003199
cBioPortal	https://github.com/cBioPortal/cbioportal/ https://github.com/cBioPortal/cbioportal/blob/master/docs/README.md	RRID:SCR_014555
Graphpad Prism 8.0.2	Graphpad software	RRID:SCR_002798
Imaris Software	Bitplane	RRID:SCR_007370
Other		
Molecular Signatures Database (MSigDB)	Liberzon et al. 2011	http://www.broadinstitute.org/msigdb
Seurat (v3.2.3)	https://github.com/satijalab/seurat	RRID:SCR_007322
Seurat (v2)	https://github.com/satijalab/seurat	RRID:SCR_007322
Seurat bioconductor package v3.2.3	Gentleman et al., 2004	RRID:SCR_006442
Cell Ranger Single-cell Software suite (3.0.2)	https://support.10xgenomics.com/single-cell-gene-expression/software/pipelines/latest/what-is-cell-ranger	RRID:SCR_017344
R v3.6	https://www.r-project.org/	RRID:SCR_001905
rsem 1.2.28	https://github.com/deweylab/RSEM	N/A
clusterProfiler (v3.14.3)	https://github.com/GuangchuangYu/clusterProfiler	RRID:SCR_016884
CellPhoneDB v2.1.4	https://github.com/Teichlab/cellphonedb	RRID:SCR_017054
inferCNV package (v. 1.6.0)	https://github.com/broadinstitute/inferCNV/	N/A
Cutadapt 1.18	https://bio.tools/cutadapt	RRID:SCR_011841
Drop-seq tool (v 2.0.0).	https://github.com/broadinstitute/Drop-seq	RRID:SCR_018142
scalop (v1.1.0)	https://github.com/jlaffy/scalop	N/A
Galaxy Version 0.9.1	Saurty et al., 2019	N/A

LEAD CONTACT AND MATERIALS AVAILABILITY

Further information and requests for resources and reagents may be directed to and will be fulfilled by Isabelle Le Roux (isabelle.leroux@icm-institute.org).

EXPERIMENTAL MODEL AND SUBJECT DETAILS

Patient samples

Fresh patient GBM samples were selected from the Pitié-Salpêtrière tumor bank Onconeurotek. They were reviewed by our senior pathologist (F.B.) to validate the histological features and confirm patients' diagnosis. Collection of tumor samples and clinical-pathological information were obtained upon patients' informed consent and ethical board approval, as stated by the Declaration of Helsinki.

Mouse and breeding

All animal care and treatment protocols complied with European legislation (no. 2010/63/UE) and national (French Ministry of Agriculture) guidelines for the use and ethical treatment of laboratory animals. All experiments on animals were approved by the local ethics committee (approval APAFIS 9131). To generate the GBM mouse model, we crossed Glast$^{creERT2/+}$ mice (Mori et al., 2006) with the Pten$^{fl/fl}$ mice (Marino et al., 2002). Glast$^{creERT2/+}$; Pten$^{fl/fl}$ males were bred with either Pten$^{fl/fl}$ or Pten$^{fl/fl}$; p16-3MR/+ females (Demaria et al., 2014) to generate Glast$^{creERT2/+}$; Pten$^{fl/fl}$ and Glast$^{creERT2/+}$; Pten$^{fl/fl}$; p16-3MR/+ mice, named WT and p16-3MR mice respectively. All animals used in the study were 6-8 week old females except for the mice used for scRNAseq at the early timepoint that were 14-week old females.

Plasmid construction

HRasV12-shp53-(IRES)-GFP-(2a)-Firefly-luciferase vector was generated from the HRasV12-shp53-(IRES)-GFP (Friedmann-Morvinski et al., 2012) construct using the Gibson Assembly technique (Gibson et al., 2009). The terminal IRES-GFP region of the initial vector and a P2A-luciferase2 sequence were both flanked with a shared sequence overlap and amplified by PCR. They were then inserted into SalI and PmlI sites of the initial vector.

METHOD DETAILS

Stereotaxic injection

We stereotaxically performed lentiviral intracranial injection of mice to induce *de novo* tumorigenesis. The mice were anesthetized with isoflurane (2-3%, 1 L/min oxygen), and subcutaneously injected in the head with lidocaine (60 µL, 2.133 mg/mL). Analgesia was injected intraperitoneally (i.p.) presurgery and up to 24h after surgery (buprenorphine, 100 µL, 15 µg/mL). The HRasV12-shp53-(IRES)-GFP (lv) or the HRasV12-shp53-(IRES)-GFP-(2a)-Firefly-luciferase lentivirus (lv-luc, 1 µL, 6 x 10^8 PFU/mL) was injected in the right subventricular zone (SVZ) of the brain (x=1mm, y=1mm, z=-2.3mm from the bregma). We used a Hamilton 30G needle with a silica fiber tip (MTI-FS) and an automatic injector (Harvard Apparatus). After injection, the skin wound was closed with surgical glue (SurgiBond®) and animals were

placed under an infra-red lamp until they recover a vigil state. From the next day, mice were injected i.p. with tamoxifen (TMX, 20 mg/mL in corn oil, Sigma #T5648-1Gi and Sigma #C8267) once per day for five consecutive days to induce the recombination of the *Pten* locus and of the *loxP-RFP-loxP* cassette of the lentivirus allowing the expression of *HRasV12*.

Bioluminescence imaging

We monitored tumor growth by *in vivo* bioluminescence twice a week from 14 days post intracranial injection. The mice were i.p. injected with Xenolight D-Luciferin (100 µL, 30 mg/mL, Perkin Elmer #122799), anesthetized with isoflurane and their head and back were shaved. Bioluminescence was recorded with an IVIS Spectrum In Vivo Imaging System (Perkin Elmer) and ratio were measured by normalizing the head signal on the back signal.

Mouse treatments

Mice were treated with vehicle (PBS, DMSO 20%, Sigma #D8418-50ML) or GCV (25 mg/kg/day, Selleckchem, #S1878) prepared in PBS, 20% DMSO at 21 days post injection (DPI). During the course of the study, we implemented bioluminescence-monitored GBM growth for the two paradigms p16-3MR+vhc vs p16-3MR+GCV and the WT+vhc vs WT+ABT263 (see below). The mice were treated when head to back bioluminescence ratio was superior or equal to 2 (around 24 DPI; n=43). GCV was administered via daily i.p. injections for 5 consecutive days per cycle, for two cycles with a 2-week interval between the two cycles. ABT263 (Selleckchem, #S1001) was prepared as previously described (Chang et al., 2016) and was administered to mice by gavage at 50 mg/kg/day for 5 days.

Kaplan-Meier mice survival studies

Kaplan-Meier survival analysis was done using Prism 8 (Graphpad software). In accordance with EU guidelines, mice were sacrificed when reaching end points (20% body weight decrease, deterioration of general condition). Mice were injected by batch. One batch always included control and experimental mice injected the same day. When control mice survival extended more than 50-52 DPI, the entire batch was removed from the analysis to exclude technical bias linked to intracranial injection.

Mice brain collection

When reaching end points, mice were sedated with CO_2 inhalation followed by an intracardiac perfusion with cold HBSS 1X. After harvesting the brain, GFP+ tumor was cut into two parts, under MZFL II stereomicroscope (Leica). Anterior part of the GFP+ tumor and the GFP- parenchyma were chopped and stored in TRI-reagent (Molecular Center Research, #TR 118)

at -80°C for RNA isolation. Posterior part was snap-frozen in dry ice cooled-isopentane for histological studies. Brains were cryosectioned at 12-µm thickness (Leica cryostat).

SA-β-gal and immunohistochemical stainings

For SA-β-gal staining, brain or GBM sections were fixed in 2% PFA, 0.02% glutaraldehyde (Sigma, #340855) 10 min at RT, washed twice in PBS pH 7.0 and once in PBS pH 5.5 for 30 min. Slides were incubated in the X-gal solution as previously described (Le Roux et al., 2015) for 5h30 at 37°C for mouse sections and overnight (O/N) for patient GBM sections. Slides were then washed in PBS and post-fixed in 4% PFA 10 min at RT.

For Immunohistochemical staining, brain or GBM sections were fixed in 4% PFA 10 min and washed in PBS. Endogenous peroxidases were inactivated in 1% H_2O_2 (in H_2O) solution for 5 min and sections were incubated in the blocking solution (PBS 1X, 10% NGS, 3% BSA and 0.25% to 0.5% Triton) for 30 min. Sections were then incubated with the primary antibody (Supplementary Table S4) in the blocking solution for either 2h at RT or O/N at 4°C. Slides were rinsed and incubated with biotinylated secondary antibodies for 45 min at RT. An amplification step was performed using VECTASTAIN Elite ABC HRP Kit (Vector Laboratories, #PK-6100-NB) for 30 min at RT and staining was revealed by a DAB reaction. Images were acquired using an Axio Scan.Z1 (Zeiss) and extracted using the ZEN 2.0 blue edition (Zeiss) software.

Surface area quantification

Quantifications were performed using Fiji software (Schindelin et al., 2012). Region of interest (ROI) corresponding to the tumor, was selected using the ellipse tool. IHC images were then color deconvoluted according to the “Giemsa” or “H DAB” vector to assess a threshold of the SA-β-gal or DAB signal respectively. The signal threshold was adjusted in order to remove the unspecific background signal without clearing the specific one. Number of pixels was measured and the values were normalized on the GFP+ tumor surface area. Four slides with three sections on each (n=12) for SA-β-gal quantification and three slides with three sections on each (n=9) for IHC quantification were analyzed per sample.

Western-Blotting

Total proteins were extracted from tumor samples following TRI-reagent protocol (Molecular Center Research, #TR 118). Protein pellets were solubilized in 1% SDS, 10M urea and stored at -80°C. Protein concentration was assayed using the Pierce BCA protein assay kit (ThermoFisher, #23225). Proteins were separated on 4-20% stain-free polyacrylamide gels (Mini-PROTEAN TGX Protein Gels, Bio Rad, #4568096) and transferred on a nitrocellulose membrane 0.45 µm (ThermoFisher, #88018). Membranes were probed with primary antibodies

(Table S4) diluted in Super Block Blocking buffer in TBS (ThermoFisher, #37535) and incubated O/N at 4°C under gentle agitation. The secondary antibodies were incubated 1h at RT. Fluorescence was detected using the Odyssey CLx (Li-cor), specific bands were quantified using Fiji software (Schindelin et al., 2012) and normalized against the corresponding β-TUBULIN band.

RNA extraction and RT-qPCR

Total RNAs were extracted from tumor and parenchyma samples following the TRI-reagent protocol (Molecular Center Research, #TR 118), and total RNAs from organoids were extracted following the Macherey-Nagel Mini kit Nucleospin protocol (Macherey-Nagel, #740955.50).

cDNAs were generated using the Maxima 1str cDNA Synth Kit (LifeTechnologies, K1642). Quantitative PCR was performed using LightCycler 480 SYBR Green I Master Mix (Roche, #4707516001) on a LightCycler® 480 Instrument II (Roche). Samples were run in duplicate or triplicate, transcript levels were normalized to TBP and GAPDH and analysis was performed using the $2^{-\Delta\Delta CT}$ method (Livak and Schmittgen, 2001). Primers used in this study are listed in Table S4.

Tumor dissociation for scRNAseq and organoids

After brain harvest, GFP+ tumors were dissected under a Leica MZFL II stereomicroscope. Tumor pieces were chopped and incubated 5 min at 37°C in a HBSS-papain based lysis buffer (Worthington PAP) containing DNAse (0.01%, Worthington #LS002139) and L-Cystein (124 µg/mL, Sigma #C78805). Papain digestion was inhibited by ovomucoid (70 µg/mL, Worthington #LS003085). Tissue was further dissociated mechanically and centrifuged 300 g, 10 min at 4°C. Cells were resuspended in cold HBSS, a debris removal step was performed (Miltenyi #130-109-398) and blood cells were removed using a blood lysis buffer (Roche 11814 389001). Cells were processed as described in (Hubert et al., 2016) to generate organoids.

For scRNAseq, cells were resuspended in cold HBSS and incubated with the eBiosciences Fixable Viability Dye Fluor 450 (Invitrogen #65-0863), to label dead cells, and washed. Cells were then sorted using the MoFlo Astrios cell sorter (Beckman Coulter) or the S3e cell sorter (Biorad). Live cells were collected in HBSS 0,1% BSA precoated tubes, centrifuged and resuspended in HBSS-0,1% BSA at a concentration of 1200 cells/µL. GFP + and GFP- cells were collected separately for the scRNAseq ddSeq experiment.

Organoids whole mount immunofluorescence

All steps of the procedure were performed at 4°C under gentle agitation and all the washes were done in a PBS-0,5% Tween20 solution (PTW). Organoids were collected in 2 mL

Eppendorf tubes, fixed O/N in a 4% PFA solution. The next day, they were extensively washed and incubated O/N in a saturation/permeabilization solution (PBS; 10% fetal calf serum (FCS); 3% BSA; 2% Triton). The organoids were incubated with the primary antibody (Table S4) in a PBS solution containing 10% FCS; 3% BSA; 1% Triton, 0.05% NaN_3 between 10-21 days and then extensively washed for 3 days. Incubation of the secondary antibody was done in the same solution as for the primary antibody, between 3-7 days and then extensively washed for 3 days. They were transferred into a cavity slide containing Rapidclear® 1.49 (SunJinLab) and sealed with a coverslip surrounded by nail varnish, the clarification took about 12h to occur. Images were acquired after 7 days in culture with a Leica SP8 DIVE microscope and after 21 days in culture with the Nikon confocal A1 R HD25 microscope. The 3D reconstructions were performed using Imaris software or Nikon NIS-Elements imaging Software.

Bulk RNA-seq and analysis

The quantity and quality of the total RNAs extracted were assessed by the Tapestation 2200 (Agilent), and sequenced with the Illumina NextSeq 500 Sequencing system using NextSeq 500/550 High Output Kit v2 (150 cycles, # 20024907), 400 million of reads, 50Gbases.

Quality of raw data was evaluated with FastQC. Poor quality sequences were trimmed or removed with Fastp software to retain only good quality paired reads. Star v2.5.3a was used to align reads on mm10 reference genome using default parameters except for the maximum number of multiple alignments allowed for a read which was set to 1. Quantification of gene and isoform abundances were done with rsem 1.2.28 on RefSeq catalogue, prior to normalisation with edgeR bioconductor package. Finally, differential analysis was conducted with the glm framework likelihood ratio test from edgeR. For malignant samples, a batch effect was detected in PCA representation. To correct it, we performed the analysis by using an additive model which includes this batch variable. Multiple hypothesis adjusted p-values were calculated with the Benjamini-Hochberg procedure to control FDR.

Functional enrichment analysis was performed with clusterProfiler (v3.14.3) bioconductor package on the differentially deregulated genes with over-representation analysis (enricher function) and on all the genes with Gene Set Enrichment analysis (GSEA function; (Subramanian et al., 2005)). Hallmark, Transcription factor targets (TFT) and Canonical pathways (CP) gene sets from MSigDB collections have been used, completed with some custom gene sets (Table S1).

CIBERSORT (Newman et al., 2015) was used to accurately quantify the relative abundances of 6 distinct immune cell types according to the ImmGen immune cell genes signature (reference GSE124829).

Single-cell RNA-seq and analysis – 10X data

Cells suspension of four dissociated GBMs (2 WT+GCV and 2 p16-3MR+GCV) were loaded with the Chromium Next GEM Chip G Single Cell Kit (10X Genomics, #PN-1000120) and a library was generated using Chromium Next GEM Single Cell 3' Reagent Kits v3.1 (10X Genomics, #20012850). The library was sequenced on an Illumina NovaSeq 6000 instrument using a 100 cycle S2 flow cell in XP mode, with the following parameters: 2050 million reads depth, 200 Gbases per run and 50 000 reads per cell.

The Cell Ranger Single-cell Software suite (3.0.2) was used to process the data. First, a custom reference genome was created with the mkref function to include 3'LTR and 3MR sequences into the mm10 reference genome. Count function was used on each GEM well that was demultiplexed by *mkfastq* to generate gene-cell matrices. Then, filtered_feature_bc_matrix output was loaded into Seurat bioconductor package v3.2.3 to filter the datasets and identify cell types using R v3.6. Genes expressed in at least 5 cells and cells with at least 200 features were retained for further analysis. To remove likely dead or multiplet cells from downstream analyses, cells were discarded when they had less than 500 UMIs (Unique Molecular Identifiers), greater than 60 000 UMIs, or expressed over 8 % mitochondrial genes.

All samples were merged together for downstream analysis. As no batch effects were observed among the four samples, no integration step was performed. Gene expression matrix was normalized using the negative binomial regression method implemented in the Seurat *SCTransform* function, via selection of the top 3000 variable genes and regressed out the mitochondrion expression percentage. The final dataset was composed of 20 293 genes and 26 237 cells.

To cluster cells, we computed a Principal Components Analysis (PCA) on scaled variable genes, as determined above, using Seurat's *RunPCA* function, and visualized it by computing a Uniform Manifold Approximation and Projection (UMAP) using Seurat's *RunUMAP* function on the top 30 PCs. We also computed the k-nearest neighbor graph on the top 30 PCs, using Seurat's *FindNeighbors* function with default parameters, and in turn used Seurat's *FindClusters* function with varying resolution values. We chose a final value of 0.5 for the resolution parameter at this stage of clustering. Clusters were assigned preliminary identities based on expression of combinations of known marker genes for major cell types. TME clusters were identified with the expression of *Ptprc* (*Cd45*) gene marker. In order to better identify other cell types, TME cells were removed and a second clustering with a resolution 0.6 was applied.

The *FindMarkers* function with the default parameters (min.LogFC = 0.25, min.pct = 0.25, test.use = Wilcox) was used to identify differentially expressed genes in different conditions : (i) p16-3MR+GCV vs WT+GCV in each cluster; (ii) cells from astrocyte and NP clusters with

Cdkn2a expression ≥ 4 (307 cells) vs all the other cells (10 280 cells) in WT+GCV GBMs. Functional enrichment analysis were done with clusterProfiler (v3.14.3) bioconductor package on the differentially deregulated genes with over-representation analysis (enricher function) and with Gene Set Enrichment analysis (GSEA function, (Subramanian et al., 2005)) on all the genes. We searched for ligand/receptor interactions between cluster 0 et *Cd45* positive clusters at 0.5 resolution in our single cell data, using CellPhoneDB v2.1.4. Copy number variations (CNVs) were inferred with inferCNV package (v. 1.6.0) with the following parameters: “denoise” and a value of 0.1 for “cutoff”.

Single-cell RNA sequencing and analysis – ddSeq data

Cell suspension of one dissociated GBM was loaded in 4 wells (3 wells with GFP+ cells or malignant cells and 1 well with GFP- cells or non-malignant cells) on the ddSEQ Single-Cell Isolator (Biorad). A library was generated using SureCell™ Whole Transcriptome Analysis 3′ Library Prep Kit for the ddSEQ System (Illumina, #20014280) and was sequenced on a Nextseq 500 Illumina sequencing system, using a High Output Kit (150 cycles), with the following parameters: 400 million reads depth, 50Gbases, and 70 million reads per sample.

Cutadapt 1.18 was used to trim nextera adapters in 3’ on reads, then a quality control of sequences was done with FastQC. Cellular and UMIs barcodes were extracted with the ddSeeker (v 0.9.0) tool with default parameters. The following steps were done with Drop-seq tool (v 2.0.0). Trimming of 5’ adapter sequences and of polyA tails was performed. Unaligned BAM were transformed to fastq with Picard tool, prior to alignment with STAR on mm10 reference genome. Ddseeker bam outputs previously tagged with molecular/cell barcode were merged with aligned BAM files, according to Drop-seq tool cookbook. Finally, TagReadWithGeneExonFunction was used to annotate each read with the gene it belongs to, and DigitalExpression was used to count gene transcripts in each cell. The output DGE matrix file is a matrix with a row for each gene, a column for each cell, containing the number of transcripts observed. This output was loaded into the Seurat (v2) R package for further analysis keeping only cells where at least 200 features were detected, and genes detected in at least 5 cells. The final dataset contains 1740 cells and 15 448 genes. To normalize the data, we applied the global-scaling normalization method “LogNormalize” that normalizes the feature expression measurements for each cell by the total expression, multiplies this by a scale factor (10 000 by default), and log-transforms the result. Then, highly variable genes were detected prior to scaling transformation. To cluster cells, we computed a Principal Components Analysis (PCA) on scaled variable genes, as determined above, using Seurat’s *RunPCA* function, and visualized it by computing a Uniform Manifold Approximation and Projection (UMAP) using Seurat’s *RunUMAP* function on the top 10 PCs. We used *FindClusters* function with a resolution of 0.6 resulting in 8 clusters. TME and malignant

clusters cells were identified according to the expression of the GFP transgene. Then, the *FindAllMarkers* function was used to extract top differentially expressed genes of each cluster, and to annotate them.

Signature expression analyses

We analyzed the senescence signature through our tumoral SCT normalized dataset and the Smartseq2 dataset of Neftel et al., 2019 corresponding to patient GBMs. This dataset was retrieved via the single cell portal (singlecell.broadinstitute.org) and processed via Seurat (v3.2.3). For both murine and patient GBM dataset, we filtered out transcriptomes expressing the *CD45* (*PTPRC*) gene and pediatric GBMs (Neftel et al., 2019) and we calculated a senescence score resulting from the geometric mean of the expression of the signature genes as previously described (Saurty et al., 2019) using the *gsc_signature_score* tool in Galaxy (Galaxy Version 0.9.1) and excluding genes that were not detected in at least 5% of transcriptomes. Then two sets of data were treated separately, one corresponding to GBMs mutated for *CDNK2A* and/or *CDK4* (Figure S7), the other to non-mutated GBMs (Figure 7). For these two datasets, we sliced the signature score distribution into deciles to determine the HIGH senescence cells (last decile), the LOW senescence cells (1st decile), and the others with an average senescence potential (MEDIUM).

Cellular state attribution

We determined the cellular states (AC-like, OPC-like, NPC-like, MES-like) using the signature lists provided by Neftel et al., 2019 by using the scalop (v1.1.0) *sigScores* function (5, https://github.com/jlaffy/scalop). It computes a score for each signature and the signature with the highest score ascertained the cellular state of a transcriptome.

TCGA survival analysis

Normalized intensities from TCGA microarray data were obtained from cBioPortal (cbioportal.org), filtering for GBM TCGA, Firehose Legacy dataset. First, geometric means of senescence genes signature and NRF2 targets signature were calculated. Secondly, we extracted the High and Low groups of patients for each signature, corresponding to the 25% patients with the highest and the lowest signature scores, respectively. Then, the *survfit* function from survival R package (v.2.44-1.1) was used to display Kaplan-Meier survival curve.

Statistical Analysis

Data are presented as mean with standard error to the mean (SEM) unless otherwise specified. Statistical comparisons were performed using Wilcoxon-Mann-Whitney, p-values unless

otherwise specified (*, p<0.05; **, p<0.01; ***, p<0.001). For Kaplan-Meier survival curves, statistical significance was determined by Mantel-Cox log-rank test (*, p<0.05).

Data and code availability

Generated data in this study are available through the Gene Expression Omnibus (GEO: GSE168014).

REFERENCES

Acosta, J.C., O'Loghlen, A., Banito, A., Guijarro, M. V., Augert, A., Raguz, S., Fumagalli, M., Da Costa, M., Brown, C., Popov, N., et al. (2008). Chemokine Signaling via the CXCR2 Receptor Reinforces Senescence. Cell 133, 1006–1018.

Angel, I., Pilo Kerman, O., Rousso-Noori, L., and Friedmann-Morvinski, D. (2020). Tenascin C promotes cancer cell plasticity in mesenchymal glioblastoma. Oncogene 39, 6990–7004.

Baker, D.J., Wijshake, T., Tchkonia, T., LeBrasseur, N.K., Childs, B.G., van de Sluis, B., Kirkland, J.L., and van Deursen, J.M. (2011). Clearance of p16Ink4a-positive senescent cells delays ageing-associated disorders. Nature 479, 232–236.

Balakrishnan, I., Danis, E., Pierce, A., Madhavan, K., Wang, D., Dahl, N., Sanford, B., Birks, D.K., Davidson, N., Metselaar, D.S., et al. (2020). Senescence Induced by BMI1 Inhibition Is a Therapeutic Vulnerability in H3K27M-Mutant DIPG. Cell Rep. 33.

Banasavadi-Siddegowda, Y.K., Russell, L., Frair, E., Karkhanis, V.A., Relation, T., Yoo, J.Y., Zhang, J., Sif, S., Imitola, J., Baiocchi, R., et al. (2017). PRMT5-PTEN molecular pathway regulates senescence and self-renewal of primary glioblastoma neurosphere cells. Oncogene 36, 263–274.

Basisty, N., Kale, A., Jeon, O.H., Kuehnemann, C., Payne, T., Rao, C., Holtz, A., Shah, S., Sharma, V., Ferrucci, L., et al. (2020). A Proteomic Atlas of Senescence-Associated Secretomes for Aging Biomarker Development. PLoS Biol.

Bhaduri, A., Di Lullo, E., Jung, D., Müller, S., Crouch, E.E., Espinosa, C.S., Ozawa, T., Alvarado, B., Spatazza, J., Cadwell, C.R., et al. (2020). Outer Radial Glia-like Cancer Stem Cells Contribute to Heterogeneity of Glioblastoma. Cell Stem Cell 26, 48-63.e6.

Bhat, K.P.L., Balasubramaniyan, V., Vaillant, B., Ezhilarasan, R., Hummelink, K., Hollingsworth, F., Wani, K., Heathcock, L., James, J.D., Goodman, L.D., et al. (2013). Mesenchymal Differentiation Mediated by NF-κB Promotes Radiation Resistance in Glioblastoma. Cancer Cell 24, 331–346.

Bowman, R.L., Klemm, F., Akkari, L., Pyonteck, S.M., Sevenich, L., Quail, D.F., Dhara, S., Simpson, K., Gardner, E.E., Iacobuzio-Donahue, C.A., et al. (2016). Macrophage Ontogeny Underlies Differences in Tumor-Specific Education in Brain Malignancies. Cell Rep. 17, 2445–2459.

Brösicke, N., and Faissner, A. (2015). Role of tenascins in the ECM of gliomas. Cell Adhes. Migr. 9, 131–140.

Castellan, M., Guarnieri, A., Fujimura, A., Zanconato, F., Battilana, G., Panciera, T., Sladitschek, H.L., Contessotto, P., Citron, A., Grilli, A., et al. (2020). Single-cell analyses reveal YAP/TAZ as regulators of stemness and cell plasticity in glioblastoma. Nat. Cancer.

Chang, J., Wang, Y., Shao, L., Laberge, R.M., Demaria, M., Campisi, J., Janakiraman, K., Sharpless, N.E., Ding, S., Feng, W., et al. (2016). Clearance of senescent cells by ABT263 rejuvenates aged hematopoietic stem cells in mice. Nat. Med. 22, 78–83.

Chen, P., Zhao, D., Li, J., Liang, X., Li, J., Chang, A., Henry, V.K., Lan, Z., Spring, D.J., Rao, G., et al. (2019). Symbiotic Macrophage-Glioma Cell Interactions Reveal Synthetic Lethality in PTEN-Null Glioma. Cancer Cell 35, 868-884.e6.

Chen, Z., Trotman, L.C., Shaffer, D., Lin, H.K., Dotan, Z.A., Niki, M., Koutcher, J.A., Scher, H.I., Ludwig, T., Gerald, W., et al. (2005). Crucial role of p53-dependent cellular senescence in suppression of Pten-deficient tumorigenesis. Nature 436, 725–730.

Chien, Y., Scuoppo, C., Wang, X., Fang, X., Balgley, B., Bolden, J.E., Premsrirut, P., Luo, W., Chicas, A., Lee, C.S., et al. (2011). Control of the senescence-associated secretory phenotype by NF-κB promotes senescence and enhances chemosensitivity. Genes Dev. 25, 2125–2136.

Coppé, J.-P., Desprez, P.-Y., Krtolica, A., and Campisi, J. (2010). The Senescence-Associated Secretory Phenotype: The Dark Side of Tumor Suppression. Annu. Rev. Pathol. Mech. Dis. 5, 99–118.

Couturier, C.P., Ayyadhury, S., Le, P.U., Nadaf, J., Monlong, J., Riva, G., Allache, R., Baig, S., Yan, X., Bourgey, M., et al. (2020). Single-cell RNA-seq reveals that glioblastoma recapitulates a normal neurodevelopmental hierarchy. Nat. Commun. 11.

Darmanis, S., Sloan, S.A., Croote, D., Mignardi, M., Chernikova, S., Samghababi, P., Zhang, Y., Neff, N., Kowarsky, M., Caneda, C., et al. (2017). Single-Cell RNA-Seq Analysis of Infiltrating Neoplastic Cells at the Migrating Front of Human Glioblastoma. Cell Rep. 21, 1399–1410.

Demaria, M., Rodier, F., Laberge, R.-M., Campisi, J., Ohtani, N., Hara, E., Youssef, S., deBruin, A., Toussaint, W., Mitchell, J., et al. (2014). An essential role for senescent cells in optimal wound healing through secretion of PDGF-AA. Dev. Cell 31, 722–733.

Demaria, M., O'Leary, M.N., Chang, J., Shao, L., Liu, S., Alimirah, F., Koenig, K., Le, C., Mitin, N., Deal, A.M., et al. (2017). Cellular senescence promotes adverse effects of chemotherapy and cancer relapse. Cancer Discov. 7, 165–176.

Faget, D. V., Ren, Q., and Stewart, S.A. (2019). Unmasking senescence: context-dependent effects of SASP in cancer. Nat. Rev. Cancer 19, 439–453.

Friedmann-Morvinski, D., Soda, Y., Marumoto, T., Singer, O., Verma, I.M., Bushong, E.A., Ke, E., and Ellisman, M.H. (2012). Dedifferentiation of neurons and astrocytes by oncogenes can induce gliomas in mice. Science (80-.). 338, 1080–1084.

Gao, B., Doan, A., and Hybertson, B.M. (2014). The clinical potential of influencing Nrf2 signaling in degenerative and immunological disorders. Clin. Pharmacol. Adv. Appl. 6, 19–34.

Geraldo, L.H.M., Garcia, C., da Fonseca, A.C.C., Dubois, L.G.F., de Sampaio e Spohr, T.C.L., Matias, D., de Camargo Magalhães, E.S., do Amaral, R.F., da Rosa, B.G., Grimaldi, I., et al. (2019). Glioblastoma Therapy in the Age of Molecular Medicine. Trends in Cancer 5, 46–65.

Gibson, D.G., Young, L., Chuang, R.-Y., Venter, J.C., Hutchison, C.A., and Smith, H.O. (2009). Enzymatic assembly of DNA molecules up to several hundred kilobases. Nat. Methods 6, 343–345.

Gilder, A.S., Natali, L., Van Dyk, D.M., Zalfa, C., Banki, M.A., Pizzo, D.P., Wang, H., Klemke, R.L., Mantuano, E., and Gonias, S.L. (2018). The Urokinase Receptor Induces a Mesenchymal Gene Expression Signature in Glioblastoma Cells and Promotes Tumor Cell Survival in Neurospheres. Sci. Rep. 8, 1–16.

Gorgoulis, V., Adams, P.D., Alimonti, A., Bennett, D.C., Bischof, O., Bishop, C., Campisi, J., Collado, M., Evangelou, K., Ferbeyre, G., et al. (2019). Cellular Senescence: Defining a Path Forward. Cell 179, 813–827.

Guerrero, A., Herranz, N., Sun, B., Wagner, V., Gallage, S., Guiho, R., Wolter, K., Pombo, J., Irvine, E.E., Innes, A.J., et al. (2019). Cardiac glycosides are broad-spectrum senolytics. Nat. Metab. 1, 1074–1088.

Haage, V., Semtner, M., Vidal, R.O., Hernandez, D.P., Pong, W.W., Chen, Z., Hambardzumyan, D., Magrini, V., Ly, A., Walker, J., et al. (2019). Comprehensive gene expression meta-analysis identifies signature genes that distinguish microglia from peripheral monocytes/macrophages in health and glioma. Acta Neuropathol. Commun. 7, 1–18.

Harris, I.S., and DeNicola, G.M. (2020). The Complex Interplay between Antioxidants and ROS in Cancer. Trends Cell Biol. 30, 440–451.

Hayashi, M., Kuga, A., Suzuki, M., Panda, H., Kitamura, H., Motohashi, H., and Yamamoto, M. (2020). Microenvironmental Activation of Nrf2 Restricts the Progression of Nrf2-Activated Malignant Tumors. Cancer Res. 80, 3331–3344.

Hiebert, P., Wietecha, M.S., Cangkrama, M., Haertel, E., Mavrogonatou, E., Stumpe, M., Steenbock, H., Grossi, S., Beer, H.D., Angel, P., et al. (2018). Nrf2-Mediated Fibroblast Reprogramming Drives Cellular Senescence by Targeting the Matrisome. Dev. Cell 46, 145-161.e10.

Hubert, C.G., Rivera, M., Spangler, L.C., Wu, Q., Mack, S.C., Prager, B.C., Couce, M., McLendon, R.E., Sloan, A.E., and Rich, J.N. (2016). A three-dimensional organoid culture system derived from human glioblastomas recapitulates the hypoxic gradients and cancer stem cell heterogeneity of tumors found in vivo. Cancer Res. 76, 2465–2477.

Inoue, D., Suzuki, T., Mitsuishi, Y., Miki, Y., Suzuki, S., Sugawara, S., Watanabe, M., Sakurada, A., Endo, C., Uruno, A., et al. (2012). Accumulation of p62/SQSTM1 is associated with poor prognosis in patients with lung adenocarcinoma. Cancer Sci. 103, 760–766.

Kang, T.W., Yevsa, T., Woller, N., Hoenicke, L., Wuestefeld, T., Dauch, D., Hohmeyer, A., Gereke, M., Rudalska, R., Potapova, A., et al. (2011). Senescence surveillance of pre-malignant hepatocytes limits liver cancer development. Nature 479, 547–551.

Kohlhapp, F.J., Haribhai, D., Mathew, R., Duggan, R., Ellis, P.A., Wang, R., Lasater, E.A., Shi, Y., Dave, N., Riehm, J.J., et al. (2021). Venetoclax Increases Intratumoral Effector T Cells and

Antitumor Efficacy in Combination with Immune Checkpoint Blockade. Cancer Discov. 11, 68–79.

Kuleshov, M. V., Jones, M.R., Rouillard, A.D., Fernandez, N.F., Duan, Q., Wang, Z., Koplev, S., Jenkins, S.L., Jagodnik, K.M., Lachmann, A., et al. (2016). Enrichr: a comprehensive gene set enrichment analysis web server 2016 update. Nucleic Acids Res. 44, W90–W97.

Litak, J., Mazurek, M., Grochowski, C., Kamieniak, P., and Roliński, J. (2019). PD-L1/PD-1 axis in glioblastoma multiforme. Int. J. Mol. Sci. 20.

Livak, K.J., and Schmittgen, T.D. (2001). Analysis of relative gene expression data using real-time quantitative PCR and the 2-ΔΔCT method. Methods 25, 402–408.

Louis, D.N., Ohgaki, H., Wiestier, O.D., Cavenee, W.K., Ellison, D.W., Figarella-Branger, D., Perry, A., Reifenberger, G., and Von Deimling, A. WHO Classification of Tumours of the Central Nervous System.

Marino, S., Krimpenfort, P., Leung, C., van der Korput, H. a G.M., Trapman, J., Camenisch, I., Berns, A., and Brandner, S. (2002). PTEN is essential for cell migration but not for fate determination and tumourigenesis in the cerebellum. Development 129, 3513–3522.

Marumoto, T., Tashiro, A., Friedmann-Morvinski, D., Scadeng, M., Soda, Y., Gage, F.H., and Verma, I.M. (2009). Development of a novel mouse glioma model using lentiviral vectors. Nat. Med. 15, 110–116.

Menegon, S., Columbano, A., and Giordano, S. (2016). The Dual Roles of NRF2 in Cancer. Trends Mol. Med. 22, 578–593.

Mirzaei, R., Sarkar, S., Dzikowski, L., Rawji, K.S., Khan, L., Faissner, A., Bose, P., and Yong, V.W. (2018). Brain tumor-initiating cells export tenascin-C associated with exosomes to suppress T cell activity. Oncoimmunology 7, 1–14.

Mitsuishi, Y., Taguchi, K., Kawatani, Y., Shibata, T., Nukiwa, T., Aburatani, H., Yamamoto, M., and Motohashi, H. (2012). Nrf2 Redirects Glucose and Glutamine into Anabolic Pathways in Metabolic Reprogramming. Cancer Cell 22, 66–79.

Moiseeva, O., Deschênes-Simard, X., St-Germain, E., Igelmann, S., Huot, G., Cadar, A.E., Bourdeau, V., Pollak, M.N., and Ferbeyre, G. (2013). Metformin inhibits the senescence-associated secretory phenotype by interfering with IKK/NF-κB activation. Aging Cell 12, 489–498.

Mori T., Tanaka K., Buffo A., Wurst W., Kuhn R., G.M. (2006). Inducible Gene Deletion in Astroglia and Radial Glia—A Valuable Tool for Functional and Lineage Analysis. Glia.

Morita, T., and Hayashi, K. (2018). Tumor progression is mediated by Thymosin-b4 through a TGFb/MRTF signaling axis. Mol. Cancer Res. 16, 880–893.

Neftel, C., Laffy, J., Filbin, M.G., Hara, T., Shore, M.E., Rahme, G.J., Richman, A.R., Silverbush, D., Shaw, M.L., Hebert, C.M., et al. (2019). An Integrative Model of Cellular States, Plasticity, and Genetics for Glioblastoma. Cell 178, 835-849.e21.

Newman, A.M., Liu, C.L., Green, M.R., Gentles, A.J., Feng, W., Xu, Y., Hoang, C.D., Diehn, M., and Alizadeh, A.A. (2015). Robust enumeration of cell subsets from tissue expression profiles. Nat. Methods 12, 453–457.

Osswald, M., Jung, E., Sahm, F., Solecki, G., Venkataramani, V., Blaes, J., Weil, S., Horstmann, H., Wiestler, B., Syed, M., et al. (2015). Brain tumour cells interconnect to a functional and resistant network. Nature 528, 93–98.

Ostrom, Q.T., Gittleman, H., Farah, P., Ondracek, A., Chen, Y., Wolinsky, Y., Stroup, N.E., Kruchko, C., and Barnholtz-Sloan, J.S. (2013). CBTRUS statistical report: Primary brain and central nervous system tumors diagnosed in the United States in 2006-2010. Neuro. Oncol. 15.

Philips, A., Henshaw, D.L., Lamburn, G., and O'Carroll, M.J. (2018). Brain tumours: Rise in glioblastoma multiforme incidence in England 1995-2015 Suggests an Adverse Environmental or Lifestyle Factor. J. Environ. Public Health 2018.

Pölönen, P., Jawahar Deen, A., Leinonen, H.M., Jyrkkänen, H.K., Kuosmanen, S., Mononen, M., Jain, A., Tuomainen, T., Pasonen-Seppänen, S., Hartikainen, J.M., et al. (2019). Nrf2 and SQSTM1/p62 jointly contribute to mesenchymal transition and invasion in glioblastoma. Oncogene 38, 7473–7490.

Quail, D.F., and Joyce, J.A. (2017). The Microenvironmental Landscape of Brain Tumors. Cancer Cell 31, 326–341.

Richards, L.M., Whitley, O.K.N., MacLeod, G., Cavalli, F.M.G., Coutinho, F.J., Jaramillo, J.E., Svergun, N., Riverin, M., Croucher, D.C., Kushida, M., et al. (2021). Gradient of Developmental and Injury Response transcriptional states defines functional vulnerabilities underpinning glioblastoma heterogeneity. Nat. Cancer 2, 157–173.

Rojo de la Vega, M., Chapman, E., and Zhang, D.D. (2018). NRF2 and the Hallmarks of Cancer. Cancer Cell 34, 21–43.

Le Roux, I., Konge, J., Le Cam, L., Flamant, P., and Tajbakhsh, S. (2015). Numb is required to prevent p53-dependent senescence following skeletal muscle injury. Nat. Commun. 6, 8528.

Ruhland, M.K., Loza, A.J., Capietto, A.-H., Luo, X., Knolhoff, B.L., Flanagan, K.C., Belt, B.A., Alspach, E., Leahy, K., Luo, J., et al. (2016). Stromal senescence establishes an immunosuppressive microenvironment that drives tumorigenesis. Nat. Commun. 7, 11762.

Ruscetti, M., Leibold, J., Bott, M.J., Fennell, M., Kulick, A., Salgado, N.R., Chen, C.-C., Ho, Y.-J., Sanchez-Rivera, F.J., Feucht, J., et al. (2018) NK cell-mediated cytotoxicity contributes to tumor control by a cytostatic drug combination. Science 362,1416.

Saurty, M.S., Bellenger, L., El-Habr, E.A., Delaunay, V., Chneiweiss, H., Antoniewski, C., Morvan-Dubois, G., and Junier, M.P. (2019). Capture at the single cell level of metabolic modules distinguishing aggressive and indolent glioblastoma cells. BioRxiv 1–16.

Schindelin, J., Arganda-Carreras, I., Frise, E., Kaynig, V., Longair, M., Pietzsch, T., Preibisch, S., Rueden, C., Saalfeld, S., Schmid, B., et al. (2012). Fiji: An open-source platform for biological-image analysis. Nat. Methods 9, 676–682.

Schmitt, M.J., Company, C., Dramaretska, Y., Barozzi, I., Göhrig, A., Kertalli, S., Großmann, M., Naumann, H., Sanchez-Bailon, M.P., Hulsman, D., et al. (2020). Phenotypic mapping of pathological crosstalk between glioblastoma and innate immune cells by synthetic genetic tracing. Cancer Discov. CD-20-0219.

Sieben, C.J., Sturmlechner, I., van de Sluis, B., and van Deursen, J.M. (2018). Two-Step Senescence-Focused Cancer Therapies. Trends Cell Biol. 28, 723–737.

Stupp, R., Mason, W.P., Van Den Bent, M.J., Weller, M., Fisher, B., Taphoorn, M.J.B., Belanger, K., Brandes, A.A., Marosi, C., Bogdahn, U., et al. Radiotherapy plus Concomitant and Adjuvant Temozolomide for Glioblastoma.

Subramanian, A., Tamayo, P., Mootha, V.K., Mukherjee, S., Ebert, B.L., Gillette, M.A., Paulovich, A., Pomeroy, S.L., Golub, T.R., Lander, E.S., et al. (2005). Gene set enrichment analysis: A knowledge-based approach for interpreting genome-wide expression profiles.

Toso, A., Revandkar, A., DiMitri, D., Guccini, I., Proietti, M., Sarti, M., Pinton, S., Zhang, J., Kalathur, M., Civenni, G., et al. (2014). Enhancing chemotherapy efficacy in pten-deficient prostate tumors by activating the senescence-associated antitumor immunity. Cell Rep.

Triana-Martínez, F., Picallos-Rabina, P., Da Silva-Álvarez, S., Pietrocola, F., Llanos, S., Rodilla, V., Soprano, E., Pedrosa, P., Ferreirós, A., Barradas, M., et al. (2019). Identification and characterization of Cardiac Glycosides as senolytic compounds. Nat. Commun. 10, 1–12.

Verhaak, R.G.W., Hoadley, K.A., Purdom, E., Wang, V., Qi, Y., Wilkerson, M.D., Miller, C.R., Ding, L., Golub, T., Mesirov, J.P., et al. (2010). Integrated Genomic Analysis Identifies Clinically Relevant Subtypes of Glioblastoma Characterized by Abnormalities in PDGFRA, IDH1, EGFR, and NF1. Cancer Cell.

Wang, H., Lathia, J.D., Wu, Q., Wang, J., Li, Z., Heddleston, J.M., Eyler, C.E., Elderbroom, J., Gallagher, J., Schuschu, J., et al. (2009). Targeting interleukin 6 signaling suppresses glioma stem cell survival and tumor growth. Stem Cells 27, 2393–2404.

Wang, L., Babikir, H., Müller, S., Yagnik, G., Shamardani, K., Catalan, F., Kohanbash, G., Alvarado, B., Di Lullo, E., Kriegstein, A., et al. (2019). The phenotypes of proliferating glioblastoma cells reside on a single axis of variation. Cancer Discov. 9, 1708–1719.

Wang, Q., Hu, B., Hu, X., Kim, H., Squatrito, M., Scarpace, L., deCarvalho, A.C., Lyu, S., Li, P., Li, Y., et al. (2017). Tumor Evolution of Glioma-Intrinsic Gene Expression Subtypes Associates with Immunological Changes in the Microenvironment. Cancer Cell 32, 42-56.e6.

Weng, Q., Wang, J., Wang, J., He, D., Cheng, Z., Zhang, F., Verma, R., Xu, L., Dong, X., Liao, Y., et al. (2019). Single-Cell Transcriptomics Uncovers Glial Progenitor Diversity and Cell Fate Determinants during Development and Gliomagenesis. Cell Stem Cell 24, 707-723.e8.

Winkler, J., Abisoye-Ogunniyan, A., Metcalf, K.J., and Werb, Z. (2020). Concepts of extracellular matrix remodelling in tumour progression and metastasis. Nat. Commun. 11, 1–19.

Wyld, L., Bellantuono, I., Tchkonia, T., Morgan, J., Turner, O., Foss, F., George, J., Danson, S., and Kirkland, J.L. (2020). Senescence and cancer: A review of clinical implications of senescence and senotherapies. Cancers (Basel). 12, 1–20.

Xue, W., Zender, L., Miething, C., Dickins, R.A., Hernando, E., Krizhanovsky, V., Cordon-Cardo, C., and Lowe, S.W. (2007). Senescence and tumour clearance is triggered by p53 restoration in murine liver carcinomas. Nature 445, 656–660.

Yoshimoto, S., Loo, T.M., Atarashi, K., Kanda, H., Sato, S., Oyadomari, S., Iwakura, Y., Oshima, K., Morita, H., Hattori, M., et al. (2013). Obesity-induced gut microbial metabolite promotes liver cancer through senescence secretome. Nature 499, 97–101.

Yuan, Z.S., Cao, Y., and Li, Z.Y. (2017). IGFBP2 induces SPRY1 expression via NF-κB signaling pathway in glioblastoma multiforme (GBM). Eur. Rev. Med. Pharmacol. Sci. 21, 5072–5080.

Yue, H., Xu, Q., and Xie, S. (2018). High EMP3 expression might independently predict poor overall survival in glioblastoma and its expression is related to DNA methylation. Med. (United States) 97, 1–5.

Zhu, Y., Tchkonia, T., Pirtskhalava, T., Gower, A.C., Ding, H., Giorgadze, N., Palmer, A.K., Ikeno, Y., Hubbard, G.B., Lenburg, M., et al. (2015). The achilles' heel of senescent cells: From transcriptome to senolytic drugs. Aging Cell 14, 6.

Discussion and perspectives

Discussion and perspectives

Our data reveal the pro-tumorigenic action of malignant senescent cells in mouse and patient GBMs. We performed single-cell and bulk RNA sequencing, at the early and the end time points of the tumorigenesis on mouse GBMs in order to define the underlying mechanisms of $p16^{Ink4a\ Hi}$ senescent cells. Their elimination delays tumor growth and remodels both the malignant and the immune compartments. Indeed, senescence removal increases the malignant oligodendroglial lineage and overall decreases the mesenchymal cell identity of glioma cells. In addition, senolysis mitigates the anti-inflammatory and the immunosuppressive phenotypes of the GBM microenvironment (Figures 4D, 4E and 4F). On the one hand, senescence removal decreases the number of BMDMs and increases the T cell fraction. On the other hand, it modifies TAM activity/polarization via a decrease in BMDM anti-inflammatory genes and in microglia cMyc pathway. The cMyc pathway is expressed in M2-TAMs where it controls expression of protumoral genes in human cancer cell lines (Pello et al., 2012). Importantly, we established a senescent signature of 31 genes from the scRNAseq data at the early timepoint and confirmed its conservation in single-cell transcriptomic data of patient GBMs (Neftel et al., 2019).

The discussion will cover the advantages and limits of our model of study, the potential senescence inducers in this model and the pleiotropic functions of senescence during gliomagenesis. Importantly, our results open new avenues for improving patient prognosis and accordingly for adapting a personalized treatment based on the development of senotherapies.

1. Mouse GBM as a translatable model for a patient GBM

Developing mouse models of GBM faithfully recapitulating patient gliomagenesis is crucial to better understand GBM biological processes and develop preclinical antitumor therapies. It is therefore important to identify the strengths and limitations of each model and technique to improve the translation of fundamental research outputs into clinical studies.

One of the most important advantages of the GBM mouse model developed in this project is the strong conservation of histological features and senescent mechanisms between mouse and patient GBMs, which was rather unexpected. First, the presence of *in situ* SA-β-gal+ Ki67- $p19^{ARF}$+ senescent cells in murine GBMs and SA-β-gal+ Ki67- $p16^{INK4A}$+ senescent cells in patient GBMs encouraged us to use this model to study cellular senescence in GBM (Figures 1A and 1D). Second, the murine GBM recapitulates patient GBM at a histopathological level with palissadic necrosis, immune infiltrates, hypervascularization and invasiveness among others (Figure S1B). Noteworthy, these histological features are enriched in GBM-MES which validated the combination of genetic alterations (loss of *Nf1* (via HRasV12), *Pten* and *p53*) in

the model (Louis et al., 2016; Verhaak et al., 2010). The mesenchymal subtype and cellular state of the mouse tumors, were further validated at bulk and single cell transcriptomics levels. Interestingly, upon senescence removal, these GBM characteristics were partially lost at an early and late timepoint (Figures S3I and S3J). Third, the senescence signature identified in the GBM mouse model was conserved in patient GBMs (Figures 7C and 7F). The senescent cells in mouse GBM display a MES-like state and senescent cells in patient GBMs display an AC-like and MES-like states, which strengthens the relevance of our model to understand the biology of patient GBMs.

The mouse model also presents secondary mutations in a rather short period of time (around 32 days post lentivirus injection) upon the introduction of solely three genetic alterations. For instance, inferring copy number variations analysis demonstrates the loss of MHC on chromosome 17, recapitulating the deletion of HLA locus at the 6p21 chromosomic region in patient GBMs, essential for adaptive immune functions (Figure S3E) (Yeung et al., 2013). Nevertheless, the quadrant representation of cellular states captures murine GBM cells as less heterogenous, (cells are less spread out from the center) than patient GBM cells (Figures 3J, 3K, 7E and 7G). This analysis suggests that the induction of secondary mutations is not sufficient to increase cellular state heterogeneity or that intratumoral heterogeneity requires a longer timeline to be established. Yet, bulk RNAseq heatmaps depicts relative intertumoral heterogeneity (Figures S2A and S2D) in line with intertumoral heterogeneity of patient GBMs.

2. Mouse GBM as functional model to study cellular senescence

We chose to use an immunocompetent mouse model of GBM with conserved immune compartments for two main reasons: (i) senescent cells can interact and modulate the activity of immune cells (Eggert et al., 2016; Iannello et al., 2013; Di Mitri and Alimonti, 2016; Ruhland et al., 2016b) and (ii) patient GBM-MES displays a high infiltration of immune cells (Bhat et al., 2013; Wang et al., 2017). Furthermore, the lentiviral induction of gliomagenesis in neural stem cells (*Glast* expressing cells of the subventricular zone) reproduces more closely the initiation steps of gliomagenesis compared with the grafting of glioma cells into syngeneic mouse model and develops relatively faster than patient-derived xenograft immunodeficient mouse models (Robertson et al., 2019). The tumor growth between lentivirus-injected mice is relatively reproducible in time, which makes the model ideal for testing various treatment protocols.
In the study, I consistently included control and experimental mice in each cohort to limit the technical variability due to mouse surgery. In addition, we implemented the Firefly Luciferase cassette into the lentiviral construct during the course of the project, for *in vivo* monitoring of tumor progression. This further enables a close control of treatment delivery at a same timepoint of the tumor progression for each animal. Indeed, the cohorts with bioluminescence

monitoring of tumor progression are more homogeneous and the increased survival upon senolytic treatments is statistically more significant (Figures 2D and 2E) than without the monitoring of tumor growth (Figure 2B).

To investigate the senescence functions *in vivo* in GBM, we introduced the p16-3MR transgene into the GBM mouse model (Demaria et al., 2014). GCV treatments enable the efficient elimination of $p16^{Ink4a\ Hi}$ senescent cells within p16-3MR GBMs. The $p16^{Ink4a\ Hi}$ senescent cells account for less than 10% of the whole tumor cells (Figures 2G and 3I) and corresponds to the SA-β-gal area quantified in the tumor (Figure 2G). Yet their removal strikingly remodels the tumor ecosystem. It decreases the mesenchymal subtype and cellular state at an early and late timepoint (Figures S3I and S3J). Furthermore, it increases the oligodendroglial lineage, and induces a shift of the cellular state of pri-OPC (the GBM transient amplifying cells) from MES-like to AC-like state (Figures 3I, 3J, 3K and 3L). These results suggest that senescence removal remodels GBM cellular states and induces, directly or indirectly, a more differentiated and overall less aggressive GBM phenotype.

Multiple studies use two ways to eliminate senescent cells to confirm their function in the phenotype of interest (Bussian et al., 2018; Chang et al., 2016b; Farr et al., 2017). Remarkably, senolytic ABT263 treatment seems to affect mouse GBM-derived organoids via the same mechanisms of senescence identified in the p16-3MR paradigm, and further validates the role of NRF2 pathway in $p16^{Ink4a\ Hi}$ malignant cells. *In vivo* analysis of the ABT263 paradigm remains to be done to verify whether the p16-independent senescent cell removal will target the same or a broader pool of senescent malignant cells, or may also affects the senescent TAM identified in mouse and patient GBMs (SA-β-gal+ IBA1+, Figures 1A and 1D). The subsequent changes triggered in GBM upon ABT263 will also be analyzed.

3. Technical approaches to decipher the functions of senescence

The use of single cell transcriptomics in GBM upon senescence removal allowed us to take a significant step forward in the identification of $p16^{Ink4a\ Hi}$ senescent cells. In addition, it provided insights into the functions of $p16^{Ink4a\ Hi}$ senescent cells on the GBM biology at multiple levels, including their cellular identity and state, their interactions with distinct malignant and immune clusters, and the identification of NRF2, a pro-tumorigenic regulatory gene in senescent cells.

However, one limitation of the scRNAseq method is the underrepresentation or lack of cell types described in the GBM microenvironment such as neurons, dendritic cells, endothelial cells or immune subpopulations. Beforehand, the scRNAseq technique requires a single cell suspension for the droplet-based cell encapsulation. Thus, we optimized the obtention a single

cell suspension from murine GBM by papain enzymatic digestion, which can potentially deplete fragile cell types (e.g., neurons, endothelial cells). As an example, deconvoluted CIBERSORT analysis from bulk RNAseq data suggests the presence of dendritic cells (Figure S4D), which are antigen-presenting cells playing important role in T cell stimulation, but these cells were absent from scRNAseq clusters (Figures 3C and 3F). To overcome this issue and increase the cell number of specific populations such as CD45+ (myeloid compartment) or CD3+ (T cells) immune cells, FACS enrichment could be performed, in the future, prior to scRNAseq. Of note, FACS sorted data of mouse GBMs depict an inherent proportion of 80% of GFP+ malignant cells and 20% of GFP- TME cells (data not shown) which was preserved by the droplet-based cell encapsulation in scRNAseq (Figure 4D).

Other methods of transcriptomics or immunolabeling can be used to retrieve the absent cell types of GBM. On the one hand, the single-nucleus RNAseq, which consists of single isolated nuclei sequencing, replaces the challenging whole cell isolation of certain cell types. On the other hand, methods for efficient immunostaining of a cleared whole organ, such as the iDISCO method, allow the three-dimensional imaging of specific cell types (Renier et al., 2014). The iDISCO method was co-developed by Nicolas Renier with whom we collaborated during the course of my PhD. As an example, Tomek Topilko, a PhD student in Renier's team, labeled the whole brain blood of a brain bearing a GBM, using a secondary anti-mouse IgG antibody (Alexa 647) to visualize the entire brain vasculature (***Figure 18***). Interestingly, the observed vascular system reproduces the GBM regionalization of a vascularized invasive periphery and a necrotic core of patient GBMs (Louis et al., 2016). In the brain parenchyma, blood vessels appear compressed, the tumor periphery displaying large irregular vessels while the tumor core is poorly vascularized with small venules and arterioles. One question we could not address in our study is the role of senescence on angiogenesis during gliomagenesis. The use of an upgraded method developed in the Renier's team to compare GBM vasculature of mice treated or not with senolytic treatment could provide insights on the effects of senescent cells on vascularization (Kirst et al., 2020). Indeed, SASP factors of therapy-induced senescent cells remodel pancreatic cancer vascularization which increases drug delivery (Ruscetti et al., 2020). Thus, senolytic treatment could potentially reduce drug delivery in GBM but also decrease the adverse effects of angiogenesis in tumor progression. This study is of particular interest as GSEA performed on the tumor bulk RNAseq at the endpoints of the mice showed a decrease of the angiogenesis pathway upon $p16^{Ink4a\ Hi}$ cells removal (Figures S2B and S2E).

Although scRNAseq reflects the intratumoral heterogeneity, it does not provide information on the cellular and structural regionalization of the tumor. The use of spatial transcriptomics could comprehensively characterize the spatial organization of GBM cellular heterogeneity. This promising technique opens the possibility to address various questions including the profiling

of rare and unique cell type (e.g., T cell subpopulations), the cell location of senescent cells within the GBM regions (e.g., hypoxic or infiltrative) as well as the immune cell polarization state according to the relative proximity with other cell types (e.g., senescent cells).

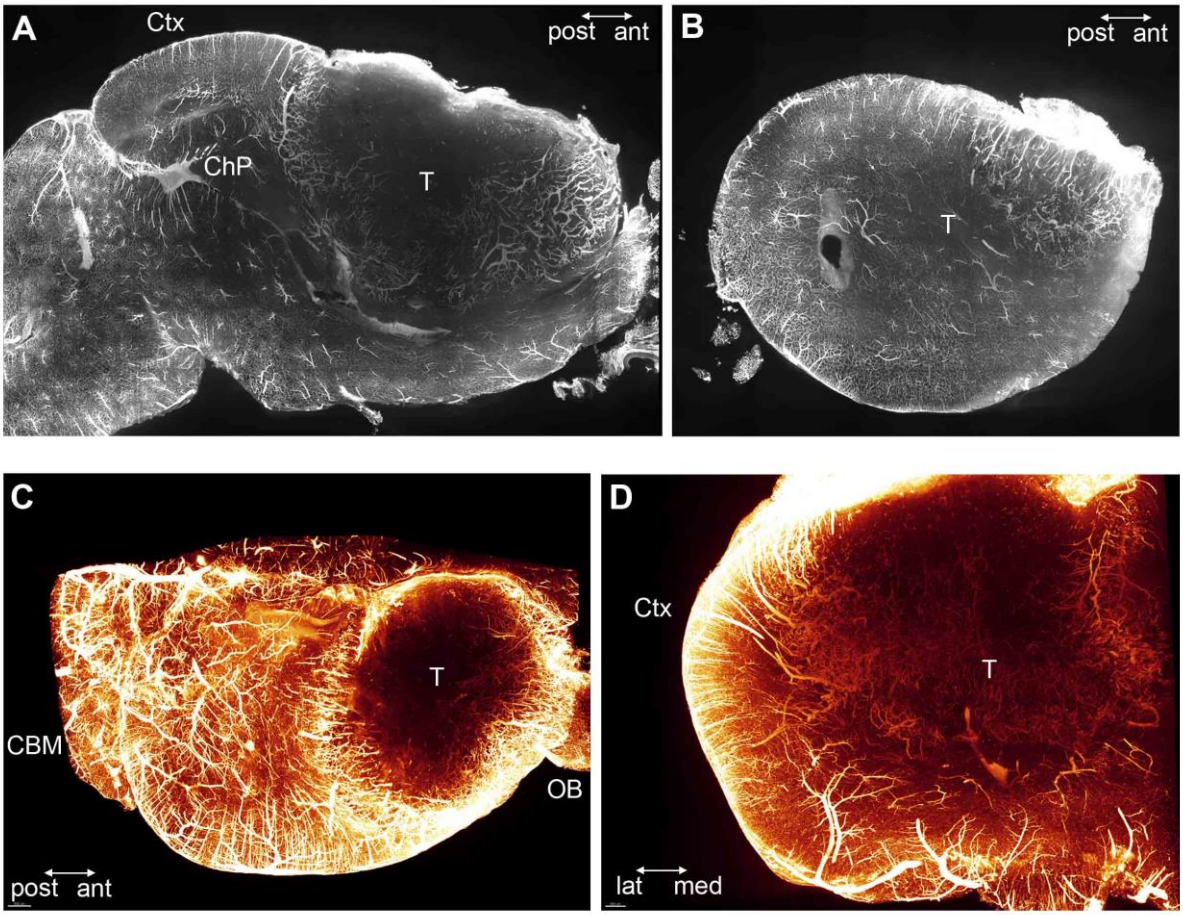

Figure 18. **Light sheet acquisitions of a murine brain with GBM immunolabelled for the vasculature**
The mouse was collected at the end points.
A. Sagittal view of the mouse brain.
B. Projection of the tumor lateral periphery.
C. Dorsal view of the mouse brain.
D. Coronal view of the tumor.
ChP: choroid plexus CBM: cerebellum; ctx: cortex; OB: olfactory bulb; T: tumor; ant: anterior; post: posterior; lat: lateral; med: medial.

Novel techniques are being developed, such as the GeoMx^{TM} Digital Spatial Profiler (launched in 2019) which combines single-cell antigen and RNA profiling at a spatial resolution. To this end, sections of a FFPE or frozen sample are simultaneously stained with imaging and profiling reagents. Imaging reagents consist of up to four antibodies coupled with fluorochrome as morphological markers, to stain for instance CD45+ myeloid cells, CD3+ T cells, GFP+

malignant cells, or hypoxic regions and be able to locate several regions of interest (ROI, of 100 µm) within the tissue. Profiling reagents correspond to a range of thousands of antibodies or RNA probes coupled with a DNA indexing oligonucleotide sequence, and cleaved when exposed to UV light. Once the ROIs are located, they are sequentially exposed to UV light to decouple to oligonucleotides from the profiling reagents. The oligonucleotides indexed to each ROI are then aspired and sequenced on an nCounter system.

One major advantage of this technology is the possible integration of our generated scRNAseq analysis to the GeoMx™ data in order to phenotype and locate already identified cell types within the tumor. The study of GBM upon senescence removal at a spatial transcriptomics level could improve insights into the potential rewiring of the immune infiltration/polarization and the differentiation of malignant cells in specific GBM regions.

4. Senescence inducers in GBM

Besides the cellular identity of senescent cells, considering the tissue context and the inducers of senescence is important to better understand the impact of cellular senescence during tumorigenesis (Faget et al., 2019). In the GBM mouse model, the potential senescence inducers are multiple and could include the oncogenic expression of HRasV12, the loss of *Pten* expression and ROS production notably from hypoxic regions (Sieben et al., 2018). Likewise, in patient GBMs, loss of *Nf1* and *Pten* and increased ROS could be potential candidates for senescence inducers during primary gliomagenesis, as the GBM mouse model recapitulates faithfully patient GBM biology.

Previous studies described that the activation of oncogenic RasV12 induces a widespread and p53-dependent SA-β-gal activity in the mouse GBM, and the loss of *Pten* in GBM neurospheres induces senescence (Banasavadi-Siddegowda et al., 2017; Marumoto et al., 2009). However, GBM genomic alterations are complex and rely on more than one mutation. Introducing Pten floxed allele along with RasV12 expression and the shp53 not only recapitulates GBM-MES alterations but also cumulates potential senescent inducers as it would occur in patient GBMs. Interestingly, although p53 is a senescence mediator, reduced p53 expression triggers a more developed SASP in cultured human cancer cells (Coppé et al., 2008) and our data cannot exclude this possibility.

One additional senescence inducer we did not address in the present study is aging. Senescent cells accumulate during lifetime and is associated with tumorigenesis onset (Baker et al., 2011). In addition, the median age of patients with GBM at diagnosis is 62 years old which makes GBM, and cancer in general, an age-related disease (Louis et al., 2016). One approach to analyze the contribution of aging as an inducer of cellular senescence in GBM would be to trigger gliomagenesis in both young (6-to-8 week old) and aged (1.5-to-2 years

old) mice, and compare their respective tumor size and survival. Nevertheless, the aged mouse model includes several challenges related to the intracranial injection procedure that I encountered in my attempts of developing this paradigm, including lower resistance to anesthesia and slower recovery from the surgery.

5. NRF2 partly mediates the pro-tumoral senescence in GBM

NRF2 and hypoxia

Senescent cells are mostly located in proliferative areas and adjacent to necrotic regions (Figure S1C). These regions are subjected to hypoxia and consequently high levels of ROS (Guzy et al., 2005). When cells are exposed to high ROS levels, the transcription factor NRF2 is no longer bound to KEAP1, which under basal condition mediates its proteasomal degradation, and thus allows NRF2 to translocate to the nucleus (Harris and DeNicola, 2020). NRF2 in turn binds to antioxidant responsive element (ARE) sequence to activate the expression of target genes which products control tumor growth, metastasis, treatment resistance (Rojo de la Vega et al., 2018). NRF2 can induce cellular senescence in fibroblasts *in vitro* and which is associated with a cancer-associated phenotype *in vivo* (Hiebert et al., 2018).

Importantly, we identify NRF2 as an upstream regulator of SASP factors (*Plaur, Tnc, Areg, Igfbp3, Tgif1*) regulating the pro-tumoral actions of $p16^{Ink4a}$ senescent cells. Further chromatin immunoprecipitation sequencing experiments on murine and patient GBMs will validate the direct or indirect activation of SASP factors by NRF2. Interestingly, recent studies emphasize the diversity of the senescence programs initiated by hypoxia and NRF2 according to the context. Van Vliet and colleagues showed that hypoxia reduces SASP expression in physiological and chemotherapy-treatment contexts (van Vliet et al., 2021). Along the same line, Lee and colleagues demonstrated that in therapy-induced and replicative senescence models, the senescence-associated selective autophagy of KEAP1 via p62 promotes the activation of the NRF2 pathway contributing to the redox homeostasis and not, in this context, to the activation of SASP (Lee et al., 2021).

Interestingly, hypoxia can inhibit OPC differentiation (Singh et al., 2018), a phenomenon that could occur in GBM. Upon senescence removal, p16-3MR GBMs display an increased in the number of committed OPC-like cells (COP) and in myelinating oligodendrocytes (mOL) (Figure 3I). In addition, the removal of senescent cells decreases the hypoxic environment at least at the end points of the mice (Figure S2B) and could therefore promote oligodendroglial differentiation. Likewise, senescence removal could mimic the use of myelination-promoting

agents (e.g., dibutyril cAMP and Pranlukast) that increases oligodendroglial differentiation and reduces tumor growth in a mouse model of GBM (Brooks et al., 2021).

NRF2 in tumor growth

Our results strongly suggest that NRF2 modulates the pro-tumorigenic function of p16$^{Ink4a\ Hi}$ senescent cells. Several studies have demonstrated the association between NRF2 and GBM aggressiveness. Indeed, the p62-mediated degradation of NRF2 promotes *in vitro* GSC survival and is hyperactivated in the MES-GBM subtype (Pölönen et al., 2019). In addition, NRF2 uses the Hippo pathway effector TAZ to induce GBM growth and decreases GBM-bearing mice survival (Escoll et al., 2020). TAZ also regulates the GBM-MES differentiation and is a master regulator, along with YAP, of the GSC G-STEM state (Bhat et al., 2011; Castellan et al., 2020). Similarly, *Nfe2l2* (encoding for NRF2) is expressed in glycolytic/plurimetabolic GSCs which correlated with a MES-like state (Garofano et al., 2021).

The identified NRF2 targets in our study are associated with tumor aggressiveness. The expressions of *Tnc*, *Igfbp3* and *Plaur* are higher in GBM-MES and are associated with a worse patient prognosis (Angel et al., 2020; Chen et al., 2020; Verhaak et al., 2010). Gja1, another NRF2 target, also promotes GBM growth and reduces GBM-bearing mouse survival (Osswald et al., 2015). However, the functions of NRF2 in cancer is complex. As an illustration, in the GBM mouse model, *Nfe2l2* expression is enriched in: (i) *p16$^{Ink4a\ Hi}$* cells within the malignant compartment and (ii) in the immune compartment (in cells with a *p16^{Ink4a}* gene expression<1, Figure 5H). Noteworthy, NRF2, in immune cells, plays beneficial roles during tumorigenesis by inhibiting the immunosuppressive functions of MDSCs and T reg cells (Hayashi et al., 2020; Hiramoto et al., 2014; Maj et al., 2017).

One missing aspect of our study to confirm the pro-tumorigenic function of NRF2 in senescent malignant cells, is a functional investigation of NRF2 specifically in these cells. We are currently doing experiments in that direction. We introduced a micro-RNA (miR) targeting either NRF2 (miR NRF2) or a no-targeting scrambled oligonucleotide (miR ctl) into the lentiviral construct that induces gliomagenesis (**Figure *19***). Beforehand, we validated the miR NRF2 efficacy in mouse glioma cells (GL261) in culture. This strategy should downregulate NRF2 specifically in malignant cells. To date, two cohorts of 10 mice each, have been injected with the lentivirus containing the miR ctl (lv-miR) or the lv-miR NRF2. We will perform survival, histological and transcriptomic studies on the mice and the corresponding GBMs.

Importantly, our data showed that a high senescence signature score and a high NRF2 targets score are correlated with a worse survival of patients with GBM. Nonetheless, patients with GBM harboring a low senescent score show a better survival from 6 months onwards while

patients with GBMs harboring a low NRF2 targets score show better survival only from one year onwards (Figure 7H and 7J). This result suggests that NRF2 may only in part modulate the pro-tumoral functions of p16$^{Ink4a\ Hi}$ senescent malignant cells.

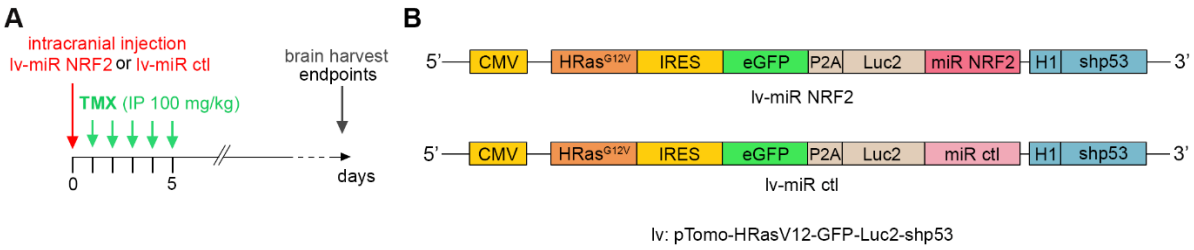

Figure 19. Strategy targeting Nrf2 in GBM malignant cells
A. Timeline of the mouse GBM generation using either the lv-miR NRF2 or the lv-miR ctl.
B. Lentiviral construct of the corresponding lv-miR NRF2 and lv-miR ctl.
lv: lentivirus; miR: micro-RNA; ctl: control.

6. Senescence and the immune compartment

Our results suggest that the pro-tumoral functions of senescence in GBM includes tumor growth, cellular plasticity but also immunosuppression. The paracrine function of the p16$^{Ink4a\ Hi}$ senescent cells are mediated by their SASP among which several factors could promote an immunosuppressive microenvironment (Figure 7C and Table S3). Indeed, *Lgals1* contribute to M2-macrophages and MDSCs-mediated immunosuppression in a syngeneic mouse GBM (Chen et al., 2019). In addition, *Plxnd1*, *Anxa2* and *Timp1* are known anti-inflammatory M2 markers which could also trigger GBM immunosuppression (Darmanis et al., 2017).

SASP factors are further enriched in ECM components. The ECM acts as a reservoir of cytokines and growth factors that can be released upon ECM degradation. ECM remodeling can control differentiation, activation, and polarization of immune cells in the TME (Henke et al., 2020) and could potentially be endorsed by the components of the SASP (e.g., MMP and ADAM metalloproteases). For instance, TNC, an ECM glycoprotein, can bind to the αVβ3 integrin receptor in various cancer tissues (Yoshida et al., 2015). Our *in silico* analysis suggests that malignant cells expressing *Tnc* interacts with T cells expressing the *αVβ3 integrin*. One model could be that the decrease of TNC expression following senescence removal partly decreases T cell exhaustion as observed at early timepoint in p16-3MR GBMs (Figures 4D and 4F).

Altogether, these results suggest that SASP-mediated ECM remodeling could inhibit T cell infiltration/activity, fuel the immunosuppression, and thus contributing to the overall establishment of the GBM-MES subtype (Doucette et al., 2013; Wang et al., 2017b; Zanotto-Filho et al., 2017).

7. Developing senotherapy for patients with GBM

We established a senescence signature based on the scRNAseq analysis of control mouse GBMs (Figures 7C and 7D). The conservation of this signature in malignant cells from patient GBMs further strengthened its specificity (Figure 7F). Importantly, the high score of the senescence signature correlates with a worse patient survival (Figures 7H). Other teams identified either single genes or a gene panel signature in GBM which are associated with worse patient survival. However the studies are solely based on TGCA and the Chinese Glioma Genome Atlas (CGGA) data without functional validation experiments (Jia et al., 2018; Zuo et al., 2019). Similarly, very few studies identified senescence signatures in cancer (Wyld et al., 2020). Xiang and colleagues identified a 7-gene senescence signature co-expressed in replicative-induced and OIS cells, while Althubiti and colleagues found a 10-gene senescence signature in p16- and p21-bladder cancer cell lines. Single gene expression of both signatures correlates negatively with hepatocarcinoma and breast cancer patient survival respectively but the combined contribution of all genes was not studied (Althubiti et al., 2014; Xiang et al., 2019). None of these described genes were found in the GBM senescence signature we unveiled in the study.

Additionally, our results suggest that the identified senescent signature can be used as survival prognostic method for patients with GBM. Further multivariate analysis should be performed to determine the contribution of senescence in survival according to age, gender, or treatment of patients. Notably, single nuclei RNAseq opens the possibility to analyze an increasing number of patient frozen GBM samples from the tumor bank Onconeurotek accessible on site and identify at a single cell level the cells expressing the signature. The direct correlation of the senescence signature at a single cell level, with patient survival will better refine the cell identity and the senescent mechanisms leading to a worse survival in patients. In addition, the identification of the senescent signature should be extended to lower grade gliomas, and also to other CNS pathologies and neurodegenerative diseases considering (i) the presence of molecules restricted to the CNS (e.g., TNC) and (ii) the known contribution of senescence in some of these diseases (Bhat et al., 2012; Bussian et al., 2018; Chinta et al., 2018; Zhang et al., 2019).

A direct application of my PhD work could be the senescence scoring of patient biopsies or resected samples in order to improve the design of personalized treatment and determine the

most effective combinatorial strategy, including eventually senolytics. To achieve this purpose, developing selective senotherapeutic agents of GBMs becomes a priority. Ideally, a senotherapeutics should preferably cross the BBB and thus possess several physicochemical parameters (e.g. the size of the molecule, its interaction with efflux pumps and transporters) (Dréan et al., 2016). Nonetheless, this requirement is not mandatory as the ultrasound-based opening of the BBB using technologies such as the SonoCloud® device can bypass the BBB restriction and increase treatment penetration (Idbaih et al., 2019).

Our data strongly suggest that senotherapeutics could be an effective therapeutic strategy solely or in combination for patients with GBM to delay tumor growth or recurrence. For instance, senotherapy can be envisioned in combination with conventional therapies to reduce the side effects of the TIS induced by conventional therapies and to delay GBM recurrence. Although immunotherapies have gained much success in various cancers such as melanoma and non-small cell lung cancers, they are yet inefficient in GBMs (Jackson et al., 2019). These tumors are qualified as “cold” tumors as they display a highly intrinsic and adaptive resistance to immunotherapies. The malignant-intrinsic resistance includes acquired genetic alteration such as *Pten* loss which induces PD-L1 expression and contributes to immunoresistance in GBM xenograft mice (Parsa et al., 2007). Conversely, adaptive resistance is promoted by cells from the TME including immunosuppressive immune cells and the reduced number of immune effector cells (Quail and Joyce, 2017). Therefore, GBM largely escapes the immunosurveillance mechanisms (Jackson et al., 2019). Here, we reported an increase in T cell number which displayed a decreased expression of immune checkpoint receptors (*Ctl4a*, *Lag3*, *Pdcd1*), upon senescence removal (Figures 4D and 4F). We propose a model in which senotherapy could partly initiate an immunosurveillance response to become “warm” the tumor, and provide a rational for combining senotherapeutics with immunotherapies in GBM.

As a conclusion, we unveiled the role of cellular senescence during primary gliomagenesis. We used an original approach consisting of analyzing a tumor with and without treatment at the single cell level to comprehensively understand the underlying mechanism of the drug. The massive amount of transcriptomic data generated during this study will open the road for many upcoming explorations. In parallel, the conception and the fast expansion of novel leading-edge technologies, such as spatial transcriptomics and proteomics, will further enrich our current knowledge on GBM. Altogether, our work along with many future studies will hopefully pave the way for the development of personalized treatment strategies to finally defeat the therapy resistance of GBM.

Bibliography

Bibliography

Aasland, D., Gotzinger, L., Hauck, L., Berte, N., Meyer, J., Effenberger, M., Schneider, S., Reuber, E.E., Roos, W.P., Tomicic, M.T., et al. (2019). Temozolomide induces senescence and repression of DNA repair pathways in glioblastoma cells via activation of ATR–Chk1, p21, and NF-kB. Cancer Res. *79*, 99–113.

Acosta, J.C., O'Loghlen, A., Banito, A., Guijarro, M. V., Augert, A., Raguz, S., Fumagalli, M., Da Costa, M., Brown, C., Popov, N., et al. (2008). Chemokine Signaling via the CXCR2 Receptor Reinforces Senescence. Cell *133*, 1006–1018.

Acosta, J.C., Banito, A., Wuestefeld, T., Georgilis, A., Janich, P., Morton, J.P., Athineos, D., Kang, T.-W., Lasitschka, F., Andrulis, M., et al. (2013). A complex secretory program orchestrated by the inflammasome controls paracrine senescence. Nat. Cell Biol. *15*, 978–990.

Alban, T.J., Alvarado, A.G., Sorensen, M.D., Bayik, D., Volovetz, J., Serbinowski, E., Mulkearns-Hubert, E.E., Sinyuk, M., Hale, J.S., Onzi, G.R., et al. (2018). Global immune fingerprinting in glioblastoma reveals immune-suppression signatures associated with prognosis. JCI Insight *3*.

Alcantara Llaguno, S., Chen, J., Kwon, C.H., Jackson, E.L., Li, Y., Burns, D.K., Alvarez-Buylla, A., and Parada, L.F. (2009). Malignant Astrocytomas Originate from Neural Stem/Progenitor Cells in a Somatic Tumor Suppressor Mouse Model. Cancer Cell *15*, 45–56.

Alcantara Llaguno, S., Sun, D., Pedraza, A.M., Vera, E., Wang, Z., Burns, D.K., and Parada, L.F. (2019). Cell-of-origin susceptibility to glioblastoma formation declines with neural lineage restriction. Nat. Neurosci. *22*, 545–555.

Alcantara Llaguno, S.R., Wang, Z., Sun, D., Chen, J., Xu, J., Kim, E., Hatanpaa, K.J., Raisanen, J.M., Burns, D.K., Johnson, J.E., et al. (2015). Adult Lineage-Restricted CNS Progenitors Specify Distinct Glioblastoma Subtypes. Cancer Cell *28*, 429–440.

Allen, M., Bjerke, M., Edlund, H., Nelander, S., and Westermark, B. (2016). Origin of the U87MG glioma cell line: Good news and bad news. Sci. Transl. Med. *8*, 354re3 LP-354re3.

Althubiti, M., Lezina, L., Carrera, S., Jukes-Jones, R., Giblett, S.M., Antonov, A., Barlev, N., Saldanha, G.S., Pritchard, C.A., Cain, K., et al. (2014). Characterization of novel markers of senescence and their prognostic potential in cancer. Cell Death Dis. *5*, e1528-10.

Amor, C., Feucht, J., Leibold, J., Ho, Y.J., Zhu, C., Alonso-Curbelo, D., Mansilla-Soto, J., Boyer, J.A., Li, X., Giavridis, T., et al. (2020). Senolytic CAR T cells reverse senescence-associated pathologies. Nature *583*, 127–132.

Angel, I., Pilo Kerman, O., Rousso-Noori, L., and Friedmann-Morvinski, D. (2020). Tenascin C promotes cancer cell plasticity in mesenchymal glioblastoma. Oncogene *39*, 6990–7004.

Baar, M.P., Brandt, R.M.C., Putavet, D.A., Klein, J.D.D., Derks, K.W.J., Bourgeois, B.R.M., Stryeck, S., Rijksen, Y., van Willigenburg, H., Feijtel, D.A., et al. (2017). Targeted Apoptosis of Senescent Cells Restores Tissue Homeostasis in Response to Chemotoxicity and Aging. Cell *169*, 132-147.e16.

Baker, D.J., Perez-Terzic, C., Jin, F., Pitel, K., Niederländer, N.J., Jeganathan, K., Yamada, S., Reyes, S., Rowe, L., Hiddinga, H.J., et al. (2008). Opposing roles for p16Ink4a and p19Arf in senescence and ageing caused by BubR1 insufficiency. Nat. Cell Biol. *10*, 825–836.

Baker, D.J., Wijshake, T., Tchkonia, T., Lebrasseur, N.K., Childs, B.G., Van De Sluis, B., Kirkland, J.L., and Van Deursen, J.M. (2011). Clearance of p16 Ink4a-positive senescent cells delays ageing-associated disorders. Nature *479*, 232–236.

Balakrishnan, I., Danis, E., Pierce, A., Madhavan, K., Wang, D., Dahl, N., Sanford, B., Birks, D.K., Davidson, N., Metselaar, D.S., et al. (2020). Senescence Induced by BMI1 Inhibition Is a Therapeutic Vulnerability in H3K27M-Mutant DIPG. Cell Rep. *33*.

Banasavadi-Siddegowda, Y.K., Russell, L., Frair, E., Karkhanis, V.A., Relation, T., Yoo, J.Y., Zhang, J., Sif, S., Imitola, J., Baiocchi, R., et al. (2017). PRMT5-PTEN molecular pathway regulates senescence and self-renewal of primary glioblastoma neurosphere cells. Oncogene *36*, 263–274.

Bao, S., Wu, Q., McLendon, R.E., Hao, Y., Shi, Q., Hjelmeland, A.B., Dewhirst, M.W., Bigner, D.D., and Rich, J.N. (2006). Glioma stem cells promote radioresistance by preferential activation of the DNA damage response. Nature *444*, 756–760.

Basisty, N., Kale, A., Jeon, O.H., Kuehnemann, C., Payne, T., Rao, C., Holtz, A., Shah, S., Sharma, V., Ferrucci, L., et al. (2020). A Proteomic Atlas of Senescence-Associated Secretomes for Aging Biomarker Development. PLoS Biol.

Bhaduri, A., Di Lullo, E., Jung, D., Müller, S., Crouch, E.E., Espinosa, C.S., Ozawa, T., Alvarado, B., Spatazza, J., Cadwell, C.R., et al. (2020). Outer Radial Glia-like Cancer Stem Cells Contribute to Heterogeneity of Glioblastoma. Cell Stem Cell *26*, 48-63.e6.

Bhat, K.P.L., Salazar, K.L., Balasubramaniyan, V., Wani, K., Heathcock, L., Hollingsworth, F., James, J.D., Gumin, J., Diefes, K.L., Kim, S.H., et al. (2011). The transcriptional coactivator TAZ regulates mesenchymal differentiation in malignant glioma. Genes Dev. *25*, 2594–2609.

Bhat, K.P.L., Balasubramaniyan, V., Vaillant, B., Ezhilarasan, R., Hummelink, K., Hollingsworth, F., Wani, K., Heathcock, L., James, J.D., Goodman, L.D., et al. (2013). Mesenchymal Differentiation Mediated by NF-κB Promotes Radiation Resistance in Glioblastoma. Cancer Cell *24*, 331–346.

Bhat, R., Crowe, E.P., Bitto, A., Moh, M., Katsetos, C.D., Garcia, F.U., Johnson, F.B., Trojanowski, J.Q., Sell, C., and Torres, C. (2012). Astrocyte Senescence as a Component of Alzheimer's Disease. PLoS One *7*, 1–10.

Birch, J., and Gil, J. (2020). Senescence and the SASP: Many therapeutic avenues. Genes Dev. *34*, 1565–1576.

Borghesan, M., Fafián-Labora, J., Eleftheriadou, O., Carpintero-Fernández, P., Paez-Ribes, M., Vizcay-Barrena, G., Swisa, A., Kolodkin-Gal, D., Ximénez-Embún, P., Lowe, R., et al. (2019). Small Extracellular Vesicles Are Key Regulators of Non-cell Autonomous Intercellular Communication in Senescence via the Interferon Protein IFITM3. Cell Rep. *27*, 3956-3971.e6.

Bowman, R.L., Klemm, F., Akkari, L., Pyonteck, S.M., Sevenich, L., Quail, D.F., Dhara, S., Simpson, K., Gardner, E.E., Iacobuzio-Donahue, C.A., et al. (2016). Macrophage Ontogeny Underlies Differences in Tumor-Specific Education in Brain Malignancies. Cell Rep. *17*, 2445–2459.

Bracken, A.P., Kleine-Kohlbrecher, D., Dietrich, N., Pasini, D., Gargiulo, G., Beekman, C., Theilgaard-Mönch, K., Minucci, S., Porse, B.T., Marine, J.C., et al. (2007). The Polycomb group proteins bind throughout the INK4A-ARF locus and are disassociated in senescent cells. Genes Dev. *21*, 525–530.

Brooks, L.J., Clements, M.P., Burden, J.J., Kocher, D., Richards, L., Devesa, S.C., Zakka, L., Woodberry, M., Ellis, M., Jaunmuktane, Z., et al. (2021). The white matter is a pro-differentiative niche for glioblastoma. Nat. Commun. *12*.

Brösicke, N., and Faissner, A. (2015). Role of tenascins in the ECM of gliomas. Cell Adhes. Migr. *9*, 131–140.

Brösicke, N., Van Landeghem, F.K.H., Scheffler, B., and Faissner, A. (2013). Tenascin-C is expressed by human glioma in vivo and shows a strong association with tumor blood vessels. Cell Tissue Res. *354*, 409–430.

Brugarolas, J., Lei, K., Hurley, R.L., Manning, B.D., Reiling, J.H., Hafen, E., Witters, L.A., Ellisen, L.W., and Kaelin, W.G. (2004). Regulation of mTOR function in response to hypoxia by REDD1 and the TSC1/TSC2 tumor suppressor complex. Genes Dev. *18*, 2893–2904.

Burma, S., Chen, B.P., Murphy, M., Kurimasa, A., and Chen, D.J. (2001). ATM Phosphorylates Histone H2AX in Response to DNA Double-strand Breaks. J. Biol. Chem. *276*, 42462–42467.

Bussian, T.J., Aziz, A., Meyer, C.F., Swenson, B.L., van Deursen, J.M., and Baker, D.J. (2018). Clearance of senescent glial cells prevents tau-dependent pathology and cognitive decline. Nature *562*, 578–582.

Calabrese, C., Poppleton, H., Kocak, M., Hogg, T.L., Fuller, C., Hamner, B., Oh, E.Y., Gaber, M.W., Finklestein, D., Allen, M., et al. (2007). A Perivascular Niche for Brain Tumor Stem Cells. Cancer Cell *11*, 69–82.

Campisi, J., and D'Adda Di Fagagna, F. (2007). Cellular senescence: When bad things happen to good cells. Nat. Rev. Mol. Cell Biol. *8*, 729–740.

Canino, C., Mori, F., Cambria, A., Diamantini, A., Germoni, S., Alessandrini, G., Borsellino, G., Galati, R.Z., Battistini, L., Blandino, R., et al. (2012). SASP mediates chemoresistance and tumor-initiating-activity of mesothelioma cells. Oncogene *31*, 3148–3163.

Carro, M.S., Lim, W.K., Alvarez, M.J., Bollo, R.J., Zhao, X., Snyder, E.Y., Sulman, E.P., Anne, S.L., Doetsch, F., Colman, H., et al. (2010). The transcriptional network for mesenchymal transformation of brain tumours. Nature *463*, 318–325.

Carvalho, C., L'Hôte, V., Courbeyrette, R., Kratassiouk, G., Pinna, G., Cintrat, J.C., Denby-Wilkes, C., Derbois, C., Olaso, R., Deleuze, J.F., et al. (2019). Glucocorticoids delay RAF-induced senescence promoted by EGR1. J. Cell Sci. *132*.

Castellan, M., Guarnieri, A., Fujimura, A., Zanconato, F., Battilana, G., Panciera, T., Sladitschek, H.L., Contessotto, P., Citron, A., Grilli, A., et al. (2020). Single-cell analyses reveal YAP/TAZ as regulators of stemness and cell plasticity in glioblastoma. Nat. Cancer.

Chang, A.L., Miska, J., Wainwright, D.A., Dey, M., Rivetta, C. V., Yu, D., Kanojia, D., Pituch, K.C., Qiao, J., Pytel, P., et al. (2016a). CCL2 produced by the glioma microenvironment is essential for the recruitment of regulatory t cells and myeloid-derived suppressor cells. Cancer Res. *76*, 5671–5682.

Chang, J., Wang, Y., Shao, L., Laberge, R.M., Demaria, M., Campisi, J., Janakiraman, K., Sharpless, N.E., Ding, S., Feng, W., et al. (2016b). Clearance of senescent cells by ABT263 rejuvenates aged hematopoietic stem cells in mice. Nat. Med. *22*, 78–83.

Chen, C.H., Chen, P.Y., Lin, Y.Y., Feng, L.Y., Chen, S.H., Chen, C.Y., Huang, Y.C., Huang, C.Y., Jung, S.M., Chen, L.Y., et al. (2020). Suppression of tumor growth via IGFBP3 depletion as a potential treatment in glioma. J. Neurosurg. *132*, 168–179.

Chen, J., Li, Y., Yu, T.S., McKay, R.M., Burns, D.K., Kernie, S.G., and Parada, L.F. (2012). A restricted cell population propagates glioblastoma growth after chemotherapy. Nature *488*, 522–526.

Chen, Q., Han, B., Meng, X., Duan, C., Yang, C., Wu, Z., Magafurov, D., Zhao, S., Safin, S., Jiang, C., et al. (2019). Immunogenomic analysis reveals LGALS1 contributes to the immune heterogeneity and immunosuppression in glioma. Int. J. Cancer *145*, 517–530.

Chen, Q.M., Liu, J., and Merrett, J.B. (2000). Apoptosis or senescence-like growth arrest: Influence of cell-cycle position, p53, p21 and bax in H2O2 response of normal human fibroblasts. Biochem. J. *347*, 543–551.

Chen, Z., Trotman, L.C., Shaffer, D., Lin, H.K., Dotan, Z.A., Niki, M., Koutcher, J.A., Scher, H.I., Ludwig, T., Gerald, W., et al. (2005). Crucial role of p53-dependent cellular senescence in suppression of Pten-deficient tumorigenesis. Nature *436*, 725–730.

Chiche, A., Le Roux, I., von Joest, M., Sakai, H., Aguín, S.B., Cazin, C., Salam, R., Fiette, L., Alegria, O., Flamant, P., et al. (2017). Injury-Induced Senescence Enables In Vivo Reprogramming in Skeletal Muscle. Cell Stem Cell *20*, 407-414.e4.

Chien, Y., Scuoppo, C., Wang, X., Fang, X., Balgley, B., Bolden, J.E., Premsrirut, P., Luo, W., Chicas, A., Lee, C.S., et al. (2011). Control of the senescence-associated secretory phenotype by NF-κB promotes senescence and enhances chemosensitivity. Genes Dev. *25*, 2125–2136.

Childs, B.G., Baker, D.J., Kirkland, J.L., Campisi, J., and Deursen, J.M. (2014). Senescence and apoptosis: dueling or complementary cell fates? EMBO Rep. *15*, 1139–1153.

Childs, B.G., Durik, M., Baker, D.J., and Van Deursen, J.M. (2015). Cellular senescence in aging and age-related disease: From mechanisms to therapy. Nat. Med. *21*, 1424–1435.

Childs, B.G., Baker, D.J., Wijshake, T., Conover, C.A., Campisi, J., and Van Deursen, J.M. (2016). Senescent intimal foam cells are deleterious at all stages of atherosclerosis. Science (80-.). *354*, 472–477.

Childs, B.G., Gluscevic, M., Baker, D.J., Laberge, R.M., Marquess, D., Dananberg, J., and Van Deursen, J.M. (2017). Senescent cells: An emerging target for diseases of ageing. Nat. Rev. Drug Discov. *16*, 718–735.

Chinta, S.J., Woods, G., Demaria, M., Rane, A., Zou, Y., McQuade, A., Rajagopalan, S., Limbad, C., Madden, D.T., Campisi, J., et al. (2018). Cellular Senescence Is Induced by the Environmental Neurotoxin Paraquat and Contributes to Neuropathology Linked to Parkinson's Disease. Cell Rep. *22*, 930–940.

Cho, S., and Hwang, E.S. (2012). Status of mTOR activity may phenotypically differentiate senescence and quiescence. Mol. Cells *33*, 597–604.

Collado, M., Gil, J., Efeyan, A., Guerra, C., Schuhmacher, A.J., Barradas, M., Benguría, A., Zaballos, A., Flores, J.M., Barbacid, M., et al. (2005). Tumour biology: Senescence in premalignant tumours. Nature *436*, 642.

Collado, M., Blasco, M.A., and Serrano, M. (2007). Cellular Senescence in Cancer and Aging. Cell *130*, 223–233.

Coppé, J.-P., Desprez, P.-Y., Krtolica, A., and Campisi, J. (2010). The Senescence-Associated Secretory Phenotype: The Dark Side of Tumor Suppression. Annu. Rev. Pathol. Mech. Dis. *5*, 99–118.

Coppé, J.P., Kauser, K., Campisi, J., and Beauséjour, C.M. (2006). Secretion of vascular endothelial growth factor by primary human fibroblasts at senescence. J. Biol. Chem. *281*, 29568–29574.

Coppé, J.P., Patil, C.K., Rodier, F., Sun, Y., Muñoz, D.P., Goldstein, J., Nelson, P.S., Desprez, P.Y., and Campisi, J. (2008). Senescence-associated secretory phenotypes reveal cell-nonautonomous functions of oncogenic RAS and the p53 tumor suppressor. PLoS Biol. *6*.

Couturier, C.P., Ayyadhury, S., Le, P.U., Nadaf, J., Monlong, J., Riva, G., Allache, R., Baig, S., Yan, X., Bourgey, M., et al. (2020). Single-cell RNA-seq reveals that glioblastoma recapitulates a normal neurodevelopmental hierarchy. Nat. Commun. *11*.

Darmanis, S., Sloan, S.A., Croote, D., Mignardi, M., Chernikova, S., Samghababi, P., Zhang, Y., Neff, N., Kowarsky, M., Caneda, C., et al. (2017). Single-Cell RNA-Seq Analysis of Infiltrating Neoplastic Cells at the Migrating Front of Human Glioblastoma. Cell Rep. *21*, 1399–1410.

Davalos, A.R., Kawahara, M., Malhotra, G.K., Schaum, N., Huang, J., Ved, U., Beausejour, C.M., Coppe, J.P., Rodoer, F., and Campisi, J. (2013). p53-dependent release of Alarmin HMGB1 is a central mediator of senescent phenotypes. J. Cell Biol. *201*, 613–629.

Debacq-Chainiaux, F., Boilan, E., Dedessus Le Moutier, J., Weemaels, G., and Toussaint, O. (2010). p38(MAPK) in the senescence of human and murine fibroblasts. Adv. Exp. Med. Biol. *694*, 126–137.

Demaria, M., Rodier, F., Laberge, R.-M.M., Campisi, J., Ohtani, N., Hara, E., Youssef, S.A., DeBruin, A., Toussaint, W., Mitchell, J.R., et al. (2014). An essential role for senescent cells in optimal wound healing through secretion of PDGF-AA. Dev. Cell *31*, 722–733.

Demaria, M., O'Leary, M.N., Chang, J., Shao, L., Liu, S., Alimirah, F., Koenig, K., Le, C., Mitin, N., Deal, A.M., et al. (2017). Cellular senescence promotes adverse effects of chemotherapy and cancer relapse. Cancer Discov. *7*, 165–176.

Dimri, G.P., Lee, X., Basile, G., Acosta, M., Scott, G., Roskelley, C., Medrano, E.E., Linskens, M., Rubelj, I., and Pereira-Smith, O. (1995). A biomarker that identifies senescent human cells in culture and in aging skin in vivo. Proc. Natl. Acad. Sci. *92*, 9363–9367.

Doucette, T., Rao, G., Rao, A., Shen, L., Aldape, K., Wei, J., Dziurzynski, K., Gilbert, M., and Heimberger, A.B. (2013). Immune heterogeneity of glioblastoma subtypes: extrapolation from the cancer genome atlas. Cancer Immunol. Res. *1*, 112–122.

Dréan, A., Goldwirt, L., Verreault, M., Canney, M., Schmitt, C., Guehennec, J., Delattre, J.-Y., Carpentier, A., and Idbaih, A. (2016). Blood-brain barrier, cytotoxic chemotherapies and glioblastoma. Expert Rev. Neurother. *16*, 1285–1300.

Duan, Q., Zhang, H., Zheng, J., and Zhang, L. (2020). Turning Cold into Hot: Firing up the Tumor Microenvironment. Trends in Cancer *6*, 605–618.

Dubinski, D., Wölfer, J., Hasselblatt, M., Schneider-Hohendorf, T., Bogdahn, U., Stummer, W., Wiendl, H., and Grauer, O.M. (2016). CD4+ T effector memory cell dysfunction is associated with the accumulation of granulocytic myeloid-derived suppressor cells in glioblastoma patients. Neuro. Oncol. *18*, 807–818.

Eggert, T., Wolter, K., Ji, J., Ma, C., Yevsa, T., Klotz, S., Medina-Echeverz, J., Longerich, T., Forgues, M., Reisinger, F., et al. (2016). Distinct Functions of Senescence-Associated Immune Responses in Liver Tumor Surveillance and Tumor Progression. Cancer Cell *30*, 533–547.

Escoll, M., Lastra, D., Pajares, M., Robledinos-Antón, N., Rojo, A.I., Fernández-Ginés, R., Mendiola, M., Martínez-Marín, V., Esteban, I., López-Larrubia, P., et al. (2020). Transcription factor NRF2 uses the Hippo pathway effector TAZ to induce tumorigenesis in glioblastomas. Redox Biol. *30*.

Essers, J., Van Steeg, H., De Wit, J., Swagemakers, S.M.A., Vermeij, M., Hoeijmakers, J.H.J., and Kanaar, R. (2000). Homologous and non-homologous recombination differentially affect DNA damage repair in mice. EMBO J. *19*, 1703–1710.

Faget, D. V., Ren, Q., and Stewart, S.A. (2019). Unmasking senescence: context-dependent effects of SASP in cancer. Nat. Rev. Cancer *19*, 439–453.

Farr, J.N., Xu, M., Weivoda, M.M., Monroe, D.G., Fraser, D.G., Onken, J.L., Negley, B.A., Sfeir, J.G., Ogrodnik, M.B., Hachfeld, C.M., et al. (2017). Targeting cellular senescence prevents age-related bone loss in mice. Nat. Med. *23*, 1072–1079.

Franceschi, C., and Campisi, J. (2014). Chronic inflammation (inflammaging) and its potential contribution to age-associated diseases. J. Gerontol. A. Biol. Sci. Med. Sci. *69 Suppl 1*, S4-9.

Freund, A., Laberge, R.M.R.-M., Demaria, M., and Campisi, J. (2012). Lamin B1 loss is a senescence-associated biomarker. Mol. Biol. Cell *23*, 2066–2075.

Friedmann-Morvinski, D., Bushong, E.A., Ke, E., Soda, Y., Marumoto, T., Singer, O., Ellisman, M.H., and Verma, I.M. (2012). Dedifferentiation of neurons and astrocytes by oncogenes can induce gliomas in mice. Science (80-.). *338*, 1080–1084.

Fulci, G., Labuhn, M., Maier, D., Lachat, Y., Hausmann, O., Hegi, M.E., Janzer, R.C., Merlo, A., and Van Meir, E.G. (2000). P53 Gene Mutation and Ink4a-Arf-Deletion Appear To Be Two Mutually Exclusive Events in Human Glioblastoma. Oncogene *19*, 3816–3822.

Fumagalli, M., Rossiello, F., Mondello, C., and D'Adda Di Fagagna, F. (2014). Stable cellular senescence is associated with persistent DDR activation. PLoS One *9*, 44–46.

Gal, H., Lysenko, M., Stroganov, S., Vadai, E., Youssef, S.A., Tzadikevitch-Geffen, K., Rotkopf, R., Biron-Shental, T., Bruin, A., Neeman, M., et al. (2020). Molecular pathways of senescence regulate placental structure and function. EMBO J. *39*.

Galan-Moya, E.M., Le Guelte, A., Fernandes, E.L., Thirant, C., Dwyer, J., Bidere, N., Couraud, P.O., Scott, M.G.H., Junier, M.P., Chneiweiss, H., et al. (2011). Secreted factors from brain endothelial cells maintain glioblastoma stem-like cell expansion through the mTOR pathway. EMBO Rep. *12*, 470–476.

Gangoso, E., Southgate, B., Bradley, L., Rus, S., Galvez-Cancino, F., McGivern, N., Güç, E., Kapourani, C.-A., Byron, A., Ferguson, K.M., et al. (2021). Glioblastomas acquire myeloid-affiliated transcriptional programs via epigenetic immunoediting to elicit immune evasion. Cell 1–17.

Garofano, L., Migliozzi, S., Oh, Y.T., D'Angelo, F., Najac, R.D., Ko, A., Frangaj, B., Caruso, F.P., Yu, K., Yuan, J., et al. (2021). Pathway-based classification of glioblastoma uncovers a mitochondrial subtype with therapeutic vulnerabilities. Nat. Cancer *2*, 141–156.

Geng, Y.Q., Guan, J.T., Xu, X.H., and Fu, Y.C. (2010). Senescence-associated beta-galactosidase activity expression in aging hippocampal neurons. Biochem. Biophys. Res. Commun. *396*, 866–869.

Gielen, P.R., Schulte, B.M., Kers-Rebel, E.D., Verrijp, K., Bossman, S.A.J.F.H., Ter Laan, M., Wesseling, P., and Adema, G.J. (2016). Elevated levels of polymorphonuclear myeloid-derived suppressor cells in patients with glioblastoma highly express S100A8/9 and arginase and suppress T cell function. Neuro. Oncol. *18*, 1253–1264.

Gil, J., Bernard, D., Martínez, D., and Beach, D. (2004). Polycomb CBX7 has a unifying role in cellular lifespan. Nat. Cell Biol. *6*, 67–72.

Gilder, A.S., Natali, L., Van Dyk, D.M., Zalfa, C., Banki, M.A., Pizzo, D.P., Wang, H., Klemke, R.L., Mantuano, E., and Gonias, S.L. (2018). The Urokinase Receptor Induces a Mesenchymal Gene Expression Signature in Glioblastoma Cells and Promotes Tumor Cell Survival in Neurospheres. Sci. Rep. *8*, 1–16.

Glück, S., Guey, B., Gulen, M.F., Wolter, K., Kang, T.W., Schmacke, N.A., Bridgeman, A., Rehwinkel, J., Zender, L., and Ablasser, A. (2017). Innate immune sensing of cytosolic chromatin fragments through cGAS promotes senescence. Nat. Cell Biol. *19*, 1061–1070.

González-Gualda, E., Pàez-Ribes, M., Lozano-Torres, B., Macias, D., Wilson, J.R., González-López, C., Ou, H.L., Mirón-Barroso, S., Zhang, Z., Lérida-Viso, A., et al. (2020). Galacto-conjugation of Navitoclax as an efficient strategy to increase senolytic specificity and reduce platelet toxicity. Aging Cell *19*, 1–19.

Gorgoulis, V., Adams, P.D., Alimonti, A., Bennett, D.C., Bischof, O., Bishop, C., Campisi, J., Collado, M., Evangelou, K., Ferbeyre, G., et al. (2019). Cellular Senescence: Defining a Path Forward. Cell *179*, 813–827.

Grosse, L., Wagner, N., Emelyanov, A., Molina, C., Lacas-Gervais, S., Wagner, K.D., and Bulavin, D. V. (2020). Defined p16High Senescent Cell Types Are Indispensable for Mouse Healthspan. Cell Metab. *32*, 87-99.e6.

Guarnaccia, L., Navone, S.E., Trombetta, E., Cordiglieri, C., Cherubini, A., Crisà, F.M., Rampini, P., Miozzo, M., Fontana, L., Caroli, M., et al. (2018). Angiogenesis in human brain tumors: Screening of drug response through a patient-specific cell platform for personalized therapy. Sci. Rep. *8*, 1–13.

Guerrero, A., Herranz, N., Sun, B., Wagner, V., Gallage, S., Guiho, R., Wolter, K., Pombo, J., Irvine, E.E., Innes, A.J., et al. (2019). Cardiac glycosides are broad-spectrum senolytics. Nat. Metab. *1*, 1074–1088.

Guerrero, A., Guiho, R., Herranz, N., Uren, A., Withers, D.J., Martínez-Barbera, J.P., Tietze, L.F., and Gil, J. (2020). Galactose-modified duocarmycin prodrugs as senolytics. Aging Cell *19*, 1–13.

Günther, W., Pawlak, E., Damasceno, R., Arnold, H., and Terzis, A.J. (2003). Temozolomide induces apoptosis and senescence in glioma cells cultured as multicellular spheroids. Br. J. Cancer *88*, 463–469.

Gupta, M.K., Polisetty, R.V., Sharma, R., Ganesh, R.A., Gowda, H., Purohit, A.K., Ankathi, P., Prasad, K., Mariswamappa, K., Lakshmikantha, A., et al. (2019). Altered transcriptional regulatory proteins in glioblastoma and YBX1 as a potential regulator of tumor invasion. Sci. Rep. *9*, 1–15.

Guzy, R.D., Hoyos, B., Robin, E., Chen, H., Liu, L., Mansfield, K.D., Simon, M.C., Hammerling, U., and Schumacker, P.T. (2005). Mitochondrial complex III is required for hypoxia-induced ROS production and cellular oxygen sensing. Cell Metab. *1*, 401–408.

Hall, B.M., Balan, V., Gleiberman, A.S., Strom, E., Krasnov, P., Virtuoso, P., Rydkina, E., Vujcic, S., Balan, K., Gitlin, I.I., et al. (2017). p16 and SAbetaGal can be induced in macrophages as part of a reversible response to physiological stimuli. Aging (Albany. NY). *9*, 1867–1884.

Hambardzumyan, D., Gutmann, D.H., and Kettenmann, H. (2015). The role of microglia and macrophages in glioma maintenance and progression. Nat. Neurosci. *19*, 20–27.

Hanif, F., Muzaffar, K., Perveen, K., Malhi, S.M., and Simjee, S.U. (2017). Glioblastoma Multiforme: A Review of its Epidemiology and Pathogenesis through Clinical Presentation and Treatment. Asian Pacific J. Cancer Prev. J Cancer Prev *18*, 3–9.

Harris, I.S., and DeNicola, G.M. (2020). The Complex Interplay between Antioxidants and ROS in Cancer. Trends Cell Biol. *30*, 440–451.

Hayashi, M., Kuga, A., Suzuki, M., Panda, H., Kitamura, H., Motohashi, H., and Yamamoto, M. (2020). Microenvironmental Activation of Nrf2 Restricts the Progression of Nrf2-Activated Malignant Tumors. Cancer Res. *80*, 3331–3344.

Hayflick, L. (1965). The limited in vitro lifetime of human diploid cell strains. Exp. Cell Res. *37*, 614–636.

Hegi, M.E., Diserens, A.-C., Gorlia, T., Hamou, M.-F., de Tribolet, N., Weller, M., Kros, J.M., Hainfellner, J.A., Mason, W., Mariani, L., et al. (2005). MGMT Gene Silencing and Benefit from Temozolomide in Glioblastoma . N. Engl. J. Med. *352*, 997–1003.

Henke, E., Nandigama, R., and Ergün, S. (2020). Extracellular Matrix in the Tumor Microenvironment and Its Impact on Cancer Therapy. Front. Mol. Biosci. *6*, 1–24.

Hernandez-Segura, A., de Jong, T. V., Melov, S., Guryev, V., Campisi, J., and Demaria, M. (2017). Unmasking Transcriptional Heterogeneity in Senescent Cells. Curr. Biol. *27*, 2652-2660.e4.

Herranz, N., Gallage, S., Mellone, M., Wuestefeld, T., Klotz, S., Hanley, C.J., Raguz, S., Acosta, J.C., Innes, A.J., Banito, A., et al. (2015). mTOR regulates MAPKAPK2 translation to control the senescence-associated secretory phenotype. Nat. Cell Biol. *17*, 1205–1217.

Hiebert, P., Wietecha, M.S., Cangkrama, M., Haertel, E., Mavrogonatou, E., Stumpe, M., Steenbock, H., Grossi, S., Beer, H.D., Angel, P., et al. (2018). Nrf2-Mediated Fibroblast Reprogramming Drives Cellular Senescence by Targeting the Matrisome. Dev. Cell *46*, 145-161.e10.

Hiramoto, K., Satoh, H., Suzuki, T., Moriguchi, T., and Pi, J. (2014). Myeloid Lineage – Speci fi c Deletion of Antioxidant System Enhances Tumor Metastasis. 835–845.

Hoare, M., Ito, Y., Kang, T.W., Weekes, M.P., Matheson, N.J., Patten, D.A., Shetty, S., Parry, A.J., Menon, S., Salama, R., et al. (2016). NOTCH1 mediates a switch between two distinct secretomes during senescence. Nat. Cell Biol. *18*, 979–992.

Huang, J.-Y., Cheng, Y.-J., Lin, Y.-P., Lin, H.-C., Su, C.-C., Juliano, R., and Yang, B.-C. (2010). Extracellular Matrix of Glioblastoma Inhibits Polarization and Transmigration of T Cells: The Role of Tenascin-C in Immune Suppression. J. Immunol. *185*, 1450–1459.

Hubackova, S., Krejcikova, K., Bartek, J., and Hodny, Z. (2012). IL1-and TGFβ-Nox4 signaling, oxidative stress and DNA damage response are shared features of replicative, oncogene-induced, and drug-induced paracrine "Bystander senescence." Aging (Albany. NY). *4*, 932–951.

Hubert, C.G., Rivera, M., Spangler, L.C., Wu, Q., Mack, S.C., Prager, B.C., Couce, M., McLendon, R.E., Sloan, A.E., and Rich, J.N. (2016). A three-dimensional organoid culture system derived from human glioblastomas recapitulates the hypoxic gradients and cancer stem cell heterogeneity of tumors found in vivo. Cancer Res. *76*, 2465–2477.

Hussain, S.F., Yang, D., Suki, D., Aldape, K., Grimm, E., and Heimberger, A.B. (2006). The role of human glioma-infiltrating microglia/macrophages in mediating antitumor immune responses. Neuro. Oncol. *8*, 261–279.

Iannello, A., Thompson, T.W., Ardolino, M., Lowe, S.W., and Raulet, D.H. (2013). p53-dependent chemokine production by senescent tumor cells supports NKG2D-dependent tumor elimination by natural killer cells. J. Exp. Med. *210*, 2057–2069.

Idbaih, A., Canney, M., Belin, L., Desseaux, C., Vignot, A., Bouchoux, G., Asquier, N., Law-Ye, B., Leclercq, D., Bissery, A., et al. (2019). Safety and feasibility of repeated and transient blood-brain barrier disruption by pulsed ultrasound in patients with recurrent glioblastoma. Clin. Cancer Res. *25*, 3793–3801.

Jackson, C.M., Choi, J., and Lim, M. (2019). Mechanisms of immunotherapy resistance: lessons from glioblastoma. Nat. Immunol. *20*, 1100–1109.

Jacob, F., Salinas, R.D., Zhang, D.Y., Nguyen, P.T.T., Schnoll, J.G., Wong, S.Z.H., Thokala, R., Sheikh, S., Saxena, D., Prokop, S., et al. (2020). A Patient-Derived Glioblastoma Organoid Model and Biobank Recapitulates Inter- and Intra-tumoral Heterogeneity. Cell *180*, 188-204.e22.

Jacobs, J.L., Kieboom, K., Marino, S., DePinho, R.A., and Van Lohuizen, M. (1999). The oncogene and Polycombgroup gene bmi-1 regulates cell proliferation and senescence through the ink4a locus. Nature *397*, 164–168.

Jeon, O.H., Kim, C., Laberge, R.M., Demaria, M., Rathod, S., Vasserot, A.P., Chung, J.W., Kim, D.H., Poon, Y., David, N., et al. (2017). Local clearance of senescent cells attenuates the development of post-traumatic osteoarthritis and creates a pro-regenerative environment. Nat. Med. *23*, 775–781.

Jeong, T., and Yee, G. (2014). Glioblastoma in a Patient with Neurofibromatosis Type 1 : A Case Report and Review of the Literature. *2*, 36–38.

Jia, D., Li, S., Li, D., Xue, H., Yang, D., and Liu, Y. (2018). Mining TCGA database for genes of prognostic value in glioblastoma microenvironment. Aging (Albany. NY). *10*, 592–605.

Kaffes, I., Szulzewsky, F., Chen, Z., Herting, C.J., Gabanic, B., Velázquez Vega, J.E., Shelton, J., Switchenko, J.M., Ross, J.L., McSwain, L.F., et al. (2019). Human Mesenchymal glioblastomas are characterized by an increased immune cell presence compared to Proneural and Classical tumors. Oncoimmunology *8*.

Kamran, N., Kadiyala, P., Saxena, M., Candolfi, M., Li, Y., Moreno-Ayala, M.A., Raja, N., Shah, D., Lowenstein, P.R., and Castro, M.G. (2017). Immunosuppressive Myeloid Cells' Blockade in the Glioma Microenvironment Enhances the Efficacy of Immune-Stimulatory Gene Therapy. Mol. Ther. *25*, 232–248.

Kang, C., Xu, Q., Martin, T.D., Li, M.Z., Demaria, M., Aron, L., Lu, T., Yankner, B.A., Campisi, J., and Elledge, S.J. (2015). The DNA damage response induces inflammation and senescence by inhibiting autophagy of GATA4. Science (80-.). *349*, 1–7.

Kang, T.W., Yevsa, T., Woller, N., Hoenicke, L., Wuestefeld, T., Dauch, D., Hohmeyer, A., Gereke, M., Rudalska, R., Potapova, A., et al. (2011). Senescence surveillance of pre-malignant hepatocytes limits liver cancer development. Nature *479*, 547–551.

Karpel-Massler, G., Ishida, C.T., Bianchetti, E., Zhang, Y., Shu, C., Tsujiuchi, T., Banu, M.A., Garcia, F., Roth, K.A., Bruce, J.N., et al. (2017). Induction of synthetic lethality in IDH1-mutated gliomas through inhibition of Bcl-xL. Nat. Commun. *8*.

Knobbe, C.B., and Reifenberger, G. (2003). Genetic alterations and aberrant expression of genes related to the phosphatidyl-inositol-3'-kinase/protein kinase B (Akt) signal transduction pathway in glioblastomas. Brain Pathol. *13*, 507–518.

Kohlhapp, F.J., Haribhai, D., Mathew, R., Duggan, R., Ellis, P.A., Wang, R., Lasater, E.A., Shi, Y., Dave, N., Riehm, J.J., et al. (2021). Venetoclax Increases Intratumoral Effector T Cells and Antitumor Efficacy in Combination with Immune Checkpoint Blockade. Cancer Discov. *11*, 68–79.

Kohli, J., Wang, B., Brandenburg, S.M., Basisty, N., Evangelou, K., Campisi, J., Schilling, B., Gorgoulis, V., and Demaria, M. (2021). Algorithmic assessment of cellular senescence in experimental and clinical specimens (Springer US).

Krtolica, A., Parrinello, S., Lockett, S., Desprez, P.-Y., and Campisi, J. (2001). Senescent fibroblasts promote epithelial cell growth and tumorigenesis: A link between cancer and aging. Proc. Natl. Acad. Sci. *98*, 12072–12077.

Kruiswijk, F., Labuschagne, C.F., and Vousden, K.H. (2015). p53 in survival, death and metabolic health: a lifeguard with a licence to kill. Nat. Rev. Mol. Cell Biol. *16*, 393–405.

Kuilman, T., Michaloglou, C., Vredeveld, L.C.W., Douma, S., van Doorn, R., Desmet, C.J., Aarden, L.A., Mooi, W.J., and Peeper, D.S. (2008). Oncogene-Induced Senescence Relayed by an Interleukin-Dependent Inflammatory Network. Cell *133*, 1019–1031.

Laberge, R.M., Adler, D., DeMaria, M., Mechtouf, N., Teachenor, R., Cardin, G.B., Desprez, P.Y., Campisi, J., and Rodier, F. (2013). Mitochondrial DNA damage induces apoptosis in senescent cells. Cell Death Dis. *4*.

Laberge, R.M., Sun, Y., Orjalo, A. V., Patil, C.K., Freund, A., Zhou, L., Curran, S.C., Davalos, A.R., Wilson-Edell, K.A., Liu, S., et al. (2015). MTOR regulates the pro-tumorigenic senescence-associated secretory phenotype by promoting IL1A translation. Nat. Cell Biol. *17*, 1049–1061.

Lathia, J.D., Mack, S.C., Mulkearns-Hubert, E.E., Valentim, C.L.L., and Rich, J.N. (2015). Cancer stem cells in glioblastoma.

Lee, J., Kotliarova, S., Kotliarov, Y., Li, A., Su, Q., Donin, N.M., Pastorino, S., Purow, B.W., Christopher, N., Zhang, W., et al. (2006). Tumor stem cells derived from glioblastomas cultured in bFGF and EGF more closely mirror the phenotype and genotype of primary tumors than do serum-cultured cell lines. Cancer Cell *9*, 391–403.

Lee, J.H., Lee, J.E., Kahng, J.Y., Kim, S.H., Park, J.S., Yoon, S.J., Um, J.Y., Kim, W.K., Lee, J.K., Park, J., et al. (2018). Human glioblastoma arises from subventricular zone cells with low-level driver mutations. Nature *560*, 243–247.

Lee, Y., Kim, J., Kim, M., Kim, J., Elledge, S.J., Kang, C., Lee, Y., Kim, J., Kim, M., Kwon, Y., et al. (2021). Coordinate regulation of the senescent state by selective autophagy. Dev. Cell 1–14.

Lesina, M., Wörmann, S.M., Morton, J., Diakopoulos, K.N., Korneeva, O., Wimmer, M., Einwächter, H., Sperveslage, J., Demir, I.E., Kehl, T., et al. (2016). RelA regulates CXCL1/CXCR2-dependent oncogene-induced senescence in murine Kras-driven pancreatic carcinogenesis. J. Clin. Invest. *126*, 2919–2932.

Li, G.M. (2008). Mechanisms and functions of DNA mismatch repair. Cell Res. *18*, 85–98.

Litak, J., Mazurek, M., Grochowski, C., Kamieniak, P., and Roliński, J. (2019). PD-L1/PD-1 axis in glioblastoma multiforme. Int. J. Mol. Sci. *20*.

Louis, D.N., Ohgaki, H., Wiestier, O.D., Cavenee, W.K., Ellison, D.W., Figarella-Branger, D., Perry, A., Reifenberger, G., and Von Deimling, A. WHO Classification of Tumours of the Central Nervous System.

Louis, D.N., Perry, A., Reifenberger, G., von Deimling, A., Figarella-Branger, D., Cavenee, W.K., Ohgaki, H., Wiestler, O.D., Kleihues, P., and Ellison, D.W. (2016). The 2016 World Health Organization Classification of Tumors of the Central Nervous System: a summary. Acta Neuropathol. *131*, 803–820.

Lu, F., Chen, Y., Zhao, C., Wang, H., He, D., Xu, L., Wang, J., He, X., Deng, Y., Lu, E.E., et al. (2016). Olig2-Dependent Reciprocal Shift in PDGF and EGF Receptor Signaling Regulates Tumor Phenotype and Mitotic Growth in Malignant Glioma. Cancer Cell *29*, 669–683.

Lujambio, A., Akkari, L., Simon, J., Grace, D., Tschaharganeh, D.F., Bolden, J.E., Zhao, Z., Thapar, V., Joyce, J.A., Krizhanovsky, V., et al. (2013). Non-cell-autonomous tumor suppression by p53. Cell *153*, 449–460.

Madisen, L., Zwingman, T.A., Sunkin, S.M., Oh, S.W., Zariwala, H.A., Gu, H., Ng, L.L., Palmiter, R.D., Hawrylycz, M.J., Jones, A.R., et al. (2010). A robust and high-throughput Cre reporting and characterization system for the whole mouse brain. Nat. Neurosci. *13*, 133–140.

Maj, T., Wang, W., Crespo, J., Zhang, H., Wang, W., Wei, S., Zhao, L., Vatan, L., Shao, I., Szeliga, W., et al. (2017). Oxidative stress controls regulatory T cell apoptosis and suppressor activity and PD-L1-blockade resistance in tumor. *18*.

Malaquin, N., Vercamer, C., Bouali, F., Martien, S., Deruy, E., Wernert, N., Chwastyniak, M., Pinet, F., Abbadie, C., and Pourtier, A. (2013). Senescent Fibroblasts Enhance Early Skin Carcinogenic Events via a Paracrine MMP-PAR-1 Axis. PLoS One *8*.

Marumoto, T., Tashiro, A., Friedmann-Morvinski, D., Scadeng, M., Soda, Y., Gage, F.H., and Verma, I.M. (2009). Development of a novel mouse glioma model using lentiviral vectors. Nat. Med. *15*, 110–116.

McFaline-Figueroa, J.L., Braun, C.J., Stanciu, M., Nagel, Z.D., Mazzucato, P., Sangaraju, D., Cerniauskas, E., Barford, K., Vargas, A., Chen, Y., et al. (2015). Minor changes in expression of the mismatch repair protein MSH2 exert a major impact on glioblastoma response to temozolomide. Cancer Res. *75*, 3127–3138.

McLendon, R., Friedman, A., Bigner, D., Van Meir, E.G., Brat, D.J., Mastrogianakis, G.M., Olson, J.J., Mikkelsen, T., Lehman, N., Aldape, K., et al. (2008). Comprehensive genomic characterization defines human glioblastoma genes and core pathways. Nature *455*, 1061–1068.

Mehta, S., Huillard, E., Kesari, S., Maire, C.L., Golebiowski, D., Harrington, E.P., Alberta, J.A., Kane, M.F., Theisen, M., Ligon, K.L., et al. (2011). The Central Nervous System-Restricted Transcription Factor Olig2 Opposes p53 Responses to Genotoxic Damage in Neural Progenitors and Malignant Glioma. Cancer Cell *19*, 359–371.

Di Micco, R., Krizhanovsky, V., Baker, D., and d'Adda di Fagagna, F. (2021). Cellular senescence in ageing: from mechanisms to therapeutic opportunities. Nat. Rev. Mol. Cell Biol. *22*, 75–95.

Michaloglou, C., Vredeveld, L.C.W., Soengas, M.S., Denoyelle, C., Kuilman, T., Van Der Horst, C.M.A.M., Majoor, D.M., Shay, J.W., Mooi, W.J., and Peeper, D.S. (2005). BRAFE600-associated senescence-like cell cycle arrest of human naevi. Nature *436*, 720–724.

Milanovic, M., Fan, D.N.Y., Belenki, D., Däbritz, J.H.M., Zhao, Z., Yu, Y., Dörr, J.R., Dimitrova, L., Lenze, D., Monteiro Barbosa, I.A., et al. (2018). Senescence-associated reprogramming promotes cancer stemness. Nature *553*, 96–100.

Di Mitri, D., and Alimonti, A. (2016). Non-Cell-Autonomous Regulation of Cellular Senescence in Cancer. Trends Cell Biol. *26*, 215–226.

Di Mitri, D., Mirenda, M., Vasilevska, J., Calcinotto, A., Delaleu, N., Revandkar, A., Gil, V., Boysen, G., Losa, M., Mosole, S., et al. (2019). Re-education of Tumor-Associated Macrophages by CXCR2 Blockade Drives Senescence and Tumor Inhibition in Advanced Prostate Cancer. Cell Rep. *28*, 2156-2168.e5.

Mosteiro, L., Pantoja, C., Alcazar, N., Marión, R.M., Chondronasiou, D., Rovira, M., Fernandez-Marcos, P.J., Muñoz-Martin, M., Blanco-Aparicio, C., Pastor, J., et al. (2016). Tissue damage and senescence provide critical signals for cellular reprogramming in vivo. Science (80-.). *354*, aaf4445.

Muñoz-Espín, D., Cañamero, M., Maraver, A., Gómez-López, G., Contreras, J., Murillo-Cuesta, S., Rodríguez-Baeza, A., Varela-Nieto, I., Ruberte, J., Collado, M., et al. (2013). XProgrammed cell senescence during mammalian embryonic development. Cell *155*, 1104.

Musi, N., Valentine, J.M., Sickora, K.R., Baeuerle, E., Thompson, C.S., Shen, Q., and Orr, M.E. (2018). Tau protein aggregation is associated with cellular senescence in the brain. Aging Cell *17*.

Narita, M., Nũnez, S., Heard, E., Narita, M., Lin, A.W., Hearn, S.A., Spector, D.L., Hannon, G.J., and Lowe, S.W. (2003). Rb-mediated heterochromatin formation and silencing of E2F target genes during cellular senescence. Cell *113*, 703–716.

Neftel, C., Laffy, J., Filbin, M.G., Hara, T., Shore, M.E., Rahme, G.J., Richman, A.R., Silverbush, D., Shaw, M.L., Hebert, C.M., et al. (2019). An Integrative Model of Cellular States, Plasticity, and Genetics for Glioblastoma. Cell *178*, 835-849.e21.

Noushmehr, H., Weisenberger, D.J., Diefes, K., Phillips, H.S., Pujara, K., Berman, B.P., Pan, F., Pelloski, C.E., Sulman, E.P., Bhat, K.P., et al. (2010). Identification of a CpG Island Methylator Phenotype that Defines a Distinct Subgroup of Glioma. Cancer Cell.

Ogawa, J., Pao, G.M., Shokhirev, M.N., and Verma, I.M. (2018). Glioblastoma Model Using Human Cerebral Organoids. Cell Rep. *23*, 1220–1229.

Ogrodnik, M., Zhu, Y., Zglinicki, T. Von, Kirkland, J.L., Jurk, D., Victorelli, S., Ruswhandi, R.A., Giorgadze, N., Pirtskhalava, T., Podgorni, O., et al. (2019). Obesity-Induced Cellular Senescence Drives Anxiety and Impairs Neurogenesis Article Obesity-Induced Cellular Senescence Drives Anxiety and Impairs Neurogenesis. 1061–1077.

Ohtani, N., Yamakoshi, K., Takahashi, A., and Hara, E. (2010). Real-time in vivo imaging of p16Ink4agene expression: A new approach to study senescence stress signaling in living animals. Cell Div. *5*, 1–8.

Osswald, M., Jung, E., Sahm, F., Solecki, G., Venkataramani, V., Blaes, J., Weil, S., Horstmann, H., Wiestler, B., Syed, M., et al. (2015). Brain tumour cells interconnect to a functional and resistant network. Nature *528*, 93–98.

Ostrom, Q.T., Patil, N., Cioffi, G., Waite, K., Kruchko, C., and Barnholtz-Sloan, J.S. (2020). CBTRUS statistical report: Primary brain and other central nervous system tumors diagnosed in the United States in 2013-2017. Neuro. Oncol. *22*, IV1–IV96.

Otvos, B., Silver, D.J., Mulkearns-Hubert, E.E., Alvarado, A.G., Turaga, S.M., Sorensen, M.D., Rayman, P., Flavahan, W.A., Hale, J.S., Stoltz, K., et al. (2016). Cancer Stem Cell-Secreted Macrophage Migration Inhibitory Factor Stimulates Myeloid Derived Suppressor Cell Function and Facilitates Glioblastoma Immune Evasion. Stem Cells *34*, 2026–2039.

Ovadya, Y., Landsberger, T., Leins, H., Vadai, E., Gal, H., Biran, A., Yosef, R., Sagiv, A., Agrawal, A., Shapira, A., et al. (2018). Impaired immune surveillance accelerates accumulation of senescent cells and aging. Nat. Commun. *9*.

Parisotto, M., Grelet, E., Bizri, R. El, Dai, Y., Terzic, J., Eckert, D., Gargowitsch, L., Bornert, J.M., and Metzger, D. (2018). PTEN deletion in luminal cells of mature prostate induces replication stress and senescence in vivo. J. Exp. Med. *215*, 1749–1763.

Parsa, A.T., Waldron, J.S., Panner, A., Crane, C.A., Parney, I.F., Barry, J.J., Cachola, K.E., Murray, J.C., Tihan, T., Jensen, M.C., et al. (2007). Loss of tumor suppressor PTEN function increases B7-H1 expression and immunoresistance in glioma. Nat. Med. *13*, 84–88.

Patel, A.P., Tirosh, I., Trombetta, J.J., Shalek, A.K., Gillespie, S.M., Wakimoto, H., Cahill, D.P., Nahed, B. V., Curry, W.T., Martuza, R.L., et al. (2014). Single-cell RNA-seq highlights intratumoral heterogeneity in primary glioblastoma. Science (80-.). *344*, 1396–1401.

Pello, O.M., De Pizzol, M., Mirolo, M., Soucek, L., Zammataro, L., Amabile, A., Doni, A., Nebuloni, M., Swigart, L.B., Evan, G.I., et al. (2012). Role of c-MYC in alternative activation of human macrophages and tumor-associated macrophage biology. Blood *119*, 411–421.

Philips, A., Henshaw, D.L., Lamburn, G., and O'Carroll, M.J. (2018). Brain tumours: Rise in glioblastoma multiforme incidence in England 1995-2015 Suggests an Adverse Environmental or Lifestyle Factor. J. Environ. Public Health *2018*.

Pietras, A., Katz, A.M., Ekström, E.J., Wee, B., Halliday, J.J., Pitter, K.L., Werbeck, J.L., Amankulor, N.M., Huse, J.T., and Holland, E.C. (2014). Osteopontin-CD44 signaling in the glioma perivascular niche enhances cancer stem cell phenotypes and promotes aggressive tumor growth. Cell Stem Cell *14*, 357–369.

Pine, A.R., Cirigliano, S.M., Nicholson, J.G., Hu, Y., Linkous, A., Miyaguchi, K., Edwards, L., Singhania, R., Schwartz, T.H., Ramakrishna, R., et al. (2020). Tumor microenvironment is critical for the maintenance of cellular states found in primary glioblastomas. Cancer Discov. *10*, 964–979.

Pölönen, P., Jawahar Deen, A., Leinonen, H.M., Jyrkkänen, H.K., Kuosmanen, S., Mononen, M., Jain, A., Tuomainen, T., Pasonen-Seppänen, S., Hartikainen, J.M., et al. (2019). Nrf2 and SQSTM1/p62 jointly contribute to mesenchymal transition and invasion in glioblastoma. Oncogene *38*, 7473–7490.

Pyonteck, S.M., Akkari, L., Schuhmacher, A.J., Bowman, R.L., Sevenich, L., Quail, D.F., Olson, O.C., Quick, M.L., Huse, J.T., Teijeiro, V., et al. (2013). CSF-1R inhibition alters macrophage polarization and blocks glioma progression. Nat. Med. *19*, 1264–1272.

Quail, D.F., and Joyce, J.A. (2017). The Microenvironmental Landscape of Brain Tumors. Cancer Cell *31*, 326–341.

Reni, M., Mazza, E., Zanon, S., Gatta, G., and Vecht, C.J. (2017). Central nervous system gliomas. Crit. Rev. Oncol. Hematol. *113*, 213–234.

Renier, N., Wu, Z., Simon, D.J., Yang, J., Ariel, P., and Tessier-Lavigne, M. (2014). IDISCO: A simple, rapid method to immunolabel large tissue samples for volume imaging. Cell *159*, 896–910.

Richards, L.M., Whitley, O.K.N.N., MacLeod, G., Cavalli, F.M.G.G., Coutinho, F.J., Jaramillo, J.E., Svergun, N., Riverin, M., Croucher, D.C., Kushida, M., et al. (2021). Gradient of Developmental and Injury Response transcriptional states defines functional vulnerabilities underpinning glioblastoma heterogeneity. Nat. Cancer *2*, 157–173.

Ritschka, B., Storer, M., Mas, A., Heinzmann, F., Ortells, M.C., Morton, J.P., Sansom, O.J., Zender, L., and Keyes, W.M. (2017). The senescence-associated secretory phenotype induces cellular plasticity and tissue regeneration. Genes Dev. *31*, 172–183.

Ritschka, B., Knauer-Meyer, T., Gonçalves, D.S., Mas, A., Plassat, J.L., Durik, M., Jacobs, H., Pedone, E., Vicino, U. Di, Cosma, M.P., et al. (2020). The senotherapeutic drug ABT-737 disrupts aberrant p21 expression to restore liver regeneration in adult mice. Genes Dev. *34*, 489–494.

Robbins, E., Levine, E.M., and Eagle, H. (1970). Morphologic changes accompanying senescence of cultured human diploid cells. J. Exp. Med. *131*, 1211–1222.

Roberts, L.M., and Munson, J. (2020). Modulating Microenvironments for Treating Glioblastoma. Curr. Tissue Microenviron. Reports *1*, 99–111.

Robertson, F.L., Marqués-Torrejón, M.A., Morrison, G.M., and Pollard, S.M. (2019). Experimental models and tools to tackle glioblastoma. DMM Dis. Model. Mech. *12*.

Rodier, F., Coppé, J.P., Patil, C.K., Hoeijmakers, W.A.M., Muñoz, D.P., Raza, S.R., Freund, A., Campeau, E., Davalos, A.R., and Campisi, J. (2009). Persistent DNA damage signalling triggers senescence-associated inflammatory cytokine secretion. Nat. Cell Biol. *11*, 973–979.

Rodier, F., Muñoz, D.P., Teachenor, R., Chu, V., Le, O., Bhaumik, D., Coppé, J.P., Campeau, E., Beauséjour, C.M., Kim, S.H., et al. (2011). DNA-SCARS: Distinct nuclear structures that sustain damage-induced senescence growth arrest and inflammatory cytokine secretion. J. Cell Sci. *124*, 68–81.

Rojo de la Vega, M., Chapman, E., and Zhang, D.D. (2018). NRF2 and the Hallmarks of Cancer. Cancer Cell *34*, 21–43.

Rosenberg, S., Verreault, M., Schmitt, C., Guegan, J., Guehennec, J., Levasseur, C., Marie, Y., Bielle, F., Mokhtari, K., Hoang-Xuan, K., et al. (2017). Multi-omics analysis of primary glioblastoma cell lines shows recapitulation of pivotal molecular features of parental tumors. Neuro. Oncol. *19*, 219–228.

Le Roux, I., Konge, J., Le Cam, L., Flamant, P., and Tajbakhsh, S. (2015). Numb is required to prevent p53-dependent senescence following skeletal muscle injury. Nat. Commun. *6*, 8528.

Rowland, B.D., Denissov, S.G., Douma, S., Stunnenberg, H.G., Bernards, R., and Peeper, D.S. (2002). E2F transcriptional repressor complexes are critical downstream targets of p19ARF/p53-induced proliferative arrest. Cancer Cell *2*, 55–65.

Ruhland, M.K., Coussens, L.M., and Stewart, S.A. (2016a). Senescence and cancer: An evolving inflammatory paradox. Biochim. Biophys. Acta - Rev. Cancer *1865*, 14–22.

Ruhland, M.K., Loza, A.J., Capietto, A.-H.H., Luo, X., Knolhoff, B.L., Flanagan, K.C., Belt, B.A., Alspach, E., Leahy, K., Luo, J., et al. (2016b). Stromal senescence establishes an immunosuppressive microenvironment that drives tumorigenesis. Nat. Commun. *7*, 11762.

Rupp, T., Langlois, B., Koczorowska, M.M., Radwanska, A., Sun, Z., Hussenet, T., Lefebvre, O., Murdamoothoo, D., Arnold, C., Klein, A., et al. (2016). Tenascin-C Orchestrates Glioblastoma Angiogenesis by Modulation of Pro- and Anti-angiogenic Signaling. Cell Rep. *17*, 2607–2619.

Ruscetti, M., Leibold, J., Bott, M.J., Fennell, M., Kulick, A., Salgado, N.R., Chen, C.C., Ho, Y. jui, Sanchez-Rivera, F.J., Feucht, J., et al. (2018). NK cell–mediated cytotoxicity contributes to tumor control by a cytostatic drug combination.

Ruscetti, M., Morris, J.P., Mezzadra, R., Russell, J., Leibold, J., Romesser, P.B., Simon, J., Kulick, A., Ho, Y. jui, Fennell, M., et al. (2020). Senescence-Induced Vascular Remodeling Creates Therapeutic Vulnerabilities in Pancreas Cancer. Cell *181*, 424-441.e21.

Sanders, Y.Y., Liu, H., Zhang, X., Hecker, L., Bernard, K., Desai, L., Liu, G., and Thannickal, V.J. (2013). Histone modifications in senescence-associated resistance to apoptosis by oxidative stress. Redox Biol. *1*, 8–16.

Sanson, M., Marie, Y., Paris, S., Idbaih, A., Laffaire, J., Ducray, F., Hallani, S. El, Boisselier, B., Mokhtari, K., Hoang-Xuan, K., et al. (2009). Isocitrate dehydrogenase 1 codon 132 mutation is an important prognostic biomarker in gliomas. J. Clin. Oncol. *27*, 4150–4154.

Schafer, M.J., White, T.A., Iijima, K., Haak, A.J., Ligresti, G., Atkinson, E.J., Oberg, A.L., Birch, J., Salmonowicz, H., Zhu, Y., et al. (2017). Cellular senescence mediates fibrotic pulmonary disease. Nat. Commun. *8*.

Schindelin, J., Arganda-Carreras, I., Frise, E., Kaynig, V., Longair, M., Pietzsch, T., Preibisch, S., Rueden, C., Saalfeld, S., Schmid, B., et al. (2012). Fiji: An open-source platform for biological-image analysis. Nat. Methods *9*, 676–682.

Serrano, M., Lin, A.W., McCurrach, M.E., Beach, D., and Lowe, S.W. (1997). Oncogenic ras provokes premature cell senescence associated with accumulation of p53 and p16(INK4a). Cell *88*, 593–602.

Shapiro, G.I., Edwards, C.D., Kobzik, L., Godleski, J., Richards, W., Sugarbaker, D.J., and Rollins, B.J. (1995). Reciprocal Rb Inactivation and p16INK4 Expression in Primary Lung Cancers and Cell Lines. Cancer Res. *55*, 505–509.

Sharpless, N.E., and Sherr, C.J. (2015). Forging a signature of in vivo senescence. Nat. Rev. Cancer *15*, 397–408.

Sieben, C.J., Sturmlechner, I., van de Sluis, B., and van Deursen, J.M. (2018). Two-Step Senescence-Focused Cancer Therapies. Trends Cell Biol. *28*, 723–737.

da Silva, B., Mathew, R.K., Polson, E.S., Williams, J., and Wurdak, H. (2018). Spontaneous Glioblastoma Spheroid Infiltration of Early-Stage Cerebral Organoids Models Brain Tumor Invasion. SLAS Discov. *23*, 862–868.

Singh, D.K., Ling, E.-A., and Kaur, C. (2018). Hypoxia and myelination deficits in the developing brain. Int. J. Dev. Neurosci. Off. J. Int. Soc. Dev. Neurosci. *70*, 3–11.

Soda, Y., Marumoto, T., Friedmann-Morvinski, D., Soda, M., Liu, F., Michiue, H., Pastorino, S., Yang, M., Hoffman, R.M., Kesari, S., et al. (2011). Transdifferentiation of glioblastoma cells into vascular endothelial cells. Proc. Natl. Acad. Sci. U. S. A. *108*, 4274–4280.

Sone, H., and Kagawa, Y. (2005). Pancreatic beta cell senescence contributes to the pathogenesis of type 2 diabetes in high-fat diet-induced diabetic mice. Diabetologia *48*, 58–67.

de Souza, C.F., Sabedot, T.S., Malta, T.M., Stetson, L., Morozova, O., Sokolov, A., Laird, P.W., Wiznerowicz, M., Iavarone, A., Snyder, J., et al. (2018). A Distinct DNA Methylation Shift in a Subset of Glioma CpG Island Methylator Phenotypes during Tumor Recurrence. Cell Rep. *23*, 637–651.

De Souza, N. (2018). Organoids. Nat. Methods *15*, 23.

Srividya, M.R., Thota, B., Shailaja, B.C., Arivazhagan, A., Thennarasu, K., Chandramouli, B.A., Hegde, A.S., and Santosh, V. (2011). Homozygous 10q23/PTEN deletion and its impact on outcome in glioblastoma: A prospective translational study on a uniformly treated cohort of adult patients. Neuropathology.

Storer, M., Mas, A., Robert-Moreno, A., Pecoraro, M., Ortells, M.C., Di Giacomo, V., Yosef, R., Pilpel, N., Krizhanovsky, V., Sharpe, J., et al. (2013). Senescence is a developmental mechanism that contributes to embryonic growth and patterning. Cell *155*, 1119–1130.

Stupp, R., Mason, W.P., Van Den Bent, M.J., Weller, M., Fisher, B., Taphoorn, M.J.B., Belanger, K., Brandes, A.A., Marosi, C., Bogdahn, U., et al. Radiotherapy plus Concomitant and Adjuvant Temozolomide for Glioblastoma.

Stupp, R., Mason, W.P., Van Den Bent, M.J., Weller, M., Fisher, B., Taphoorn, M.J.B., Belanger, K., Brandes, A.A., Marosi, C., Bogdahn, U., et al. (2005). 2005STUPP rt + tmz. N Engl J Med *352*, 987–996.

Sturm, D., Witt, H., Hovestadt, V., Khuong-Quang, D.A., Jones, D.T.W., Konermann, C., Pfaff, E., Tönjes, M., Sill, M., Bender, S., et al. (2012). Hotspot Mutations in H3F3A and IDH1 Define Distinct Epigenetic and Biological Subgroups of Glioblastoma. Cancer Cell *22*, 425–437.

Suvà, M.L., and Tirosh, I. (2020). The Glioma Stem Cell Model in the Era of Single-Cell Genomics. Cancer Cell *37*, 630–636.

Takasugi, M., Okada, R., Takahashi, A., Virya Chen, D., Watanabe, S., and Hara, E. (2017). Small extracellular vesicles secreted from senescent cells promote cancer cell proliferation through EphA2. Nat. Commun. *8*, 1–11.

Tang, M., Xie, Q., Gimple, R.C., Zhong, Z., Tam, T., Tian, J., Kidwell, R.L., Wu, Q., Prager, B.C., Qiu, Z., et al. (2020). Three-dimensional bioprinted glioblastoma microenvironments model cellular dependencies and immune interactions. Cell Res. *30*, 833–853.

Tasdemir, N., Banito, A., Roe, J.S., Alonso-Curbelo, D., Camiolo, M., Tschaharganeh, D.F., Huang, C.H., Aksoy, O., Bolden, J.E., Chen, C.C., et al. (2016). BRD4 connects enhancer remodeling to senescence immune surveillance. Cancer Discov. *6*, 613–629.

Thompson, P.J., Shah, A., Ntranos, V., Van Gool, F., Atkinson, M., and Bhushan, A. (2019). Targeted Elimination of Senescent Beta Cells Prevents Type 1 Diabetes. Cell Metab. *29*, 1045-1060.e10.

Thorsson, V., Gibbs, D.L., Brown, S.D., Wolf, D., Bortone, D.S., Ou Yang, T.H., Porta-Pardo, E., Gao, G.F., Plaisier, C.L., Eddy, J.A., et al. (2018). The Immune Landscape of Cancer. Immunity *48*, 812-830.e14.

Todorova, P.K., Fletcher-Sananikone, E., Mukherjee, B., Kollipara, R., Vemireddy, V., Xie, X.J., Guida, P.M., Story, M.D., Hatanpaa, K., Habib, A.A., et al. (2019). Radiation-induced DNA damage cooperates with heterozygosity of TP53 and PTEN to generate high-grade gliomas. Cancer Res. *79*, 3749–3761.

Toso, A., Revandkar, A., DiMitri, D., Guccini, I., Proietti, M., Sarti, M., Pinton, S., Zhang, J., Kalathur, M., Civenni, G., et al. (2014). Enhancing chemotherapy efficacy in pten-deficient prostate tumors by activating the senescence-associated antitumor immunity. Cell Rep.

Touat, M., Li, Y.Y., Boynton, A.N., Spurr, L.F., Iorgulescu, J.B., Bohrson, C.L., Cortes-Ciriano, I., Birzu, C., Geduldig, J.E., Pelton, K., et al. (2020). Mechanisms and therapeutic implications of hypermutation in gliomas. Nature *580*, 517–523.

Treps, L., Perret, R., Edmond, S., Ricard, D., and Gavard, J. (2017). Glioblastoma stem-like cells secrete the pro-angiogenic VEGF-A factor in extracellular vesicles. J. Extracell. Vesicles *6*.

Triana-Martínez, F., Picallos-Rabina, P., Da Silva-Álvarez, S., Pietrocola, F., Llanos, S., Rodilla, V., Soprano, E., Pedrosa, P., Ferreirós, A., Barradas, M., et al. (2019). Identification and characterization of Cardiac Glycosides as senolytic compounds. Nat. Commun. *10*, 1–12.

Tuveson, D.A., Weinberg, B., Bradley, A., Berns, A., and Copeland, N. (2021). Fighting the sixth decade of the cancer war with better cancer models. Cancer Discov. 801–805.

Ventura, A., Kirsch, D.G., McLaughlin, M.E., Tuveson, D.A., Grimm, J., Lintault, L., Newman, J., Reczek, E.E., Weissleder, R., and Jacks, T. (2007). Restoration of p53 function leads to tumour regression in vivo. Nature *445*, 661–665.

Verhaak, R.G.W., Hoadley, K.A., Purdom, E., Wang, V., Qi, Y., Wilkerson, M.D., Miller, C.R., Ding, L., Golub, T., Mesirov, J.P., et al. (2010). Integrated Genomic Analysis Identifies Clinically Relevant Subtypes of Glioblastoma Characterized by Abnormalities in PDGFRA, IDH1, EGFR, and NF1. Cancer Cell *17*, 98–110.

van Vliet, T., Varela-Eirin, M., Wang, B., Borghesan, M., Brandenburg, S.M., Franzin, R., Evangelou, K., Seelen, M., Gorgoulis, V., and Demaria, M. (2021). Physiological hypoxia restrains the senescence-associated secretory phenotype via AMPK-mediated mTOR suppression. Mol. Cell 1–12.

Wakita, M., Takahashi, A., Sano, O., Loo, T.M., Imai, Y., Narukawa, M., Iwata, H., Matsudaira, T., Kawamoto, S., Ohtani, N., et al. (2020). A BET family protein degrader provokes senolysis by targeting NHEJ and autophagy in senescent cells. Nat. Commun. *11*, 1–13.

Wang, C., Jurk, D., Maddick, M., Nelson, G., Martin-ruiz, C., and Von Zglinicki, T. (2009a). DNA damage response and cellular senescence in tissues of aging mice. Aging Cell *8*, 311–323.

Wang, C., Vegna, S., Jin, H., Benedict, B., Lieftink, C., Ramirez, C., de Oliveira, R.L., Morris, B., Gadiot, J., Wang, W., et al. (2019a). Inducing and exploiting vulnerabilities for the treatment

of liver cancer. Nature *574*, 268–272.

Wang, H., Lathia, J.D., Wu, Q., Wang, J., Li, Z., Heddleston, J.M., Eyler, C.E., Elderbroom, J., Gallagher, J., Schuschu, J., et al. (2009b). Targeting interleukin 6 signaling suppresses glioma stem cell survival and tumor growth. Stem Cells *27*, 2393–2404.

Wang, L., Leite de Oliveira, R., Wang, C., Fernandes Neto, J.M., Mainardi, S., Evers, B., Lieftink, C., Morris, B., Jochems, F., Willemsen, L., et al. (2017a). High-Throughput Functional Genetic and Compound Screens Identify Targets for Senescence Induction in Cancer. Cell Rep. *21*, 773–783.

Wang, L., Babikir, H., Müller, S., Yagnik, G., Shamardani, K., Catalan, F., Kohanbash, G., Alvarado, B., Di Lullo, E., Kriegstein, A., et al. (2019b). The phenotypes of proliferating glioblastoma cells reside on a single axis of variation. Cancer Discov. *9*, 1708–1719.

Wang, Q., Hu, B., Hu, X., Kim, H., Squatrito, M., Scarpace, L., deCarvalho, A.C., Lyu, S., Li, P., Li, Y., et al. (2017b). Tumor Evolution of Glioma-Intrinsic Gene Expression Subtypes Associates with Immunological Changes in the Microenvironment. Cancer Cell *32*, 42-56.e6.

Wang, S.I., Puc, J., Li, J., Bruce, J.N., Cairns, P., Sidransky, D., Parsons ', R., and Surgery, N. (1997). in Glioblastoma Multiforme PTEN Somatic Mutations of Somatic Mutations of PTEN in Glioblastoma Multiforme. Cancer Res *57*, 4183–4186.

Weller, M., van den Bent, M., Tonn, J.C., Stupp, R., Preusser, M., Cohen-Jonathan-Moyal, E., Henriksson, R., Rhun, E. Le, Balana, C., Chinot, O., et al. (2017). European Association for Neuro-Oncology (EANO) guideline on the diagnosis and treatment of adult astrocytic and oligodendroglial gliomas. Lancet Oncol. *18*, e315–e329.

Wen, P.Y., Weller, M., Lee, E.Q., Alexander, B.M., Barnholtz-Sloan, J.S., Barthel, F.P., Batchelor, T.T., Bindra, R.S., Chang, S.M., Antonio Chiocca, E., et al. (2020). Glioblastoma in adults: A Society for Neuro-Oncology (SNO) and European Society of Neuro-Oncology (EANO) consensus review on current management and future directions. Neuro. Oncol. *22*, 1073–1113.

Wikstrand, C.J., McLendon, R.E., Friedman, A.H., and Bigner, D.D. (1997). Cell surface localization and density of the tumor-associated variant of the epidermal growth factor receptor, EGFRvIII. Cancer Res. *57*, 4130–4140.

Wiley, C.D., and Campisi, J. (2016). From Ancient Pathways to Aging Cells - Connecting Metabolism and Cellular Senescence. Cell Metab. *23*, 1013–1021.

Winkler, J., Abisoye-Ogunniyan, A., Metcalf, K.J., and Werb, Z. (2020). Concepts of extracellular matrix remodelling in tumour progression and metastasis. Nat. Commun. *11*, 1–19.

Wyld, L., Bellantuono, I., Tchkonia, T., Morgan, J., Turner, O., Foss, F., George, J., Danson, S., and Kirkland, J.L. (2020). Senescence and cancer: A review of clinical implications of senescence and senotherapies. Cancers (Basel). *12*, 1–20.

Xiang, X.H., Yang, L., Zhang, X., Ma, X.H., Miao, R.C., Gu, J.X., Fu, Y.N., Yao, Q., Zhang, J.Y., Liu, C., et al. (2019). Seven-senescence-associated gene signature predicts overall survival for Asian patients with hepatocellular carcinoma. World J. Gastroenterol. *25*, 1715–1728.

Xu, M., Pirtskhalava, T., Farr, J.N., Weigand, B.M., Palmer, A.K., Weivoda, M.M., Inman, C.L., Ogrodnik, M.B., Hachfeld, C.M., Fraser, D.G., et al. (2018). Senolytics improve physical function and increase lifespan in old age. Nat. Med. *24*, 1246–1256.

Xue, W., Zender, L., Miething, C., Dickins, R.A., Hernando, E., Krizhanovsky, V., Cordon-Cardo, C., and Lowe, S.W. (2007). Senescence and tumour clearance is triggered by p53

restoration in murine liver carcinomas. Nature *445*, 656–660.

Yamada, S., Matsuda, R., Nishimura, F., Nakagawa, I., Motoyama, Y., Park, Y.S., Nakamura, M., Nakase, H., Ouji, Y., and Yoshikawa, M. (2012). Carnitine-induced senescence in glioblastoma cells. Exp. Ther. Med. *4*, 21–25.

Yang, H., Wang, H., Ren, U., Chen, Q., and Chena, Z.J. (2017). CGAS is essential for cellular senescence. Proc. Natl. Acad. Sci. U. S. A. *114*, E4612–E4620.

Yang, Y., Shao, N., Luo, G., Li, L., Zheng, L., Nilsson-Ehle, P., and Xu, N. (2010). Mutations of PTEN gene in gliomas correlate to tumor differentiation and short-term survival rate. Anticancer Res.

Yeung, J.T., Hamilton, R.L., Ohnishi, K., Ikeura, M., Potter, D.M., Nikiforova, M.N., Ferrone, S., Jakacki, R.I., Pollack, I.F., and Okada, H. (2013). LOH in the HLA class I region at 6p21 is associated with shorter survival in newly diagnosed adult glioblastoma. Clin. Cancer Res. *19*, 1816–1826.

Yosef, R., Pilpel, N., Tokarsky-Amiel, R., Biran, A., Ovadya, Y., Cohen, S., Vadai, E., Dassa, L., Shahar, E., Condiotti, R., et al. (2016). Directed elimination of senescent cells by inhibition of BCL-W and BCL-XL. Nat. Commun. *7*.

Yoshida, T., Akatsuka, T., and Imanaka-Yoshida, K. (2015). Tenascin-C and integrins in cancer. Cell Adhes. Migr. *9*, 96–104.

Yoshimoto, S., Loo, T.M., Atarashi, K., Kanda, H., Sato, S., Oyadomari, S., Iwakura, Y., Oshima, K., Morita, H., Hattori, M., et al. (2013). Obesity-induced gut microbial metabolite promotes liver cancer through senescence secretome. Nature *499*, 97–101.

Zanotto-Filho, A., Gonçalves, R.M., Klafke, K., de Souza, P.O., Dillenburg, F.C., Carro, L., Gelain, D.P., and Moreira, J.C.F. (2017). Inflammatory landscape of human brain tumors reveals an NFκB dependent cytokine pathway associated with mesenchymal glioblastoma. Cancer Lett. *390*, 176–187.

Zezula, J., Casaccia-Bonnefil, P., Ezhevsky, S.A., Osterhout, D.J., Levine, J.M., Dowdy, S.F., Chao, M. V., and Koff, A. (2001). P21cip1 is required for the differentiation of oligodendrocytes independently of cell cycle withdrawal. EMBO Rep. *2*, 27–34.

Zhang, P., Kishimoto, Y., Grammatikakis, I., Gottimukkala, K., Cutler, R.G., Zhang, S., Abdelmohsen, K., Bohr, V.A., Misra Sen, J., Gorospe, M., et al. (2019). Senolytic therapy alleviates Aβ-associated oligodendrocyte progenitor cell senescence and cognitive deficits in an Alzheimer's disease model. Nat. Neurosci. *22*, 719–728.

Zhang, R., Poustovoitov, M. V., Ye, X., Santos, H.A., Chen, W., Daganzo, S.M., Erzberger, J.P., Serebriiskii, I.G., Canutescu, A.A., Dunbrack, R.L., et al. (2005). Formation of macroH2A-containing senescence-associated heterochromatin foci and senescence driven by ASF1a and HIRA. Dev. Cell *8*, 19–30.

Zhang, X., Chen, L., Dang, W. qi, Cao, M. fu, Xiao, J. fang, Lv, S. qing, Jiang, W. jie, Yao, X. hong, Lu, H. min, Miao, J. ya, et al. (2020). CCL8 secreted by tumor-associated macrophages promotes invasion and stemness of glioblastoma cells via ERK1/2 signaling. Lab. Investig. *100*, 619–629.

Zuo, S., Zhang, X., and Wang, L. (2019). A RNA sequencing-based six-gene signature for survival prediction in patients with glioblastoma. Sci. Rep. *9*, 1–10.

The schemes in the manuscript were created with BioRender.com.

Abstract

Glioblastoma (GBM) is the most common primary brain tumor in adults yet with limited treatment efficacy. In cancer, recent studies describe senescent cells removal as a new emerging therapeutic strategy. Senescent cells are characterized by a stable cell cycle arrest and by the secretion of a plethora of factors referred as the senescence-associated secretory phenotype (SASP). The aim of my thesis was to decipher the role of cellular senescence in GBM progression. We first identified senescent cells in patient and in a mouse model of GBM. We then showed that the removal of senescent cells expressing high levels of *p16^{Ink4a}*, using the p16-3MR transgene, significantly increased the survival of GBM-bearing mice. Single-cell RNA sequencing (scRNAseq) analysis revealed that senescent p16$^{Ink4a\ Hi}$ cells are malignant, they represent less than 10% of the tumor cells and their removal modify the tumoral ecosystem. By combining scRNAseq and bulk RNAseq with immunohistochemistry, we identified NRF2 transcription factor as a regulator of the SASP. Moreover, we defined a specific senescence signature in the mouse model of GBM. Remarkably, the senescence signature is conserved in patient GBMs and its high score is correlated with a lower survival. These results pave the way for the use of senotherapy as a companion therapy for patients with GBM.

Key words: Glioblastoma, Cellular Senescence, NRF2, scRNAseq, Senotherapy

Résumé

Le glioblastome (GBM) est une tumeur cérébrale maligne primitive la plus fréquente chez l'adulte. L'efficacité des traitements reste très limitée et le taux de survie très faible. Dans le domaine du cancer, l'élimination des cellules sénescentes a récemment émergé comme une potentielle stratégie thérapeutique. Les cellules sénescentes sont caractérisées par un arrêt stable du cycle cellulaire ainsi que par la sécrétion d'une multitude de facteurs regroupés sous le terme phénotype sécrétoire associé à la sénescence (SASP). Le but de mon projet de thèse a été d'étudier le rôle de ces cellules au cours de la progression tumorale des GBM. Nous les avons tout d'abord identifiées dans les GBM de patients et de souris. En utilisant le modèle transgénique p16-3MR, nous avons montré que l'élimination des cellules sénescentes exprimant des niveaux élevés de *p16^{Ink4a}* améliore significativement la survie des souris porteuses d'un GBM. Des analyses de séquençage d'ARN en cellule unique (scRNAseq) ont révélé que les cellules sénescentes p16$^{Ink4a\ Hi}$ ont une identité maligne, qu'elles représentent moins de 10% de la tumeur totale, et qu'elles modifient l'écosystème tumoral.

En combinant les techniques de séquençage de l'ARNm sur tissu (bulk RNAseq) et sur cellule unique (scRNAseq) avec l'immunohistochimie, nous avons identifié le facteur de transcription NRF2 comme régulateur du SASP. Enfin, nous avons identifié une signature de la sénescence, spécifique dans notre modèle souris et qui est conservée dans les GBM de patients. De manière remarquable, l'expression élevée de la signature sénescente est corrélée un mauvais pronostic chez les patients. Ces résultats ouvrent la voie à l'utilisation d'une sénothérapie en combinaison avec les thérapies conventionnelles pour les patients atteints de GBM.

Mots-clés : Glioblastome, Sénescence Cellulaire, NRF2, scRNAseq, Sénothérapie

Abstract

Glioblastoma (GBM) is the most common primary brain tumor in adults yet with limited treatment efficacy. In cancer, recent studies describe senescent cells removal as a new emerging therapeutic strategy. Senescent cells are characterized by a stable cell cycle arrest and by the secretion of a plethora of factors referred as the senescence-associated secretory phenotype (SASP). The aim of my thesis was to decipher the role of cellular senescence in GBM progression. We first identified senescent cells in patient and in a mouse model of GBM. We then showed that the removal of senescent cells expressing high levels of *p16*^{Ink4a}, using the p16-3MR transgene, significantly increased the survival of GBM-bearing mice. Single-cell RNA sequencing (scRNAseq) analysis revealed that senescent p16$^{Ink4a\ Hi}$ cells are malignant, they represent less than 10% of the tumor cells and their removal modify the tumoral ecosystem. By combining scRNAseq and bulk RNAseq with immunohistochemistry, we identified NRF2 transcription factor as a regulator of the SASP. Moreover, we defined a specific senescence signature in the mouse model of GBM. Remarkably, the senescence signature is conserved in patient GBMs and its high score is correlated with a lower survival. These results pave the way for the use of senotherapy as a companion therapy for patients with GBM.

Key words: Glioblastoma, Cellular Senescence, NRF2, scRNAseq, Senotherapy

Résumé

Le glioblastome (GBM) est une tumeur cérébrale maligne primitive la plus fréquente chez l'adulte. L'efficacité des traitements reste très limitée et le taux de survie très faible. Dans le domaine du cancer, l'élimination des cellules sénescentes a récemment émergé comme une potentielle stratégie thérapeutique. Les cellules sénescentes sont caractérisées par un arrêt stable du cycle cellulaire ainsi que par la sécrétion d'une multitude de facteurs regroupés sous le terme phénotype sécrétoire associé à la sénescence (SASP). Le but de mon projet de thèse a été d'étudier le rôle de ces cellules au cours de la progression tumorale des GBM. Nous les avons tout d'abord identifiées dans les GBM de patients et de souris. En utilisant le modèle transgénique p16-3MR, nous avons montré que l'élimination des cellules sénescentes exprimant des niveaux élevés de *p16*^{Ink4a} améliore significativement la survie des souris porteuses d'un GBM. Des analyses de séquençage d'ARN en cellule unique (scRNAseq) ont révélé que les cellules sénescentes p16$^{Ink4a\ Hi}$ ont une identité maligne, qu'elles représentent moins de 10% de la tumeur totale, et qu'elles modifient l'écosystème tumoral.

En combinant les techniques de séquençage de l'ARNm sur tissu (bulk RNAseq) et sur cellule unique (scRNAseq) avec l'immunohistochimie, nous avons identifié le facteur de transcription NRF2 comme régulateur du SASP. Enfin, nous avons identifié une signature de la sénescence, spécifique dans notre modèle souris et qui est conservée dans les GBM de patients. De manière remarquable, l'expression élevée de la signature sénescente est corrélée un mauvais pronostic chez les patients. Ces résultats ouvrent la voie à l'utilisation d'une sénothérapie en combinaison avec les thérapies conventionnelles pour les patients atteints de GBM.

Mots-clés : Glioblastome, Sénescence Cellulaire, NRF2, scRNAseq, Sénothérapie